Density-Based Separations in Aqueous Multiphase Systems: Tools for Biological Research and Low-Cost Diagnostics

Density-Based Separations in Aqueous Multiphase Systems:

Tools for Biological Research and Low-Cost Diagnostics

A dissertation presented

by

Ashok Ashwin Kumar

to

The School of Engineering and Applied Sciences

in partial fulfillment of the requirements

for the degree of

Doctor of Philosophy

in the subject of

Applied Physics

Harvard University

Cambridge, Massachussetts

May, 2014

Dissertation Advisors:

Professor George M. Whitesides

Professor Robert M. Westervelt

Submitted by:

Ashok Ashwin Kumar

Density-Based Separations in Aqueous Multiphase Systems:

Tools for Biological Research and Low-Cost Diagnostics

Abstract

Cells often exist in heterogeneous mixtures. Density provides a property to separate several types of cells from the mixed sample in which they originate. Density-based separation methods provide a standard method to quickly separate or enrich specific populations of cells, such as lymphocytes from whole blood. This dissertation explores the use of aqueous multiphase systems (AMPS) as self-forming step-gradients in density for the separation of cells. AMPS were first discovered over a hundred years ago as aqueous two-phase systems. Density as a tool to separate cells is at least as old. Despite this long history, the work in this thesis is the first work to use AMPS to perform density-based separations on cells. This combination provides a powerful technique to separate cells and enable new testing at the point-of-care. Chapter 1 provides a short overview of aqueous multiphase systems and density-based separations of cells. Chapter 2 describes the process of taking technology, including AMPS, from a demonstration in a laboratory to a large scale evaluation in a field setting. In Chapter 3 and Appendix I, AMPS provide a means to enrich reticulocytes from whole blood as a means to grow malaria parasites.

Chapter 4 and Appendix II describe the development and proof-of-prinicple of a density-based diagnostic test for sickle cell disease (SCD) using AMPS. Chapter 5 and Appendix III detail the results of a large scale field evaluation of a rapid test for SCD using AMPS in Zambia. Demonstrations of AMPS for density- and size-based separations are provided in Appendices IV and V. Appendix VI demonstrates the general usefulness of density to separate crystal polymorphs with another density-based separation method: magnetic levitation in a paramagnetic fluid. Beyond density, novel combinations of technology, such as electrochemistry and telecommunications provide opportunities for enabling global health (Appendix VII).

Table of Contents

Dedicated to my family

and to those in South Africa that adopted me as their family as a Peace Corps Volunteer

Acknowledgments

Several hands and minds go into the creation of any PhD. I would not have been able to do the work that I did if I had not joined the Whitesides group, and that event would never have happened without Hayat Sindi. After seeing her present about Diagnostics for All at a symposium, I discussed my aspirations as a graduate student with her. She was kind enough to send an introductory email to George based on that simple interaction. From there, I was able to join the group. The work in this thesis began and ended with the mentorship of Charlie Mace. As a postdoctoral fellow, he provided guidance to me as a new graduate student sharing his vision with me about aqueous multiphase systems (AMPS) and their potential to separate cells. Five years later as a professor at Tufts, he continued to provide guidance in writing papers and designing experiments to understand how AMPS behave under different conditions.

I have had the privilege of working alongside over a hundred postdoctoral fellows, dozens of visiting scholars, and about a dozen graduate students in the Whitesides group. Lizzy Hulme, Kat Mirica, Bill Reus, Sindy Tang, and Darren Lipomi deserve special mention for taking time to explain to me how to be a successful graduate student in the group. Darren, in particular, provided wise words, a well stocked bench to inherit, and enough free furniture to deck out my apartment as a graduate student.

Other group members that deserve special mention are Ozge Akbulut, Jon Hennek, Shuji Fujita, Barb Smith, Alex Nemiroski, Dionysius Christodouleous, Matt Lockett, Gulden Camci-Unal, Jerome Fox, Jane Maxwell, Heiko Lange, Mathieu Gonidec, Nathan Shapiro, Manza Atkinson, and David Bwambok who have been wonderful team members on various projects. Outside of work, Bobak Mosadegh and Phillip Rothemund ensured my muscled did not atrophy by providing motivation to climb as much as possible.

I have had the privilege of working with and mentoring many talented students who have contributed to my projects: Matt Patton, Ryan Lee, Gaetana D'Alesio-Spina, Abeer Syed, Phillip Aguilar, Bhavin Patel, and Will Bloxham. Outside of the lab, many students have contributed to my projects: Caeul Lim, Yovany Moreno, Daria Van Tyne, Kate Fernandez, and Amy Bei.

Harvard has provided several resources that have allowed me to grow as a researcher and a person. I would not have been able to have pursued AMPS without the tireless advocacy of Mick Sawka at Harvard's Office of Technology Development. Jim MacArthur and Stan Coutreau in Physics provided me with an education in electronics and machining. Laura Frahm, Pamela Pollock, Marlon Kuzmick, Sarah Jessop, and John Girash helped me develop as a speaker and a teacher through Harvard Horizons and the Bok Center. Fanny Ennever at the Committee on the Use of Human Subjects provided me with guidance navigating IRB reviews. T.J. Martin, Melissa LeGrand, and Tracie Smart helped me navigate my way in a large lab full of postdocs.

Several people in Zambia provided a capstone to my PhD work. Dr. Catherine Chunda-Liyoka and Dr. Hamakwa Mantina were wonderful partners who enabled me to set up a field trial. Ali, the taxi driver who became my friend, helped me navigate the ins and outs of Lusaka and procure supplies for our study. The entire study staff and the Peace Corps in Zambia were incredibly helpful and dedicated to making an impact on Zambia.

I have also had the incredible opportunity to get to know two startup companies working on low-cost diagnostics. Bill Rodriguez, Marta Fernandez-Suarez, and Aaron Oppenheimer of Daktari Diagnostics, and Una Ryan, Marcus Lovell-Smith, Patrick Beattie, Jason Rolland, Shali Kumar, and Sid Jain at Diagnostics for All have provided me with insights into what it takes to make technology into products that can have an impact.

Coming home every day to wonderful people has made grad school a joy. Jonathan Pines, Lauren Hartle, Zsofia Botyanszki, Brenna Krieger, John Rutherford, Megan Clapp, Zach Gerson-Nieder, Richa Gawande, Karen Kieser, and Vivian Hemmelder were wonderful roommates. Erin Gannon and Alan Post shared their home with me for a summer when my apartment burned down. And finishing off my PhD living with Meera Krishnan has provided me with a home full of love and support.

I was fortunate to have many eminent faculty to mentor me as I embarked on medical applications; Prof. Dyann Wirth, Prof. Manoj Duraisingh, Dr. Tom Stossel, and Dr. Carlo Brugnara provided me with counsel and their students time and skills. Prof. Bob Westervelt, my advisor in SEAS, provided support and perspective on technology and electronics. Dyann and Bob also served on my Dissertation Advisory Committee along with Prof. Joanna Aizenberg. Prof. Adam Cohen also provided valuable insights as part of my Qualifying Committee.

And, of course, Prof. George Whitesides. I know no other person with a command for so many subjects, with such incredible management skills, and with such a fierce curiosity. He has provided me more than just an education about how to be a scientist. He has provided an example of drive, intellectual vigor, and holistic development; his comments and lessons to me over the years have included as much about personal skills, communications, and leadership as they have about science. As a physics student at Stanford and a Peace Corps Volunteer in South Africa, I had no idea who George was, but I am incredibly thankful that I found him soon after arriving at Harvard.

Finally, I could not have gone far in life without my family. My sister, Anita, has been a constant friend and support. Her husband, Nile, has added a mischievous fun to our family. My mom, Kausalya, and my father, Ashok, provided incredible role models growing up. Even

though I developed my skills in the hard sciences, their dedication as doctors made it impossible for me to ignore the immediacy of medicine and health. If my work is inspired by anything, it is inspired by my mom and dad.

Chapter 1

Aqueous Multiphase Systems: A Tool for Separating Cells by Density

Ashok A. Kumar[1], Jenna Walz[2], Charles R. Mace[2]

and George M. Whitesides[3]

[1]School of Engineering and Applied Sciences, Harvard University, Cambridge, MA 02138

[2]Department of Chemistry, Tufts University, Medford, MA 02155

[3]Department of Chemistry and Chemical Biology, Harvard University, Cambridge, MA 02138

Abstract

This chapter reviews the use of aqueous multiphase systems (AMPS)—immiscible solutions of polymers, salts, surfactants, and/or ionic liquids—as a tool for the density-based separation of cells. AMPS provide self-assembling step-gradients with molecularly-sharp interfaces to collect and concentrate cells. Osmolality, pH, and viscosity provide additional parameters of the solution to improve separations. Centrifugation of cells through these systems provides a simple means to enrich cells as a preparative step—such as the enrichment of reticulocytes for the cultivation of malaria parasites—or for the separation and identification of a specific subset of cells—such as the separation of dense, sickled cells to diagnose sickle cell disease.

1. Introduction

1.1. Aqueous Multiphase Systems

When a mixture of polymers, surfactants, salts, and/or ionic liquids are dissolved in water, they often spontaneously form immiscible phases. Although these phases are primarily composed of water, they are separated by distinct, molecularly sharp interfaces. The combinations of components that form two phases are called aqueous two-phase systems (ATPS), and have been reviewed extensively.[1] Combinations can also be found that result in the formation of more than two phases.[2] These systems can be, thus, more generally described as aqueous multiphase systems (AMPS). AMPS possess four qualities that make them particularly appealing for separations: i) they are self-forming, ii) they are scalable in volume, iii) they can be made biocompatible, and iv) their physical properties are tunable.

Biochemists have used AMPS for the purification and extraction of proteins and other biomolecules.[3–5] Recently, the partitioning ability of AMPS has been extended to enrich nanoparticles and other non-biological materials.[6] The combination of AMPS in microfluidic systems also provides new techniques to exploit partitioning to separate materials.[7] In addition to partitioning, the physical properties of AMPS (e.g., density and viscosity) have been exploited to create new methods for separations and provide the opportunity for far broader use.[2,8] The phases of an AMPS form layers based on density; these systems are self-assembling step-gradients in density with well defined, molecularly sharp steps in density between phases.[2] As such, AMPS provide a simple tool to separate cells by density.

1.2. Why separate cells?

Whether in tissues, a tumor, or blood, cells often appear in mixtures in nature. Sometimes, only one type of cell is of particular interest; scientists have developed a number of

methods to separate and enrich particular cells from heterogeneous mixtures. Separating cells is an important ability in three aspects of biomedicine: 1) diagnostics, 2) biological research, and 3) therapeutics. In diagnostic applications, separation is generally a means for identification. The identification of cells present at low concentrations in blood (e.g., circulating tumor cells) is greatly enabled by the prior removal of cells present in much higher concentrations (e.g., erythrocytes and leukocytes).[9–11] In research applications, separation makes it possible for scientists to perform experiments on specific populations of cells. Pure populations of cells enable studies on genomics, cellular function, and differentiation. For example, the ability to separate and enrich cells enabled immunologists to understand the role of dendritic cells[12] and study the ways in which natural killer cells and T-lymphocytes defend against bacteria.[13] Separations are also important for therapeutics. Plasma enriched in platelets has been used to treat a variety of musculoskeletal injuries and disorders.[14–16] Stem cells enriched from adipose tissue may be useful for tissue engineering.[17,18]

Labeling a cell using an antibody conjugated to a marker (e.g., a fluorophore or a magnetic bead) allows the separation of specific cells using molecular recognition. Both fluorescence-activated cell sorting (FACS) and magnetically activated cell sorting (MACS) allow a wide range of cell separations.[19] While label-based separations are often useful, in some cases, label-free methods offer advantages.[20] Biochemical labels may trigger internal signals in a cell. For assays of immune response—where the objective is to understand the behavior of white blood cells—labeling may affect cell membranes or produce a phenotype that does not represent the state of the original sample.[21] Similarly, certain therapeutics require unlabeled cells; labels on stem cells may affect differentiation.[22] The use of labels, and the associated washing required to remove excess reagents, can increase the number of steps necessary for a

separation. In point-of-care applications, limits on time, the stability of reagents, and the availability of trained users may be easier to overcome with label-free separation methods. Separating cells without labels, however, requires the identification of properties or characteristics of a cell that provide a degree of specificity to the population of cells of interest. Among the physical properties that have been exploited to separate cells are morphology,[23] size,[24,25] stiffness,[26,27] and dielectric constant.[19,28]

1.3. Density and Cells

Density—the mass over the volume—has also been exploited in the research of many different cell types from various biological samples. **Table 1.1** provides a list of some of the most frequent cellular separations by density. The density of a cell is a biophysical indicator dependent on the phenotype and environment of a cell. As such, biophysical indicators can provide useful information for managing diseases[29] or understanding cellular differentiation.[30]

In cells, changes in density are generally the result of two processes: 1) dehydration or swelling, and 2) the production or consumption of proteins. These processes can be the result of invasion by a parasite, cellular responses to the environment, differentiation, or aging.[31–34] Compared to mass and volume separately, density may provide a more robust parameter to monitor changes in cells.[35]

Centrifugation over AMPS allows the label-free separation of cells by small ($\Delta\rho < 0.001$ g/cm^3) differences in density. The self-forming nature of AMPS allows for their use over a wide range of volumes. A drop of blood from a fingerprick can be separated in a capillary tube, or a unit of blood can be separated in large conical tubes. The use of AMPS to separate cells can not only improve the ease of separations currently done with other methods, but also enables new applications of density-based separations of cells, such as point-of-care diagnostics.

Table 1.1. Examples of cell types separated by density.

Enriched cell type(s)	Method	Original suspension	Density of Barrier(s) (g/cm^3)[a]	Purity
Lymphocytes	Nycoprep	Human Leukocyte Suspension	1.072	98.6 ± 0.4[36]
Granulocytes	Layered Gradient	Whole blood	1.075, 1.096–1.098	99.7% of leukocytes, purity of total cells not reported[37]
Mononuclear cells	Lymphoprep	Whole blood	*NA*	94.5% ± 6.2[b][38]
Myeloblasts + promyeloblasts	Lymphoprep	Bone marrow	*NA*	8.6 ± 3.7%[38]
P. falciparum infected RBCs	Ficoll solution	Blood cultures of *P. falciparum*	*NA*	76.2%[39]
Disseminated tumor cells	Ficoll & oncoquick	Whole blood	*NA*	84–87%[40]
P. falciparum schizonts	Continuous Percoll gradient	Blood cultures of *P. falciparum*	*NA*	66.6%[41]
Spermatozoa	Discontinuous Percoll gradient	Semen	*NA*	85.2%, based on vitality[42]
Candida albicans	Discontinuous sucrose gradient	Polymorphic cell culture	*NA*	80%, hyphal from yeast forms[43]
Alveolar macrophages	Discontinuous Percoll gradient	Bronchoalveolar lavage	1.045, 1.055, 1.065, 1.075	>94%[44]

[a] Note that many references provide only the concentrations of substances used but do not characterize the density of these systems.

[b] calculated based on reported values

1.4. Scope of the Review

Previous work on AMPS has largely focused on the subclass of systems with two phases, ATPS. These systems have been reviewed extensively and several good books have been written about their use in partitioning of biomolecules.[1,45,46] In this review, we will provide a sketch of the historical context of AMPS and refer the reader to previous works for more detailed information on ATPS. This work focuses primarily on advances in the use of AMPS to separate cells by density. Previous work on AMPS has focused most heavily on applications in the separation of small biomolecules, such as proteins. This review does not cover work on AMPS as a tool for synthesis, such as their use for the formation of particles of hydrogels or other aqueous structures.[47]

1.5. History and Previous Work

Previous reviews have covered the formation of phases in AMPS,[1] the design and use of AMPS[46] for partitioning biomolecules, and theoretical models of phase separation.[48] Phase separation of aqueous polymers was first noted by Beijerinck[49] in 1896, but the use of these systems became popular after Albertsson demonstrated their use to partition biomolecules in the 1950's.[50] Since then, AMPS have been applied to separate numerous proteins, cells, and nanoparticles (**Table 1.2**).[51–53] AMPS have been formed using polymers, salts, surfactants, and, more recently, ionic liquids.[54–56]

As the use of AMPS grew, theoreticians began to devise models of phase separation and partitioning behavior. These models include osmotic virial expansion, lattice theories, Flory-Huggins theory, and excluded volume models.[48,57] Debye-Huckel theory can be added to many of these models to account for charged species.[48] All models rely on measured parameters to characterize a particular interaction; to our knowledge, no model exists to predict phase

Table 1.2. Applications of AMPS

Method	Application	Examples
Partitioning	Separation of enzymes	laccases,[58] lipases[54]
	Separation of organelles	spinach leaf mitochondria,[59] rat brain mitochondria[60]
	Separation of cells	lymphosarcoma tumor cells,[61] erythrocytes,[62–64] plant cells[65]
	Purification of nanoparticles	gold nanoparticles,[66] carbon nanotubes[67]
	Separation of antibodies	monoclonal antibodies[3,68,69]
	Oligonucleotides	DNA, RNA[70,71]
Density centrifugation	Separation of cells	reticulocytes (Ch. 3), sickled cells (Ch. 4)
	Separation of polymers	nylon[2]
Rate-zonal centrifugation	Purification of nanoparticles	nanorods from nanospheres [8]

separation based on the chemical structure and concentration of components alone. Despite this lack of a comprehensive, fundamental mechanism for phase separation, the models that have been developed provide guidance about the ways in which changes to experimental parameters, such as temperature, molecular weight, ionic strength, and concentrations of components, can affect phase separation.

1.6. Use of AMPS with Cells

Although the use of AMPS for the density-based separation of cells is quite recent (Chapters 3, 4, and 5) previous work on AMPS demonstrated the enrichment or separation of cells by partitioning (**Table 1.2**).[65,72] This work with partitioning demonstrates that AMPS can be used as a biocompatible medium in which to separate cells.

2. Density-based Separations of Cells

Several methods exist to separate cells by density. Different methods may be appropriate for a specific application depending on the requirements for speed, simplicity, throughput, and the level of purity of the separated population.

2.1. Differential Centrifugation

The simplest method of density separation, differential centrifugation, involves nothing more than a centrifuge and a suspension of cells in a liquid medium (e.g., plasma or cell-culture media).[73] Under centrifugation, the natural sedimentation of cells accelerates. Denser cells sediment faster than less dense cells. These cells migrate until they pack against the bottom of the container. Less dense cells pack above denser cells, which create a gradient of packed cells that are ordered by density. In blood, the "buffy coat" (i.e., the leukocyte and platelet rich layer) that is found on top of packed red blood cells after centrifugation is a result of the lower density of white blood cells compared to red blood cells.

Higher speeds and longer centrifugation times allow finer separations in density. Within the population of red blood cells, less dense, immature reticulocytes can be enriched in the top quarter of the packed red cells through differential centrifugation.[73] Removing purified populations from cells packed by differential centrifugation can be difficult because the cells themselves form a gradient in densities. The boundaries between types of cells is no bigger than the size of a single cell. In the example of the buffy coat, significant skill and a steady hand are required to remove this desired layer of cells fully without also removing red blood cells just below the layer and compromising the purity of the isolate.

2.2. Centrifugation Over a Solution

The removal of cells separated by density is improved by the use of separation media. These media often include additives (e.g., salts, sucrose, Ficoll, and Nycodenz). designed to provide liquid layers of a specific density.[36,74,75] Layering a suspension of cells above these media and centrifuging them allows the cells to separate into bands above and below the solution separated by a distance commensurate with the amount of media used. The solution provides a liquid barrier in density that only allows cells to pass to the bottom of the solution if they are denser than the liquid. Other additives are used in part to control the properties of the medium required to maintain physiological conditions (e.g., pH and tonicity). For example, Lymphoprep—a combination of salts and Ficoll—is a commercial medium to separate lymphocytes from red blood cells and has an osmolality of 295 mOsm/kg to match that of blood plasma.[76]

Solutions may also be prepared with non-physiological tonicities to enhance separation of a specific cell type, combining responses to osmotic stress with density.[75] For example, hypertonic solutions of Nycodenz or Polymorphprep can separate granulocytes from red blood

cells by exploiting the difference in dehydration experienced by these cells in response to a hypertonic environment; the selective dehydration of the red blood cells increases their density, allowing them to be separated from the granulocytes.[77,78]

Recovering cells from these systems is simpler than recovering cells from differential centrifugation; in differential centrifugation, the desired cells are adjacent to the rest of the cells while, in the case of centrifugation over a solution with a specific density, desired cells are separated from the rest of the cells by the liquid media. Obtaining reproducible results from these systems requires gently layering cells on top of the media.[79,80] With the exception of Polymorphprep, these systems only allow the separation of a single population of cells by density.

2.3. Centrifugation in Colloidal Media

An alternative to creating a solution with a specific density is to use a colloidal suspension, such as Percoll. Percoll is a suspension of silica spheres of polydisperse sizes that are coated with polyvinylpyrrolidone (PVP).[81] The polymer coating provides steric stabilization of the suspension. Percoll provides a solution capable of achieving high densities (~ 1.13 g/cm^3) with low osmolality (< 25 mOsm/kg), and low viscosity (~ 10 cP). The microspheres of silica contribute to the relative density of the solution without contributing directly to the osmolality of of the solution because the spheres are suspended rather than dissolved. Solutions of Percoll, thus, are often used as media for density separations.

Percoll can also form a gradient in density *in situ.*[41,82] Under centrifugation, large particles will sediment faster than small particles; the resulting continuous gradient in particle size is also a gradient in density. A continuous gradient can be formed using a fixed-angle rotor and controlled timing. The use of density-standard beads allows users to create a calibration

curve of the densities so that fractions of cells at a particular position within the gradient can be matched to their density. Percoll has found wide uses in the separation of cells.[44,83,84]

2.4. Centrifugation Over Layered Gradients

Both solutions and colloidal suspensions can be used to create layered gradients.[44,85] Media of different densities are layered sequentially with media of lower densities placed on top of media of higher densities. Cells sediment through the gradient and stop at the boundary above a layer that has a higher density than the cells. Layered gradients allow multiple populations to be separated in a single step. Assembling layers, however, can be tedious and great care must be taken to create reproducible gradients. Manual assembly of gradients has limited the minimum volume that these systems can be used to milliliters.[85,86]

2.5. Separation in Microfluidic Systems

Microfluidics allow separations of cells by density and can be particularly useful when volumes of samples are limited.[20] In the simplest implementations, sedimentation under gravity provides a means to separate cells vertically in a microchannel.[87,88] By adding features, such as herringbone structures, to microchannels, the flow of particles and cells can be made density- and size-dependent.[89] Similarly a double spiral microchannel can effectively enrich cells based on a combination of size and density.[90] Another way to use the density of cells to change the flow of cells is acoustic focusing. Standing waves generated in a microchannel push cells to flow along nodes or peaks depending on their densities.[91] These methods have been demonstrated to separate cells with differences in density on the order of 0.1 g/cm^3.

The growth of "lab-on-a-disc" technologies also could exploit differences in density between cells to perform separations. Devices in this field already exploit the sedimentation of cells to extract plasma for assays.[92]

Combining microfluidics with micro-electromechanical systems (MEMS) provides higher resolution in density. A system using microfluidic channels running through a cantilever measures the density of individual cells with a resolution of < 0.001 g/cm^3.[35]

Although the management of small volumes is advantageous for point-of-care applications where only a drop of blood may be available, microfluidic systems are less useful for applications that require high-throughput (e.g., therapeutics) or those applications limited by cost of equipment or complexity of an assay.

2.6. Centrifugation Over AMPS

AMPS provide an additional centrifugation method to separate cells by density. The self-forming characteristic of AMPS allows step-gradients over a wide range of volumes (from liters to microliters). AMPS for density-based separations could even be implemented in microfluidics, as they have already been implemented for phase separation in such devices.[7,93]

3. AMPS as a Tool for Density-based Separations

3.1. Properties & Comparison to Other Methods

As a media-based separation method, AMPS provide a means to separate different populations of density by significant distances to facilitate the subsequent removal of cells. Like layered gradients, AMPS separate multiple populations of density in a single system. Unlike layered systems, the boundary between layers is molecularly sharp and easily reforms if perturbed. The self-forming nature of the layers in AMPSs reduces variability and increases the ease-of-use compared to layered systems.

The density between phases can be quite small (as low as 0.0005 g/cm^3); these small steps in density allow fine resolution of populations separated by density. The step-gradients formed by AMPS are independent of the angle of the rotor used for centrifugation, unlike the

continuous gradients formed by Percoll. When applications require high throughput separations, AMPS can be used in large volumes. For point-of-care applications, AMPS can be used in microcapillary tubes with small, portable hematocrit centrifuges. The versatility of AMPS can provide a useful density separation method that covers applications ranging from those covered by conventional density-gradient centrifugation techniques to point-of-care applications covered by microfluidic density-separation methods.

3.2. Applications in Cells: Enriching Reticulocytes

The fine resolution of AMPS allows the enrichment of cells even when the population of interest has a distribution of densities that overlaps with background cells. Erythrocytes are a heterogeneous mixture of cells of different ages.[33,73] Reticulocytes are a particular subclass of erythrocytes; immature erythrocytes. Reticulocytes have a larger size[94] and a lower density,[95] on average, than mature erythrocytes. Despite this difference, the density distributions of both cell types overlap significantly.[96] Using density alone, therefore, may be unable to separate a pure population of reticulocytes. With fine control of density and well-defined interfaces, however, enrichment is possible.[73]

An AMPS designed to have densities necessary to isolate the least dense fraction of all erythrocytes can enrich reticulocytes (**Figure 1.1A**) (Chapter 3). Tuning the density can increase the total yield of erythrocytes or the total purity of the erythrocytes. The maximum purity obtained was 64 ± 3%.

Specific applications dictate the desired level of yield and purity. Several species of malaria preferentially invade reticulocytes.[97–99] To grow these species in continuous culture requires a higher purity of reticulocytes than is typically present in whole blood. Growing substantial numbers of parasites for experiments also requires a volume of > 10 uL of packed

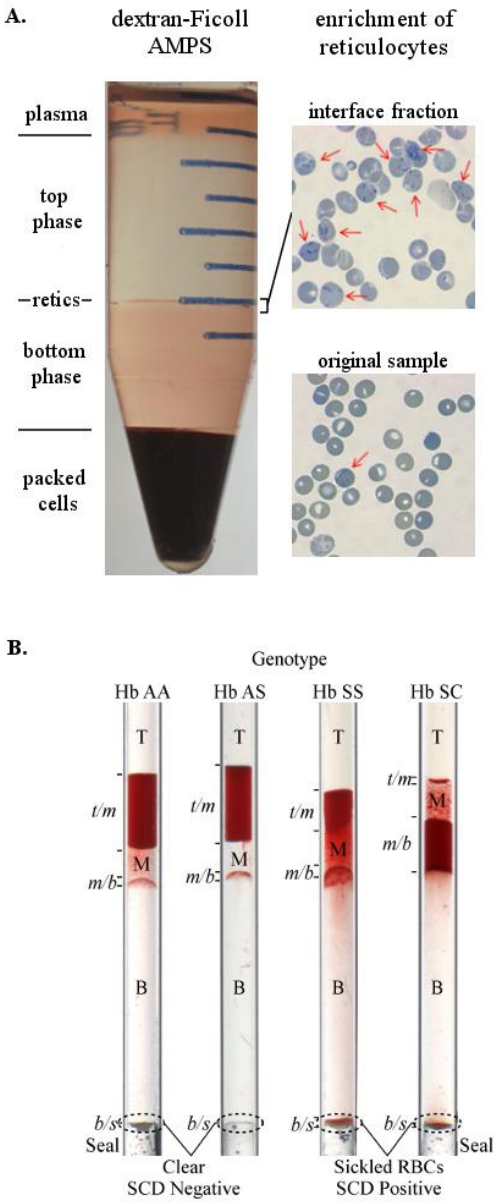

Figure 1.1. Density-based separations of cells with AMPS. (A) Reticulocytes (red arrows) are enriched by centrifugation over an AMPS with two phases. (B) The bands of red blood cells at the interfaces (*t/m*, *m/b*, *b/s*) of a three phase system (with phases, T, M, and B) enables the identification of sickle cell disease (SCD positive) and can help distinguish subtypes (Hb SS from Hb SC).

cells and, thus, higher yield allows cultivation with less whole blood. Tuning an AMPS to produce an enrichment of >15% while maintaining a yield of >1% allowed the growth of *Plasmodium knowlesi* that had not been adapted to grow in human blood.

3.3. Applications in Cells: Identifying Sickle Cell Disease

In some cases, the difference in densities between the population of cells of interest and background cells is large enough that separation can be achieved. With these cells, not only are pure separations possible, but simple diagnostics devices can be created.

Sickle cell disease (SCD) is a genetic disorder that causes a mutation in hemoglobin (Hb S). This mutation leads to the formation of sickle cells and leads to a population of dense, dehydrated cells in blood.[84,100] The dense cells present in SCD are ~ 0.02 g/cm^3 more dense than normal erythrocytes and the most dense cells present in SCD do not overlap with the tails of the distribution of normal cells.[101,102] Using AMPS to separate the dense cells present in SCD from cells with normal densities provides a way to identify SCD (**Figure 1.1B**) (Chapter 4). Implementation of the test in a capillary tube with a hematocrit centrifuge enables a simple test for SCD in low-resource settings (Chapter 5).

4. Principles in Designing Systems

4.1. Choosing a system

Several components are available to form an AMPS: polymers, salts, ionic liquids, and surfactants. For separating cells, the phases of the AMPS must be biocompatible. This requirement rules out salts and surfactants, as the concentrations of these components in their dominant phase would generally disrupt cell membranes or cause significant osmotic stress. A number of ionic liquids have been tested on mice and seem to be biocompatible.[103] To the best of our knowledge, AMPS using ionic liquids have not yet been used to separate cells. In general,

density-based separations of cells are limited to the subclass of AMPS that comprise polymers. A number of polymers that form AMPS have been used extensively with cells.[64] Reviews on polymers used in biological applications provide guidance on using polymers with cells.[104,105] For any specific application, however, one must demonstrate that the polymers used do not interfere with cellular function and viability. For example, while some studies demonstrate low cytotoxicity associated with polyethyleneimine when used as a vector for gene transfer,[106] other studies demonstrate that polycations may indeed have adverse effects on cells.[107] Biocompatibility may be a function of the concentration of a polymer.[106]

The number of desired subpopulations to be separated sets the minimum number of phases needed. A system with *n* phases has *n-1* liquid-liquid interfaces, a liquid-container interface, and a liquid-air interface; the total number of interfaces where populations can be separated in an AMPS is thus *n+1*. In many applications, a solution containing cells—such as blood—may be layered on top of an AMPS. The boundary between this layer and the top phase will be a diffuse boundary rather than a well-defined interface, leaving *n* molecularly sharp interfaces for separation (**Figure 1.2**).

4.2. Density of the Phases

The difference in density between the desired cells and the background cells determines the differences in densities between phases. The step in density between phases depends on the composition of phases. The composition of phases is a function of the specific polymers used, the concentrations of those polymers, and the molecular weight of the polymers used. In ATPS, ternary phase diagrams can provide some guidance on the initial concentrations to use for a specific molecular weight.[5,108] AMPS with more than two phases can be harder to predict, but

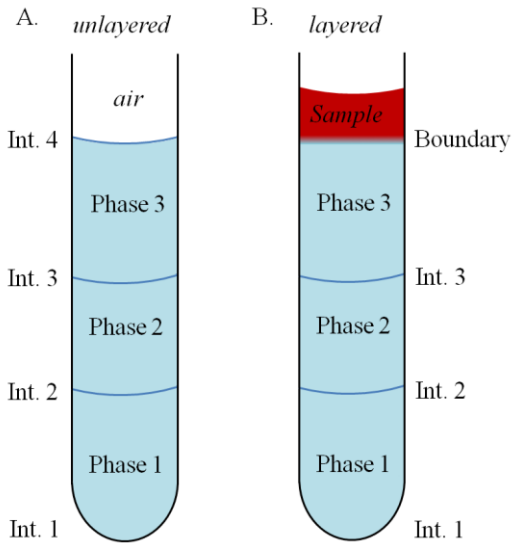

Figure 1.2. An AMPS with three phases has four interfaces (Int. 1-4) when no liquid is layered on top of the system. If a liquid is added over the AMPS, the *air*/Phase 3 interface is no longer a stable interface and becomes a diffuse boundary, *Sample/*Phase 3.

phase diagrams of each two phase combination comprising the AMPS can provide parameters to understand how each polymer affects the other.

Adding other solutes, such as salts or Nycodenz, can increase the overall density of the system while, generally, maintaining the steps in density between phases.[2] For this reason, it is often easier to first identify mixtures of polymers that provide the needed difference in density and then adjust the overall density of the system through additives.

4.3. Considering Other Properties

Besides the choice of polymers and the densities, several other considerations are specific to the kind of separation desired. In general, when the targeted cells are desired for use in assays after separation by density, the environment of the cells should be maintained as close to physiological conditions as possible. The use of buffers and adjusting pH can be important, especially in cases where cells change their density in response to pH. In some cases, differences in density can be increased if the targeted population of cells responds to pH, osmolality, or tonicity in a different way than background cells.[109]

Often, the volumes of different phases can be adjusted without varying the density of each phase. In ATPS, this variation is accomplished by changing the initial concentrations of each polymer while remaining on a tie-line between the binodal curve.[1] The composition of the top and the bottom phase, and hence the densities of each phase, are constant along the tie-line. Increasing the volume between two interfaces makes the subsequent removal of cells from the interfaces easier than if they were closer. This increased ease comes with a tradeoff; the time of centrifugation necessary to allow cells to all sediment to their equilibrium position in density increases with increased volume between phases.

The minimum volume between phases has a practical limit that is dependent on the size of the container and the interfacial tension between phases. In general, the interfacial tension between phases is remarkably low (100 nJ/m^2–100 µJ/m^2)[1] because both phases contain, predominantly, water. The differences in the polymers that contribute to phase separation, however, can lead to differences in surface interactions with a surface. As a result, the interface between two phases will have a contact angle (θ) with the wall of the container used that is dependent on the material of the container and the composition of the AMPS. The competition between the surface tension and gravitational forces shapes the meniscus between two phases. When the gravitational term dominates the balance of forces, the meniscus is almost flat. When the surface tension dominates, the meniscus may be quite pronounced. This effect is most pronounced when the distance (d) between opposing walls of a container is small (< 1 mm), as is the case with many capillary tubes.

In a regime with a low Bond number (i.e., a regime where surface tension dominates over gravity), the Young-Laplace equation provides a simple solution to the meniscus between two liquids in a cylindrical capillary; the meniscus will have spherical curvature with a radius (R) that is a function of θ and d. Equation 1 describes the distance (h) between the depression in the meniscus and the intersection of the meniscus with the container.

$$h = \frac{d(1-sin\theta)}{2cos\theta} \qquad \text{(Equation 1)}$$

The shape of the interfaces between phases has important implications for the design of AMPS for density-based separations. In a three phase system, an interface with positive curvature above an interface with negative curvature reduces the effective distance between the top and the bottom phase. Assuming a minimal influence of gravity, we can use Equation 1 to

derive the maximum distance (*D*) that two interfaces—with contact angles θ and φ—could deform towards each other (Equation 2).

$$D = \frac{d}{2}\left(\frac{(1-sin\theta)}{cos\theta} + \frac{1-sin\phi}{cos\phi}\right) \quad \text{(Equation 2)}$$

The distance between phases, and the corresponding volume of the phases, should be chosen to be greater than the distance of deflection given by Equation 2. For the extreme case of contact angles of 90º, *D* is the same as *d*, the diameter as a capillary. As a rule of thumb, the distance between phases (*H*) should be greater than the distance between the walls of the container (*d*) to ensure that cells at the two interfaces can be distinguished and separated (**Figure 1.3**). For systems that do not have asymptotically small or large Bond numbers, the work of Concus provides a comprehensive mathematical description of the shape of a meniscus in a cylinder.[110] In situations where AMPS are used in larger containers (d > 1 cm) than capillaries, one can often separate cells at interfaces separated by less than the diameter of the tube.

The choice of the container depends on the specific application. Separations of large volumes (> 10 mL at a time) can be done in conical tubes or any containers that fit in a centrifuge. Separations for point-of-care applications or where the volume of the sample is limited should be done in capillary tubes. Using polycarbonate microhematocrit tubes allows interfaces to be isolated by cutting the tube with a razor blade in the phases between the interfaces.

The densities of the phases of AMPS will change with temperature. Choosing compositions of AMPS within the phase-separated region of the phase diagram ensures that variations in temperature will not strongly impact the composition of each phase. With water as

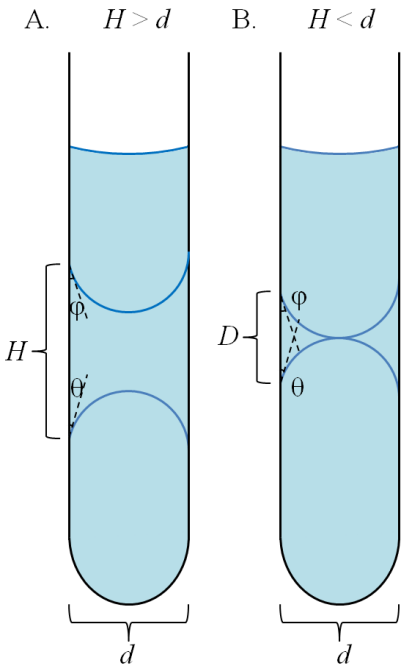

Figure 1.3. The distance between the phases of an AMPS must be chosen such that the curvature of the interfaces does not interfere with the separation of cells, especially in cases where capillaries are used as the container. The contact angles of the interfaces around a phase (θ and φ) along with the diameter of the capillary (d) dictates the distance (H) that should be used to separate the phases by a distance (h). By choosing $H > d$ in capillaries, the interfaces between phases will not interfere with separations.

the predominant component, the behavior of water with temperature dictates the behavior of AMPS.

To quantify the effect of temperature on AMPS, we investigated one of AMPS used for the enrichment of reticulocytes from blood: a mixture of 12% (w/w) Ficoll with a molecular weight of 400 kDa and 12% (w/w) dextran with a molecular weight of 500 kDa in a hypertonic buffered solution. During continuous mixing, we aliquoted small volumes of the AMPS into six sets of smaller batches. Each set contained three technical replicates and incubated at a specific temperature for over 30 minutes before centrifugation at the same temperature. Upon phase separation, we immediately removed pure volumes of each phase.

Using a temperature controlled density meter (Anton Paar DMA 4100M), we measured both the density and the specific gravity (density of solution/density of water at the same temperature) of each phase at the temperature at which the AMPS was formed. Measuring both density and specific gravity allowed us to estimate the contribution of water to the change in density as a function of temperature.

The densities of both phases decreased as temperature increased (**Figure 1.4A**). Variations in specific gravity as a function of temperature are much less (**Figure 1.4B**). Between 20–40 ºC, the maximum change in density of each phase is over four times greater than the maximum change in specific density. This relatively small variation in specific gravity implies that the variation in density in phases in this range of temperatures is dominated by water. The 20–40 ºC range is relevant for many settings where point-of-care diagnostics may be used. For separations of cells—whose mass is dominated by water—media whose densities mirror the changes in density of water with temperature could be useful over a range of pertinent temperatures for point-of-care hematology.

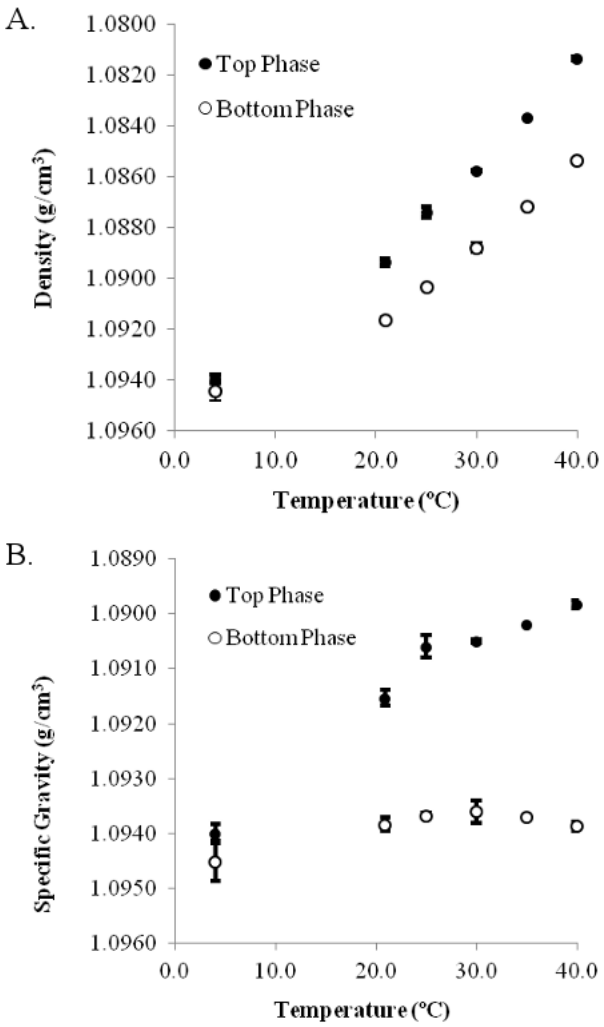

Figure 1.4.The density of the phases of a dextran-Ficoll AMPS as a function of temperature. (A) In both phases, the density decreases as temperature increases. (B) Between 20–40 °C, the change in the specific gravity in the phases is small (< 0.002 g/cm^3); most of the change in density of the phases in this range of temperatures can be attributed to the change in density of water. Error bars depict the standard error of the mean for technical replicates (n = 3).

4.4. Expanding the Range of Cells Accessible by Density-based Separation

In instances where populations of cells have distributions of density that overlap, natural differences in density alone may not be enough to achieve a desired separation. As discussed previously, some parameters, such as pH, tonicity, and osmolality can be used to increase differences in density. Sometimes these parameters may still not provide enough resolution between populations. In these cases, coupling other properties with AMPS can expand their applications.

Cells that are very similar in density but have a different size or shape will have the same isodensity point in a density gradient, but will approach the equilibrium position with different dynamics. By stopping centrifugation before equilibrium positions are achieved, hydrodynamic differences can provide a way to resolve different populations of cells. These differences can be further amplified by changing the viscosity of phases. This method successfully separated gold nanorods from gold nanospheres in AMPS.[8]

When the end goal of a separation is detection, labeling cells may not be a limitation. In these instances, biochemical labels attached to particles with high densities (e.g., lead or gold) can act as anchors to pull specific cells to a desired interface. This approach has been exploited in simple single layer density media separations to pre-enrich CTCs[111] and to separate CD4+ T-lymphocytes for CD4 counts.[112] If label-free isolates are required, density-tags could still be helpful to selectively deplete or remove background cells. Although this method has not been explicitly employed with AMPS or other density separation methods, it has proven to be effective in microfluidic systems.[11]

5. Conclusions

As a method that uses a biophysical marker, AMPS fill a niche separate from techniques that rely on biochemical markers, such as cell sorting techniques assisted by fluorescence (i.e., FACS) or magnetic actuation (i.e., MACS). AMPS offer a tool for separating cells where at least one of the following three criteria are required: 1) the cells desired for separation should be free of biochemical labels, 2) several populations of cells require separation, and 3) ease-of-use and simplicity are critical. The ability of AMPS to form across a large range of volumes (nL to L) provides a degree of versatility uncommon in other density-separation methods.

When populations of cells have overlapping density distributions, enrichments of cells are still possible and can be improved by modulating other properties, such as osmolality. In these cases, however, pure separations of cells are difficult to obtain. For certain applications, such as the enrichment of reticulocytes for the cultivation of malaria, enrichment may be suitable even without high purities. Given the large number of cell types that are currently separated by layered gradients, AMPS should find plentiful applications where the reproducibility and simplicity of self-assembling gradients offers an advantage over manually creating layered gradients.

The ability of AMPS to provide density-gradient centrifugation over small volumes (nL to μL) is particularly exciting as a prospect for point-of-care hematology. As the development of a rapid test for SCD demonstrates, density-based separations in AMPS can provide useful clinical information. Digital analysis with a cell phone camera, variations in timing, and additional phases could provide ways to estimate other parameters from a single test, such as white blood cell counts, mean corpuscular hemoglobin concentration (related to density), hematocrit, and red blood cell distribution width. The future development of AMPS and

supporting analytical methods could enable a wealth of hematological information at the point-of-care.

Acknowledgements

A.A.K. acknowledges a Graduate Research Fellowship from the National Science Foundation. This work was supported, in part, by the Department of Chemistry at Tufts University.

References

(1) Hatti-Kaul, R. *Mol. Biotechnol.* **2001**, *19*, 269.

(2) Mace, C. R.; Akbulut, O.; Kumar, A. A.; Shapiro, N. D.; Derda, R.; Patton, M. R.; Whitesides, G. M. *J. Am. Chem. Soc.* **2012**, *134*, 9094.

(3) Lutwyche, P.; Norris-Jones, R.; Brooks, D. E. *Appl. Environ. Microbiol.* **1995**, *61*, 3251.

(4) Albertsson, P.-Å. *Biochemistry* **1973**, *12*, 2525.

(5) Diamond, A.; Hsu, J. *Biotechnol. Bioeng.* **1989**, *34*, 1000.

(6) Khripin, C. Y.; Fagan, J. A.; Zheng, M. *J. Am. Chem. Soc.* **2013**.

(7) Hardt, S.; Hahn, T. *Lab Chip* **2012**, *12*, 434.

(8) Akbulut, O.; Mace, C. R.; Martinez, R. V; Kumar, A. A.; Nie, Z.; Patton, M. R.; Whitesides, G. M. *Nano Lett.* **2012**, *12*, 4060.

(9) Lagoudianakis, E. E.; Kataki, A.; Manouras, A.; Memos, N.; Papadima, A.; Derventzi, A.; Zografos, G.; Papadopoulos, S.; Katergiannakis, V.; Konstadoulakis, M. M. *J. Surg. Res.* **2009**, *155*, 183.

(10) Königsberg, R.; Gneist, M.; Jahn-Kuch, D.; Pfeiler, G.; Hager, G.; Hudec, M.; Dittrich, C.; Zeillinger, R. *Cancer Lett.* **2010**, *293*, 117.

(11) Karabacak, N. M.; Spuhler, P. S.; Fachin, F.; Lim, E. J.; Pai, V.; Ozkumur, E.; Martel, J. M.; Kojic, N.; Smith, K.; Chen, P.-I.; Yang, J.; Hwang, H.; Morgan, B.; Trautwein, J.; Barber, T. a; Stott, S. L.; Maheswaran, S.; Kapur, R.; Haber, D. a; Toner, M. *Nat. Protoc.* **2014**, *9*, 694.

(12) Hart, D. N. *Blood* **1997**, *90*, 3245.

(13) Agerberth, B.; Charo, J.; Werr, J.; Olsson, B.; Idali, F.; Lindbom, L.; Kiessling, R.; Jörnvall, H.; Wigzell, H.; Gudmundsson, G. H. *Blood* **2000**, *96*, 3086.

(14) Arora, N. S.; Ramanayake, T.; Ren, Y.-F.; Romanos, G. E. *Implant Dent.* **2009**, *18*, 303.

(15) Raft, S. I. G.; Art, S. U. P.; Lozada, J. L.; Caplanis, N.; Proussaefs, P.; Willardsen, J.; Kammeyer, G. *J. Oral Implantol.* **2001**, *XXVII*, 38.

(16) Anitua, E.; Sánchez, M.; Nurden, A. T.; Nurden, P.; Orive, G.; Andía, I.; Sa, M. *Trends Biotechnol.* **2006**, *24*, 227.

(17) Zuk, P. A.; Zhu, M.; Mizuno, H.; Huang, J.; Futrell, J. W.; Katz, A. J.; Benhaim, P.; Lorenz, H. P.; Hedrick, M. H. *Tissue Eng.* **2001**, *7*, 211.

(18) García-Olmo, D.; García-Arranz, M.; Herreros, D.; Pascual, I.; Peiro, C.; Rodríguez-Montes, J. A. *Dis. Colon Rectum* **2005**, *48*, 1416.

(19) Pappas, D.; Wang, K. *Anal. Chim. Acta* **2007**, *601*, 26.

(20) Gossett, D. R.; Weaver, W. M.; Mach, A. J.; Hur, S. C.; Tse, H. T. K.; Lee, W.; Amini, H.; Di Carlo, D. *Anal. Bioanal. Chem.* **2010**, *397*, 3249.

(21) Seidl, J.; Knuechel, R.; Kunz-Schughart, L. A. *Cytometry* **1999**, *36*, 102.

(22) Kostura, L.; Kraitchman, D. L.; Mackay, A. M.; Pittenger, M. F.; Bulte, J. W. M. *NMR Biomed.* **2004**, *17*, 513.

(23) Beech, J. P.; Holm, S. H.; Adolfsson, K.; Tegenfeldt, J. O. *Lab Chip* **2012**, *12*, 1048.

(24) Desitter, I.; Guerrouahen, B. S.; Benali-Furet, N.; Wechsler, J.; Jänne, P. A.; Kuang, Y.; Yanagita, M.; Wang, L.; Berkowitz, J. A.; Distel, R. J.; Cayre, Y. E. *Anticancer Res.* **2011**, *31*, 427.

(25) Kang, Y.; Li, D.; Kalams, S. A.; Eid, J. E. *Biomed. Microdevices* **2008**, *10*, 243.

(26) Wang, G.; Mao, W.; Byler, R.; Patel, K.; Henegar, C.; Alexeev, A.; Sulchek, T. *PLoS One* **2013**, *8*, e75901.

(27) Hou, H. W.; Bhagat, A. A. S.; Chong, A. G. L.; Mao, P.; Tan, K. S. W.; Han, J.; Lim, C. T. *Lab Chip* **2010**, *10*, 2605.

(28) Hunt, T. P.; Issadore, D.; Westervelt, R. M. *Lab Chip* **2008**, *8*, 81.

(29) Wood, D. K.; Soriano, A.; Mahadevan, L.; Higgins, J. M.; Bhatia, S. N. *Sci. Transl. Med.* **2012**, *4*, 123ra26.

(30) Shortman, B. Y. K.; Brunner, K. T.; Cerottini, J. **1972**, *135*, 1375.

(31) Brugnara, C.; Bunn, H. F.; Tosteson, D. C. *Science1* **1986**, *232*, 388.

(32) Miller, L. H.; Chien, S. *Exp. Parasitol.* **1971**, *466*, 451.

(33) Branch, D.; Hian, A.; Carlson, F.; Maslow, W.; Petz, L. *Am. J. Clin. Pathol.* **1983**, *80*, 453.

(34) Weiskirchen, R.; Gressner, A. M. *Methods Mol. Med.* **2005**, *117*, 99.

(35) Grover, W. H.; Bryan, A. K.; Diez-Silva, M.; Suresh, S.; Higgins, J. M.; Manalis, S. R. *Proc. Natl. Acad. Sci. U. S. A.* **2011**, *108*, 10992.

(36) Bøyum, A.; Brincker Fjerdingstad, H.; Martinsen, I.; Lea, T.; Løvhaug, D.; Fjerdingstad, H. B.; Lovhaug, D. *Scand. J. Immunol.* **2002**, *56*, 76.

(37) Jepsen, L. V; Skottun, T. *Scand. J. Clin. Lab. Investig.* **1982**, *42*, 235.

(38) Koistinen, P. *Scand. J. Clin. Lab. Invest.* **1987**, *47*, 709.

(39) Mrema, J. E.; Campbell, G. H.; Miranda, R.; Jaramillo, A. L.; Rieckmann, K. H. *Bull. World Health Organ.* **1979**, *57*, 133.

(40) Rosenberg, R.; Gertler, R.; Friederichs, J.; Fuehrer, K.; Dahm, M.; Phelps, R.; Thorban, S.; Nekarda, H.; Siewert, J. R. *Cytometry* **2002**, *49*, 150.

(41) Rivadeneira, E. M.; Wasserman, M.; Espinal, C. T. *J. Protozool.* **1983**, *30*, 367.

(42) Hammadeh, M. E.; Kühnen, A.; Amer, A. S.; Rosenbaum, P.; Schmidt, W. *Int. J. Androl.* **2001**, *24*, 360.

(43) Fu, X.-H.; Meng, F.-L.; Hu, Y.; Zhou, J.-Q. *Aging Cell* **2008**, *7*, 746.

(44) Calhoun, W. J.; Reed, H. E.; Moest, D. R.; Stevens, C. a. *Am. Rev. Respir. Dis.* **1992**, *145*, 317.

(45) Fisher, D. *Biochem. J.* **1981**, *196*, 1.

(46) *Partitioning in Aqueous Two-Phase Systems: Theory, Methods, Uses, and Applications to Biotechnology*; Walter, H.; Brooks, D. E.; Fisher, D., Eds.; New York, 1986; pp. 1–704.

(47) Ziemecka, I.; van Steijn, V.; Koper, G. J. M.; Rosso, M.; Brizard, A. M.; van Esch, J. H.; Kreutzer, M. T. *Lab Chip* **2011**, *11*, 620.

(48) Cabezas, H. *J. Chromatogr. B. Biomed. Appl.* **1996**, *680*, 3.

(49) Beijerinck, M. W. *Zentralbl. Bakteriol.* **1896**, *2*, 698.

(50) Albertsson, P.-Å. *Biochim. Biophys. Acta* **1958**, *27*, 378.

(51) Oelmeier, S. A.; Dismer, F.; Hubbuch, J. *Biotechnol. Bioeng.* **2011**, *108*, 69.

(52) Eggersgluess, J. K.; Richter, M.; Dieterle, M.; Strube, J. *Chem. Eng. Technol.* **2014**, 1.

(53) Rosa, P. a J.; Azevedo, A. M.; Sommerfeld, S.; Mutter, M.; Bäcker, W.; Aires-Barros, M. R. *Biotechnol. J.* **2013**, *8*, 352.

(54) Ventura, S. P. M.; de Barros, R. L. F.; de Pinho Barbosa, J. M.; Soares, C. M. F.; Lima, Á. S.; Coutinho, J. A. P. *Green Chem.* **2012**, *14*, 734.

(55) He, C.; Li, S.; Liu, H.; Li, K.; Liu, F. *J. Chromatogr. A* **2005**, *1082*, 143.

(56) Pei, Y.; Wang, J.; Wu, K.; Xuan, X.; Lu, X. *Sep. Purif. Technol.* **2009**, *64*, 288.

(57) Johansson, H.; Karlström, G.; Tjerneld, F.; Haynes, C. A. *J. Chromatogr. B* **1998**, *711*, 3.

(58) Prinz, A.; Koch, K.; Górak, A.; Zeiner, T. *Process Biochem.* **2014**.

(59) Gardeström, P.; Ericson, I. *Methods Enzymol.* **1987**, *148*, 434.

(60) López-Pérez, M. J.; París, G.; Larsson, C. *Biochim. Biophys. Acta - Bioenerg.* **1981**, *635*, 359.

(61) Miner, K. M.; Walter, H.; Nicolson, G. L. *Biochemistry* **1981**, *20*, 6244.

(62) Walter, H.; Krob, E. J.; Brooks, D. E. *Biochemistry* **1976**, *15*, 2959.

(63) Karr, L.; Shafer, S.; Harris, J. *J. Chromatogr. A* **1986**, *354*, 269.

(64) Walter, H.; Johansson, G.; Brooks, D. E. *Anal. Biochem.* **1991**, *197*, 1.

(65) Yamada, M.; Kasim, V.; Nakashima, M.; Edahiro, J.; Seki, M. *Biotechnol. Bioeng.* **2004**, *88*, 489.

(66) Helfrich, M. R.; El-Kouedi, M.; Etherton, M. R.; Keating, C. D. *Langmuir* **2005**, *21*, 8478.

(67) Tang, M. S. Y.; Show, P. L.; Lin, Y. K.; Woon, K. L.; Tan, C. P.; Ling, T. C. *Sep. Purif. Technol.* **2014**, *125*, 136.

(68) Wu, Q.; Lin, D.-Q.; Zhang, Q.-L.; Gao, D.; Yao, S.-J. *J. Sep. Sci.* **2014**, *37*, 447.

(69) Mao, L. N.; Rogers, J. K.; Westoby, M.; Conley, L.; Pieracci, J. *Biotechnol. Prog.* **2010**, *26*, 1662.

(70) Luechau, F.; Ling, T. C.; Lyddiatt, A. *Biochem. Eng. J.* **2011**, *55*, 230.

(71) Kula, M.; Frerix, A.; Geilenkirchen, P.; Mu, M. **2007**, *96*, 57.

(72) Fisher, D. *Biochem. J.* **1981**, *196*, 1.

(73) Rushing, D.; Vengelen-Tyler, V. *Transfusion* **1987**, *27*, 86.

(74) Martínez-Salas, E.; Martín, J. A.; Vicente, M. *J. Bacteriol.* **1981**, *147*, 97.

(75) Bøyum, A. *Scand. J. Immunol.* **1983**, *17*, 429.

(76) Kratz, A.; Ferraro, M.; Sluss, P. M.; Lewandrowski, K. B. *N. Engl. J. Med.* **2004**, *351*, 1548.

(77) Bøyum, A.; Løvhaug, D.; Tresland, L.; Nordlie, E. M. *Scand. J. Immunol.* **1991**, *34*, 697.

(78) Sovershaev, M. A.; Lind, K. F.; Devold, H.; Jørgensen, T. Ø.; Hansen, J.-B.; Østerud, B.; Egorina, E. M. *J. Thromb. Haemost.* **2008**, *6*, 1742.

(79) Park, J. J.-M.; Lee, J. J.-G. J.-Y. J.; Jeong, H.; Oh, J.-M. H.; Kim, Y. J.; Park, D.; Kim, M. S.; Lee, H. J.; Lee, S. S.; Lee, W.-Y.; Huh, N. *Anal. Chem.* **2012**, *84*, 7400.

(80) Goodman, S. R.; Hughes, K. M. H.; Kakhniashvili, D. G.; Neelam, S. *Exp. Biol. Med. (Maywood).* **2007**, *232*, 1470.

(81) Gärtner, I. *Immunology* **1980**, *40*, 133.

(82) Arrowood, M.; Sterling, C. *J. Parasitol.* **1987**, *73*, 314.

(83) Trang, D. T. X.; Huy, N. T.; Kariu, T.; Tajima, K.; Kamei, K. *Malar. J.* **2004**, *3*, 7.

(84) Kaul, D. K.; Fabry, M. E.; Windisch, P.; Baez, S.; Nagel, R. L. *J. Clin. Invest.* **1983**, *72*, 22.

(85) Glinski, W.; Gershwin, M. E.; Budman, D. R.; Steinberg, a D. *Clin. Exp. Immunol.* **1976**, *26*, 228.

(86) Redgrave, T.; Roberts, D.; West, C. *Anal. Biochem.* **1975**, *49*, 42.

(87) Oh, A. G.; Lee, D. W.; Cho, Y.-H. *Sensors Actuators B Chem.* **2012**, *166-167*, 24.

(88) Sugiyama, D.; Teshima, Y.; Yamanaka, K.; Briones-Nagata, M. P.; Maeki, M.; Yamashita, K.; Takahashi, M.; Miyazaki, M. *Anal. Methods* **2014**, *6*, 308.

(89) Hsu, C.-H.; Di Carlo, D.; Chen, C.; Irimia, D.; Toner, M. *Lab Chip* **2008**, *8*, 2128.

(90) Sun, J.; Li, M.; Liu, C.; Zhang, Y.; Liu, D.; Liu, W.; Hu, G.; Jiang, X. *Lab Chip* **2012**, *12*, 3952.

(91) Petersson, F.; Aberg, L.; Swärd-Nilsson, A.-M.; Laurell, T. *Anal. Chem.* **2007**, *79*, 5117.

(92) Haeberle, S.; Brenner, T.; Zengerle, R.; Ducrée, J. *Lab Chip* **2006**, *6*, 776.

(93) Soohoo, J. R.; Walker, G. M. *Biomed. Microdevices* **2009**, *11*, 323.

(94) Vömel, T.; Platt, D.; Strobelt, W. *Mech. Ageing Dev.* **1980**, *13*, 357.

(95) Leif, R. C.; Vinograd, J. *Proc. Natl. Acad. Sci. U. S. A.* **1964**, *51*, 520.

(96) D'Alessandro, A.; Blasi, B.; D'Amici, G. M.; Marrocco, C.; Zolla, L. *Blood Transfus.* **2013**, *11*, 75.

(97) Martín-jaular, L.; Elizalde-torrent, A.; Thomson-luque, R.; Ferrer, M.; Segovia, J. C.; Herreros-aviles, E.; Fernández-becerra, C.; Portillo, H. A. **2013**, 1.

(98) Galinski, M. R.; Medina, C. C.; Ingravallo, P.; Barnwell, J. W. *Cell* **1992**, *69*, 1213.

(99) Lim, C.; Hansen, E.; Desimone, T. M.; Moreno, Y.; Junker, K.; Bei, A.; Brugnara, C.; Buckee, C. O.; Duraisingh, M. T. *Nat. Commun.* **2013**, *4*, 1638.

(100) Bartolucci, P.; Brugnara, C.; Teixeira-Pinto, A.; Pissard, S.; Moradkhani, K.; Jouault, H.; Galacteros, F. *Blood* **2012**, *120*, 3136.

(101) Fabry, M. E.; Kaul, D. K.; Raventos-Suarez, C.; Chang, H.; Nagel, R. L. *J. Clin. Invest.* **1982**, *70*, 1315.

(102) Embury, S.; Clark, M. *J. Clin. Invest.* **1984**, *73*, 116.

(103) Elliott, G. D.; Kemp, R.; Macfarlane, D. R. **2010**, 95.

(104) Kadajji, V. G.; Betageri, G. V. *Polymers (Basel).* **2011**, *3*, 1972.

(105) Jen, A. C.; Wake, M. C.; Mikos, A. G. *Biotechnol. Bioeng.* **1996**, *50*, 357.

(106) Boussif, O.; Lezoualc'h, F.; Zanta, M. A.; Mergny, M. D.; Scherman, D.; Demeneix, B.; Behr, J. P. *Proc. Natl. Acad. Sci. U. S. A.* **1995**, *92*, 7297.

(107) Fischer, D.; Li, Y.; Ahlemeyer, B.; Krieglstein, J.; Kissel, T. *Biomaterials* **2003**, *24*, 1121.

(108) Diamond, A.; Hsu, J. *Biotechnol. Tech.* **1989**, *3*, 119.

(109) Sorette, M. P.; Shiffer, K.; Clark, M. R. *Blood* **1992**, *80*, 249.

(110) Concus, P. *J. Fluid Mech.* **1968**, *34*, 481.

(111) Adams, A. A.; Okagbare, P. I.; Feng, J.; Hupert, M. L.; Patterson, D.; Göttert, J.; McCarley, R. L.; Nikitopoulos, D.; Murphy, M. C.; Soper, S. A. *J. Am. Chem. Soc.* **2008**, *130*, 8633.

(112) Glynn, M. M. T.; Kinahan, D. J. D.; Ducrée, J. *Lab Chip* **2013**, *13*, 2731.

Chapter 2

From the Bench to the Field: Two Case Studies in the Development of Low-Cost Diagnostics

Ashok A. Kumar[1], Barbara S. Smith[2], Jonathan W. Hennek[2], Shailendra Kumar[3] and George M. Whitesides[2,4]

[1]School of Engineering and Applied Sciences, Harvard University, 29 Oxford St., Cambridge, MA 02138

[2]Department of Chemistry and Chemical Biology, Harvard University, 12 Oxford St., Cambridge, MA 02138

[3]Diagnostics for All, 840 Memorial Drive, Cambridge, MA 02139

[4]Wyss Institute for Biologically Inspired Engineering, Harvard University, 60 Oxford St., Cambridge, MA 02138

Abstract

Despite the growth of research on point-of-care (POC) diagnostics for global health, many devices never leave the laboratory. This chapter describes a framework for the process of moving diagnostic technology from the laboratory to the field to perform evaluations of operation and performance. Two case studies illustrate the framework: 1) the development of a paper-based device to measure liver function tested in Vietnam, and 2) the development of a density-based device to diagnose sickle cell disease tested in Zambia. General lessons drawn from these experiences may aid scientists and engineers designing rapid tests aimed at having an impact in developing countries.

1. Introduction

Over the past two decades the advent of lab-on-a-chip technologies and the expansion of mobile phone technology have each led to tremendous activity in the field of point-of-care (POC) testing and diagnostics. The growth in publications on this topic has risen at an exponential rate over the last two decades (**Figure 2.1**). Despite this activity, the promise of devices that will allow personalized and low-cost healthcare, to a large extent, remains just that: a promise.

What steps are necessary to bridge the gap between publications on POC tests and POC tests that are actually being used to improve healthcare?

Transitioning from a concept in a laboratory to a product is a hard task in any field, but the task can become Herculean in medical applications. Large clinical trials and regulatory approval require long times and substantial resources. As a first step, a POC test must go from the bench to the field; a device needs to demonstrate performance in a real field setting.

Some might argue that scientists should be concerned only with discovering new methods and enabling new technologies; testing in the field should be left to companies. This model works well when potential profits are large and risks are low; market forces will then encourage companies (either startups or large companies) to invest in early-stage technologies. Technologies aimed for the bottom of the pyramid, however, do not fit this model because they often provide little or no financial incentive and a higher risk.

By performing initial field evaluations, scientists can improve their technologies and reduce the uncertainty about whether a company should invest to develop a POC diagnostic. This translational step is itself no small task because it requires a set of skills and experiences

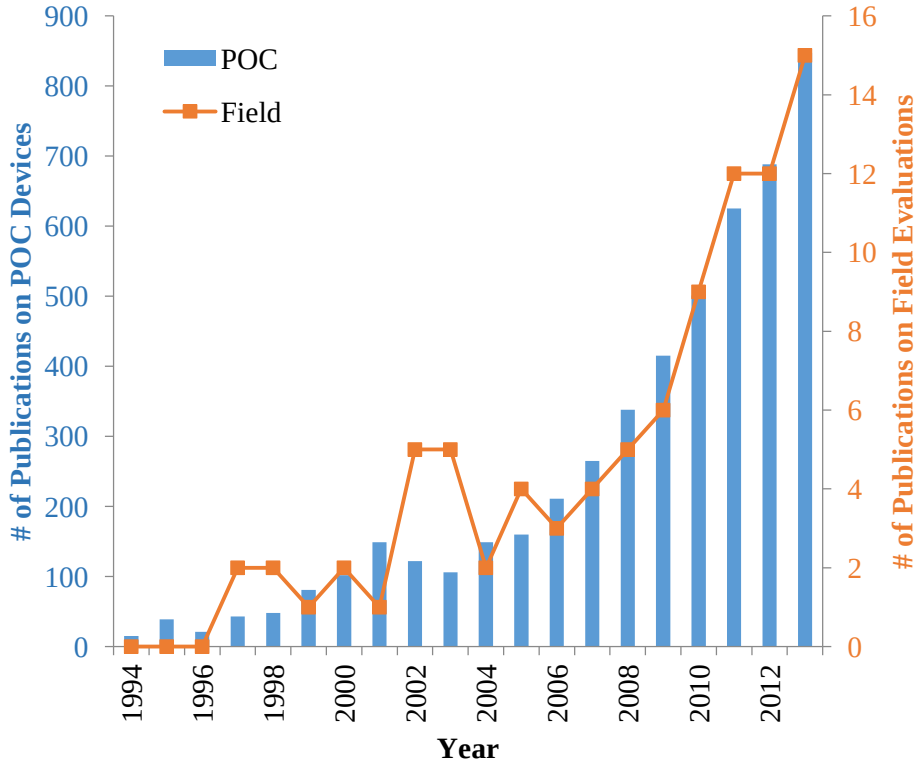

Figure 2.1. The number of publications with the topic of point-of-care tests or diagnostics (POC) and publications on the field evaluation of such devices (Field) have both increased exponentially over the past decade. Publications on the devices themselves are about 60 times more frequent than publications about the field evaluation of the devices.

that—while common in fields like public health—are rare among engineers and applied scientists.

Publications on field trials and evaluations of POC devices illustrate the difficulty of going from the bench to the field. Each year, only one paper is published about field testing or evaluation of POC devices for every 60 papers published about laboratory tests of devices pointed toward POC diagnostics. This ratio has been fairly consistent for the past two decades (**Figure 2.1**). We hope that this ratio might be changed by sharing experiences and creating a more open discussion about the less scientific, but still quite imposing, challenges that scientists face when testing a technology in the field.

Here we present a general framework for creating POC diagnostics, and illustrate its structure with two case studies from our own experience. In the last 7 years, we have taken two technologies from the bench[1–3] to the field.[4] For each technology, we have adopted a slightly different approach. In one case, development and field testing were done through a strong partnership with a non-profit company and other organizations. In the other case, development and field testing was led by our academic laboratory. By sharing these details, we hope that others interested in testing their devices can benefit from the lessons we have learned, and anticipate some of the challenges of this phase of development of a fielded technology.

1.1. What is a Field Trial?

A scientist who has designed a new method to detect a disease in a simple, portable device may believe that the most appropriate way to test the device in the field would be to travel to rural clinics in a low- and middle-income countries (LMICs) and begin using the devices with patients. If the device is designed for the POC, should not the POC be the best place to test the

device? Testing the performance of a device at the POC is essential, but not necessarily the first work that should be done in the field.

Field trials and, more generally, field work refers to a wide range of activities (**Figure 2.2**). Work in field settings can be broken down into four tiers: Tier 1) needs—identifying a problem and understanding its context, Tier 2) evaluation—testing a prototype of a device in the field to identify aspects of the test to improve, Tier 3) validation—demonstrating clinical performance in a field setting, and Tier 4) efficacy—testing whether the use of the device has an impact on outcomes in health. The two cases we describe were at a stage between Tier 2 and Tier 3 when they were evaluated in the field. In both cases, however, field work began much earlier, and included an assessment of needs and an evaluation of designs with potential end-users.

2. A Framework for Development

2.1. Defining a Problem

A successful technology must solve a real problem. For a diagnostic device intended for LMICs to make an impact, the problem addressed by the device should have four characteristics: 1) a sufficiently large number of people should be impacted by the disease for a research program intended to ameliorate the problem to receive adequate attention from funding agencies, non-governmental organizations (NGOs), and governments, 2) the diagnostic device being designed should provide actionable information that can improve the wellbeing of the patient, 3) simple interventions should already exist to treat the patient once a diagnosis has been provided, and 4) existing solutions to the problem should be inadequate. The last criterion is especially important when the final goal is to create a useful product. Analyzing the market for current solutions provides an idea of the level of performance that must be surpassed to make a

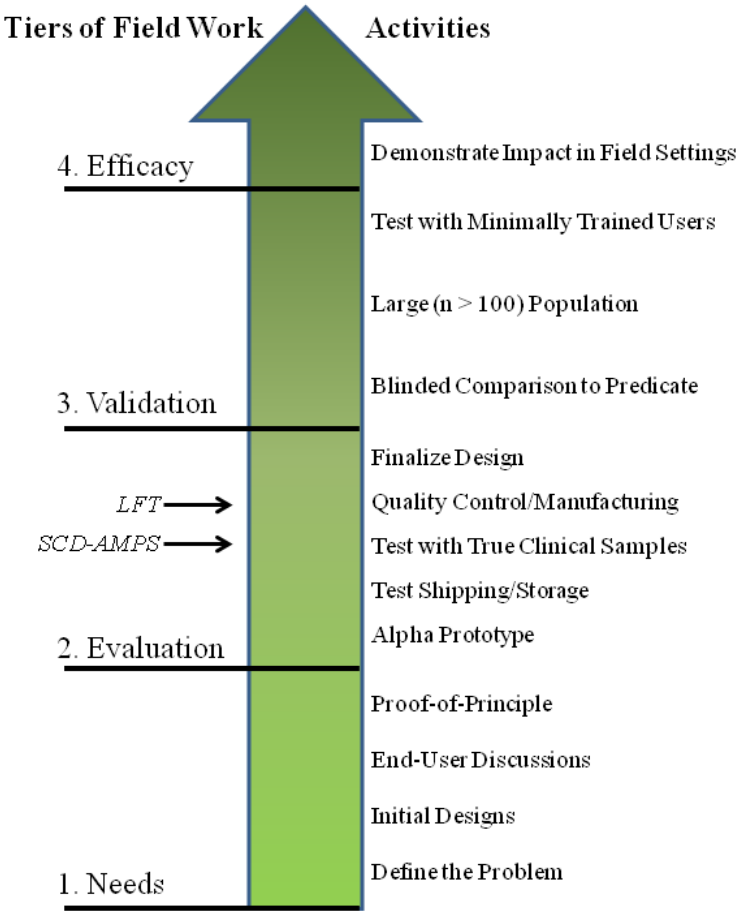

Figure 2.2. The spectrum of field work can be broken down into four tiers. Progressing upwards from an initial assessment of needs, the activities and milestones that a device must pass requires increased time and resources. Field trials of a POC diagnostic for LMICs can refer to testing in an LMIC done anywhere above Tier 2. Field trials of the paper-based liver function test (LFT) and the density-based test for sickle cell disease (SCD-AMPS) were between Tier 2 and Tier 3.

substantial impact. Several reviews provide detailed examples for these characteristics applied to different diseases.[5–8]

To identify needs and outstanding problems in global health, it is not enough to simply read reports from the World Health Organization (WHO) or look at the latest grand challenges list from the Bill and Melinda Gates Foundation (BMGF), although both organizations do extensive research on the ground to come up with these lists. By their nature, lists neglect the details, and in POC applications, the detail is where the devil lives.

To better understand problems that could be addressed by technology, experience at the point-of-care is necessary, whether it be in rural villages in Africa, urban slums in India, or a forward deployed military unit in a combat zone. When this experience is not available to us as scientists, we must find partners that understand the needs, and can explain them in the context of technical challenges. Once one has a team that brings together technical capabilities, medical expertise, and an understanding of field work, it is—in principle—possible to identify a problem properly, where new technology could have an impact.

2.2. Building a Team

Creating an interdisciplinary team with global scope requires little more than searching for potential partners, sharing ideas, and valuing what every member brings to the discussion. For scientists and engineers in academic departments, attending symposia or lectures aimed at medical audiences, or simply emailing doctors and researchers at local hospitals or nearby schools of public health are easy ways to find partners who can guide your capabilities toward real problems.

International collaborations can often be initiated without boarding an airplane. In the U.S. and Europe, many hospitals and medical schools have at least some doctors who have

worked in LMICs. Many of these doctors operate, or work with, NGOs that may be a resource for conducting trials. In developing countries, Ministries of Health and local NGOs can be valuable partners.

Trust and mutual understanding are important aspects to any partnership, but especially so in international collaborations. Online communities and forums, such as Global Health Delivery Online (www.ghdonline.org) and Engineering for Change (www.engineeringforchange.org), make it much easier to begin communicating with potential partners, but establishing a good working partnership is often best done in person. Over the last several years, international conferences and workshops on POC diagnostics have been held around the world; in 2012 a workshop on "Bringing Diagnostic Prototypes to the Point-of-Care" was held in Nairobi, Kenya and in 2013 the "Micro Med A" workshop was held in Pilanesberg, South Africa. Several universities have also begun to offer courses that take students and professors abroad to work with organizations in the field. Taking advantage of these opportunities can lead to partnerships and new research programs. Partnering with organizations that have experience doing field work is another option. Engineers Without Borders (EWB) provide a grassroots network with global connections. Larger institutions like the Program for Appropriate Technologies in Health (PATH) and the Foundation for Innovative New Diagnostics (FIND) are particularly well suited to help evaluate diagnostics. **Table 2.1** lists these and other resources to help establish partnerships.

2.3. Design Considerations

A well-defined problem requires solutions to fit within specific constraints. The ASSURED criteria (affordable, sensitive, specific, user-friendly, robust, equipment-free, delivered), developed by the WHO, provide a rough guide to, and check-list for, design, but

Table 2.1. List of potential partner organizations with global reach.

Organizations	Type	Headquarters	Countries of Collaboration	Experience Developing Diagnostics
Center for Integration of Medical Innovation and Technology (CIMIT) & Center for Global Health (CGH)	Consortium	Boston, MA, USA	> 20 countries worldwide	Yes
Global Scientific Solutions for Health, Inc. (GSSHealth)	Consultants	MD, USA	> 15 countries (Africa & Asia)	Yes
John Snowe Inc.	Consultants	Boston, MA, USA	> 75 countries worldwide	Yes
Clinton Health Access Initiative (CHAI)	Foundation	Boston, MA, USA	> 25 coutnries worldwide	Yes
USAID	Government Agency	Washington, DC, USA	> 100 countries worldwide	Yes
National Center for the Advancement of Translational Science (NCATS-NIH)	Government Institute	Bethesda, MD, USA	Fund programs/initiatives worldwide	Yes
Engineers for a Sustainable World (ESW)	Network	Pittsburgh, PA, USA	> 9 countries worldwide	
Engineers Without Borders (EWB)	Network	Denver, CO, USA	> 47 countries worldwide	
Bill and Melinda Gates Foundation	NGO	Seattle, WA, USA	> 100 countries worldwide	Yes
Foundation for Innovative New Diagnostics (FIND)	NGO	Geneva, Switzerland	> 60 countries worldwide	Yes
Partners in Health (PIH)	NGO	Boston, MA, USA	> 12 countries worldwide	
Program for Appropriate Technologies in Health (PATH)	NGO	Seattle, WA, USA	> 70 countries worldwide	Yes
Center for Emerging & Neglected Diseases (CEND)	University Center	Berkeley, CA, USA	worldwide	Yes
D-Lab (MIT)	University Center	Cambridge, MA, USA	> 20 countries worldwide	Yes
National School of Tropical Medicine (Baylor)	University Center	Waco, TX, USA	> 7 countries worldwide	
Sandra Rotman Centre	University Center	Toronto, ON, Canada	worldwide	Yes
Stanford Biodesign & Center for Innovation in Global Health (Stanford)	University Center	Stanford, CA, USA	worldwide	Yes

should be understood in the specific context under which they were developed: criteria for rapid tests for sexually transmitted infections.[9] These criteria are important, but, as has been pointed out by others, they are guidelines and should not be used as a substitute for the considerations and requirements that are specific for a particular disease.[7] In some cases, the ASSURED criteria may be too constraining. For example, the "equipment-free" in ASSURED may not apply if your device would be employed in a district hospital where small scale equipment could be used. Similarly, a cell phone could count as a piece of equipment, but simple mobile phones are readily found, even in many remote villages (more advanced cell-phones that are now often proposed for POC use in resource-limited, POC applications often are not). Some problems require quantitative measurements while others only need a simple yes/no answer.

Scientists developing POC technology can visit sites where they intend their devices to function or can work with clinical and international collaborators to learn the detailed context around their diagnostic target.[10,11] Designing a device with a specific context and problem in mind prevents unnecessary restrictions while retaining constraints that are crucial to success in a field evaluation.

2.4. How to obtain funding

Finding funding for field trials can be a challenge. A first step is to understand costs. Depending on the size and scope of the field evaluation, costs can range from $15,000 (e.g., a week-long program in a rural setting to get end-user feedback) to over $100,000 (e.g., a six-month clinical evaluation of performance on several hundred subjects). By working with the international partners on the team and maintaining clear communications, one will be able to estimate costs for personnel, equipment, and local transportation for your specific device. With a realistic set of costs, the team can factor field testing into budgets for grants from traditional

funding agencies, like the NIH, or foundations sympathetic to global health causes, such as the BMGF.

Many institutions and non-profit organizations offer "accelerator", "innovation", or "translational" grants, designed to position a technology in such a fashion that it becomes easier to obtain funding from companies or venture capitalists. Design competitions or "hack-a-thons" are also becoming popular and can provide money, insight from others in the field, and a mechanism to build a team.

Funding may also be available from LMICs interested in technologies that will be of benefit to their citizens. Even when money is not available, in-kind services—such as access to space in a clinical laboratory or accommodations in dormitories—may reduce the amount of funding needed from external sources. Close connections to partners in the country can be crucial to take advantage of such opportunities.

Companies that make diagnostic instruments and other supplies (e.g., Beckman Coulter) are sometimes willing to donate ancillary supplies and equipment when there is a potential benefit to the public; these kinds of donations can further reduce the costs of a field evaluation.

2.5. When is a device ready for field work?

Ideally, one would test a device in field settings early and often throughout the entire spectrum of field work (**Figure 2.2**).[12] The constraints of time and funding, however, require a more judicious use of resources. Much preliminary work can be done in a laboratory or with medical partners in developed countries. The state of development that a device must attain before testing in the field depends on specific problem being addressed and the objectives of the field work. Diagnostic devices developed in academic laboratories can often benefit from an

early evaluation of operability in the field. Sometimes a device may advance farther to some point on the spectrum below Tier 3 (Validation) where a more advanced field evaluation could provide feedback on performance as well as operational issues. How can one tell whether a device is in a phase of development that will benefit from evaluation in the field?

A field evaluation of a prototype device (between Tier 2 and 3) can quickly identify the most critical weaknesses of the device. The effect of environmental conditions (e.g., temperature and humidity), variations in biological specimens (i.e., testing on true samples versus surrogates), and problems with use and interpretation are all critical challenges that can be identified. These kind of studies can be short (< 1 month) and require a more modest number (n ~ 30) of subjects than a higher tier field trial because the objective is to identify critical issues with the device rather than subtle influences.

Despite the expectation of some area of failure, some degree of confidence in the device is necessary to undertake a field evaluation. A proof-of-principle—demonstrations that the device works in a laboratory setting using clinically relevant samples or surrogates (e.g., serum or artificial urine spiked with an antigen)—provides a degree of confidence that, given proper settings and conditions, the device should work. Although initial validation on 30 or more samples is desirable to provide statistical power,[13] smaller sample sizes may still provide confidence in a result depending on the size of the effect being detected and the sensitivity required. As a minimum, however, one should not use less than seven independent samples.[13] Make sure that experiments with surrogate samples are independent; spiking different levels of an antigen into aliquots of plasma from the same sample would not provide the same amount of variation in the background as spiking antigen into plasma from different samples. If using surrogate samples, scientists should consult closely with a clinical specialist to understand

limitations of the surrogate for the test that the device performs. Using a sample representative of the sample in the field provides the best test of a device. A device designed tested only on blood from venipuncture may behave differently with fresh blood from a fingerprick; obtaining a reproducible and high quality sample from a fingerprick requires care and technique to avoid hemolysis or inclusion of large volumes of interstitial fluid.[14]

Testing the device with naive users—people who were not involved in the development of the device—can provide important information about design and operations for the use of the device. Not only does a naive user provide feedback about the usability of the test, the performance of the test being run and interpreted by such a user provides a more realistic estimate of performance in the field than use and interpretation by the developers. With both the technologies we describe in this piece, most testing before field work was done with some involvment of the developers of each technology. If naive users had been introduced in testing in the laboratory, perhaps we could have reduced the time spent on pilot trials or identified areas to imrpove on the devices before they were evaluated in the field.

Devices designed to give a binary readout (i.e. "positive" or "negative") must be sensitive (able to detect positives) as well as specific (avoid classification of a negative sample as positive). If a threshold is used to define whether a measurement is classified as positive or negative, a receiver operating characteristic (ROC) curve can provide a simple visual tool to understand the performance of the test.[15] If the device provides a quantitative measurement, comparison to measurements from a standard diagnostic test using a Bland-Altman plot can identify potential bias in the measurement.[16]

With confidence that the biological and technical side of your device *can* work, development efforts should focus on reducing the sources of confounding factors. In preparation

for field evaluations, one needs to develop quality controls, identify suitable packaging, set storage requirements, and set shipping methods. Packaging devices and then storing them in an oven or a high humidity environment can provide quick tests for stability under extreme storage conditions. Packing some devices and sending them by a courier (e.g. FedEx, DHL, or UPS) with a return service provides exposure to different shipping environments. The degree to which all these factors are understood and accounted for sets the level of confidence that a device will perform as expected in a clinical trial and provide a true measure of performance.

Field evaluations conducted during this phase of development, before the final design has been frozen, provide an important opportunity to test a device on clinically relevant samples and to identify unexpected problems before conducting a field trial on the level of the third tier of field work (**Figure 2.2**), such as a trial for regulatory approval. In both of the case studies that follow, the design was not finalized but work to test for shipping, stability, and quality control had been done to different degrees. **Table 2.2** provides a representative example of a timeline for development and field evaluation.

A field trial at or above Tier 3 requires high confidence that the device will work and a fixed design (including packaging and storage conditions). This level of confidence requires demonstration of diagnostic accuracy (both sensitivity and specificity) on larger numbers of clinically relevant samples ($n > 30$) on devices produced in different lots. Multiple users should both perform and interpret tests. The intention of a field trial at Tier 3 is no longer to troubleshoot the device, but to demonstrate validity of the rapid test (often as a means towards regulatory approval). A field trial above Tier 4 requires a device that has passed a field trial at Tier 3 and is essentially in the form of a product. At Tier 4, field work aims to establish whether the use of the device at the POC provides a significant health outcome. Above Tier 3, the

Table 2.2. Representative timeline for moving a device from the laboratory to a field evaluation.

	Timeline - 5 Year Plan				
Task	**1**	**2**	**3**	**4**	**5**
1. Defining the Problem					
a. Team building					
b. Needs assessment					
2. Device Design & Testing					
a. Prototyping					
b. End-user feedback					
c. Validation on clinical samples					
d. Quality Control/Stability/Storage					
3. Supporting Activities					
a. Grant Writing					
b. IRB approvals					
c. Institutional agreements					
3. Field Evaluation					
a. Trial Design					
b. Shipment/Purchasing of Supplies					
c. Training					
d. Pilot Phase					
e. Full Study					
4. Next steps					
a. Analysis of Results					
b. Publication					
c. Discussion with companies/providers					

support of a company is often critical to bring manufacturing standards and scale to validation and efficacy testing.

2.6. Ethical Considerations

Research involving human subjects generally requires the approval of an Institutional Review Board (IRB)—these are committees common at universities and hospitals that review research proposals involving human subjects to ensure that the study is designed ethically and participants are properly informed and protected. An important exception relevant to diagnostics is the use of existing samples that are either publicly available or obtained in such a manner that subjects are unidentifiable. In any case, researchers involved in a field evaluation should complete training on human subject research. The IRB review process, while sometimes cumbersome, is essential to protect the trial subjects from physical or emotional harm. In fact, if approached properly, committees on the use of human subjects and IRB committees can provide guidance to ensure the ethical and proper collection of data. Often, these committees are knowledgeable about regulatory requirements, and they can provide advice to ensure that the study is designed in a manner appropriate for regulatory approval. In general, field trials carried out abroad must be approved both by an IRB in the country of the trial and by a separate IRB in the country where the research project originates. Each IRB committee may have different requirements and standards; the process of reconciling these differences can take several months.

2.7. Designing a study

Once the prototype is ready to be tested in the field at or above Tier 2 (Evaluation), significant focus should go into the design of the study. With the medical and local team, lay out clear goals for the study. The entire team should know which tier of field work is expected because, as discussed earlier, the objectives and requirements for each varies significantly.

During the design process, an institutional agreement between the research institution and the site of the field work should be established. This agreement can take the form of a subcontract or a memorandum of understanding. Clear expectations of work and commitments should be laid out, including precise language about financial commitments and oversight.

During a field evaluation, one may want to take a device to rural clinics to obtain feedback about the operation, interpretation, and design of the device. Such field work falls in Tier 1 and has different requirements for partners in LMICs and for the design of the study. A field evaluation and an evaluation of usability at the POC can be done concurrently, but each requires a specific set of goals and objectives. In some cases, they may each require separate approvals from the IRB.

Field evaluations past Tier 2 and before final efficacy testing (Tier 4) usually include checking the performance of the device on clinically relevant samples. Estimating performance requires comparison of measurements from the device to a gold standard test (i.e., a widely accepted, standard clinical test). Often, these tests are not available at the POC. The requirement to compare results to a gold standard may mean that initial trials must be done in a regional hospital in-country, where the necessary equipment is available to perform a gold standard test, rather than at the POC. If one aims to characterize device performance, make sure to follow best practices[17,18] and sound statistics[19] (e.g., ensure adequate sample sizes for statistical power,[20] proper blinding of samples,[17] well-defined inclusion and exclusion criteria[17]).

Recruiting and training staff to carry out the study can require weeks to months; the investment in time used to find qualified and committed staff members will allow a study to be more robust against external events. Training requires clear instructions on recruitment, workflow, sample collection and distribution, carrying out the rapid test, carrying out the

standard test, and recording results. In addition to time for training, time should be set aside for a pilot study before the main study begins. A pilot phase allows logistical problems to be identified and remedied without compromising the quality of the data from the trial.

Data collection instruments (i.e., questionnaires and laboratory logs) should include as much information as possible without becoming cumbersome. Moving from the lab to the field introduces many variables; unless you have tracked the externalities, the results of the study may be difficult to interpret. Events that could affect a device occur from the moment devices are prepared in the laboratory to the time that they are used, but some factors are not immediately apparent. For example, including a temperature logger when devices are shipped is often overlooked (indeed, see the Lessons Learned section).

2.8. Context and Culture

Establishing a working relationship with partners overseas early in the development of a device reduces the risk of a misunderstanding later during the implementation of a field trial or evaluation. Partners may not have protected research time, especially in clinical settings, preventing them from devoting as much time to run the study as needed. In such cases, it may be appropriate to hire a dedicated study coordinator for the project. Different countries have different hierarchical structures. Understanding the local culture can prevent a social faux-pas that can undermine a study or put a partnership at risk.

2.9. Challenges

With all the complications of carrying out an international collaboration and field evaluation, unexpected challenges will arise. Strikes, natural disasters, and regional instability are just a few examples of unrelated events that can threaten a project. Set timelines, but be

flexible. Take each obstacle in stride because each challenge is an indication that your device is slowly making its way to becoming something truly useful.

3. Case Study 1: Liver Function Test

3.1. The Problem

In recent years, international efforts to combat HIV have enabled access to anti-retroviral therapy (ART) in LMICs. As of last year, over 10 million people were being treated with ART.[21] Drug-induced liver injury (DILI) is a significant side effect associated with ARTs. DILI associated with nevirapine-based ART—widely used in the developing world—is of particular concern; rates of nevirapine-associated hepatotoxicity (a type of liver damage) exceed 13%.[22,23] Monitoring liver function provides an important tool to manage ART;[23,24] dosages and treatments can be adjusted if signs of liver damage or hepatitis appear. Tests to monitor liver function, however, are often unavailable in low-resource settings where many patients with HIV receive care. Levels of serum transaminases (aspartate aminotransferase, AST, and alanine aminotrasferase, ALT) provide a standard for monitoring DILI, but generally require centralized labs and venipuncture.[25]

3.2. The Team

We built a team combining academia, industry, and medicine. A business plan competition at the Harvard Business School brought together business students and scientists from the Whitesides group. The Whitesides group had developed the initial idea of 3D paper microfluidic devices that formed the architecture of the test.

With the assistance of Carmichael Roberts, a former postdoctoral fellow in the Whitesides group, at that time a venture capitalist, Diagnostics for All (DFA) was formed as a

non-profit organization to develop paper-based devices as diagnostics. Academic groups excel at basic research and innovation but lack both the proper resources and incentives to do the detail oriented engineering required to execute manufacturing and quality control for a product. A company provided a vehicle to do high quality engineering. The decision to create a non-profit stemmed from the idea that a for-profit entity driven by stakeholders might be forced to focus on developed world applications of paper-based diagnostics rather than first apply the technology to address needs in the developing world.

The team identified enzymatic tests for liver function early on and discussions with doctors in Boston-area hospitals and experts in public health confirmed the importance of the problem, especially in countries with large populations of patients being treated for HIV or TB. After initially considering seven different assays, the team settled on ALT and AST based on the counsel of medical experts.

Scientists from Diagnostics for All (DFA) developed a robust assay and integrated sample acquisition, preparation, and evaluation into a single device. Dr. Nira Pollock at Beth Israel Deaconess Medical Center (BIDMC) provided medical guidance and led clinical validation in Boston. Dr. Pollock identified a site in Vietnam to evaluate the test in a field setting. After initial validation, DFA called Bernhard Weigl, the director of NIH-funded Center for Point-of-Care Testing at PATH, for assistance in running a field evaluation.

3.3. Designing a Solution

To monitor DILI at the POC in LMICs, we created a low-cost, rapid, liver function test (LFT) for serum transaminases using paper-based microfluidics.[3] Paper provides an inexpensive substrate for immunoassays. Patterning paper allows multiplexed flow and small test zones which reduce the need for large volumes of costly reagents. Paper-based microfluidic devices

provide an attractive system to develop POC tests where low cost is a key design criterion. Tests that are performed frequently and potentially at high volume, such as tests to monitor liver function, are particularly sensitive to cost.

The specific problem of measuring liver function provided guidance on the design of the test. Although standard tests for serum transaminases provide a quantitative measurement, these measurements are generally interpreted in three bins. In practice, this binning means that a rapid test needs to provide a semi-quanitative readout that will allow results to be placed into three bins. To meet this requirement, we made a colorimetric test with a read guide (a standard color bar) that would allow users to provide a semi-quantitative measurement of each test (**Figure 2.3**). Benchmark values for ALT and AST are based on measurements in blood serum. In order to measure transaminases from serum, we incorporated a plasma separation membrane (PSM) into the paper device.

With end-users at the POC in mind, the device was designed to be simple to use and interpreted by eye. The device was covered in plastic lamination to protect the paper test zones from the outside environment and a small hole in the lamination over the PSM provided an entry to directly add blood from a fingerprick. Positive and negative controls are built into the device to provide a metric to know if test results are valid (e.g., reagents are working, blood has not lysed). Several iterations of design have incorporated improvements to the ease-of-use, sensitivity, and interpretation of the test (**Figure 2.4**).

3.4. Validation and Preparation for Field Evaluation

In Cambridge and Boston, we tested analytical, operational and clinical performance of the LFT device.[3] Briefly, these studies included defining the limit of detection, assessing repeatability, checking for cross-reactivity and interference, optimizing the time for the assay,

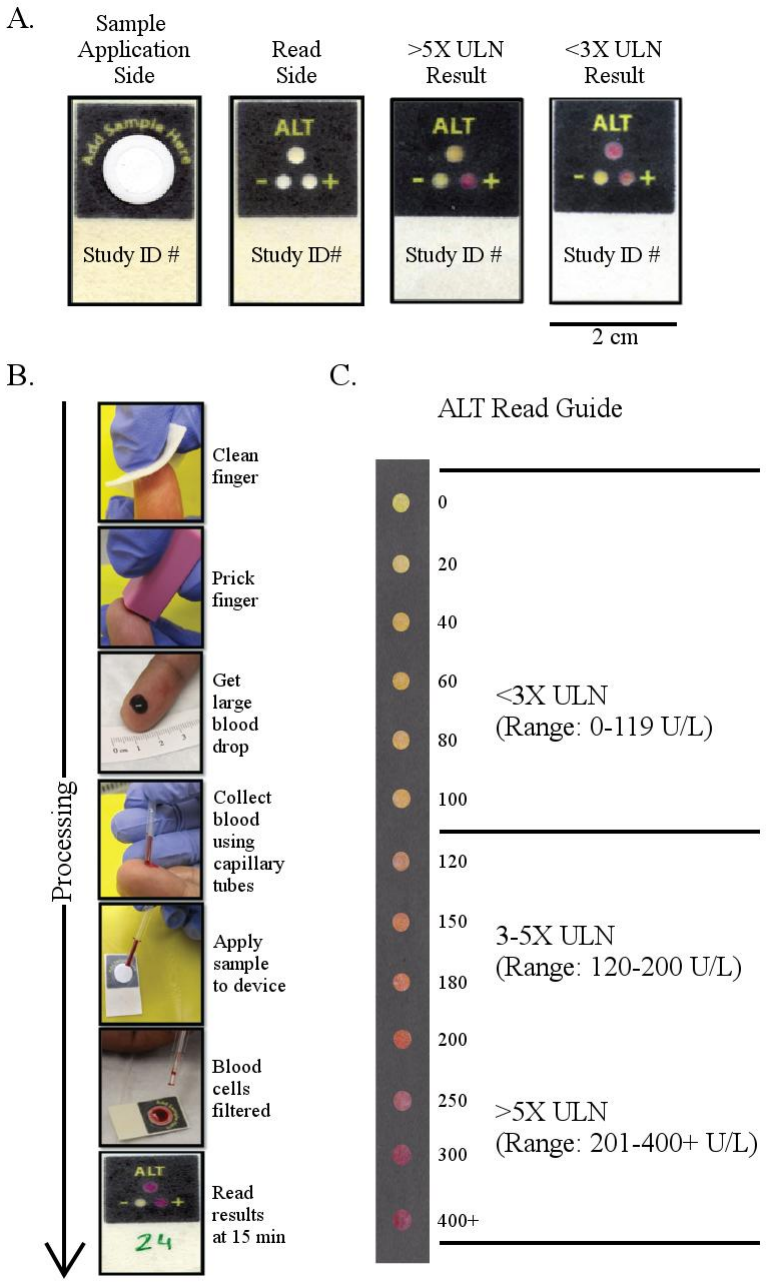

Figure 2.3. The design of a paper-based LFT provides a semi-quantitative test for LFT for serum transaminases. (A) The stamp-sized devices receive a sample of blood on the "application side" and provide a colorimetric readout on the "read side." (B) The entire process of running the test requires minimal sample manipulation. (C) Valid results are interpreted and binned into three levels using a read guide.

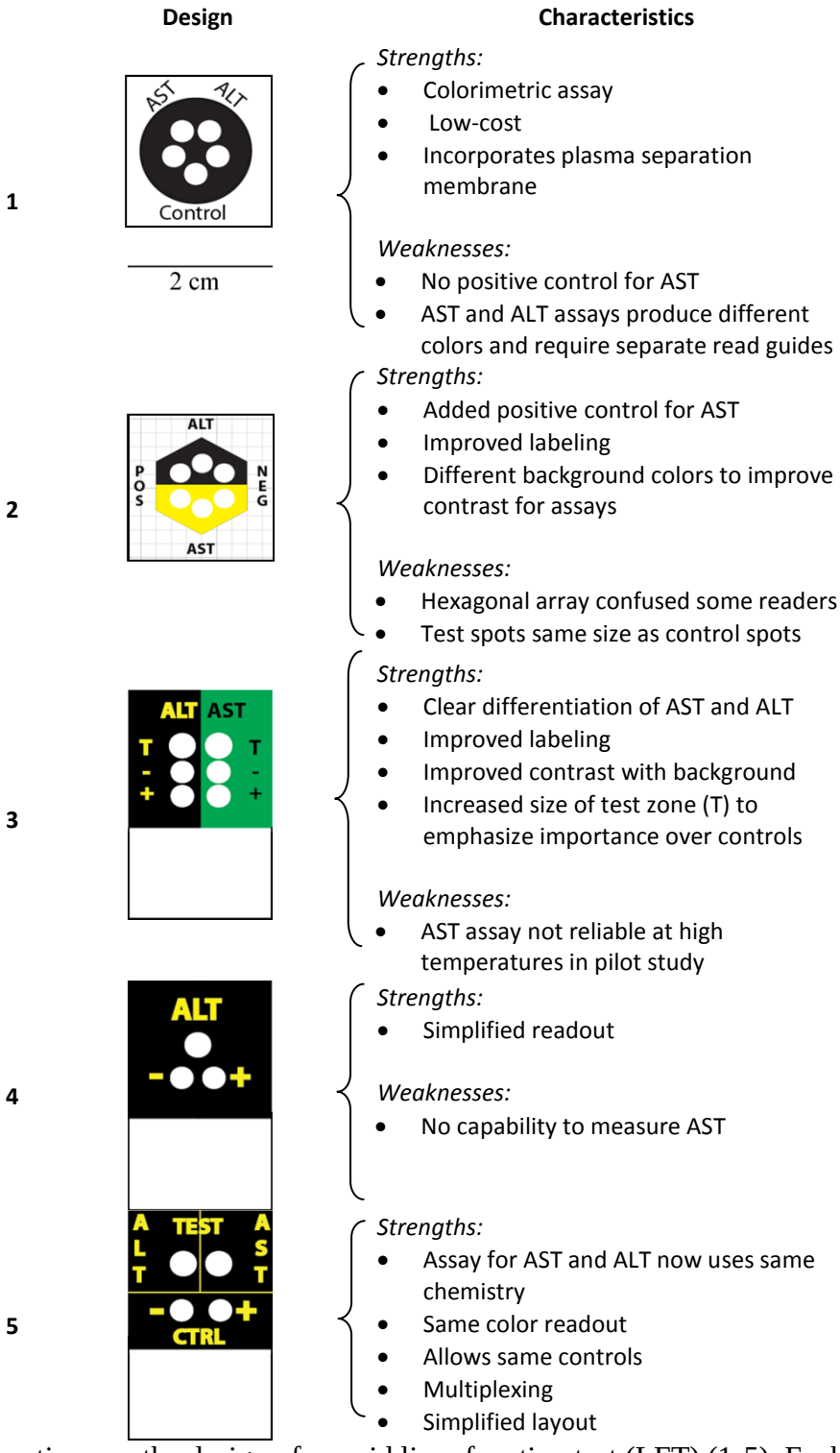

Figure 2.4. Iterations on the design of a rapid liver function test (LFT) (1-5). Each design has the same scale. The characteristics of each iteration demonstrate improvements to the design to create a user-friendly device.

designing methods for metering the sample, comparing the performance of the device to gold standard methods, and testing the stability of the device. These studies were intended to validate the device and provide adequate supporting data to warrant initiation of field testing. During this time, members of the team from DFA had opportunities to travel to different countries for conferences and meetings with potential end-users in different healthcare settings. A trip to India in 2010 allowed a DFA member to show the design of the LFT at the time (**Figure 2.4: Iteration 2**) to clinical laboratory workers. Workers at the clinic felt that the test was too small, and ceiling fans in the hot environment had the potential to cause samples toevaporate and change the dynamics of the test. Later iterations of the device increased the size and added a small white tab to hold (**Figure 2.4: Iteration 3 onward**). Protocols for running the test were modified to include placing the tests under a glass dish to prevent excessive evaporation.

After three years of development, the team decided to perform a field evaluation to produce high quality data for use in refining the device. Field evaluation would also assist in freezing aspects of the design that worked well; this step would then enable future trials for regulatory validation and enable manufacturing to be scaled up. Most importantly, we hoped the field study would provide a test to see if the device could perform as a POC diagnostic in a setting where it could have a major impact. This study enrolled 600 patients and was intended to provide the evidence that prototype test performed well in a controlled field setting.

3.5. How Funding was Obtained

The initial work to develop the test on paper-based microfluidics was supported by a grant from BMGF (51308–Zero-Cost Diagnostics). This grant also enabled some early travel to countries where a large number of patients on ART could benefit from a test to monitor DILI.

Dr. Pollock was supported by an NIH K23 grant to carry out the clinical validation in Boston (5 K23 AI074638-04). By working with PATH, we were able to fund the field evaluation. PATH had an NIH funded Center to Advance Point-of-Care Diagnostics for Global Health (NIBIBU54-EB007949).

3.6. Study Design

Working with BIDMC, we sought an international partner who worked with a large number of patients on ART and who would both be able to benefit from a POC LFT. The partner also needed to have the infrastructure in place to measure serum transaminases as a gold standard comparison to our test. BIDMC had a long-standing partnership with hospitals in Vietnam through the Harvard AIDS Initiative in Vietnam (HAIVN). Dr. Pollock connected with Dr. Donn Colby who had spent years living and working with hospitals in Vietnam as part of this program. Dr. Colby provided an essential link who had a longstanding relationship with both the medical team developing the device and the local site in Vietnam where the device would be connected. With Dr. Colby's assistance, the Hospital for Trpical Diseases (HTD) in Ho Chi Minch City was identified as a site for testing.

The HIV clinic at the HTD provided the right combination of appropriate patient population and supporting infrastructure. The clinic we chose saw 3,000 HIV-positive patients on ART, provided free through the Vietnam Ministry of Health. Of these, a significant proportion were on nevirapine-based ART (known to confer risk of DILI) or were at risk for co-infection with hepatitis B (HBV, 15% prevalence) and/or hepatitis C (HCV, 25% prevalence). The clinic also had an existing practice of routine transaminase monitoring (once every six months) for patients receiving HIV treatment, following Vietnamese national guidelines.[26] As a

result, the clinic had capabilities to do standard tests, but also could benefit from a POC LFT that could enable more frequent and less expensive monitoring.

The study recruited patients scheduled for routine clinical ALT testing (specimen collected by venipuncture) by their physicians; after venipuncture, subjects proceeded to fingerstick collection for LFT testing. Working with PATH and HTD, DFA and Dr. Pollock chose a target population of adults since this population would be one of the largest to benefit from the LFT and would be able to provide informed consent themselves (an important consideration to simplify IRB approval and the consenting process). The Vietnam field study was evaluated and approved by the Institutional Review Boards of the Hospital for Tropical Diseases, Ho Chi Minh City, as well as by Research Ethics Committees at PATH and Beth Israel Deaconess Medical Center. All participants in the study provided informed consent.

Working with HTD rather than a rural clinic enabled validation of results using standard tests. Using resources at HTD, automated ALT testing was performed in parallel (Roche Cobas 6000 analyzer) using blood obtained by venipuncture. In order to collect additional information that could be relevant to the devices performance, the study was designed to collect more clinical information, as available, for each subject: hepatitis B virus (HBV) status, hepatitis C virus (HCV) status, current HIV medications, current TB medications, and most recent CD4 count. Results of any laboratory tests ordered concurrently with ALT on the day of enrollment were also captured as available (e.g., AST, hemoglobin, hematocrit, platelet count, creatinine, and CD4).

Outside of clinical information, we also tried to record other variables that could have an impact on the performance of the LFT. Packaged LFTs were stored in ambient conditions, and, thus, a temperature and humidity logger, combined with historical weather data from Weather

Underground (wunderground.com) provided a log of ambient environmental conditions. Initially, no data loggers were included during the shipment of LFTs to Vietnam. The team carrying out the trial, however, added data loggers to the second batch of LFTs that were sent to the study site.

Three activities occurred at the site of the study: 1) training, 2) pilot phase, 3) study phase. The training was meant to familiarize all staff with the study and establish competency reading the LFT. The pilot phase was designed to recruit 50 subjects and ensure that study procedures were working as expected before beginning the study phase and recruiting 600 participants over six months.

3.7. Implementation

Approximately one month prior to the beginning of the study, representatives from PATH and DFA traveled to HTD and provided training to nurses who would carry out the study. The training curriculum included review of the study objectives and recruitment procedures, overview of the device structure and function, steps for completing the fingerstick and transferring sample to the device, and practice reading with mock devices. In addition, nurses were specifically instructed to read and record device results privately, without interaction with any other individual. The study nurses were required to pass a proficiency test using the mock devices (pass criteria: > 80% bin placement accuracy and 100% determination of invalids) before patient enrollment could start. If they failed this test, they were retrained with the mock devices and given another test. Each nurse was allowed a maximum of two trials to pass the test. During the pilot phase, the study nurses received immediate feedback on correct and incorrect use (including fingerstick, sample transfer procedure, and device reading) from an expert DFA

representative. No additional training or feedback was given once evaluation study enrollment began.

The temperatures during the pilot phase were often higher than the range the LFT was designed for (4-30 ^{0}C). The read-time for the test was adjusted for the higher temperature and the AST test was removed from the device due to poor stability of reagents for that test at higher temperatures (current improvements in the AST test have addressed these issues and will be evaluated in future trials).

All tests were performed following a set of instructions provided with each product by the DFA, the details of which are described elsewhere.[4] Notably, each test was read by two nurses. Neither the patients nor their doctors were informed of the results of their fingerstick testing. Although the field work took only six months, the total time to plan for the study, obtain IRB approval and carry out the work at the field site took over a year.

3.8. Context and Culture

Working with multiple partners—academics (Harvard and BIDMC), a non-profit company (DFA), an NGO (PATH), and a hospital (HTD)—provided the benefit of specialized knowledge and experience from each partner. Managing such a multi-institutional collaboration, however, also has challenges. Each partner has their own needs and their own timeframe. Academics want to publish results, hospitals need to maintain enough staff for their primary operations outside the study, companies want to learn as much as possible about their test for use in development, and NGOs needs to ensure that the device is at a mature enough stage to merit investing time and resources into a trial. In the case of the field trial in Vietnam, we believe everyone was able to meet their needs effectively, but this success required clear and open communication from the outset and throughout the study. For example, DFA and PATH had

wanted to have ten nurses reading tests independently in order to estimate concordance for the visual test. HTD was not comfortable with providing so many nurses to the study based on the resources they needed. A compromise was reached and three nurses were provided by HTD for the study.

Every healthcare system operates differently and differences in norms can potentially disrupt a study. At HTD, nurses rotate their positions every six months. The team from PATH and DFA arrived and began training nurses during the pilot phase in the middle of a rotation cycle; all the trained staff would have been rotated out of the clinic halfway through the study and could have caused major inconsistencies. The practice of rotating staff came to the attention of the PATH trainers, fortunately, during the pilot phase. Working with HTD, they were able to negotiate for some of the key personnel that were trained to remain at the clinic for the duration of the trial.

Stigma associated with HIV can pose a challenge for diagnostics designed for those with the disease. Working with an established HIV clinic provided an environment where patients were comfortable. Sometimes patients may be reluctant to participate in a study when there is no direct compensation. By choosing to work with an HIV clinic where patients were already being monitored regularly for DILI, the potential future benefit of a rapid LFT was clear to patients.

3.9. Challenges

From the study, we found numerous parameters of the LFT device to improve. Some involved the ease-of-use, such as bin placement accuracy. Others related to quality control in components; several tests were invalid because of a batch of faulty plasma separation membranes. Even though DFA had performed some tests of environmental conditions (humidity and temperature) and shelf-life, the results from the study indicated that further optimization of

these parameters was necessary. Temperatures at the study site went up to 36 ^{0}C during the course of the study. This temperature was higher than the recommended storage temperature for the device.

At the beginning of the study, nurses felt that devices were difficult to read, but, but the end of the study, they reported that tests were easy to read 90% of the time and that the instructions provided with the test were "very clear and easy to follow." The most frequently mentioned challenge to using the test was matching the color on the device to the reader guide (**Figure 2.3**).

3.10. Lessons learned

Based on the characteristics of the test that were tested, we identified several aspects of the test to focus on in further development. For example, to improve bin placement, we are working to expand the dynamic range of assay for clearer visual differences between different levels of ALT. To avoid invalids, we have incorporated quality testing of incoming materials that are used in the assembly of the LFT devices. DFA has also tightened the requirements for a controlled manufacturing environment to reduce lot-to-lot variability. Finally, research has been focused on stabilization of device components to improve shelf-life.

Like many rapid tests, the LFT requires that results be read within a specific window of time to avoid false positives and false negatives. Interestingly, in discussions with the nurses using the LFT in Vietnam, several expressed a desire for tests that were not as time sensitive and could be read within several hours. As busy nurses in a hospital, managing time between patients and other duties makes it difficult for tests to be read at a very specific time.

Although much research has been done on POC diagnostics using paper-based microfluidic devices, this study was the first-ever large scale field evaluation of such a device.

As such, it provides evidence that paper-based devices could be feasible in LMICs. In particular, we found health workers performing tests on samples from a clinically relevant population had a high degree of concordance on visual readings. Successful development of this device for clinical use will require further, iterative, optimization of the device, but the initial field evaluation provided us with guidance on the aspects requiring focus.

3.11. Next Steps

In the past year, DFA has made improvements to the LFT device. The newest prototype has a better accuracy, is less sensitive to environment conditions, and more importantly is stable for over a year at 20-30^{o}C. Most of the issues identified in Vietnam have been addressed. We are currently preparing for field testing of the new prototype and beginning the process of validation of the product for regulatory approval.

The intensive training of users allowed in the context of this first field study is unlikely to be feasible or reproducible outside of study contexts. A thorough understanding of the minimal training requirements for novice users will ultimately be key to understanding the range of clinical environments in which this test can be used–whether that be in centralized clinics as performed by trained staff, decentralized clinical settings as performed by minimally trained health-care workers, or even at home as performed by patients themselves. DFA is currently planning an "Untrained User Study" with 50-100 participants in order to obtain Clinical Laboratory Improvement Amendment (CLIA) waived certification for the LFT device.

Field evaluation provided helpful information on the performance of the LFT on a large patient population as well as operational information about user-to-user variation and potential environmental conditions. This knowledge has enabled DFA to design a next generation

prototype of the LFT device that we hope will provide an accurate and easy-to-use test to monitor DILI.

4. Case Study 2: Sickle Cell Diagnostic Test

4.1. Problem

Sickle cell disease (SCD) is an example of an illness where an early diagnosis can have a major impact on health outcomes. Each year, over 300,000 children are born with SCD, most in sub-Saharan Africa and India.[27] In countries without early diagnosis and targeted treatment, the mortality rates of children under 5 years old with the disease ranges from 50-90%.[28] Interventions as simple as prophylactic penicillin and parental education can have a significant impact on child survival rates.[29] The lack of a low-cost, rapid, point-of-care test for SCD, however, means that the potential of these interventions goes largely unrealized.

4.2. The Team

Students in the Whitesides group at Harvard University had developed aqueous multiphase systems (AMPS)—mixtures of polymers in water that spontaneously form immiscible liquid phase—as a method to separate cells by density. Based on the literature[30–32], the Whitesides members recognized the potential for AMPS to identify SCD early on, but initial efforts with AMPS were focused on a variety of other applications in blood separation. A chance encounter with Dr. Thomas Stossel (Brigham and Women's Hospital, Boston) at a symposium at Harvard Medical School provided the incentive to think seriously about the underlying problem, and the real need for a rapid test for SCD. Dr. Stossel spent the better part of a decade doing medical and dental work in rural Zambia. As a hematologist, he quickly realized the large burden of undiagnosed patients with SCD in the country. He also understood the constraints that a test would have to meet to be useful in rural areas.

Table 2.3. Timeline from the conceptualization of a density-based rapid test for sickle cell disease to a field evaluation in Zambia.

	Timeline			
Task	**2011**	**2012**	**2013**	**2014**
1. Defining the Problem				
a. Team building				
b. Needs assessment				
2. Device Design & Testing				
a. Prototyping				
b. End-user feedback				
c. Validation on clinical samples				
d. Quality Control/Stability/Storage				
3. Supporting Activities				
a. Grant Writing				
b. IRB approvals				
c. Institutional agreements				
3. Field Evaluation				
a. Trial Design				
b. Shipment/Purchasing of Supplies				
c. Training				
d. Pilot Phase				
e. Full Study				
4. Next steps				
a. Analysis of Results				
b. Publication				
c. Discussion with companies/providers				

Once the team realized the potential impact of a density-based assay to identify sickle cell disease, they met with Dr. Carlo Brugnara (Children's Hospital, Boston), and recruited him onto the team. Dr. Brugnara added a depth of understanding of the density of red blood cells in SCD.[33,34] Dr. Stossel connected the team to Dr. Catherine Chunda-Liyoka, a physician at the University Teaching Hospital (UTH) in Lusaka, Zambia. Dr. Chunda-Liyoka complemented Dr. Stossel's knowledge of the needs for sickle cell diagnostics with her experience managing SCD in patients in Zambia.

The team moved from a conceptual idea to an evaluation in the field in Zambia in three years (**Table 2.3**). The speed of development was driven in part by the simplicity of the technology, and in part by the ability of team members to work together efficiently in the design and implementation of the field work.

4.3. Design Considerations

Using AMPS, we created self-assembling step gradients in density designed to separate dense cells present in sickle cell disease and provide a visual test for SCD (Chapter 4). The self-forming nature of AMPS allowed us to make large batches of AMPS and preload them into microhematocrit capillary tubes.

Based on discussions with Dr. Stossel and Dr. Chunda, we wanted to minimize the power and time requirements for the test so that it could be run in rural clinics. For cells to move through an AMPS in a short amount of time (minutes rather than hours/days), centrifugation is required. The faster the centrifuge, the more power that is required, but the less time that will be needed for the test. Consultation with our medical team along with other organizations, including DFA, brought us to the conclusion that time was the more critical component and that

a target of less than 20 minutes could be useful in rural clinics. This time target set the speed of the centrifuge and power requirements.

The use of the centrifuge brings the need for electricity. District hospitals and even many provincial hospitals in Zambia do not have the capability to diagnose SCD by standard methods due to the expense of equipment and reagents. In these hospitals, line electricity is available. Many Zambians, however, receive their care from rural clinics. A number of these clinics are equipped with solar panels. In fact, in rural parts of Zambia, usually one home can be found in a community with a car battery charged by a solar panel. This setup is often used by enterprising individuals to charge cell phones of neighbors for a small fee. Whether at a district hospital or in a rural clinic with a solar setup, we believed the unmet need for a rapid test for SCD was large enough to allow for the use of a microhematocrit centrifuge to enable a density based test to be fast.

To ensure the test was easy to use, we had to think about the entire process of the interaction of a patient with a diagnostic, from sample acquisition to reading the results (**Figure 2.5**). For ease of use and safety, we used polycarbonate capillary tubes rather than glass tubes. We designed the test so that tubes would be preloaded with polymers. Taking a sample from a subject and adding it into a device in a simple way is often a non-trivial task. We iterated several designs (**Figure 2.6**) before finding a simple method to add a fixed volume of blood to a capillary that was already sealed on one end and partially filled with an AMPS solution. Visual readout removes the need for additional equipment or computing power. Including aspects of sample acquisition and readout into the design of the device ensured a smooth interaction with an end-user. All that a user would have to do is to load a drop of blood and spin the small test in the centrifuge.

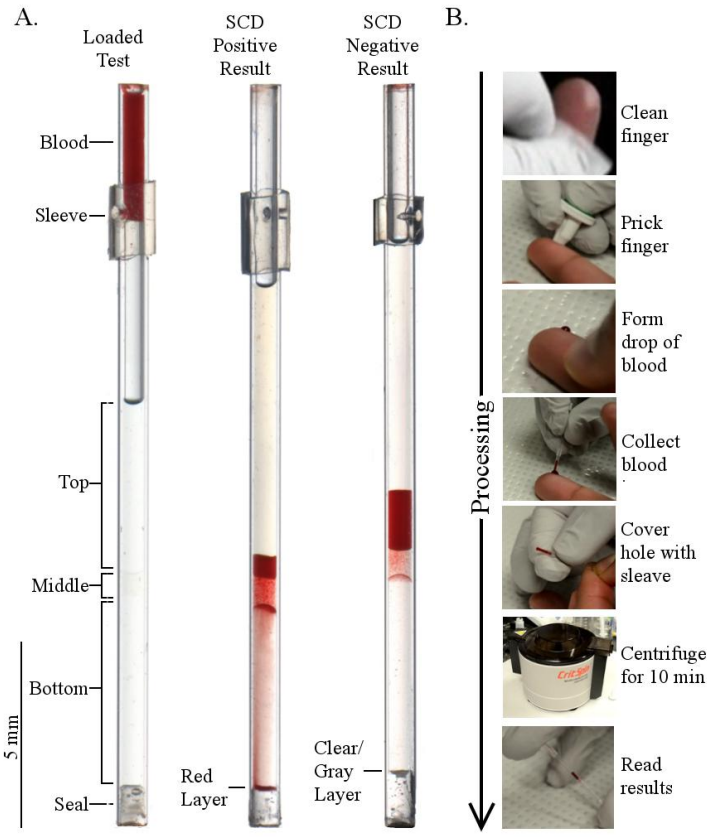

Figure 2.5. AMPS enable a simple, rapid test for SCD using density. (A) A capillary pre-loaded with AMPS wicks a fixed volume of blood into the device. After covering the hole for filling the tube with a sleeve, centrifugation enables the rapid sedimentation of cells over the AMPS and provides a result that can be read by eye. A red layer above the seal at the bottom of the tube indicates the presence of SCD. (B) The entire process of performing a test, including centrifugation, requires ~12 minutes.

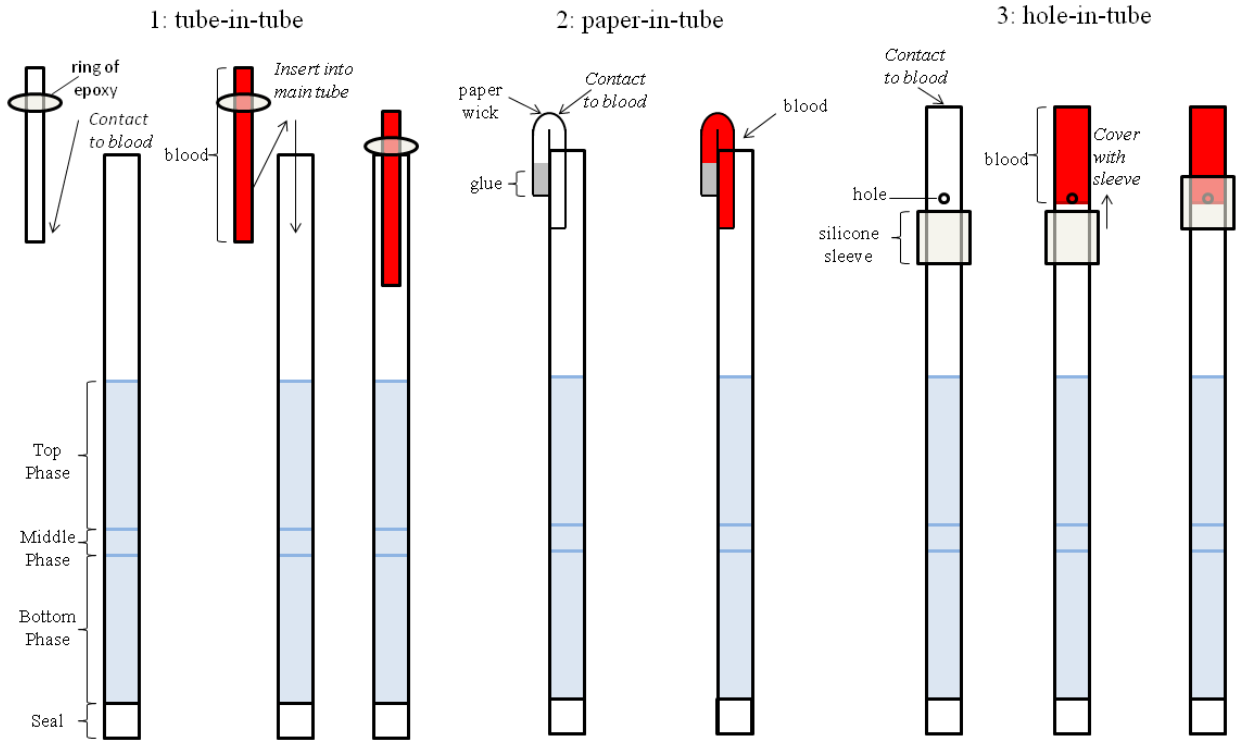

Figure 2.6. Iterations on the design of the loading mechanism for a density-based SCD test. We tested three different methods to add blood to a capillary tube that was preloaded with AMPS and sealed on one end: 1) tube-in-tube method, 2) paper-in-tube method, and 3) hole-in-tube method. The tube-in-tube method allows a fixed volume of blood to be added to the larger tube loaded with AMPS, but requires dexterity to assemble. The paper-in-tube method uses the wicking ability of a thin strip of chromatography paper with large pore sizes to add whole blood into the tube by simply touching the open end to a drop of blood, but causes lysis upon centrifugation to remove the blood from the paper. The hole-in-tube method allows a fixed volume to enter the preloaded tube via capillary action and a silicone sleeve covers the filling hole to prevent blood from leaking during centrifugation.

4.4. Validation and Preparation for Field Evaluation

Blood samples provided by our collaborators at Children's Hospital Boston allowed us to make rapid improvements on early iterations of our density-based test. Once densities of the AMPS were identified that provided discrimination between normal blood and blood from individuals with sickle cell disease, the design was frozen and testing was carried out on a larger number of samples (n = 59). To achieve this sample size, we collaborated with researchers at Tulane University and the Sickle Cell Center of Southern Louisiana, one of whom had been a postdoctoral fellow in the Whitesides group.

For the initial proof-of-principle, we included the main two genotypes of SCD (HbSS and HbSC) and also tested sickle cell trait (HbAS) along with other non-sickle cell subjects (HbAA). Initial results showed a promising ability to discriminate between SCD and non-SCD with only 10 minutes of centrifugation and a drop (~5 μL) of blood. To enable the test to leave the bench, we also began work on the issues of packaging and storage. We used various packaging materials and accelerated storage tests in an oven to assess the risk for evaporation.

4.5. How Funding was Obtained

Although the clinical need for a rapid test for SCD was clear from conversations with Dr. Stossel and Dr. Chunda-Liyoka, the way to fund such research was not apparent at first. In general, SCD suffers from a low level of funding, as is often the case with neglected tropical and orphan diseases. We began applying to a number of innovation awards focused on global health. One difficulty with these grants was pressure to already have data from the field to justify the award. Research to provide such data, however, required funding.

To obtain our initial funding for SCD, we had to think of other applications for the AMPS technology that would perhaps be more attractive to investors or granting agencies. By

proposing to useAMPS to both diagnose SCD and to explore circulating tumor cells, we were able to put together a successful proposal to the Blavatnik Biomedical Accelerator Fund. This award supported the development of the test and the field trial at UTH. A smaller award from the Harvard Global Health Institute enabled us to perform an evaluation of the usability of the test with end-users in rural clinics in Zambia.

4.6. Designing the Study

Dr. Stossel's connection to Zambia was one of the motivations for beginning work on a SCD diagnostic and, thus, work in Zambia was a natural choice for a field evaluation. Through Dr. Stossel, the team from Harvard connected with Dr. Chunda-Liyoka at UTH and began to draft grant applications, study protocols, and IRB submissions.

The site for the field evaluation was the Department of Paediatrics and the Department of Haematology at UTH in Lusaka, Zambia. The facilities at UTH could support equipment to do a gold standard measurement of SCD (i.e., hemoglobin electrophoresis) and UTH also had a large population of SCD patients. UTH regularly monitors patients with SCD through a program that included regular evaluation and follow-up. As a result of this program, over 3,000 patients with SCD are currently being managed by the program. Every Friday, roughly 50 patients visit a specific clinic in the hospital for continuing evaluation.

The primary relevance of a rapid test for SCD is for use in children, and hence, the study only enrolled subjects under 18 years of age. Working with children required consent of a guardian as well as assent for children above a certain age. Literacy and language differences also added to the requirements of the consenting process to ensure adequate protection of subjects. Working in close consultation with both the local IRB in Zambia and the Committee

on the Use of Human Subjects at Harvard was critical to ensure that all aspects of the ethics of the research were considered.

SCD screening at UTH relied primarily on solubility tests (Sickledex). Positive tests were followed up by gel electrophoresis. The electrophoresis equipment, however, was quite old and unreliable. Part of the study budget, therefore was allocated to update the clinical laboratory at UTH with a semi-automated hemoglobin electrophoresis unit (SAS1/2, Helena). In particular, this would allow quantitative measurements of different hemoglobin types, including fetal hemoglobin (HbF)—a parameter of interest for the density-based test. We also collected routine complete blood count (CBC) information on all subjects in the study and used a questionnaire to gather basic demographic information and information about factors that may constitute a confounding factor for our method (i.e., recent sickle crisis) so that we could understand the effect of these variables.

Outside of the medical data, we also designed methods to record tests that had packaging failures, temperature on the days testing was performed, and the time between the blood draw and the use of rapid and gold-standard tests. Guidelines for the use of samples for various tests (CBC, hemoglobin electrophoresis, and the rapid test) were decided based on guidelines from the manufacturers or, in the case of the rapid test, experience from initial validation. Samples that were processed on any method outside the recommended timeline would be invalid. One variable that was overlooked in the design phase of this trial was the inclusion of temperature and humidity loggers during shipment.

Through the Harvard Catalyst program, the team consulted with a biostatistician to design the size of the cohorts to be recruited in the study. The trial was designed to recruit ~600 subjects over six months. The process of designing the study, obtaining IRB approval, and

installing the new hemoglobin electrophoresis equipment took over nine months before the study could begin.

In addition to the evaluation of the performance of the test, we also wanted to evaluate the test in rural clinics for ease-of-use. Working with UTH and the U.S. Peace Corps in Zambia, we identified rural clinics to visit and designed a program to explain the test and receive feedback. The U.S.-based IRB committee declared the survey instrument to be exempt from full review as human subject research because of minimal risk and the nature of the information collected. The Zambian-based IRB committee, however, required a full review of the survey at the rural sites.

4.7. Implementation

Researchers from Harvard University traveled to Lusaka at the beginning of the trial. Over the course of a week, the trial was set up. A full day training of the study staff included the overall design of the study, workflow, recruitment, use of the rapid test, and management of data. Four readers were trained (two laboratory technicians and two nurses) using images of results of rapid tests and examples by an expert reader. A poster outlining each step of the use of the rapid test was placed prominently in the laboratory where rapid tests were run. A two-week pilot phase followed.

The pilot phase was critical for the success of the study. During this time, we evaluated initial concordance between the readers at UTH and the expert reader. We also identified and remedied potential problems with sample handling and workflow. For example, blood samples were collected in vacutainers containing ethylenediaminetetraacetic acid (EDTA) as an anticoagulant. A fraction of each sample was transferred to a second tube. One tube of the sample went to the laboratory running hemoglobin electrophoresis while the other tube went to

the laboratory running the rapid tests. Using separate laboratories aided with blinding the study. Initially, the second tube that blood was added to also contained EDTA. This additional EDTA could have caused dehydration of the cells and compromised the rapid test. This potential problem was identified during the pilot phase and all subsequent samples were aliquotted into untreated tubes after collection in anticoagulant treated tubes.

Halfway through the study, the expert reader from Harvard returned to the study site and performed a blinded test for concordance with three of the local Zambian readers. Throughout the study, the team at Harvard made batches of AMPS solutions and assembled packages with hundreds of rapid test to ship to the study site.

4.8. Context and Culture

Recruitment of subjects with SCD was generally much easier than recruitment of subjects without SCD because patients with SCD and their parents generally were more knowledgeable about the disease and the need for a rapid diagnostic test than the general population. Occasionally, parents chose not to participate in the study because there was concern about what could be done with the blood of their child. Some parents expressed a belief that a child has a finite amount of blood in their entire life and they were afraid that the child would not have blood left if they provided blood for the study in addition to a clinically indicated blood draw.

4.9. Challenges

Several unexpected obstacles threatened the completion of the study, but fortunately, all were overcome. At two points during the six month trial, nurses at UTH went on strike. Although the nurses on the study did not strike, their workload for their non-study obligations increased. The continued recruitment of subjects during this time is a testament to the commitment of these nurses to the study.

Near the middle of the study, a major fire broke out in the Nairobi International Airport in Kenya. Although far from the study site, this airport was part of the delivery route for the batches of AMPS tests shipped to Zambia. The fire occurred just after one batch had been shipped overseas and, as a result, that batch took an extra week to arrive at UTH. This extra shipping time could have compromised the tests, but unfortunately, the conditions during shipment are unknown. Indeed, the performance of the delayed batch was significantly worse than the other batches (Chapter 5), but without additional information, we could not justify exclusion from the data analysis. This experience demonstrates the importance of setting clear parameters for valid results, including shipping and storage conditions, along with the use of temperature and humidity loggers to capture the relevant data.

Although the nurses' strike did not halt the study, supply-chain problems did cause a temporary pause. Initially, we purchased about 20% more electrophoresis gels than we believed would be required for the study. A fault in the heating unit in the electrophoresis instrument meant that only eight out of twelve lanes ran properly. Delays in getting a technician to fix the instrument meant that we ran out of gels before recruitment was complete. As a result, we suffered a one month halt in the study while we waited for additional gels from the supplier. Even though we were not able to recruit the number of subjects that we had wanted due to the delays, we were still able to collect enough samples to retain statistical power before the budget for the study was spent. The dependence of the gold standard device on maintenance and technical expertise highlighted the need for simplicity in design of diagnostics for the POC.

4.10. Lessons learned

The details of the performance of the device and user feedback are described in Chapter 5. Briefly, of the two prototypes tested, the best system had a diagnostic accuracy of 77%. In

general, false positives were more frequent than false negatives (more so than was found in the initial validation studies). Variation in performance between batches was fairly significant. We are actively working on improving quality controls and developing standards to use with the rapid tests to reduce the variability between batches. Concordance between readers was high, but could be improved by clearer guides for readers and more extensive training.

Apart from the technical knowledge gained from the field evaluation, we also gained significant contextual knowledge. The visit to the rural clinics was particularly informative. We were able to verify that appropriate interventions for SCD existed in rural clinics as well as off-grid access to power through solar panels charging car batteries.

Perhaps one of the most interesting outcomes of the field evaluation came to light during exit interviews of the study staff in Zambia by the Harvard team. A number of staff members commented—without any specific prompting—that they had a new perspective when thinking about using diagnostics and developing technology for issues relevant to Zambia; if researchers abroad could come up with low-cost rapid tests, perhaps they could also come up with useful technologies. Although quantifying the impact of inspiration and modeling innovation is difficult, at best, the aspect of directly sharing knowledge and skills during such an international collaboration is a welcome side-effect of co-creation and field-evaluation.

4.11. Next Steps

Development of the next generation prototype is underway. Data from the field validation and initial work has enabled us to write new grants and has sparked conversations with companies interested in developing the technology. Although nothing is concluded at this point, the results of the field evaluation allows us to think, seriously, about real translation either as a startup or by licensing to an established company.

5. Conclusions & Recommendations

5.1. General lessons learned

In both cases presented here, the technologies are not yet products, but field evaluation has brought significant gains in understanding the technology and has identified specific deficiencies to address. Based on our experiences, we believe the following five pieces of advice will assist the scientist who has developed a POC diagnostic in setting up a field trial: 1) *Begin planning and partnerships early.* Ideally, partnerships should be in place before applying for grants. Long-standing partnerships allow clear communications that allow a team to properly identify a problem and also to work through challenges of performing a field trial while maintaining good relations; 2) *Get feedback early and often.* Even if a full field trial is not appropriate for the stage of development that a device is at, getting feedback about the design and use of a device consistently throughout development will improve its quality and the chances of success in a large field trial; 3) *Track every variable.* No matter how much validation is done, there will be variables that are not accounted for in the technical specifications of a device. Even if every variable is not controlled, most variables can be measured and these data may prove to be the key to understanding the results from the field; 4) *Aim for more subjects than the minimum needed.* Unexpected problems can pause or end a study prematurely. Be sure to understand the statistical power of your study and what your acceptable loss in recruited subjects would be before the study loses value. Within reason, aim for more than you would need so that you can be flexible with the timing of the study; 5) *Have patience.* Take the time to get IRB approval, define every part of the protocol, work out the details of the supply chain, and do a pilot study to ensure the field trial is successful.

5.2. From the Bench to the Field, and the Field to the Shelf

Field evaluations are not only the purview of companies. Although a partnership between a company (DFA) and an academic group (the Whitesides group) developed the LFT, an NGO (PATH) led the field evaluation of the LFT device. An academic group (the Whitesides group), led the field evaluation of the AMPS-based rapid test for SCD with partners at UTH. In fact, the ability to demonstrate functionality (even imperfect functionality) in the field provides an academic group the chance to leverage more funding and piques the interest of potential commercial partners.

Someday, we hope that both the LFT and the SCD-AMPS could be available on the shelf of a clinic as a finished product. When that day arrives, the experience and lessons of early field evaluations will surely have played an important role.

Acknowledgements

The authors thank Patrick Beattie (DFA), Sidhartha Jain (DFA), Nira Pollock (BIDMC), Sarah McGray (PATH), Bernhard Weigl (PATH), Sarah Vella (former Whitesides group member), Andres Martinez (former Whitesides group member), Sariah Kormee (Harvard Medical School), and Dr. Catherine Chunda-Liyoka (UTH) for helpful conversations and discussions. A.A.K. acknowledges support from a Graduate Research Fellowship from the National Science Foundation.

References

(1) Martinez, A. W.; Phillips, S. T.; Butte, M. J.; Whitesides, G. M. *Angew. Chem. Int. Ed. Engl.* **2007**, *46*, 1318–1320.

(2) Mace, C. R.; Akbulut, O.; Kumar, A. A.; Shapiro, N. D.; Derda, R.; Patton, M. R.; Whitesides, G. M. *J. Am. Chem. Soc.* **2012**, *134*, 9094–9097.

(3) Pollock, N. R.; Rolland, J. P.; Kumar, S.; Beattie, P. D.; Jain, S.; Noubary, F.; Wong, V. L.; Pohlmann, R. A.; Ryan, U. S.; Whitesides, G. M. *Sci. Transl. Med.* **2012**, *4*, 152ra129.

(4) Pollock, N. R.; McGray, S.; Colby, D. J.; Noubary, F.; Nguyen, H.; Nguyen, T. A.; Khormaee, S.; Jain, S.; Hawkins, K.; Kumar, S.; Rolland, J. P.; Beattie, P. D.; Chau, N. V; Quang, V. M.; Barfield, C.; Tietje, K.; Steele, M.; Weigl, B. H. *PLoS One* **2013**, *8*, e75616.

(5) Peeling, R. W.; Mabey, D. *Clin. Microbiol. Infect.* **2010**, *16*, 1062–1069.

(6) Mabey, D.; Peeling, R. W.; Ustianowski, A.; Perkins, M. D. *Nat. Rev. Microbiol.* **2004**, *2*, 231–240.

(7) Yager, P.; Domingo, G. J.; Gerdes, J. *Annu. Rev. Biomed. Eng.* **2008**, *10*, 107–144.

(8) Chin, C. D.; Linder, V.; Sia, S. K. *Lab Chip* **2007**, *7*, 41–57.

(9) Kettler, H.; White, K.; Hawkes, S. *Mapping the Landscape of Diagnostics for Sexually Transmitted Infections: Key Findings and Recommendations*; 2004; pp. 1–44.

(10) Pai, N. P.; Vadnais, C.; Denkinger, C.; Engel, N.; Pai, M. *PLoS Med.* **2012**, *9*, e1001306.

(11) Weigl, B. H.; Boyle, D. S.; de los Santos, T.; Peck, R. B.; Steele, M. S. *Expert Rev. Med. Devices* **2009**, *6*, 461–464.

(12) Caldwell, B. A.; Young, A.; Gomez-Marquez, J.; Olson, K. R. *IEEE Pulse* **2011**, 63–67.

(13) VanVoorhis, C.; Morgan, B. *Tutor. Quant. Methods Psychol.* **2007**, *3*, 43–50.

(14) National Committee for Clinical Laboratory Standards. *Procedures and Devices for the Collection of Diagnostic Capillary Blood Specimens (Approved Standard HA-A5)*; 5th ed.; NCCLS: Wayne, PA, 2004; Vol. 24.

(15) Metz, C. *Semin. Nucl. Med.* **1978**, *VIII*, 283–298.

(16) Bland, J. M.; Altman, D. G. *Stat. Methods Med. Res.* **1999**, *8*, 135–160.

(17) Pocock, S. J.; Friedman, L. M.; Furberg, C. D.; Demets, D. L. *Fundamentals of Clinical Trials*; 1982; Vol. 38, p. 873.

(18) Glasgow, R.; Magid, D.; Beck, A. *Med. Care* **2005**, *43*, 551–557.

(19) Lachin, J. *Control. Clin. Trials* **1981**, *113*, 93–113.

(20) Button, K. S.; Ioannidis, J. P. A.; Mokrysz, C.; Nosek, B. A.; Flint, J.; Robinson, E. S. J.; Munafò, M. R. *Nat. Rev. Neurosci.* **2013**, *14*, 365–376.

(21) United Nations. *Political Declaration on HIV and AIDS: Intensifying Our Efforts to Eliminat HIV and AIDS*; 2011; pp. 1–17.

(22) Martínez, E.; Blanco, J. L.; Arnaiz, J. A.; Pérez-Cuevas, J. B.; Mocroft, A.; Cruceta, A.; Marcos, M. A.; Milinkovic, A.; García-Viejo, M. A.; Mallolas, J.; Carné, X.; Phillips, A.; Gatell, J. M. *AIDS* **2001**, *15*, 1261–1268.

(23) Panel on Antiretroviral Guidelines for Adults and Adolescents. *Dep. Heal. Hum. Serv.* **2009**.

(24) Maartens, G.; Venter, F.; Meintjes, G.; Cohen, K. *Southern African HIV Clinicians Society Guidelines for Antiretroviral Therapy in Adults*; 2008; pp. 1–23.

(25) *Current Medical Diagnostics and Treatment*; McPhee, S. J.; Papadakis, M. A., Eds.; 49th ed.; McGraw Hill: New York, 2010; pp. 599–600.

(26) Ministry of Health (Vietnam). *Guidelines for HIV/AIDS Diagnosis and Treatment*; Ha Noi, 2009; pp. 1–193.

(27) Piel, F. B.; Hay, S. I.; Gupta, S.; Weatherall, D. J.; Williams, T. N. *PLoS Med.* **2013**, *10*, e1001484.

(28) Hankins, J.; Ware, R. E. *Lancet* **2009**, *374*, 1308–1310.

(29) Gaston, M.; Verter, J.; Woods, G.; Pegelow, C.; Kelleher, J.; Presbury, G.; Zarkowsky, H.; Vichinsky, E.; Iyer, R.; Lobel, J.; Diamond, S.; Holbrook, C.; Gill, F.; Richey, K.; Faletta, J. *N. Engl. J. Med.* **1986**, *314*, 1593–1599.

(30) Weems, H. B.; Lessin, L. S. *Acta Haematol.* **1984**, *71*, 361–370.

(31) Fabry, M. E.; Mears, J. G.; Patel, P.; Schaefer-Rego, K.; Carmichael, L. D.; Martinez, G.; Nagel, R. L. *Blood* **1984**, *64*, 1042–1046.

(32) Grover, W. H.; Bryan, A. K.; Diez-Silva, M.; Suresh, S.; Higgins, J. M.; Manalis, S. R. *Proc. Natl. Acad. Sci. U. S. A.* **2011**, *108*, 10992–10996.

(33) Brugnara, C.; Ha, T. Van; Tosteson, D. C. *Blood* **1989**, 487–495.

(34) Brugnara, C. *J. Pediatr. Hematol. Oncol.* **2003**, *25*, 927–933.

Chapter 3

Enrichment of Reticulocytes from Whole Blood using Aqueous Multiphase Systems of Polymers

Ashok A. Kumar[1], Caeul Lim[2], Yovany Moreno[2], Charles R. Mace[3], Abeer Syed[3], Daria Van Tyne[2], Dyann F. Wirth[2], Manoj T. Duraisingh[2], and George M. Whitesides[3,4]

[1]School of Engineering and Applied Sciences, Harvard University, 29 Oxford St., Cambridge, MA 02138, United States

[2]Harvard School of Public Health, Harvard University, 677 Huntington Avenue, Boston, MA 02115, United States

[3]Department of Chemistry & Chemical Biology, Harvard University, 12 Oxford St., Cambridge, MA 02138, United States

[4]Wyss Institute for Biologically Inspired Engineering, Harvard University, 60 Oxford St., Cambridge, MA 02138, United States

Abstract

This chapter demonstrates the enrichment of a reticulocytes by centrifuging whole blood through aqueous multiphase systems (AMPS)—immiscible phases of solutions of polymers that form step-gradients in density. The interfaces of an AMPS concentrate cells; this concentration facilitates the extraction of blood enriched for reticulocytes. Varying the osmolality and density of the phases of AMPS provides different levels of enrichment and yield of reticulocytes. A maximum enrichment of reticulocytemia of 64 ± 3 % was obtained. Several species of malaria parasites show a preference to invade young erythrocytes and reticulocytes; this preference complicates *in vitro* cultivation of these species in human blood. *Plasmodium knowlesi* malaria parasites invade human blood enriched for reticulocytes to 4–21% by AMPSs at a rate 2.9 times greater than they invade unenriched blood. Parasite invasion in blood enriched by AMPS was 1.3 times greater than in blood enriched to a similar reticulocytemia by differential centrifugation followed by centrifugation over Percoll.

Introduction

The characterization of different cellular components of human whole blood plays an important role in medical diagnoses and research.[1] This task is often accomplished by isolating or enriching a specific cellular sub-population from the complex mixture of cells found in whole blood. Whole blood is composed of cells—leukocytes, platelets, and erythrocytes—suspended in protein-rich plasma; each type of cell is useful in the evaluation of the health of a patient. These cells can be further subdivided into important components. For example, the isolation of reticulocytes—immature erythrocytes—is important for research on malaria.

Plasmodium (P.) vivax, *P. ovale,* and *P. knowlesi*—three causative agents of malaria in humans—preferentially invade human reticulocytes.[2–4] The study of these species of malaria suffers from the practical difficulty of *in vitro* cultures in whole human blood. Their cultivation in blood enriched for reticulocytes would provide concentrated host cells in which the parasites proliferate; continuous cultures of these parasites would make their study much more practical.[4–7] Enrichment is difficult because reticulocytes exist at a low concentration (0.5–2.5% of erythrocytes) in whole blood[8] and have a short half-life in culture (~30 hours).[9] Cryopreservation provides a method to store samples that have been enriched with reticulocytes,[10] but enriched samples must be obtained prior to freezing. A method to routinely enrich reticulocytes from normal, whole blood with high yields and reproducibility would enable more scientists to perform research with reticulocytes.

This paper describes a new method to obtain samples of cells that are enriched for reticulocytes using centrifugation through aqueous multiphase systems (AMPSs). AMPSs are systems of polymers in aqueous solutions that generate immiscible phases when mixed. These

phases provide self-assembling step-gradients in density.[11] We demonstrate that centrifugation through AMPSs separates cells based on their density, and concentrates them at interfaces. *P. knowlesi* multiplies at a higher rate in reticulocytes enriched by this method than in normal human blood or in blood enriched for reticulocytes by conventional means (differential centrifugation followed by centrifugation over Percoll). We exploit two differences between reticulocytes and mature erythrocytes—density and osmotic response to hypotonic and hypertonic environments—to enrich reticulocytes from whole blood to a maximum reticulocytemia of 64 ± 3%.

Current methods to obtain substantially enriched (> 15% of erythrocytes) samples of reticulocytes are impractical, expensive, labor-intensive, or not satisfactory for routine use for applications that require reproducible yields. These methods include culture and development of progenitors,[12] differential centrifugation,[13] centrifugation over layered gradients,[14] and affinity-based separation.[15] We describe these methods in Appendix I.

Density provides a label-free characteristic to use in enriching reticulocytes. The average density of reticulocytes is slightly lower than that of mature erythrocytes ($\Delta\rho \approx 0.009$ g/cm^3).[16,17] The reticulocyte population is concentrated in the least dense quarter of the distribution of densities of erythrocytes.[17,18] AMPSs provide steps in density suitable for enriching reticulocytes from blood.

Each phase of an AMPS consists predominantly (60–95% (w/v)) of water, and contains concentrations of polymers or surfactants ranging from 1–40% (w/v) (that is, micromolar to millimolar). These compositions determine the physical properties of the phases of an AMPS (e.g., density, viscosity, ionic strength, and refractive index). The phases order, on settling or on centrifugation, according to their densities.[19] Many AMPSs are biocompatible[20] and have been

used for separations of cells by partitioning[21–25]—that is, by a process based on the preferential interaction of the surfaces of different types of cells with the components of the different phases.[26] Partitioning methods result in relatively low enrichment of reticulocytes (< 2%).[25]

The differences in the densities of the phases of AMPSs provide a means to perform density-based separations.[11] The interfaces between phases mark discontinuities (on the molecular scale) between continuous fluid phases of different density. The densities (ρ_A and ρ_B) of the phases above and below the interface establish the range of densities for components (ρ_C) that will localize at the interface ($\rho_A > \rho_C > \rho_B$). The interfacial surface energy between the phases of an AMPSs is astonishingly low (from nJ/m^2 to mJ/m^2);[27] a low interfacial surface energy reduces the mechanical stress on cells as they pass through the interface.

Compared to layered gradients in density (e.g., Percoll, Optiprep, or Nycodenz), AMPSs offer several advantages: i) they are thermodynamically stable, ii) they self-assemble rapidly (t ~ 15 minutes, 2000 *g*) on centrifugation or slowly (t ~ 24 hours) on settling in a gravitational field, iii) they can differentiate remarkably small differences in density ($\Delta\rho < 0.001$ g/cm^3), and iv) they provide well-defined interfaces that facilitate both the identification and extraction of sub-populations of cells by concentrating them to quasi-two-dimensional surfaces.

Experimental Design and Methods

The choice of AMPSs to enrich reticulocytes from blood requires many considerations. When blood is layered on top of an AMPS, the region between the top phase and the blood forms a boundary of density like those found in layered gradients. This boundary is diffuse and unstable because plasma is soluble in the phases of AMPSs. Cells concentrated at the boundary, therefore, are not confined sharply, and the subsequent recovery of cells from the boundary region is more difficult than from a well-defined interface between two immiscible phases. The

two phases of a two-phase AMPS provide two well-defined interfaces—one between the two phases of the AMPS, and one between the denser phase and the bottom of the container—in addition to the boundary that is formed with the blood. In this arrangement, one interface (that between the two liquid phases of the AMPS) collects the enriched reticulocytes, and one interface (that between the denser phase and the bottom of the tube) collects the remaining erythrocytes. An AMPS with more than two phases could also enrich reticulocytes. Each additional phase could isolate a different population of cells, but would add to the complexity of the phase separation. To separate a reticulocyte-rich sub-population from mature erythrocytes, we thus chose to use an AMPSs with two phases, also known as an aqueous two-phase system (ATPS).[19,28]

We surveyed several previously reported AMPSs (Appendix I). A system prepared from dextran (MW ≈ 500 kD) and Ficoll (MW ≈ 400 kD) satisfied our two selection criteria: i) the ability to create a small step in density to separate reticulocytes from mature erythrocytes, and ii) the ability to maintain physiological pH while allowing the tonicity to be tuned. In blood, the physiological reference range for pH is 7.38–7.44, and for osmolality is 285–295 mOsm/kg.[8] Changes to either of these parameters will result in changes to the morphology and density of blood cells. We describe methods to prepare and characterize the AMPSs that we use in this communication in Appendix I.

We prepared a series of dextran–Ficoll AMPSs at various densities and osmolalities. We expected that differences between ion transport in reticulocytes and mature erythrocytes would enhance differences in density due to unequal responses to osmotic stress [14]. Osmolality thus provided an additional parameter to tune the separation of these cells based on density.

A range of available densities and tonicities—controlled by the concentrations of polymers and salts in each phase—allowed us to investigate the influence of these factors on both the final purity and the yield of reticulocytes concentrated at the interface of the AMPS. Based on literature precedent, we expected an AMPS with a density of the bottom phase near 1.080 g/cm^3 to isolate a band of reticulocyte-rich erythrocytes at the upper interface of the bottom phase [17]. We explored a range of densities for a bottom phase near this value. For hypertonic and hypotonic systems, we explored ranges of densities based on expected shifts in density from changes in hydration (**Appendix I; Table I.1**).

In addition to reticulocytemia, we also chose to characterize yield and scale for our separations. Yield and scale are important characteristics of reticulocyte enrichment for the cultivation of malaria parasites. Systems that scale well to large volumes (> 10 mL of blood) and attain > 10 µL of packed reticulocytes would decrease the burden of time and resources to maintain cultures of *P. knowlesi*, *P. vivax*, or *P. ovale*. Changing the volume ratio of blood to polymer affected the final enrichment of reticulocytes (**Appendix I; Figures I.1 & I.2**). A constant volume ratio of blood to polymer, however, achieves reproducible results at different scales (**Appendix I; Figure I.3**). Details of the effects of volume ratio and scale are provided in Appendix I.

Results

AMPSs can enrich reticulocytes to a high purity. Upon sedimentation of 1 mL of blood through 4 mL of a hypertonic (φ = 330 mOsm/kg) AMPS of 11.6% (w/v) of dextran and 11.6% (w/v) Ficoll (ρ_{top}= 1.086 g/cm^3 and ρ_{bottom}= 1.089 g/cm^3), we observed two layers of erythrocytes: one layer at the liquid/liquid interface between the two phases of the AMPS and

one layer between the bottom phase and the container (**Figure 3.1**). After extracting cells with a pipette and washing them in phosphate buffered saline (PBS), cells were stained either with New Methylene Blue (to visualize intracellular RNA in reticulocytes by microscopy) or with acridine orange (to quantify reticulocytes by flow cytometry).

For hypertonic, isotonic, and hypotonic systems, we found specific densities of the dextran–Ficoll AMPS that provided highly enriched reticulocytes (**Figure 3.2, Appendix I; Figure I.4**). **Appendix I; Table I.1** details the parameters of each AMPS and the results of each enrichment procedure. For small shifts in osmolality, the difference in density between an object and water scales with the osmolality (Appendix I); the density of the best-performing hypotonic system is lower than that of the best-performing hypertonic system. A hypotonic (φ = 269 mOsm/kg) AMPS of 9.3% (w/v) dextran and 9.3% (w/v) Ficoll with ρ_{top}= 1.068 g/cm^3 and ρ_{bottom}= 1.072 g/cm^3 enriched reticulocytes to 55 ± 8% at the interface of the AMPS (**Figure 3.2**). Although this system provided the highest purity of enrichment for a 1:4 volume ratio of blood to AMPS, it collected less than 10^7 cells (~1 μL of packed cells) at the interface.

We also explored different volume ratios of blood to AMPSs to see if we could attain similar purities with a lower relative volume of AMPSs (**Appendix I; Table I.4**). A 1:1 volume ratio of blood to a hypertonic (φ = 336 mOsm/kg) AMPS of 11.4% (w/v) dextran and 11.4% (w/v) Ficoll (ρ_{top}= 1.084 g/cm^3 and ρ_{bottom}= 1.088 g/cm^3) provided the greatest enrichment of reticulocytes (up to 64 ± 3%) at the interface of the AMPS (**Figure 3.2, Appendix I; Figure I.4**).

Variations between individuals can lead to significant differences in the performance of density-based separation methods. We enriched reticulocytes using four dextran–Ficoll AMPSs from the initial screen, and blood from four different donors (**Table 3.1**). Increasing the ratio

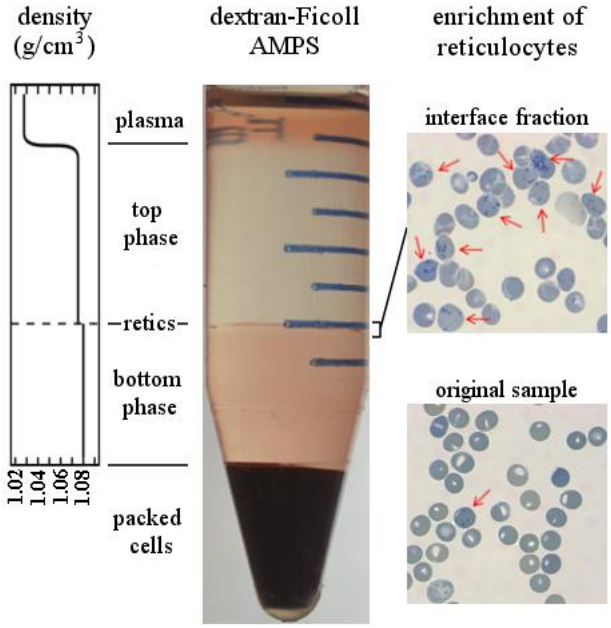

Figure 3.1. A hypertonic (φ = 330 mOsm/kg) AMPS of 11.6% (w/v) dextran and 11.6% (w/v) Ficoll (ρ_{top}= 1.086 g/cm^3 and ρ_{bottom}= 1.089 g/cm^3) provides a step-gradient in density capable of enriching reticulocytes from blood. Centrifugation of blood depleted of leukocytes over a column of the AMPS leaves the plasma above the top phase and a reticulocyte-rich layer of cells at the liquid/liquid interface (retics); the remaining erythrocytes pack below the bottom phase (packed cells). Arrows on the micrographs indicate reticulocytes. The bottom phase becomes pink from the presence of suspended cells that are nearly isodense with that phase and, hence, do not settle at an interface for the centrifugation parameters used.

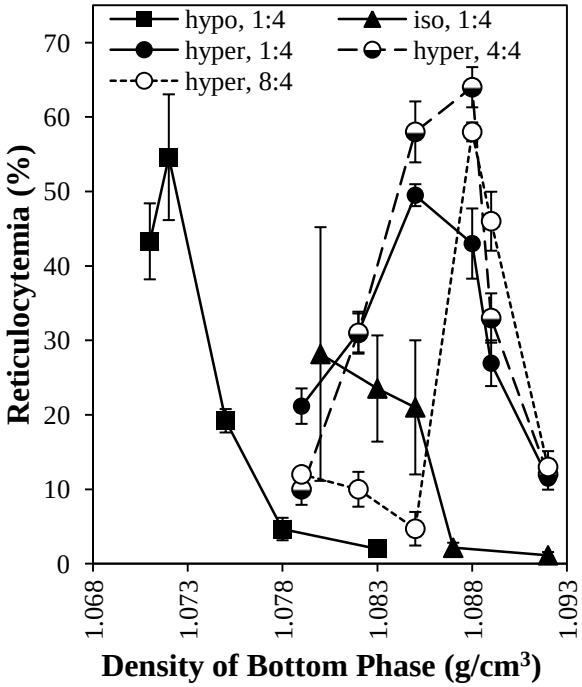

Figure 3.2. The fraction of blood at the interface of several AMPSs are enriched to a reticulocytemia over 50%. Filled, black symbols mark results from hypotonic (hypo)—square, isotonic (iso)—triangle and hypertonic (hyper)—circle—series of AMPSs where the volume ratio of blood to AMPS was kept constant at 1:4. The half-black, half-white and white circles illustrate hypertonic series with volume ratios of blood to AMPS of 4:4 and 8:4. Error bars depict the average deviation from the mean of triplicate experiments.

Table 3.1. Performance of AMPS-enrichment of reticulocytes with multiple (*n = 4*) donors compared to a combination of differential centrifugation and layered Percoll.

	Density (g/cm^3)		Osmolality	Reticulocytemia (%)		Yield of Reticulocytes[a] (%)	
ID[b]	ρ_{top}	ρ_{bot}	(mOsm/kg)	Median	[Min, Max]	Median	[Min, Max]
C1	1.089	1.092	330	19	[15, 21]	1.6	[0.24, 6]
C2	1.086	1.089	330	29	[15, 32]	0.90	[0.095, 1.7]
A5	1.076	1.080	295	36	[18, 49]	0.012	[0.0065, 1.1]
B3	1.071	1.075	260	40	[15, 45]	0.0061	[0.00079, 0.012]
DC-P[c]	--	--	--	38	[6.0, 86]	0.61	[0.12, 9.7]

[a] The percentage of the total reticulocytes from blood loaded on a system that are found in the enriched fraction.
[b] IDs refer to specific densities and tonicities of the dextran–Ficoll AMPS specified in Appendix I; Table I.1.
[c] Enrichments done by differential centrifugation followed by centrifugation over layered Percoll (DC-P).

of the volume of blood to polymer to 1:1 (i.e., 4 mL blood on 4 mL of AMPS) increased the yield of reticulocytes as measured by flow cytometry (Appendix I).

The degree of enrichment and final yield varied significantly between donors (**Appendix I; Table I.2**). The last three AMPSs from **Table 3.1** demonstrate, however, that similar enrichments can be achieved between systems with different tonicities. The density of these systems increases as a function of osmolality, reflecting the increase in the mean density of the reticulocyte and mature erythrocyte populations. Interestingly, in the systems with similar enrichments, the median yield is two times greater in the hypertonic AMPS than in the isotonic AMPS; it is more than 70 times greater in the isotonic AMPS than in the hypotonic AMPS. We also compared our systems to a common enrichment method: differential centrifugation of blood followed by centrifugation of the enriched fraction over a layered gradient of Percoll (DC-Percoll). The enrichments with DC-Percoll showed a high degree of variability, with some separations attaining high yield (9.6%) and low purity (6.0%), and others attaining low yield (0.12%) and high purity (86%). The hypertonic systems of AMPS provide a higher median yield, and their ranges for reticulocytemia and reticulocyte yield are smaller than blood enriched by DC-Percoll. Separations with AMPS provide better reproducibility than DC-Percoll.

Malaria parasites invade reticulocytes enriched by centrifugation through an AMPS. To ensure that we obtained a sufficient number of reticulocytes to perform an invasion assay after enrichment, we chose system C1 (**Table 3.1**). We layered 25 mL of blood over 25 mL of the dextran–Ficoll AMPS in 50 mL conical tubes. After centrifugation, we collected the cells from the interface using sterile technique and washed them three times in a 100-fold volume of PBS. After washing, the morphology of the cells was comparable to the morphology before exposure to AMPS (**Appendix I; Table I.3, Figure I.5**); these cells were then used for culture.

Appendix I; Table I.4 details the reticulocytemia of enrichments from different donors. We added purified late-stage parasites (e.g., late trophozoites and schizonts) of *P. knowlesi* H strain to the culture medium at a parasitemia—the percentage of erythrocytes that contain parasites—between 0.5–2.5%. This mixture of enriched reticulocytes and parasites incubated at culture conditions for 18 hours. This time is sufficient to allow late-stage parasites to mature and rupture, and then to release infectious merozoites into the suspension of erythrocytes enriched in reticulocytes.

We quantified the ability of parasites to reinvade by the parasitized erythrocyte multiplication rate (PEMR)—the ratio of the initial parasitemia to the parasitemia after 18 hours. If merozoites can invade the AMPS-enriched reticulocytes, we would expect to see an increase in the parasitemia after 18 hours (PEMR > 1); a PEMR > 1 is necessary for long-term cultivation of malaria parasites. Reinvasion is an important step in culture that depends in part on the surface of the host cells; if residual polymers on the surface of reticulocytes compromised cultivation, we expected the effect would be most pronounced during reinvasion.

Figure 3.3 shows the results from invasion assays using blood enriched by AMPS as well as results from similar invasion assays using normal human blood, blood enriched for reticulocytes by DC-Percoll, and blood from rhesus monkeys—the well-established experimental host for *P. knowlesi*.[29] In normal human blood, the PEMR was often less than one because *P. knowlesi* H strain is limited to invasion of human reticulocytes and young erythrocytes.[4] Blood enriched by DC-Percoll provides a benchmark comparison for reticulocyte enrichment. For each invasion assay, we matched the enrichment of reticulocytes from DC-Percoll with that from AMPSs by diluting the more enriched sample with whole blood. Reticulocytemia in enriched

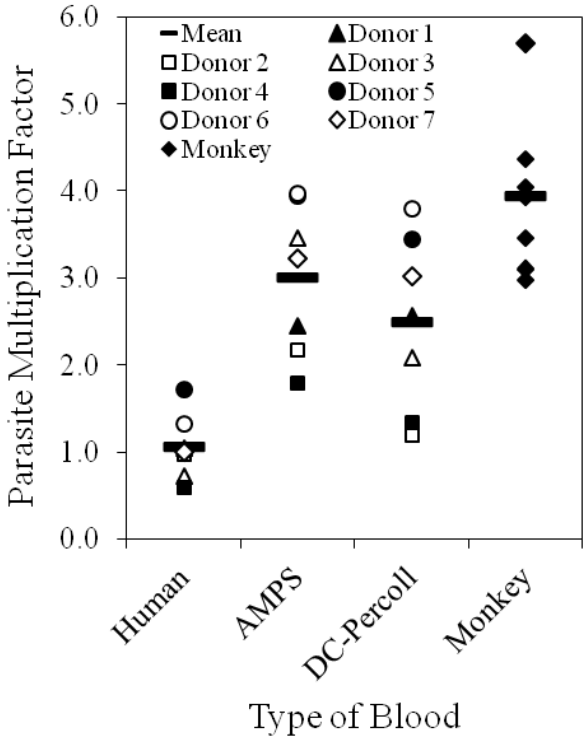

Figure 3.3. Reticulocytes enriched through a dextran–Ficoll AMPS are invaded by *P. knowlesi*. Parasites cultured in normal human blood (Human), AMPS-enriched human blood (AMPS), DC-Percoll-enriched human blood (DC-Percoll), and rhesus blood (Monkey) show invasion after 18 hours. *P. knowlesi* parasitemia increased more in media that contained blood enriched for reticulocytes by centrifugation in a dextran–Ficoll AMPS than in normal human blood. The horizontal bars indicate the mean parasitized erythrocyte multiplication rate (PEMR) for each invasion assay. For human blood (Human, AMPS, DC-Percoll) each symbol represents average results from a different donor ($n = 7$) performed in triplicate. Assays performed with blood from different monkeys are all shown with the same symbol (filled diamond).

samples was between 4–21%. Blood from a rhesus monkey provided a positive control in which multiplication of parasites was unrestricted by the availability of host cells.

Blood from seven subjects provided biological replicates. We performed three technical replicates with each subject. We prepared thin smears of the samples immediately after the introduction of late stage parasites to the blood samples and at 18 hours after cultivation. After staining the slides with Field's Stain, we quantified the parasitemia of each sample (Appendix I).

As expected, the multiplication rate in rhesus blood was greater than any of the human samples (**Figure 3.3**). The enriched blood from both AMPSs and DC-Percoll performed better than normal blood to support the invasion of *P. knowlesi.* On average, the PEMR in blood enriched by AMPSs was 2.9 times that of normal blood (p-value < 0.01). Microscopy confirmed that the parasites that had invaded the reticulocyte-rich blood from AMPSs continued to develop normally in culture. The average PEMR in blood enriched by AMPSs was 1.3 times that of blood enriched by DC-Percoll (p-value < 0.05).

Discussion

We have demonstrated that sedimentation through AMPSs is a useful technique to separate cells by density. AMPSs concentrate cells at molecularly sharp interfaces that provide well-defined steps in density, and this concentration facilitates the enrichment of cell types that differ in density. Specifically, AMPSs can enrich reticulocytes from human whole blood. *P. knowlesi* H strain invades blood enriched for reticulocytes by AMPSs at a higher rate than it invades normal blood or blood enriched for reticulocytes by DC-Percoll. The ability to reproducibly enrich reticulocytes from normal, whole blood should benefit research involving reticulocytes, such as efforts to culture malaria species that preferentially invade reticulocytes (i.e., *P. vivax, P. knowlesi*, and *P. ovale*).

Existing methods to enrich reticulocytes are not suitable for the routine enrichments that would be required for a sustainable continuous culture. Differential centrifugation provides a simple method to enrich reticulocytes, but the enrichment is low (< 3%).[13] Affinity-based separation techniques and the direct growth of reticulocytes allows high purity (> 90%) that is not matched by enrichments using AMPSs, but these methods are expensive and impractical for routine use.[15] DC-Percoll provides a means to enrich reticulocytes, but this method requires two separate centrifugation steps and two extraction steps; variation between steps compound to reduce reproducibility. Exposure to Percoll may also impair parasite development for specific strains of malaria parasites,[30] and may, partly, explain the greater invasion of reticulocytes enriched by AMPS compared to those enriched by DC-Percoll.

Enriching reticulocytes through AMPSs retains the simplicity of differential centrifugation (layering blood over an AMPS adds only one step to the general procedure), but provides much higher levels of enrichment (median reticylocytemia of 19%). The scalability of AMPSs also allows researchers to process large volumes (~1 L) of blood in a single centrifugation step. The combination of purity, scalability, and simplicity make centrifugation through AMPSs a valuable technique for separations of cells that require high throughput and routine use. The use of AMPSs to separate cells by density should aid in the cultivation of malaria species that require reticulocyte-rich blood, and facilitate the separation of other cells with natural differences in density such as lymphocytes and erythrocytes, as well as sickled erythrocytes and normal erythrocytes.

Supporting Information

Supporting Information is provided in Appendix I and includes materials and methods, experimental details, analyses of separations, study of volume and osmotic effects, and additional background.

Financial Disclosure

This work was supported by the Bill and Melinda Gates Foundation [OPP1016360 and OPP1023594]; the Office of Naval Research [NDSEG Fellowship to A.A.K.]; the Louis-Berlinguiet Program Postdoctoral Research Scholarship in Genomics – Fonds the Recherche du Quebec, Nature et Technologies to Y.M.; the Royal Society of Edinburgh's J.M. Lessell's Scholarship to A.S and the Mac Roberston Postgraduate Travel Scholarship to A.S. The funders had no role in study design, data collection and analysis, decision to publish, or preparation of the manuscript.

Acknowledgements

The authors thank Dr. Carlo Brugnara and Jessica Alves (Children's Hospital, Boston, MA) for lending their expertise and equipment for hematology analysis, Kate Fernandez (Harvard School of Public Health, MA) for valuable assistance in preliminary studies on *P. falciparum*, and Matt Patton (Harvard University, MA) for assistance preparing and characterizing solutions of polymers. The authors thank Brigham and Women's Hospital, Boston for providing blood samples.

References

(1) Bunn, H. F.; Aster, J. C. *Pathophysiology of Blood Disorders*; McGraw Hill Medical: New York, 2011; p. 342.

(2) Galinski, M.; Barnwell, J. *Parasitol. Today* **1996**, *1*, 20–29.

(3) Mons, B.; Collins, W. E.; Skinner, J. C.; van der Star, W.; Croon, J. J.; van der Kaay, H. J. *Exp. Parasitol.* **1988**, *66*, 183–188.

(4) Lim, C.; Hansen, E.; Desimone, T. M.; Moreno, Y.; Junker, K.; Bei, A.; Brugnara, C.; Buckee, C. O.; Duraisingh, M. T. *Nat. Commun.* **2013**, *4*, 1638.

(5) Mueller, I.; Galinski, M. R.; Baird, J. K.; Carlton, J. M.; Kochar, D. K.; Alonso, P. L.; del Portillo, H. A. *Lancet Infect. Dis.* **2009**, *9*, 555–566.

(6) Basco, L. K.; Le Bras, J. *Parasitol. Res.* **1994**, *80*, 262–264.

(7) Golenda, C. F.; Li, J.; Rosenberg, R. *Proc. Natl. Acad. Sci. U. S. A.* **1997**, *94*, 6786–6791.

(8) Kratz, A.; Ferraro, M.; Sluss, P. M.; Lewandrowski, K. B. *N. Engl. J. Med.* **2004**, *351*, 1548–1564.

(9) Skadberg, O.; Brun, A.; Sandberg, S. *Lab. Hematol.* **2003**, *9*, 198–206.

(10) Borlon, C.; Russell, B.; Sriprawat, K.; Suwanarusk, R.; Erhart, A.; Renia, L.; Nosten, F.; D'Alessandro, U. *Int. J. Parasitol.* **2012**, *42*, 155–160.

(11) Mace, C. R.; Akbulut, O.; Kumar, A. A.; Shapiro, N. D.; Derda, R.; Patton, M. R.; Whitesides, G. M. *J. Am. Chem. Soc.* **2012**, *134*, 9094–9097.

(12) Giarratana, M.-C.; Kobari, L.; Lapillonne, H.; Chalmers, D.; Kiger, L.; Cynober, T.; Marden, M. C.; Wajcman, H.; Douay, L. *Nat. Biotechnol.* **2005**, *23*, 69–74.

(13) Rushing, D.; Vengelen-Tyler, V. *Transfusion* **1987**, *27*, 86–89.

(14) Sorette, M. P.; Shiffer, K.; Clark, M. R. *Blood* **1992**, *80*, 249–254.

(15) Brun, A.; Gaudernack, G.; Sandberg, S. *Blood* **1990**, *76*, 2397–2403.

(16) Key, J. *Arch. Intern. Med.* **1921**, *1882*, 511–549.

(17) Leif, R. C.; Vinograd, J. *Proc. Natl. Acad. Sci. U. S. A.* **1964**, *51*, 520–528.

(18) Haidmayer, R.; Kenner, T.; Hinghofer-Szalkay, H. *Biomed. Tech.* **1980**, *25*, 258–260.

(19) Albertsson, P.-Å. *Biochim. Biophys. Acta* **1958**, *27*, 378–395.

(20) Albertsson, P.-Å. *Biochem. Pharmacol.* **1961**, *5*, 351–358.

(21) Soohoo, J. R.; Walker, G. M. *Biomed. Microdevices* **2009**, *11*, 323–329.

(22) Albertsson, P.-Å. *Partition of Cell Particles and Macromolecules*; Wiley Interscience: News York, 1986.

(23) Frampton, J. P.; Lai, D.; Sriram, H.; Takayama, S. *Biomed. Microdevices* **2011**, *13*, 1043–1051.

(24) Lutwyche, P.; Norris-Jones, R.; Brooks, D. E. *Appl. Environ. Microbiol.* **1995**, *61*, 3251–3255.

(25) Walter, H.; Miller, A.; Krob, E. J.; Ascher, G. S. *Exp. Cell Res.* **1971**, *69*, 416–424.

(26) Fisher, D. *Biochem. J.* **1981**, *196*, 1–10.

(27) Hatti-Kaul, R. *Mol. Biotechnol.* **2001**, *19*, 269–277.

(28) Huddleston, J. G.; Lyddiatt, A. *Appl. Biochem. Biotechnol.* **1990**, *26*, 249–279.

(29) Kocken, C.; Ozwara, H. *Infect. Immun.* **2002**, *70*, 655–660.

(30) Spadafora, C.; Gerena, L.; Kopydlowski, K. M. *Malar. J.* **2011**, *10*, 96.

Chapter 4

Density-based Separation in Multiphase Systems Provides a Simple Method to Identify Sickle Cell Disease

Ashok A. Kumar[1], Matthew R. Patton[2], Jonathan W. Hennek[2], S.Y. Ryan Lee[2], Gaetana D'Alesio-Spina[2], Xiaoxi Yang[3], Julie Kanter[4], Sergey S. Shevkoplyas[3], Carlo Brugnara[5], and George M. Whitesides[2,6]

[1]School of Engineering and Applied Sciences, Harvard University, 29 Oxford St., Cambridge, MA 02138, United States

[2]Department of Chemistry & Chemical Biology, Harvard University, 12 Oxford St., Cambridge, MA 02138, United States

[3]Department of Biomedical Engineering, Tulane University, New Orleans, LA 70118

[4]Department of Pediatrics, Medical University of South Carolina, Charleston, SC 29425.

[5]Department of Laboratory Medicine, Children's Hospital Boston, 300 Longwood Avenue, Boston MA 02115

[6]Wyss Institute for Biologically Inspired Engineering, Harvard University, 60 Oxford St., Cambridge, MA 02138, United States

Abstract

Although effective low-cost interventions exist, child mortality attributable to sickle cell disease (SCD) remains high in low-resource areas due, in large part, to the lack of accessible diagnostic methods. The fluid, self-assembling step-gradients in density created by aqueous multiphase systems (AMPSs) identifies SCD by detecting dense cells. AMPS separate different forms of red blood cells by density in a microhematocrit centrifuge, and provide a visual means to distinguish individuals with SCD from those with normal hemoglobin, or with non-disease, sickle-cell trait, in under 12 minutes. Visual evaluation of a simple two-phase system identified SCD with a sensitivity of 90% (73-98%) and a specificity of 97% (86-100%). A three-phase system identified SCD with a sensitivity of 91% (78-98%) and a specificity of 88% (74-98%). This system could also distinguish the main subclasses of SCD (Hb SS and Hb SC). This test demonstrates the usefulness of AMPSs in point-of-care diagnostic hematology.

Introduction

Over 300,000 children (approximately 1% of births) are born with sickle cell disease (SCD) in Africa each year.[1,2] SCD is a genetic disorder caused by an array of genotypes (e.g., homozygous sickle cell disease—Hb SS, and hemoglobin SC disease—Hb SC) that lead to the sickling of erythrocytes and associated pathologies (**Table 4.1**). Severity and specific symptoms vary between the subtypes of SCD, but the most prevalent form (Hb SS, > 75%)[3] is the associated with the most severe effects.

Children with SCD suffer high mortality due to acute vaso-occlusive crises and increased risk of bacteremia.[4,5] Although inexpensive interventions exist to limit infection (e.g., penicillin prophylaxis, vaccinations) and reduce childhood mortality, over 50% of children < 5 years of age die in low-resource areas.[4,6,7] Much of this mortality could be avoided, but to implement simple interventions, a diagnosis is necessary.[8,9] Standard diagnostic procedures, such as hemoglobin electrophoresis (HE) or high performance liquid chromatography (HPLC), which are used in well-equipped facilities to detect SCD, are either unfeasible in low-resource settings—where the disease is highly prevalent—or do not differentiate between SCD and the non-disease, sickle cell trait (Hb AS). This unmet need has motivated the recent development of creative diagnostic methods for SCD using blood stains on paper devices[10] and hemolysis in solutions of sucrose.[11]

SCD also lacks simple metrics for management.[12,13] Standard diagnostic tests lack the ability to provide prognostic information. Genetic testing only confirms that the mutations for SCD are present. HE and HPLC can quantify the level of fetal hemoglobin—a useful, but incomplete, modulator of clinical manifestations.[14] Biophysical indicators, such as the rate of jamming of erythrocytes in microfluidic channels, have been proposed as integrative sources of information that could aid the management of SCD[13]—large clinical studies are still needed to

Table 4.1. Genetic disorders classified as SCD.

Genotype	Fraction of SCD Cases[a]
Hb SS	75%
Hb SC	20%
Hb $S\beta^{+/0}$	4%
Hb SD	<1%
Hb SE	<1%

[a] estimates based on literature[3,10,15]

verify this claim. The distribution of density of red blood cells provides another biophysical indicator that is closely related to SCD pathophysiology;[16,17] the dehydration that leads to the formation of sickle cells increases the rate of the polymerization of hemoglobin S. Dehydration increases the density of the cell by reducing the volume and increasing the ratio of dense protein to less dense water in the cell. Although many of the cells with the highest density are also sickled, some may also have irregular shapes variously described as a holly leaf or wreath shape.[18–20] For simplicity, we refer to the entire class of high density cells characteristic of SCD as "dense, SCD cells."

This paper describes two rapid tests for the two most prevalent forms of SCD (Hb SS and Hb SC) based on a sensitive but convenient measurement of the density (ρ, g/cm^3) of red blood cells using aqueous multiphase systems (AMPSs)—mixtures of polymers in water that form immiscible phases.[21] AMPSs provide a method of separating particles by density;[21] the discrimination between particles of different density using an AMPS can be high ($\Delta\rho < 0.001$ g/cm^3).[21] Each phase of an AMPS is separated by an interface that defines a step in density. AMPSs are thermodynamically stable and re-form if disturbed by stirring or shaking. AMPSs can be designed to be biocompatible, and have been used to separate mammalian cells by surface interactions.[22,23]

Our tests use AMPSs to separate erythrocytes into multiple bins of density; the presence or absence of erythrocytes in the bins distinguishes individuals with the most prevalent forms of SCD from individuals with either normal hemoglobin (Hb AA) or sickle-cell trait (Hb AS). The simpler test, SCD-AMPS-2, uses two phases; the higher resolution test, SCD-AMPS-3, uses three phases. We evaluated our tests both visually and digitally in a population of 59 subjects (33

negative—Hb AA or Hb AS, 26 positive—Hb SS, Hb or SC). Both tests diagnosed SCD positive samples with a sensitivity > 90% and a specificity > 88%.

SCD-AMPS-3 is further able to distinguish between the two main forms of SCD: i) Hb SS, which accounts for the majority (~ 75%) of SCD,[3] and ii) Hb SC, which constitutes most of the remaining cases of SCD (~20%).[3] These two variants of SCD have important differences in pathophysiology; Hb SC comes with a higher risk for retinal vascular damage and otological disorders, whereas Hb SS is generally more severe and comes with a higher risk of stroke and acute chest syndrome.[24–26] Effective diagnosis of the genotype would enable management to be tailored to the appropriate risks.

Results

Bins of density provide a specific test for SCD that can distinguish sub-types. The number of sub-populations of erythrocytes of interest determines the number of phases that should be used (see Appendix II). An AMPS with three fluid phases provides enough interfaces—two liquid-liquid interfaces and a liquid-container interface—to separate the three populations of erythrocytes required in a test for SCD that can distinguish subtypes of the disease (**Figure 4.1**). An AMPS with two phases provides two well-defined interfaces: one liquid-liquid interface between the phases, and one liquid-container interface. These interfaces are sufficient to separate dense, SCD cells from cells in the normal range of densities of erythrocytes, and to provide a test for SCD. Like the three-phase system depicted in **Figure 4.1**, the presence of red cells at the bottom of the tube indicates a positive test for SCD. The simplicity of interpreting only two phases comes at the cost of the inability of this test to distinguish subtypes (Hb SS and Hb SC) of SCD.

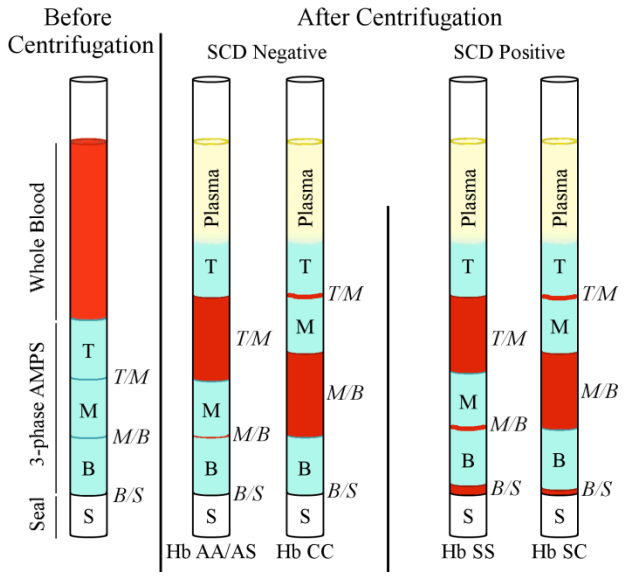

Figure 4.1. Schematic representations for the four most important outcomes of a density-based rapid test for sickle-cell disease. Upon centrifugation, erythrocytes move through the top (T), middle (M), and bottom (B) phases of the AMPS and collect at some combination of the three lower interfaces (two liquid/liquid interfaces, *T/M* and *M/B*, and one liquid/container interface, *B/S*). The distribution of cells between these interfaces will depend on the genotype; non-sickle hemoglobins (Hb AA, Hb AS, and Hb CC) are distinct from sickle hemoglobins (Hb SS and Hb SC). In all cases, the presence of red at *B/S* indicates sickle cell disease. Three interfaces allow further discrimination; a majority of erythrocytes at *M/B* indicates Hb SC or Hb CC.

The densities of the sub-populations of erythrocytes determine the desired densities of the phases of these AMPSs (see Appendix II). Although the density distribution of erythrocytes in SCD has been studied extensively, commonly used methods of separating cells by density are not suitable for use in field settings (see Appendix II). Methods that separate multiple populations require tediously layered gradient systems that are destroyed by agitation or mixing, and simple systems can only separate a single population. Centrifugation through AMPSs allows the separation of multiple populations in a thermodynamically stable (and, thus, simple to use) system. AMPS agitated by vigorous shaking readily reform quickly (minutes) under centrifugation, or more slowly (hours) under gravity.[21]

When designing an AMPS, we first seek systems whose phases are separated by the same differences in density as our target sub-populations of erythrocytes. We then use other additives to tune the overall density to the necessary levels.

An AMPS formed by mixing 7.0% (w/v) poly(ethylene glycol) (PEG) with a molecular weight (MW) of ~20 kD and 10.3% (w/v) Ficoll with a MW of ~400 kD provided phases with densities separated by the values required for a two-phase system useful in the diagnosis of SCD. An AMPS comprising 3% (w/v) PEG with a MW of ~20 kD, 10% (w/v) dextran with a MW of ~500 kD, and 5% (w/v) polymer of partially hydrolyzed poly(vinyl acetate) (containing 75% -OH and 25% $-OCOCH_3$ groups) with a MW of ~3 kD, provided phases separated by differences in density of the values required for our three-phase assay.

We added NaCl to make the system isotonic (as measured by vapor pressure osmometry) with blood. The pH of each system was adjusted to 7.40 ± 0.02 by the addition of concentrated (1-10 M) NaOH or HCl. We used a low-osmolality, high-density additive (Nycodenz, Accurate Chemical), to increase the density of each system to the proper range, and measured the density

of each phase using an oscillatory U-tube densitometer. SCD-AMPS-2 contained 9.1% (w/v) Nycodenz and had phases with densities ρ_{top} = 1.078 g/cm^3 and ρ_{bot} = 1.129 g/cm^3. SCD-AMPS-3 contained 8.7% (w/v) Nycodenz and had phases with densities ρ_{top} = 1.077 g/cm^3, ρ_{mid} = 1.108 g/cm^3, and ρ_{bot} = 1.120 g/cm^3.

A point-of-care test imposes cost and time constraints on the assay design. To demonstrate the potential use of our tests in point-of-care settings, we designed them to use ~5 µL of blood (a volume easily obtained from a finger stick). This blood was added to a plastic capillary that had been preloaded with 14 µL of the SCD-AMPS-3 or SCD-AMPS-2 (**Figure 4.2**). We sealed the capillaries with either white clay sealant—for ease of visual detection—or epoxy—for clarity when imaging tubes by transmission-mode in a scanner. Volumes were dictated by the capacity of the capillaries (see Appendix II). The total cost of reagents and materials per test is ~$0.20 at this scale; when fabrication costs and packaging materials are accounted for, the cost per test is ~$0.50 (**Appendix II; Table II.1**).

In rural settings, patients may travel for a day to seek medical care, and follow-up is challenging. Tests that can be coupled to actionable information and counseling must be rapid (ideally under 30 minutes). To meet this condition, we used a microhematocrit centrifuge (CritSpin, Iris Sample Processing) to centrifuge samples at 13,000 *g*; this centrifuge can perform 12 tests at a time and, with a simple, DC-to-DC converter can be powered by a car battery. We could distinguish blood of individuals with SCD from normal blood after six minutes; additional time in centrifugation enhanced the signal (**Appendix II; Figure II.1**). We chose to use ten minutes for our test to ensure a strong positive response, while keeping the test rapid. The rest of the procedure, including the finger-stick, sample loading, and test interpretation, took less than two minutes. By comparison, the gold standard for analysis of SCD, hemoglobin electrophoresis,

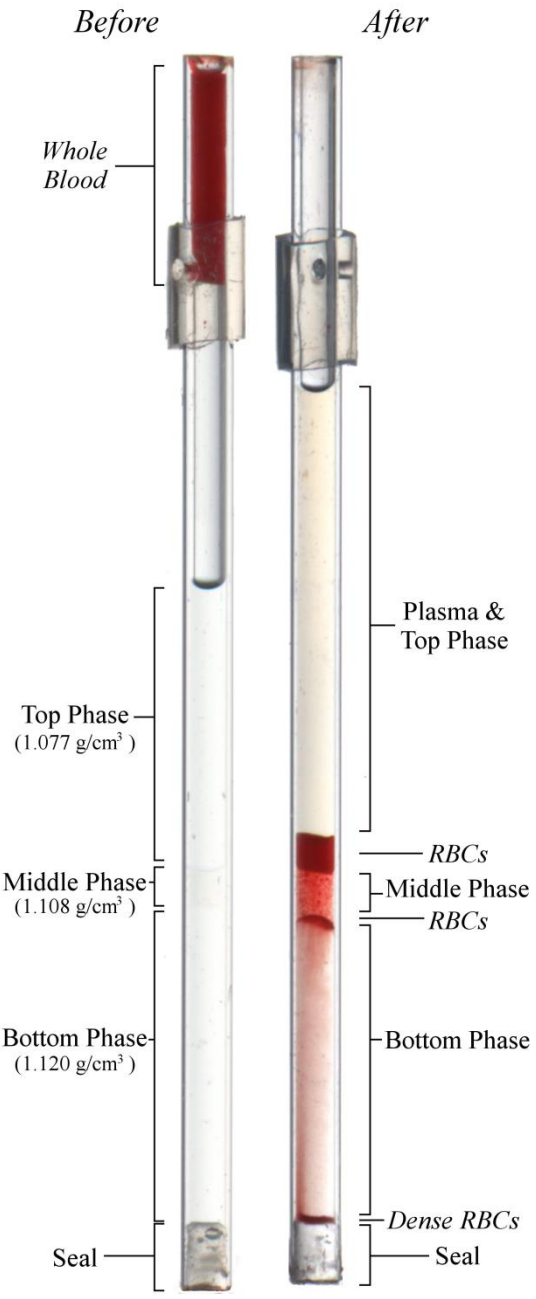

Figure 4.2. Example of an SCD-AMPS-3 rapid test loaded before and after centrifugation of blood from a sample without sickle cell disease. Blood wicks just past the hole in the side of the tube that is then covered with the silicone sleeve. After centrifugation, the cells separate from the plasma and pack between the phases of the AMPS. The test shown would be classified SCD positive because there is red below the bottom phase and above the seal.

requires more than three hours to prepare samples, run electrophoresis, stain, and wash. Laboratories often batch samples to run on a single gel and report results several days later.

In addition, ease-of-use is a critical component of a point-of-care test.[27] Capillary action provides a simple mechanism to load blood. Designing a test to diagnose SCD from a finger-stick required a method to load blood into a capillary pre-loaded with SCD-AMPS and sealed on one end. Without modification, capillaries with closed ends will not wick additional fluid due to air trapped between the fluid and the sealed end. We used a "hole-in-tube" method to load blood into the capillary; puncturing a small hole in the side of the polycarbonate capillary at a specific distance from one end allowed a standard volume of blood (~5 µL) to wick into the tube (**Appendix II; Figure II.2**).

Centrifugation of blood through the SCD-AMPS provides a visual separation of sickled cells. Over the course of ten minutes of centrifugation at 13,000 *g*, blood moved out of the loading zone and through the AMPS, and formed separated layers at the interfaces (**Figure 4.2**). In most cases, the boundary between the top phase and the plasma was not distinguishable. The total packed volume between each interface provides an estimate of the hematocrit (**Appendix II; Figure II.3**): this estimate also provides a simple, if crude, method to identify severe anemia concurrently [28]. With a diagnostic accuracy of over 90%, we could distinguish samples from individuals with SCD from normal samples; a layer of red cells sat below the bottom phase of both SCD-AMPSs, and packed against the seal of the capillary (**Figure 4.3**); this layer was dominated by sickled and dehydrated cells (**Appendix II; Figure II.6**). By comparing the volume of the packed cells at the seal, to the volume of cells at the other interfaces, we could estimate the percentage of dense cells (**Appendix II; Table II.2**).

Figure 4.3. Representative examples of positive and negative tests in the SCD-AMPS-3 (ρ_{top} = 1.077 g/cm^3, ρ_{mid} = 1.108 g/cm^3, ρ_{bot} = 1.120 g/cm^3) and the SCD-AMPS-2 (ρ_{top} = 1.078 g/cm^3, ρ_{bot} = 1.129 g/cm^3), show a clear distinction between subjects with SCD (Hb SS and Hb SC) and those without SCD (Hb AA and Hb AS). In non-SCD blood in the SCD-AMPS-2 system, all cells pack at the liquid interface (*T/B*). In the SCD-AMPS-3 system, most cells have normal morphologies and densities (normocytes) and pack at the upper liquid interface (*T/M*), the densest normal shaped cells (dense normocytes) collect at the lower liquid interface (*M/B*), and some aggregated platelets are present at the bottom of the tube (gray) (*B/S*). Erythrocytes from a subject with SCD display greater heterogeneity at high densities. Dense, SCD cells form a layer below the bottom phase of both SCD-AMPS on top of the sealant (*B/S*). In the SCD-AMPS-3 test, the distribution of cells between the liquid interfaces (*T/M* and *M/B*) differentiates Hb SS from Hb SC. The difference in the total packed volume of the cells demonstrates the difference in the hematocrit between the normal subject and the anemic subject with SCD.

Figure 4.2 (Continued).

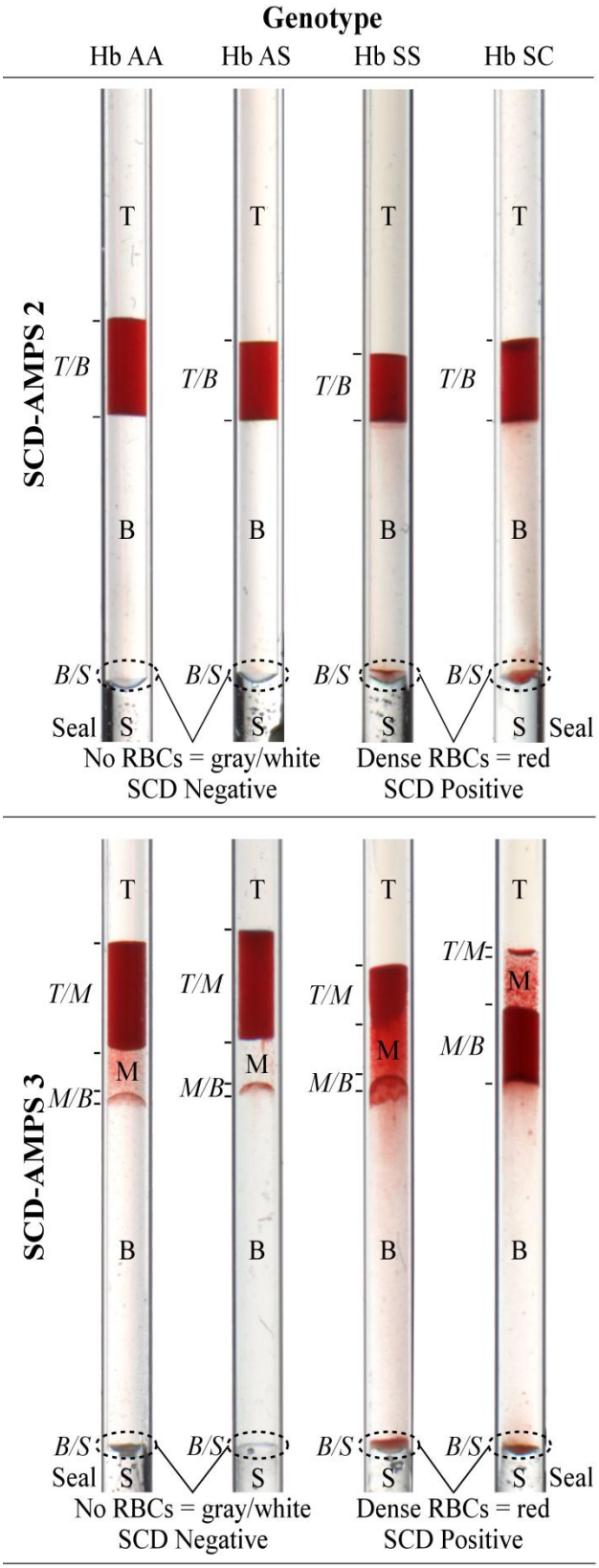

In the SCD-AMPS-3, most erythrocytes within the normal density range sat at the upper liquid/liquid interface. The densest normal erythrocytes (~1–5% of erythrocytes) collected at the lower liquid/liquid interface. In both SCD-AMPS-2 and SCD-AMPS-3, blood from individuals with sickle-cell trait appeared the same as that from normal individuals; our method does not differentiate between Hb AS and Hb AA genotypes. Although a small amount of sickled cells may exist in blood from an individual with Hb AS, the amount is below our estimated limit of detection of 2.8% dense cells (**Appendix II; Figure II.7**).

The presence of cells with a high density correlates with the presence of SCD. Samples that had a visible red band at the bottom of the AMPS correlated strongly with the presence of SCD. Conversely, samples negative for SCD rarely had red cells visibly present at the bottom of the AMPS (**Appendix II; Table II.3**). The SCD-AMPS-2 had a true positive rate (sensitivity) of 90% with a Jeffreys 95% confidence interval (C.I.) of 73%–98% and a true negative rate (specificity) of 97% (C.I. = 86%–100%). The SCD-AMPS-3 had a sensitivity of 91% (C.I. = 78%–98%), and a specificity of 88% (C.I. = 74%–98%). Admittedly, visual inspection allows room for bias in a diagnostic test. To reduce biased evaluation, each test was evaluated independently by at least two people (see Appendix II for more details). Samples negative for SCD included both Hb AA (n = 26 for SCD-AMPS-3, n = 24 for SCD-AMPS-2) and Hb AS (n = 7). Samples positive for SCD included Hb SS (n = 20 for SCD-AMPS-3, n = 15 for SCD-AMPS-2) and Hb SC (n = 6). The formulation of SCD-AMPS-2 was finalized after testing had begun on SCD-AMPS-3 and, thus, the former system was tested on fewer samples.

In about half of all tests where a clear red band was not present at the bottom of the tube, visual inspection showed a thin layer of white, yellow or pink material. Evaluation of these layers by microscopy revealed that platelets had clumped together to form large aggregates

(**Appendix II; Figure II.5**). In some cases, these aggregates appeared to have captured a small number of both red and white blood cells. In samples without SCD, we believe these aggregates may occasionally capture enough red blood cells to create a false positive.

We also evaluated scanned images of the capillaries digitally. Varying the thresholds for the intensity of the red color at the bottom of the tube produced a receiver operating characteristic (ROC) curve (**Figure 4.4**) (see Appendix II). Our sensitivity and specificity from visual evaluation matched the ROC curve for both tests; this finding suggests two interrelated procedures: i) with proper training, the visual reading of the tests by health workers could match (and be checked by) the performance of the digital analysis; or ii) with higher-technology phones, digital analysis could replace training of readers. The fact that these two methods of reading give equivalent results suggest that reading the test will not be a major source of error.

The least dense red blood cells in Hb SC have a slightly higher density than the least dense red blood cells in Hb SS [29]. In SCD-AMPS-3, blood from most individuals with Hb SC had distributions of red cells distinct from those with Hb SS. In half the cases, a thick band of red cells formed at the lower liquid interface whose height was comparable to or greater than that of the band of red cells at the upper interface (**Figure 4.3**). In some cases, an hour-glass shape of red cells connected the packed cells at the two interfaces (**Appendix II; Figure II.8**). By contrast, blood from samples with Hb SS had two distinct bands of red with a clear majority of red cells at the upper liquid interface. These differences in the distribution of cells allowed us to distinguish visually between Hb SC (n = 6) and Hb SS (n = 20), the two most prevalent forms of SCD with a sensitivity of 67% (C.I. = 29%–92%) and a specificity of 100% (C.I. = 88%–100%). Centrifugation for an additional 10 minutes increased the sensitivity to 83% (C.I. = 44%–98%).

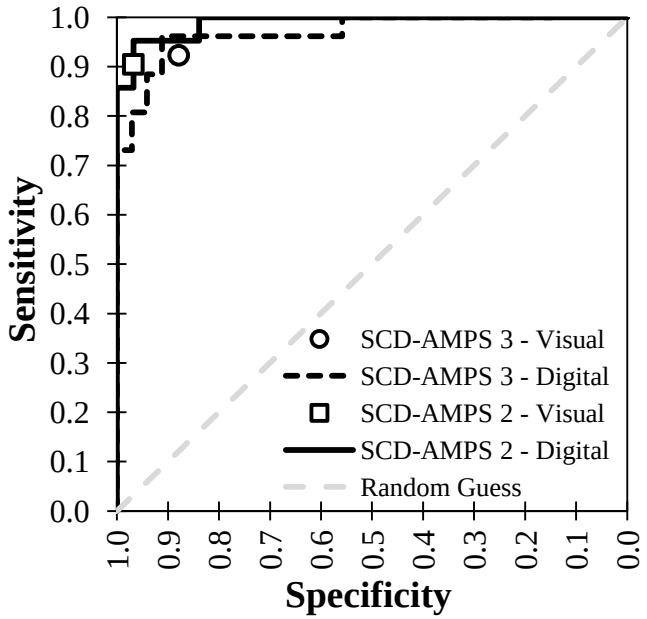

Figure 4.4. The receiver operating characteristic (ROC) curve (solid line) for the digital evaluation of the presence of a red layer at the bottom of the SCD-AMPS demonstrates good diagnostic performance. Both curves are far from the gray line that indicates no ability to detect an event. Visual evaluation of the rapid tests matched the sensitivity and specificity of the digital analysis.

In **Figure 4.3**, the red and pink, in the lower phases, indicated either that the dense cells had not all reached their equilibrium position, or that some cells had the same density as one of these phases. Additional centrifugation time (a total of 30 minutes) allowed these cells to sediment further and increased the thickness of the layer of red at the bottom of the tube (**Appendix II; Figure II.1 & II.4**), but required more time. For a diagnostic test, however, we do not need all the cells to reach their equilibrium positions as long as the difference between positive and negative tests is clear.

Discussion

An AMPS-based test for SCD is appropriate for use at the point-of-care. The World Health Organization (WHO) has defined the ASSURED criteria as guidelines for the development of point-of-care devices.[27] Devices should be affordable, sensitive, specific, user-friendly, reliable, equipment-free, and deliverable to those in need. AMPS-based tests for SCD have the characteristics of sensitivity, affordability, and ease-of-use required for them to have an impact at the POC.

The "hole-in-tube" method allows blood to fill the tube automatically. Unlike tests that require lysing and incubating blood in a solution (e.g., Sickledex), whole blood is tested directly. Minimal handling of the sample reduces errors and risks to health workers performing the test. We estimate the cost of materials and manufacturing per test to be $0.50 (see Appendix II). The centrifuge (CritSpin, Iris Sample Processing) we use in this study costs approximately $1,600, but we have verified that our system performs similarly on a basic centrifuge (SpinCrit, www.spincritcentrifuge.com) that costs $150, is portable, and runs on four AA batteries; this centrifuge can perform six tests at a time and standard AA batteries allow three separate 10 minutes spins per charge. Simple centrifuges, such as those that use mechanical actuation, solar

power, or batteries, should allow this test to reach rural and mobile clinics;[30] slower centrifuges, however, would require longer times for the tests.

Even with simplicity and low cost, AMPS-based tests still attain a sensitivity and specificity near 90%. Although they do not distinguish between Hb AS and Hb AA, they can distinguish between Hb AS and both Hb SS and Hb SC. SCD-AMPS-3 has the added ability to distinguish Hb SC from Hb SS, albeit with a lower sensitivity than that with which the test identifies SCD—the sensitivity to identify Hb SC may be improved with a slightly different density of the middle phase. In addition to providing diagnostic information, these tests measure a biophysical indicator that may help identify patients more likely to experience certain complication of the disease; the fraction of erythrocytes that have a high density correlates with certain clinical manifestations of SCD (e.g., skin ulcers, priapism, and renal disfunction).[31] Monitoring the distribution of the density of cells could also provides a way to assess sickle crises.[32]

The density of cells can be used as a diagnostic marker. The use of density as a tool for point-of-care diagnostics dates back to the spun hematocrit, in which the density difference between cells and plasma enables the measurement of the volume ratio of packed cells in blood. This measure has been helpful in the diagnosis of anemia.[28] Modifications on the spun hematocrit concept have led to systems for measuring white blood cell counts and other parameters.[33] The company Zyomyx has developed a technique to tag CD4+ cells with proprietary, high-density beads so that these cells can be separated from whole blood and quantified.[34] The measurement of the density of individual cells demonstrates that density can provide a high quality measure of cellular properties.[35]

Fractionating red blood cells by density in step-gradients generated using AMPSs provides a new method to identify SCD. The presence of dense cells correlates with the presence of SCD;[16] AMPSs provide a self-assembling step-gradient in density that makes the identification of dense cells accessible in low-resource settings. Further testing will be required to verify the performance of the SCD-AMPS on larger population with more genetic variation and concurrent conditions, but this work demonstrates that density has the potential to be a sensitive and specific biophysical marker for diagnosing SCD.

One limitation of density-based methods is that density is a colligative property; density depends on the sum of the elements (solutes, proteins) contained in a cell rather than on a specific biochemical marker. Factors that can affect the density of red blood cells, such as clotting or other genetic diseases, must be carefully assessed to develop a POC diagnostic based on density. The densities of SCD-AMPS described here should discriminate between Hb CC and SCD; if, however, dense cells in Hb CC do provide false positives, an additional low-density band to isolate reticulocytes could discriminate Hb CC from Hb SC and Hb SS.[29] Other genetic disorders that may increase density, such as hereditary spherocytosis, have little geographic overlap with SCD.[36,37]

Density-based tests, also, will not be sensitive when dense cells are not present. At birth, children with SCD have predominantly Hb F, and generally begin to express appreciable amounts of Hb S between six months and one year of age. The presence of dense, SCD cells relies on some amount of dehydration or sickling,of cells and, hence, on the presence of large amounts of Hb S; we expect a density-based test, therefore, to have significantly lower sensitivity in newborns than in one-year olds. Only one of our Hb SS samples came from a child under one year old, and it appeared negative on both digital and visual inspection. Developing

an accessible and affordable screening test for newborns remains a critical, unmet challenge. Rapid diagnostics that rely on the presence of sickled cells, such as ours, can play an important role in reducing child mortality if screenings are done near a child's first birthday; such diagnostic efforts could be carried out simultaneously with vaccination campaigns (e.g. measles) that target children between nine months and one year old.

An AMPS-based test for SCD can fill a gap in global health. With progress against infectious diseases around the world, the burden of morbidity and mortality due to hemoglobinopathies, such as SCD, will rise.[3] Standard diagnostic techniques in well-equipped laboratories, such as HE and HPLC, are too expensive and require more infrastructure than is available in many countries with high burdens of SCD, especially in rural areas.[38]

Currently, the most used, microscope-free methods for screening for sickle-cell disease in low-resource settings are solubility tests, such as Sickledex.[39] In these tests a solution lyses and deoxygenates the blood; the polymerization of deoxyhemoglobin S causes the hemoglobin to form a nematic liquid crystal and makes the solution turbid.[40,41] These tests can detect the presence of Hb S, but cannot distinguish between Hb SS and Hb AS without the use of additional, expensive equipment (i.e., a turbidimeter); this difference is non-trivial, as the former is a life-threatening condition, and the latter is, largely, benign.

Even when testing for the presence of Hb S and not specifically for SCD, solubility tests offer a sensitivity of 45% and a specificity of 85%.[39] This low sensitivity is not enough to effectively screen for sickle cell. In response to the outstanding need for rapid tests for SCD appropriate for the POC, a Request for Applications by the NIH in 2013 solicited the creation of tests for SCD with a sensitivity of at least 60% (RFA-HL-14-010). The AMPS-based tests described here have a sensitivity of over 87%.

Compared to currently available techniques, the density-based tests using AMPS combine four desirable properties: i) fieldability—they are amenable to use at the point-of-care, ii) performance—they can distinguish Hb SC and Hb SS from Hb AA or Hb AS, iii) biophysical information—by quantifying the percentage of dense, SCD cells, and iv) low cost. The AMPS-based method also compares favorably in ease-of-use to other technologies that have been developed recently to diagnose SCD (**Appendix II; Table II.4**).

The high sensitivity and specificity of SCD-AMPS in identifying SCD in tests in a laboratory described here demonstrates that a density-based approach may provide a valuable screening tool. Further testing on different genotypes and concurrent conditions will determine whether such a test is appropriate as a point-of-care diagnostic for SCD. Even if the performance is reduced, the densities could be adjusted to provide a higher sensitivity test (with lower specificity) to be used as a screening method; such a test would allow interventions where the cost-to-treat is low.

By combining simplicity and rapidity to measure a biophysical parameter (i.e., density), the density-based test using AMPSs could play an important role in diagnosing SCD at the point-of-care. Measuring the fraction of dense cells at the bottom of an SCD-AMPS could also have use beyond the diagnosis of SCD, and possibly aid in the management of the disease, but such uses will require clinical validation. More generally, density-based diagnostics illustrate how biophysical markers, such as density, and simple separation methods, such as centrifugation through AMPS, can combine to provide simple and low-cost health solutions; AMPS-based separations of blood should enable hematology at the point-of-care.

Materials and Methods

Appendix II includes detailed descriptions of all chemicals and materials used, methods for obtaining blood samples, the preparation and characterization of the AMPS, estimations of the cost per rapid test (**Appendix II; Table II.1**), analysis of test performance with different centrifugation times (**Appendix II; Figure II.1 and II.4**), experimental and rapid test design (**Appendix II; Figure II.2**), estimation of hematocrit and fraction of dense cells (**Appendix II; Figure II.3 and Table II.2**), analysis of separated fractions of cells (**Appendix II; Figure II.5 and II.6**), comparison of methods to identify SCD (**Appendix II; Table II.4**), estimation of the limit of detection using cells treated with Nystatin as a model for dense, sickled cells (**Appendix II; Figure II.7**), and detailed results on clinical samples (**Appendix II; Table II.3 and Figure II.8**).

Acknowledgements

This work was supported by the Harvard Office of Technology Development's Biomedical Accelerator Award, and the Bill and Melinda Gates Foundation under award number OPP1016360. A.A.K. acknowledges financial support from the Office of Naval Research through the NDSEG fellowship program. X.Y. and S.S.S. were supported by a 2012 NIH Director's Transformative Research Award (NHLBI R01HL117329, PI: SSS). The authors would like to thank Dr. Thomas Stossel (Brigham and Women's Hospital, Boston) for helpful discussions about sickle cell disease in low-resource settings.

References

(1) Piel, F. B.; Hay, S. I.; Gupta, S.; Weatherall, D. J.; Williams, T. N. *PLoS Med.* **2013**, *10*, e1001484.

(2) Serjeant, G. R. *Br. J. Haematol.* **2010**, *151*, 425–429.

(3) Weatherall, D. J. *Blood* **2010**, *115*, 4331–4336.

(4) Emond, A. M.; Collis, R.; Darvill, D.; Higgs, D. R.; Maude, G. H.; Serjeant, G. R. *J. Pediatr.* **1985**, *107*, 201–206.

(5) Williams, T. N.; Uyoga, S.; Macharia, A.; Ndila, C.; McAuley, C. F.; Opi, D. H.; Mwarumba, S.; Makani, J.; Komba, A.; Ndiritu, M. N.; Sharif, S. K.; Marsh, K.; Berkley, J. A.; Scott, J. A. G. *Lancet* **2009**, *374*, 1364–1370.

(6) Gaston, M.; Verter, J.; Woods, G.; Pegelow, C.; Kelleher, J.; Presbury, G.; Zarkowsky, H.; Vichinsky, E.; Iyer, R.; Lobel, J.; Diamond, S.; Holbrook, C.; Gill, F.; Richey, K.; Faletta, J. *N. Engl. J. Med.* **1986**, *314*, 1593–1599.

(7) Hankins, J.; Ware, R. E. *Lancet* **2009**, *374*, 1308–1310.

(8) Tubman, V. N.; Archer, N. M. *Am. J. Hematol.* **2013**, *88*, 983.

(9) McGann, P. T.; Ferris, M. G.; Ramamurthy, U.; Santos, B.; de Oliveira, V.; Bernardino, L.; Ware, R. E. *Am. J. Hematol.* **2013**, *88*, 984–989.

(10) Yang, X.; Kanter, J.; Piety, N. Z. N.; Benton, M. S. M.; Vignes, S. M.; Shevkoplyas, S. S. *Lab Chip* **2013**, *13*, 1464–1467.

(11) Milligan, C.; Rees, D. C.; Ellory, J. C.; Osei, A.; Browning, J. A.; Hannemann, A.; Gibson, J. S. *J. Physiol.* **2013**, *6*, 1463–1474.

(12) Steinberg, M. H. *Br. J. Haematol.* **2005**, *129*, 465–481.

(13) Wood, D. K.; Soriano, A.; Mahadevan, L.; Higgins, J. M.; Bhatia, S. N. *Sci. Transl. Med.* **2012**, *4*, 123ra26.

(14) Akinsheye, I.; Alsultan, A.; Solovieff, N.; Ngo, D.; Baldwin, C. T.; Sebastiani, P.; Chui, D. H. K.; Steinberg, M. H. *Blood* **2011**, *118*, 19–27.

(15) Ashley-Koch, A.; Yang, Q.; Olney, R. *Am. J. …* **2000**, *151*, 839–845.

(16) Fabry, M. E.; Mears, J. G.; Patel, P.; Schaefer-Rego, K.; Carmichael, L. D.; Martinez, G.; Nagel, R. L. *Blood* **1984**, *64*, 1042–1046.

(17) Brugnara, C. *J. Pediatr. Hematol. Oncol.* **2003**, *25*, 927–933.

(18) Itano, H.; Pauling, L. *Blood* **1949**, 66–68.

(19) Horiuchi, K.; Ballas, S. K.; Asakura, T. *Blood* **1988**, *71*, 46–51.

(20) Kaul, D.; Xue, H. *Blood* **1991**, 1353–1361.

(21) Mace, C. R.; Akbulut, O.; Kumar, A. A.; Shapiro, N. D.; Derda, R.; Patton, M. R.; Whitesides, G. M. *J. Am. Chem. Soc.* **2012**, *134*, 9094–9097.

(22) Brooks, D. E. *J. Colloid Interface Sci.* **1973**, *43*, 700–713.

(23) Soohoo, J. R.; Walker, G. M. *Biomed. Microdevices* **2009**, *11*, 323–329.

(24) Lionnet, F.; Hammoudi, N.; Stojanovic, K. S.; Avellino, V.; Grateau, G.; Girot, R.; Haymann, J. *Haematologica* **2012**, *97*, 1136–1141.

(25) Platt, O.; Thorington, B.; Brambilla, D. J.; Milner, P. F.; Rosse, W. F.; Vichinsky, E.; Kinney, T. R. *N. Engl. J. Med.* **1991**, *325*, 11–16.

(26) Platt, O.; Brambilla, D.; Rosse, W. F.; Milner, P. F.; Castro, O.; Steinberg, M. H.; Klug, P. P. *N. Engl. J. Med.* **1994**, *330*, 1639–1644.

(27) Kettler, H.; White, K.; Hawkes, S. *Mapping the Landscape of Diagnostics for Sexually Transmitted Infections: Key Findings and Recommendations*; 2004; pp. 1–44.

(28) Quintó, L.; Aponte, J. J.; Menéndez, C.; Sacarlal, J.; Aide, P.; Espasa, M.; Mandomando, I.; Guinovart, C.; Macete, E.; Hirt, R.; Urassa, H.; Navia, M. M.; Thompson, R.; Alonso, P. L. *Trop. Med. Int. Heal.* **2006**, *11*, 1295–1302.

(29) Fabry, M. E.; Kaul, D. K.; Raventos-Suarez, C.; Chang, H.; Nagel, R. L. *J. Clin. Invest.* **1982**, *70*, 1315–1319.

(30) Wong, A. P.; Gupta, M.; Shevkoplyas, S. S.; Whitesides, G. M.; George, M. *Lab Chip* **2008**, *8*, 2032–2037.

(31) Bartolucci, P.; Brugnara, C.; Teixeira-Pinto, A.; Pissard, S.; Moradkhani, K.; Jouault, H.; Galacteros, F. *Blood* **2012**, *120*, 3136–3141.

(32) Fabry, M. E.; Benjamin, L.; Lawrence, C.; Nagel, R. L. *Blood* **1984**, *64*, 559–563.

(33) Bark, J.; Hurst, M.; Hamer, D.; Sciences, B.; Hospital, R. B. **2013**, *70*, 67–74.

(34) Kirakossian, H. Density-based cell detection system. US 2010/0068754 A1, 2009.

(35) Grover, W. H.; Bryan, A. K.; Diez-Silva, M.; Suresh, S.; Higgins, J. M.; Manalis, S. R. *Proc. Natl. Acad. Sci. U. S. A.* **2011**, *108*, 10992–10996.

(36) Perrotta, S.; Gallagher, P. G.; Mohandas, N. *Lancet* **2008**, *372*, 1411–1426.

(37) Piel, F. B.; Patil, A. P.; Howes, R. E.; Nyangiri, O. A.; Gething, P. W.; Williams, T. N.; Weatherall, D. J.; Hay, S. I. *Nat. Commun.* **2010**, *1*, 104.

(38) Howitt, P.; Darzi, A.; Yang, G.-Z.; Ashrafian, H.; Atun, R.; Barlow, J.; Blakemore, A.; Bull, A. M. J.; Car, J.; Conteh, L.; Cooke, G. S.; Ford, N.; Gregson, S. A. J.; Kerr, K.; King, D.; Kulendran, M.; Malkin, R. A.; Majeed, A.; Matlin, S.; Merrifield, R.; Penfold, H. A.; Reid, S. D.; Smith, P. C.; Stevens, M. M.; Templeton, M. R.; Vincent, C.; Wilson, E.; Finlayson, A.; Greaves, F.; Ali, F. *Lancet* **2012**, *380*, 507–535.

(39) Okwi, A. L.; Byarugaba, W.; Parkes, A.; Ocaido, M. *Clin. Mother Child Heal.* **2010**, *7*, 1205–1210.

(40) Ballard, M.; Radel, E.; Sakhadeo, S.; Schorr, J. *J. Pediatr.* **1970**, 117–119.

(41) Nalbandian, R. M. R.; Nichols, B. B. M. B.; Camp, F. R.; Lusher, J. M.; Conte, N. F.; Henry, R. L.; Wolf, P. L.; Jeanne, M. *Clin. Chem.* **1971**, *17*, 1028–1032.

Chapter 5

Evaluation of a Density-based Rapid Diagnostic Test for Sickle Cell Disease in a Clinical Setting in Zambia

Ashok A. Kumar[1], Catherine Chunda-Liyoka[2], Jonathan W. Hennek[3], Hamakwa Mantina[2], S.Y. Ryan Lee[3], Matthew Patton[3], Pauline Sambo[2], Silvester Sinyangwe[2], Chipepo Kankasa[2], Chifumbe Chintu[2], Carlo Brugnara[4], Thomas Stossel[5], and George M. Whitesides[3,5]

[1]School of Engineering and Applied Sciences, Harvard University, 29 Oxford St., Cambridge, MA 02138, United States

[2]Department of Pediatrics, University Teaching Hospital, Nationalist Rd., Lusaka, Zambia

[3]Department of Chemistry & Chemical Biology, Harvard University, 12 Oxford St., Cambridge, MA 02138, United States

[4]Children's Hospital, Boston, MA, United States

[5]Brigham and Women's Hospital, Boston, MA, United States

[5]Wyss Institute for Biologically Inspired Engineering, Harvard University, 60 Oxford St., Cambridge, MA 02138, United States

Abstract

Although simple and low-cost interventions for sickle cell disease (SCD) exist in many developing countries, child mortality associated with SCD remains high, in part, because of the lack of access to diagnostic tests for SCD. A density-based test using aqueous multiphase systems (SCD-AMPS) showed promise as a candidate for a low-cost, point-of-care diagnostic for SCD. In this chapter, the field evaluation of SCD-AMPS in a large clinical trial in Zambia is described. Of the two variations of the SCD-AMP used, the best system (SCD-AMPS-2) demonstrated a sensitivity of 87% (82-90%) and a specificity of 60% (53-67%). Analysis identified potential sources of false positives to include clotting, variation between batches of SCD-AMPS, and shipping conditions. Interestingly, SCD-AMPS-2 remained over 80% sensitive in detecting sickle cell disease in children between 6 months and 1 year old. In addition to an evaluation of performance, an assessment of end-user operability was done with health workers in rural clinics in Zambia. Health workers in these settings rated the SCD-AMPS tests to be as simple to use as lateral flow tests for malaria and HIV.

Introduction

Timely diagnosis of sickle cell disease (SCD) is essential for the implementation of life-saving interventions. The lack of effective diagnostics in low-resource settings, however, means that over half of the more than 300,000 children born each year with SCD die before five years of age.[1,2] Detecting the presence of dense cells could provide a sensitive and specific diagnostic of SCD. Density is a particularly relevant biophysical characteristic of sickle cell disease. The dehydration associated with the sickling of cells causes an increase in the density of an erythrocyte, from approximately 1.095 g/cm^3 to over 1.120 g/cm^3.[3,4] The density of sickled cells is higher than the densest cells in the natural distribution of the density of erythrocytes.

We previously described the use of aqueous multiphase systems (AMPSs)—mixtures of polymers in water that form immiscible, liquid phases—to separate erythrocytes by density and provide a rapid visual diagnostic for SCD (Chapter 4). Four characteristics make AMPSs suitable for density-based separations at the point-of-care: i) *Thermodynamic Stability*. Step-gradients can be made centrally and will reform after disturbances from transportation. ii) *Fine Resolution in Density*. The interface between the liquid phases of AMPSs provide a molecularly sharp step in density between phases with differences in density as low as 0.001 g/cm^3.[5] iii) *Scalability*. Reproducible step gradients can be made by making large batches (> 1 L) of AMPS and then distributing them into capillary tubes appropriate for separating microliters of blood obtained from a fingerprick, and iv) *Low Cost*. Using commercially available polymers, the cost of reagents, packaging, and labor per test is ~$0.50 (Appendix II).

Although previous use of AMPS as a density-based diagnostic for sickle cell disease (SCD-AMPS) in a laboratory showed both sensitivity and specificity near or over 90%, implementing the test in point-of-care settings introduces several variables that may affect

performance, such as quality control, packaging methods, storage and shipping conditions, shelf-life, and end-user variability. To understand how these issues might affect the SCD-AMPSs tests, we undertook a 505 subject case-control study at the University Teaching Hospital (UTH) in Lusaka, Zambia. Within this cohort, we evaluated the performance of the test on three subsets: 1) children between 6 months to 1 year of age, 2) sickle cell patients who recently experienced a crisis, and 3) patients identified as having microcytic hypochromic anemia by complete blood count (CBC).

We tested two prototypes, both of which demonstrated the ability to identify SCD with a diagnostic accuracy over 69%. Based on the results of this study, we identified three key issues that could be addressed to improve the performance of future prototypes: 1) variability in the density of the bottom phase between batches, 2) conditions of shipping and storage, and 3) clotting of blood samples. We also performed surveys of health workers in two rural health centers in a part of Zambia estimated to have a high prevalence of SCD.[6] The surveys captured current knowledge of the disease, experience with other rapid tests, and feedback on the design of the proposed rapid test for SCD.

Experimental Design

Rapid Test Design. We evaluated two different density-based tests: a system with two phases, SCD-AMPS-2, and a system with three phases, SCD-AMPS-3 (**Figure 5.1**). Although SCD-AMPS-2 allows for a simpler interpretation, SCD-AMPS-3 provides a richer set of information about the distribution of densities of erythrocytes that can help distinguish between the two main genotypes of SCD: Hb SS and Hb SC (Chapter 4). We evaluated both tests in the clinical trial to see if the simplicity of the two-phase test conferred a distinguishable advantage in clinical performance.

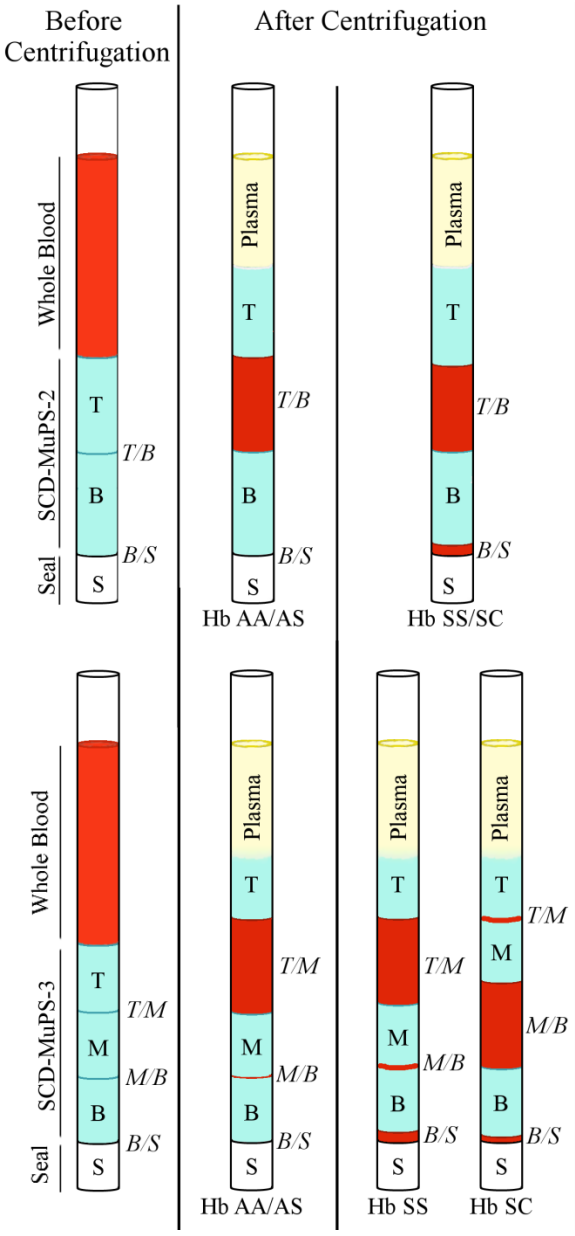

Figure 5.1. Both versions of the SCD-AMPS are designed to separate dense, sickled red blood cells from whole blood. Blood passes through the phases—T and B for SCD-AMPS-2 and T, M, and B for SCD-AMPS-3—upon centrifugation. If sickled cells are present, they collect at the *B/S* interface, providing a visual readout for the presence of SCD. In SCD-AMPS-3, the additional phase allows the discrimination of Hb SS from Hb SC by evaluating the distribution of red cells at the upper interfaces (*T/M* and *M/B*).

We used the design of the rapid test described previously (Chapter 4) with some additional modifications to enable rapid assembly of tests and improved durability for shipping and storage (**Appendix III; Figure III.1**). A mixture of 7.0% (w/v) poly(ethylene glycol) (PEG) with a molecular weight (MW) of ~20 kD, 10.3% (w/v) Ficoll with a MW of ~400 kD, and 9.1% (w/v) Nycodenz formed SCD-AMPS-2 (ρ_{top} = 1.078 g/cm^3 and ρ_{bot} = 1.129 g/cm^3). Similarly, a mixture of 3% (w/v) PEG with a MW of ~20 kD, 10% (w/v) dextran with a MW of ~500 kD, 5% (w/v) polymer of partially hydrolyzed poly(vinyl acetate) (containing 75% -OH and 25% -$OCOCH_3$ groups) with a MW of ~3 kD, and 8.7% (w/v) Nycodenz, formed SCD-AMPS-3 (ρ_{top} = 1.077 g/cm^3, ρ_{mid} = 1.108 g/cm^3, and ρ_{bot} = 1.120 g/cm^3). We buffered the systems and used NaOH and HCl to adjust the pH of the solutions and NaCl to adjust the osmolality (see Appendix III).

Appendix III; Figure III.2 outlines the process to perform a rapid test for an end-user. The self-forming steps gradient in density allows the end-user to use the AMPS out of a packet without needing to mix reagents or pipette solutions. Whole blood wicks directly into the capillary; no further handling of blood is necessary. Preparative steps common to other techniques, such as lysis or exposure to reagents to deoxygenate hemoglobin,[7,8] are not needed. These characteristics of the test reduce risks for biohazards and user error. The polycarbonate capillary tubes that house the rapid test are preloaded with AMPS and sealed on one end with white clay. The white seal provides an effective background to contrast with the red cells. A volume of ~5 µL of blood enters the rapid test via capillary action as a result of the pre-punched hole in the side of the capillary. Sliding a silicone sleeve over the hole prevents the blood from leaking, and centrifugation accelerates the density-based separation of red blood cells over the AMPS. We used a 3D printed mold and a pushpin to make repeatable holes; this standardization

allowed us to load a reproducible volume of blood with a coefficient of variance (CV) of 4% (Appendix III). After 10 minutes of centrifugation at 13,700 *g*, evaluating the interfaces of AMPS for the visible presence of red cells provides a means to identify SCD and, in the case of SCD-AMPS-3, to distinguish between the two main genotypes of SCD **(Figure 5.1)**.

Development of methods to pack, store, and ship SCD-AMPS tests. We performed a series of accelerated storage tests using various packaging materials and methods (see Appendix III). We found that foil-lined pouches partially filled with water and then sealed with an impulse sealer minimized evaporation of the AMPS in the tubes. To minimize variables for this clinical trial, we refrigerated the rapid tests after packaging at 4-8 °C and shipped them on ice to Zambia. On arrival in Zambia, the staff at UTH stored the samples at 4 °C. We brought the tests to room temperature on the day of use. Each batch of packaged tests was used within two months of the packaging date. Future work will need to focus on shelf-life and storage stability at ambient temperatures.

Characteristics of Population for the Clinical Study. The initial study in Zambia included 505 children that were seen as out-patients or in-patients during the period of the study in the Department of Paediatrics and Child Health and the out-patient haematology clinic for SCD patients. We used the broad inclusion and exclusion criteria found in **Table 5.1**, with further criteria for specific subsets of the study population: Subset 1) children fitting the inclusion criteria with the additional inclusion criteria of being over 1 year old and confirmed as SCD positive, Subset 2) children fitting the inclusion criteria above with the additional inclusion criterion of not having SCD, Subset 3) children fitting the inclsusion criteria with the additional inclusion criteria of being below 1 year old and confirmed as SCD positive, and Subset 4) children fitting inclusion criteria with the exception of the first exclusion criteria who were over

Table 5.1. Inclusion and Exclusion Criteria for Study

Inclusion Criteria	Exclusion Criteria
▪ Children aged 6 months up to, but not including 18 years ▪ Children with clinical indication for a blood draw ▪ Children whose parents give a written informed consent to be part of the study ▪ Children whose parent consent to have blood draw for clinical purposes and for the study	▪ Children who have had a sickling crisis one month prior to the blood draw (except for the subset specified below) ▪ Children who have been treated with hydroxyurea in the last four months

1 year old, confirmed as SCD positive, and had undergone a sickling crisis within the last 48 hours.

The first two subsets were recruited to achieve a population with roughly 50% SCD positive participants. These participants provide the main population of interest in the study. The last two subsets were of interest to test potential confounding factors for a field diagnostic. Before achieving 1 year of age, infants may still have a large proportion of fetal hemaglobin, HbF, in their blood. This hemoglobin could reduce the percent of the cells present that are dense, and reduce the sensitivity of a density-based assay for this subset. An evaluation of this subset allowed us to determine whether there was a difference between the predictive value of the SCD-AMPS test for children below 1 year of age and children above 1 year of age. Similarly, participants who have SCD and have recently experienced a sickle crisis may have cleared all dense cells in their blood.[9] **Table 5.2** details the the final populations used in the study.

Evaluation of samples by standard methods. Hemoglobin electrophoresis (HE) and CBCs were performed on all the samples. The rapid tests and confirmatory tests occurred at different laboratories and were performed by separate personnel to ensure proper blinding of the results. During the pilot phase of the study, we established the maximum time between sample collection and testing for each type of analysis, as well as other criteria to deem samples unusable (e.g. visible clots forming) (**Appendix III; Table III.1**). Results from HE and CBC allowed us to classify subjects as SCD, sickle cell trait, or non-SCD based on detecting the presence and quantity of Hb S as well as evaluation of the red blood cell indices (see Appendix III).

Visual inspection and validation. After a one day training, readers were instructed to evaluate each test by classifying the amount of red color that was visible at each interface using

Table 5.2. Basic Characteristics of the Study Population

Population	Zambia Subjects
Positive (HbSS)	322
≥ 1 yr, non-crisis	*270*
< 1 yr, non-crisis	*19*
>1 yr, crisis	*33*
Negative	183
HbAA	*136*
HbAS	*47*
TOTAL	**505**

the following five criteria: 1) no red cells detectable, 2) less than half a layer of red cells, 3) over half layer of red cells, 4) full layer of red cells, or 5) majority of red cells (**Appendix III; Figure III.3**). We chose to use these five classifications rather than a simple binary reading in order to understand how different cut-offs could affect test performance. Although the five levels add complexity to interpretation, they allow a greater resolution of the potential differences in the densities of cells.

Field visits to obtain feedback from end-users. We performed demonstrations of the rapid test and gathered feedback on the use of the test from the clinical staff at two rural health centers (RHCs) in the Luwingu District of Northern Province, Luena RHC and Ipusukilo RHC. The Northern Province is estimated to have a high prevalence of SCD.[6] We selected the two centers in the Northern Province for their remote location with no access to grid electricity or paved roads. At each site, over the course of two days, study staff members provided an information session about sickle cell disease and management for the clinical staff and the community, as well as an information session and demonstration of the SCD-AMPS-2 rapid test. Following these sessions, a survey of the staff members assessed their familiarity with other rapid tests, and their thoughts on the SCD-AMPS-2 rapid test.

Results and Discussion

The packaging method prevented the evaporation of samples. All rapid tests were evaluated for modes of failure before use, and the result of this inspection was logged for the vast majority of the tests used (n = 624). We found two modes of failure of the rapid test after packaging, shipping, and storing. In 3.8% of the tests, the plug from the removable rubber cap on the tube snapped, leaving the capillary plugged and unusable. 1.5% of the rapid tests had incorrect liquid levels; 1.0% were under-filled and 0.5% were over-filled. The discrepancy may

have been due to improper coverage with the silicone seal allowing water to either enter or leave the capillary tube. Notably, all tests formed the correct number of phases as verified by visual inspection. The total failure rate for the packaging of the rapid tests was 5.3%.

Performance of SCD-AMPS. We calculated the sensitivity and specificity of SCD-AMPS-2 and SCD-AMPS-3 using each of the five classifications for the level of red cells below the bottom interface. We constructed receiver operating characteristic curves using these calculations **(Figure 5.2).** The area under the curve (AUC) for SCD-AMPS-2 was 0.73 and for SCD-AMPS-3 was 0.70. This indicates an ability to discriminate sickle cell disease, but is lower than previous estimates of performance for these systems using digital analysis (AUC > 0.95) (Chapter 4).

We used the threshold at which the product of the sensitivity and specificity was highest to use as the evaluation threshold for each of the two SCD-AMPS. For SCD-AMPS-2, this level was "less than half a red layer" at the bottom of the tube or higher to be considered positive (Level 2). For SCD-AMPS-2, the cutoff was a "full layer of red" at the bottom of the tube or higher (Level 4). Using these thresholds, visual readings of SCD-AMPS-2 provided a sensitivity of 87% with a 95% confidence interval (CI) of 82-90%, a specificity of 60% (CI 53-67%), and an overall diagnostic accuracy of 77% (CI 73-81%); and SCD-AMPS-3 had a sensitivity of 75% (CI 70-79%), a specificity of 60% (CI 53-67%), and an overall diagnostic accuracy of 69% (CI 65-73%).

Part of the reduced specificity could be attributed to the bias of the readers at UTH to read samples with a higher level of redness compared to the expert reader (Appendix III). The use of a cell phone camera or portable scanner to analyze the rapid tests would eliminate the subjectivity associated with human readers.

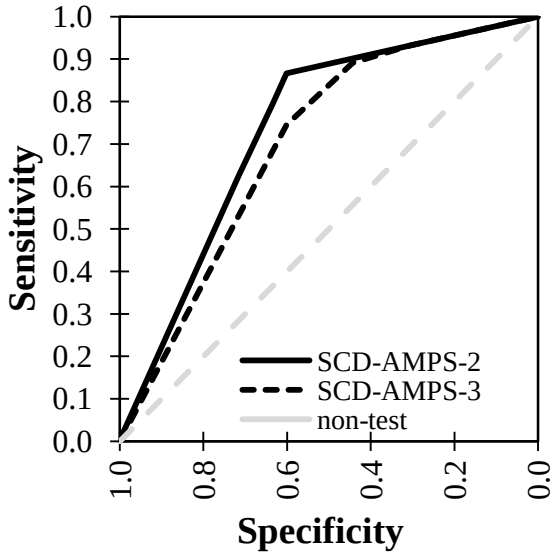

Figure 5.2. Receiver Operating Characteristic (ROC) curve of SCD-AMPS-2 and SCD-AMPS-3 including all data from Zambia shows fair discriminative ability. The amount of red cells below the bottom phase of each test was evaluated by eye and classified on a five point scale. Both tests showed an ability to discriminate sickle cell disease form non-disease. In general, the specificity was found to be lower than the sensitivity of the tests.

The trial in Zambia introduced several other variables that may have played a role in the lower performance, and are potential areas for improvement for development of a point-of-care diagnostic. These variables include: variability in batches of AMPS (**Appendix III; Figure III.4, Table III.2**), variability in manufacturing of the rapid tests, shipping and storage conditions, and clotting of blood samples. We analyzed each of these variables and concluded that three of them were the most probably causes of the reduced performance: 1) storage and shipping conditions, 2) variability in the density of the bottom phase between batches, and 3) clotting (see Appendix III).

Five batches of SCD-AMPS tests were made at Harvard and shipped to UTH during the course of the study. Slight variations in the density of the bottom phase of each batch may have impacted the performance of the tests; this issue could be addressed by implementing tighter quality control at the site of production and by developing density standard beads for the tests. All batches were shipped with ice packs and insulation via FedEx, generally arriving at UTH five days after dispatch from Harvard. The third batch, however, was delayed in transit due to a fire at the Nairobi International Airport that disrupted travel and shipping throughout sub-Saharan Africa. This batch took ten days to arrive at UTH. The SCD-AMPS-2 from Batch 3 had the second lowest diagnostic accuracy of the batches, and the SCD-AMPS-3 tests from that batch had the lowest diagnostic accuracy of all batches (**Appendix III; Figure III.4**). Without data loggers for temperature and humidity, we can only speculate about whether the additional transit time resulted in an extreme condition, and, thus, we have included the results of tests from the third batch in the overall analysis. Notably, performance improves when these results are excluded; SCD-AMPS-2 improves to a sensitivity of 90% (85-93%) and a specificity of 64%

(55-72%), and SCD-AMPS-3 improves to a sensitivity of 79% (73-83%) and a specificity of 70% (62-78%).

Variability in the total blood drawn from each subject may have led to samples receiving different concentrations of EDTA. We found that both under treatment and over treatment with EDTA could lead to false positives as a result of clotting or dehydration from high levels of EDTA (**Appendix III; Figure III.5**). The heparin coating on the capillary tubes had a negligible effect. The eventual use of SCD-AMPS directly from fingerprick samples necessitates future work to incorporate effective anti-coagulants into the blood collection aspect of the SCD-AMPS tests.

Based on our previous work (Chapter 4), we set 48 hours after blood was drawn as a cutoff for inclusion in the study. To test the effect of time after collection to running tests, we also collected samples to run after 48 hours. Binning test results based on whether they were run in the first, second, or third 24 hour time period after collection demonstrated a clear decline in specificity over time (**Figure 5.3**). Both SCD-AMPS-2 and SCD-AMPS-3 showed significant (p-value = 0.0019 and 0.012) decline between samples run within 24 hours and those run after 48 hours. Although sensitivity also showed variation between times (**Figure 5.3**), for both systems the only significant (p-value = 0.012 and 0.016) difference was a decline between samples collected between 24 to 48 hours and those over 48 hours old.

Future work on the development of SCD-AMPS as a rapid test should focus on quality control to reduce batch to batch variations in density, evaluation of shelf-life and stability in various shipping conditions, and effectiveness when used on fresh blood samples from finger pricks rather than venous blood that has been stored at 4° C.

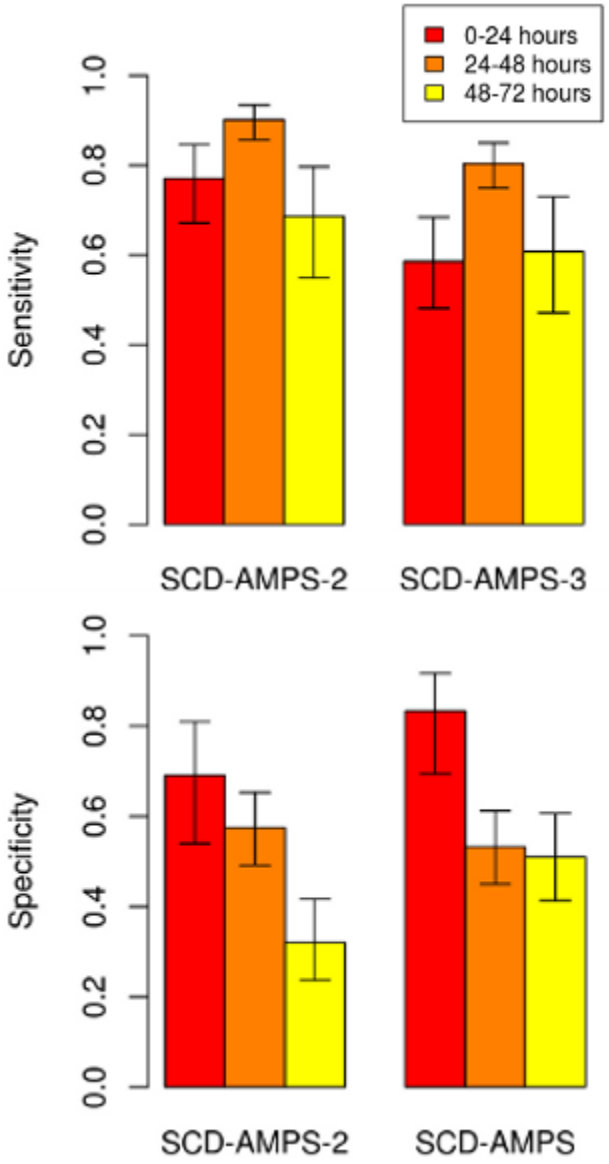

Figure 5.3. The sensitivity and specificity of SCD-AMPS as a function of the amount of time between collecting samples and running tests. The specificity shows a decline over each 24 hour increment.

Performance on Subpopulations. We evaluated several subpopulations of interest to determine whether the SCD-AMPS tests would be suitable for general screening (**Table 5.3**). One concern with a diagnostic test based on the dense cells present in SCD is that other concurrent conditions may lead to a decrease in the number of dense cells in circulation and compromise the sensitivity of the diagnostic.

The high levels of HbF in very young children (below 1 year old) has a protective effect in SCD.[10,11] To test whether this effect would reduce sensitivity, we evaluated a subpopulation of subjects with SCD that were between 6 months and 1 year of age, as well as a subpopulation of subjects with SCD that had HbF > 20%. High levels of HbF resulted in significantly decreased sensitivity in both SCD-AMPS-2 and SCD-AMPS-3 (p-value < 0.005). Interestingly, SCD-AMPS-2 showed a sensitivity for those between 6 months and 1 year of age (84%) similar to that in the general population (87%).

The occurrence of a recent vaso-occlusive crisis has been shown to reduce the percent of dense cells present in SCD;[9] we tested a subpopulation of those with SCD who self-reported to have experienced a crisis in the last 48 hours. In both SCD-AMPS-2 and SCD-AMPS-3, the sensitivity was the same or higher for this subset compared to the general population.

Severe anemia (defined as a hemoglobin concentration below 8 g/dL for children over 5 years of age and 7 g/dL for children under 5 years old)[12] is common among patients with SCD. Anemia can also result from other genetic disorders (e.g., alpha-thalassemia) or nutritional deficiencies (e.g., iron deficiency), which could result in a reduction in the density of red blood cells. In both SCD-AMPS systems, however, those with both SCD and severe anemia were detected with high sensitivity (> 85%).

Table 5.3. Sensitivity of SCD-AMPS tests on specific subpopulations

Population	SCD Subjects	*SCD-AMPS-2* Sensitivity	CI	*SCD-AMPS-3* Sensitivity	CI
All	322	87%	(82,90)	75%	(70,79)
6-12 months	19	84%	(62,94)	52%	(31,73)
Recent Crisis[a]	33	93%	(80,98)	88%	(73,95)
HbF > 20%	36	58%	(42,70)	39%	(25,55)
Micro. Hypo.[b]	89	80%	(70,87)	62%	(51,71)
Sev. Anem.[c]	89	93%	(87,96)	86%	

[a] Self-reported to have experienced body pain or vaso-occlusive crisis within previous 48 hours.
[b] Micro. Hypo. – Microcytic & hypochromic anemia defined as patients with a mean corpuscular volume below 80 fL, a mean corpuscular hemoglobin below 26 pg/cell and a hemoglobin concentration below 13.5 g/dL for males or below 21.0 g/dL for females.
[c] Sev. Anem. – Severe anemia defined as a hemoglobin concentration below 8 g/dL for those over 5 years old, and 7 g/dL for those under 5 years old.

On both tests, specificity was similar for subjects with HbAA and HbAS; sickle cell trait was not a major factor in creating false positives (**Appendix III; Table III.3**). This characteristic sets density-based tests apart from solubility tests like Sickledex.

Although the reduction in performance due to high HbF merits some caution, the high sensitivity for children between 6 months to 1 year of age, patients with a recent vaso-occlusive crisis, and those with severe anemia suggests that the SCD-AMPS-2 test could be useful as a screening or diagnostic tool for children as young as 6 months old. Similarly, SCD-AMPS-3 could be useful if used on children over 1 year of age.

Capabilities of Rural Health Centers. A point-of-care diagnostic provides benefit when it is coupled to effective interventions. Simple interventions (e.g., pneumococcal vaccine and prophylactic antibiotics) for sickle cell disease exist, and we sought to assess whether rural health centers in Zambia had the capabilities to perform an SCD-AMPS test and provide appropriate interventions.

Working with the U.S. Peace Corps in Zambia, we identified two Rural Health Centers—Luena RHC and Ipusukilo RHC—in Northern Province to carry out a demonstration of the rapid test and an assessment of capabilities to care for patients with SCD. Our survey indicated that the clinical staff at both RHCs was well acquainted with rapid tests for malaria, HIV, and syphilis and had a supply of these tests. Neither clinic had a microscope or capabilities to diagnose SCD. Although both clinics lacked the infrastructure to perform transfusions and did not have morphine, they did have the ability to provide several other interventions that have been shown to reduce mortality and ease symptoms of sickle cell disease, including folic acid supplements, intravenous fluids, antibiotics, antimalarials, and pneumococcal vaccine (PCV) (**Appendix III; Table III.4**).[13–15]

Feedback on SCD-AMPS from end-users. The SCD-AMPS tests were designed to use minimal equipment in order to be used in low-level clinics. Apart from the SCD-AMPS tests themselves, the only other equipment necessary to perform a test is a microhematocrit centrifuge. We used a centrifuge (CritSpin, Iris Sample Processing) with a custom adapter to run off of a car battery. The tests, supplies to safely perform a finger-prick, the centrifuge, and the battery all fit into a backpack (**Figure 5.4**) and were transported from Lusaka to the RHCs by bus, shared taxis, and hitch-hiking.

We assessed the ability of the clinical staff to perform SCD-AMPS test by presenting an education session and a demonstration of the rapid test with a focus on four steps: i) checking rapid tests for defects, ii) loading blood, iii) centrifugation of tests, and iv) interpretation of rapid test results. The staff was able to handle the rapid test and ask questions about the protocol and interpretation. Afterwards, participants were surveyed to assess their comfort with each of the four steps. Their familiarity and comfort with common lateral flow rapid tests was also assessed as a benchmark for usability. Participants rated tests using a five point scale with 1 being "very difficult to use", 3 being "okay to use", and 5 being "very easy to use." The clinical staff rated the ease of use of lateral flow tests, such a rapid diagnostic test for malaria, as 3.4.

Evaluation of the rapid test was broken into four sections: Step 1) initial setup, Step 2) loading blood, Step 3) running tests (centrifugation), and Step 4) reading results. Each step was rated for ease on the same 5 point scale. The initial set up was given an average rating of 3.3. The loading step was given an average rating of 3.4. Running the tests was given an average rating of 3.3. Reading results was given an average rating of 3.3. Every step was, thus, comparable to the ease of use of existing rapid tests.

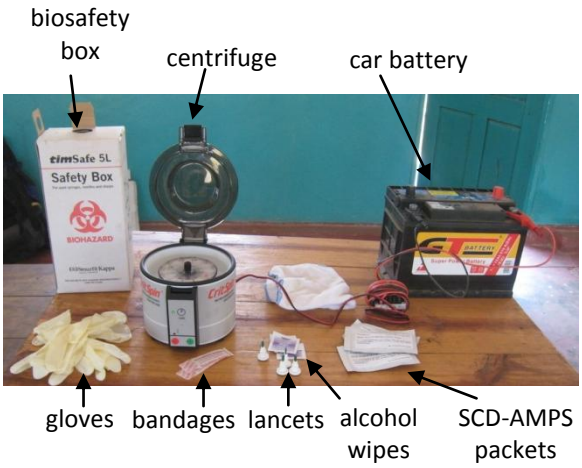

Figure 5.4. All the equipment necessary to run the rapid test in a rural clinic fits inside a backpack and were evaluated at rural health centers in Zambia.

Conclusions

A density-based diagnostic for sickle cell disease using AMPS has the potential to fill a critical healthcare gap in low-resource settings. Although sensitivity and specificity are not as high as those of gold standard methods like HPLC and IEF, these tests could provide actionable information when coupled with patient history and clinical presentation. Many clinics, such as those visited in Zambia, do not have the infrastructure to support the equipment needed for gold standard methods, but could run SCD-AMPS tests. Solubility tests, such as Sickledex™, are often used to screen for SCD in clinics in India and sub-Saharan Africa, but they cannot differentiate between the non-disease, carrier sickle cell trait and SCD. Although SCD-AMPSs do not distinguish HbAA from sickle cell trait, SCD-AMPSs do discriminate between SCD and sickle cell trait.

The diagnostic ability of the SCD-AMPS depends on the presence of dense, sickled cells in the blood. These cells will not be present in newborns, and hence SCD-AMPS would not be appropriate for neonatal screening. After 6 months, however, the amount of dense cells present is sufficient to allow use of SCD-AMPS-2. Coupled with vaccination programs, screening children for SCD with an SCD-AMPS test could provide useful information on prevalence.

SCD-AMPS are also simple to use; Initial demonstrations with staff at rural clinics in Zambia indicate that SCD-AMPS tests are comparable to standard rapid diagnostic tests for malaria in ease-of-use. The capability to diagnose sickle cell disease at primary health centers and rural health centers in places like Zambia would allow the targeted use of appropriate interventions (e.g., vaccines, prophylactic penicillin, and supplements for folate and iron). These interventions could reduce child mortality and improve the quality of life for those that live with undiagnosed sickle cell disease.

Acknowledgement

The authors thank Mubanga Mutale, Titus Kaira, Gloria Muyunda, Euphrasia Phiri, and Nicholas Aulelyo for their dedication as members of the UTH study staff; the U.S. Peace Corps Office in Zambia and Peace Corps Volunteers Erica Orange and Dan Osterhange for arranging rural site visits; and Dr. Leslie Kalish (Children's Hospital, Boston) for helpful consultation on biostatistics. This work was supported by a Blavatnik Biomedical Accelerator Award and by a Research Grant from the Harvard Global Health Insitute. A.A.K. acknowledges support from the Office of Naval Research through the NDSEG Fellowship Program and from a Graduate Research Fellowship from the National Science Foundation.

References

(1) Grosse, S. D.; Odame, I.; Atrash, H. K.; Amendah, D. D.; Piel, F. B.; Williams, T. N. *Am. J. Prev. Med.* **2011**, *41*, S398–405.

(2) Piel, F. B.; Hay, S. I.; Gupta, S.; Weatherall, D. J.; Williams, T. N. *PLoS Med.* **2013**, *10*, e1001484.

(3) Embury, S.; Clark, M. *J. Clin. Invest.* **1984**, *73*, 116–123.

(4) Fabry, M. E.; Mears, J. G.; Patel, P.; Schaefer-Rego, K.; Carmichael, L. D.; Martinez, G.; Nagel, R. L. *Blood* **1984**, *64*, 1042–1046.

(5) Mace, C. R.; Akbulut, O.; Kumar, A. A.; Shapiro, N. D.; Derda, R.; Patton, M. R.; Whitesides, G. M. *J. Am. Chem. Soc.* **2012**, *134*, 9094–9097.

(6) Piel, F. B.; Patil, A. P.; Howes, R. E.; Nyangiri, O. A.; Gething, P. W.; Williams, T. N.; Weatherall, D. J.; Hay, S. I. *Nat. Commun.* **2010**, *1*, 104.

(7) Louderback, A. L.; Youhne, Y.; Fontana, A.; Natland, M. *Clin. Chem.* **1974**, *20*, 761–764.

(8) Yang, X.; Kanter, J.; Piety, N. Z. N.; Benton, M. S. M.; Vignes, S. M.; Shevkoplyas, S. S. *Lab Chip* **2013**, *13*, 1464–1467.

(9) Fabry, M. E.; Benjamin, L.; Lawrence, C.; Nagel, R. L. *Blood* **1984**, *64*, 559–563.

(10) Steinberg, M. H. *Br. J. Haematol.* **2005**, *129*, 465–481.

(11) Akinsheye, I.; Alsultan, A.; Solovieff, N.; Ngo, D.; Baldwin, C. T.; Sebastiani, P.; Chui, D. H. K.; Steinberg, M. H. *Blood* **2011**, *118*, 19–27.

(12) WHO. *Haemoglobin concentrations for the diagnosis of anaemia and assessment of severity*; World Health Organization: Geneva, 2011; pp. 1–6.

(13) Gaston, M.; Verter, J.; Woods, G.; Pegelow, C.; Kelleher, J.; Presbury, G.; Zarkowsky, H.; Vichinsky, E.; Iyer, R.; Lobel, J.; Diamond, S.; Holbrook, C.; Gill, F.; Richey, K.; Faletta, J. *N. Engl. J. Med.* **1986**, *314*, 1593–1599.

(14) McGann, P. T.; Ferris, M. G.; Ramamurthy, U.; Santos, B.; de Oliveira, V.; Bernardino, L.; Ware, R. E. *Am. J. Hematol.* **2013**, *88*, 984–989.

(15) Quinn, C. T.; Rogers, Z. R.; McCavit, T. L.; Buchanan, G. R. *Blood* **2010**, *115*, 3447–3452.

Appendix I

Supporting Information

Enrichment of Reticulocytes from Whole Blood using Aqueous Multiphase Systems of Polymers

Ashok A. Kumar, Caeul Lim, Yovany Moreno, Charles R. Mace, Abeer Syed, Daria Van Tyne, Dyann F. Wirth, Manoj T. Duraisingh, and George M. Whitesides

Materials and Methods

Materials. We purchased the following polymers: poly(ethylene glycol) (Sigma-Aldrich; MW = 20000 Da), Ficoll (Sigma-Aldrich; MW = 70000 Da and 400000 Da), dextran (Spectrum Chemical; 500000 Da), and poly(vinyl alcohol) (Polysciences; MW = 3000 Da). We purchased phosphate-buffered saline (Lonza) at 10× concentration and diluted it to 1× using distilled, deionized water from a Milli-Q water purification system (Millipore). For stains, we used New Methylene Blue for slides and ReticONE (acridine orange) for flow cytometry. We used all reagents without further purification. We purchased Lymphoprep from Accurate Chemical, fluorescein isothiocyanate from Thermo Scientific, and Percoll from GE healthcare. For the parasite culture media, we purchased RPMI, hypoxanthine and sodium bicarbonate from Sigma, HEPES from EMD Biosciences, and Albumax from Invitrogen.

We purchased human whole blood, collected over sodium heparin as an anticoagulant, from single healthy donors (vendor certified syphilis$^-$, HTLV$^-$, HIV$^-$, HepB$^-$, and HepC$^-$) from Research Blood Components (Boston, MA). Whole blood units (approximately 500 mL in volume) collected from hemochromatosis patients undergoing therapeutic phlebotomy were obtained from the blood donor center at Brigham and Women's Hospital, Boston, MA.
The H Strain of *Plasmodium knowlesi* was obtained from the Biomedical Primate Research Center (Rijswijk, The Netherlands). The 3D7 Strain of *Plasmodium falciparum* was obtained from the Harvard School of Public Health (Boston, MA, USA).

Formation and Analysis of AMPSs. The system C1 that was used for the invasion assays was created in the following way: 1) measure 12% (w/v) Ficoll and 12% dextran (w/v) into a volumetric flask (i.e. 12 grams of each into a 100 mL flask), 2) add 5 mM disodium ethylenediaminetetraacetic acid (EDTA) to prevent coagulation, 3) add 5 mM of sodium

phosphate monobasic and 5 mM of sodium phosphate dibasic to buffer the system, 4) add deionized water (MilliQ) to dissolve all the components and attain the final volume, 5) mix the solution well, measure the pH (Orion Star, Thermo Scientific), and adjust to 7.40 ± 0.02 by titrating with concentrated (1-10 M) NaOH and HCl, 6) remove a small aliquot (100 µL) of the mixture and centrifuge to separate phases, 7) measure the osmolality by vapor pressure osmometry (Vapro 5600, Wescor), 8) add solid NaCl to adjust osmolality to the desired level (1 M of NaCl ~ 2 Osm/kg), 9) check and adjust pH again. After these steps, we centrifuged 4 mL of the solution in a polycarbonate conical tube and separated the phases using a pipette to remove the top phase and a syringe to puncture the bottom of the tube and remove the bottom phase. We then characterized the pH, osmolality, and density of each phase. An oscillating U-tube densitometry (Anton Paar DM35N) measured the density of each phase.

For initial screening of different AMPS, we followed the same steps above to prepare stock solutions of AMPS at concentrations higher (15% (w/v) of each polymer) and lower (5% (w/v) of each polymer) than those used in applications of aqueous multiphase systems (AMPSs). We then mixed these solutions in different ratios to attain a series of AMPS with different densities.

Measurements of density characterized stock solutions and to ensure uniformity across multiple preparations of each solution. To prepare AMPSs, we added solutions of polymers (either at stock concentrations or a dilution) into a container (e.g., conical tubes), thoroughly mixed the solutions by vortex for 30 seconds, and accelerated phase separation by centrifugation. Phase separation in AMPSs due to gravity alone may occur inconveniently slowly (hours) because the difference in density between layers of an AMPS can be small ($\Delta\rho \approx 0.001–0.100$

g/cm^3). Centrifugation (2 – 30 minutes at 2000 g) increased the rate of separation of phases in AMPSs.

Separations of Blood with AMPS. We performed separation experiments within one week of the blood being drawn. Blood was stored at 4 °C and brought to room temperature before use. We introduced the blood to the top phase of the AMPS as a layer in all of our experiments. Samples were spun at 4000 *g* for one hour at a temperature of 32 °C.

DC-Percoll Separations. To compare our enrichment method to a standard technique, we used a standard density separation with Percoll. Centrifugation of blood in 50 mL tubes at 4000 *g* for one hour packed cells. After removing the serum, the top 4 mL of packed blood was collected and resuspended in the previously collected serum at ~50% hematocrit. We layered 5 mL of this blood on top of 6 mL of 70% isotonic Percoll. Centrifugation for 15 minutes at 1200 *g* at 30 °C in a swinging bucket rotor (SX4750A, Beckman Coulter) left a band of erythrocytes above the Percoll and a pellet of erythrocytes at the bottom. A pipette collected the band from above the Percoll. Washing the collected samples with PBS three times removed excess Percoll before analysis and the introduction of parasites.

Characteristics of blood samples used. We used blood from two sources: a commercial supplier (Research Blood Components) and a hematology clinic (Brigham and Women's Hospital, Boston). The blood from the commercial supplier was collected with an anti-coagulant from normal, healthy individuals. The blood from the hematology clinic came from hemochromatosis patients undergoing treatment. Despite the hemochromatosis, the blood from many of these patients did not reveal a level of reticulocytes that was significantly higher than normal. In this work, all the blood that was used contained the clinically normal range of 0.5–2.5% reticulocytes before enrichment.[1] Blood from hemochromatosis patients was used only in

the work to screen different AMPS. All experiments with parasites were done with normal human blood. White blood cells were removed from the blood prior to use by passage through a leukocyte filtration device (Sepacell R-500). The removal of white blood cells is necessary for the cultivation of *Plasmodium* parasites.

Extraction of Fractions of Cells after Separation. For separations on whole blood performed in conical tubes with AMPS, blood enriched for reticulcoytes concentrated at the liquid/liquid interface. After blunting a pipette, we removed the clumps of packed red cells that could be seen by eye at this interface. Depending on the yield and the tube used, the total volume extracted ranged from 100 μL to 1 mL. 5 μL of packed cells from the pellet at the bottom of the tube were also collected for analysis.

For screening experiments, washing extracted cells in roughly a five-fold volume of isotonic PBS a total of three times removed excess polymers for analysis (i.e., microscopy on thin smears or flow cytometry). During each wash, we suspended the cells gently with a pipette and then spun the cells to a pellet at 1,500 *g* for 6 minutes. After the supernatant was removed, the cells were suspended again until all washes were completed. For invasion experiments, increasing the volume of PBS to be 20-fold the volume of the sample provided a more thorough washing to remove excess polymers.

Analysis of the Fractions of Blood. We counted reticulocytes by flow cytometry (MACS Quant). Reticulocytes were stained with acridine orange (Retic ONE) following the manufacturer's protocol. Using known volumes of sample, we counted cells and also quantified the fraction of all cells that were reticulocytes. Comparing samples before and after enrichment allowed us to estimate the total number of reticulocytes that were added to each AMPS, and the

total number of reticulocytes recovered. The fraction of these two numbers provided a measure of the yield of reticulocytes.

We also made thin smears stained with New Methylene Blue (Retic Stain) and quantified reticulocytemia by microscopy. To analyze other cell parameters, we used a hematology analyzer (Advia 2120, Siemens).

Statistical Methods. We used a paired, two-sided Student's T-test to test for significant differences between the logarithms of the parasitized erythrocyte multiplication rates (PEMRs) to compare blood from donors with different treatments. For reticulocytemias and yields of reticulocytes from different donors enriched over several AMPS (**Chapter 3; Table 3.1**), we provide the median, minimum, and maximum for biological replicates to provide a clearer representation of the actual experimental data than means and standard deviations would provide with four biological replicates. Results from technical replicates are reported as means of the technical replicates.

Experimental Details

Selection of AMPSs. The dextran–Ficoll AMPS exhibited a small difference in density between the top and bottom phases. Without additives, dextran–Ficoll AMPSs prepared in distilled, deionized water that are in the density range of blood cells are acidic and hypotonic. We titrated the pH to 7.40 with NaOH and HCl. We added NaCl to the solutions to reach a final osmolality of 295 ± 15 mOsm/kg (i.e., isotonic).

The small step in density in the dextran–Ficoll AMPS allowed us to create a bottom phase with a low enough density to allow mature erythrocytes to pass through it, and a top phase dense enough to prevent the blood from mixing instantaneously after being layered over the

AMPS. We explored two other systems—a poly(ethylene glycol)–Ficoll AMPS and a poly(ethylene glycol)–dextran AMPS—as alternative systems.

The poly(ethylene glycol)–Ficoll AMPS exhibited differences in density between phases that were greater than 0.030 g/cm^3. We could not produce a top phase with a density significantly greater than that of plasma (ρ = 1.026 g/cm^3) while keeping the osmolality of the phases isotonic; this AMPS was, thus, not suitable for blood separations.

The poly(ethylene glycol)–dextran AMPS had similar characteristics to the poly(ethylene glycol)–Ficoll AMPS. The poly(vinyl alcohol)–poly(ethylene glycol) AMPS could not produce a bottom phase that was dense enough to separate most reticulocytes from mature erythrocytes in the range of osmolality that is required for the separation of cells.

Centrifugation Parameters. Our separations used swinging-bucket rotors for centrifugation to avoid smearing cells along the walls of centrifuge tubes during sedimentation. Centrifugation at a relative centrifugal force (RCF) of 4000 *g* for one hour provided a clear separation between blood cells at the liquid/liquid interface of the two-phase AMPS and cells below the bottom phase for a sedimentation distance of 40 mm (e.g., 4 mL of AMPS in a 15 mL conical tube) (**Chapter 3; Figure 3.1**). Experiments with a greater distance for sedimentation (e.g., 60 mm for 25 mL blood over 25 mL AMPS in a 50 mL conical tube) required additional centrifugation time. For larger volumes that had up to a 50% increase in the sedimentation distance (i.e., 25 mL of AMPS in a 50 mL conical tube) the centrifugation time was increased to 90 minutes. The limitation of a long period of centrifugation can be overcome by using a centrifuge that operates at higher relative centrifugal forces.

Detailed Results from Enrichment of Reticulocytes from Whole Blood. Table I.1 details the parameters of the different AMPS that were screened as well as the results from

Table I.1. The enrichment of reticulocytes at the interface of dextran–Ficoll AMPSs with varying density and osmolality.

ID	Concentration (% w/v) Ficoll	dextran	Tonicity (mOsm/kg)	Density (g/cm^3) Top	Bottom	AMPS Interface Retic[a]	S.D.[b]	Initial Retic[a]
Isotonic Systems (295 ± 15 mOsm)								
A1	12.0	12.0	299	1.089	1.092	1.1	0.4	1.1
A2	11.4	11.4	295	1.084	1.087	2.1	0.7	1.1
A3	11.1	11.1	306	1.082	1.085	21	5.2	1.8
A4	10.8	10.8	301	1.080	1.083	24	4.1	1.8
A5	10.3	10.3	289	1.076	1.080	28	10	1.8
Hypotonic Systems (260 ± 10 mOsm)								
B1	10.5	10.5	250	1.079	1.083	2.0	1.0	1.1
B2	10.0	10.0	252	1.074	1.078	4.7	1.5	1.1
B3	9.5	9.5	252	1.071	1.075	19	1.6	1.1
B4	**9.3**	**9.3**	**269**	**1.068**	**1.072**	**55**	**8.4**	**1.8**
B5	9.0	9.0	264	1.067	1.071	43	5.1	1.8
Hypertonic Systems (330 ± 10 mOsm)								
C1	12.0	12.0	327	1.089	1.092	12	0.7	2.4
C2	11.6	11.6	340	1.086	1.089	27	3.1	2.4
C3	11.4	11.4	336	1.084	1.088	43	4.7	2.4
C4	11.0	11.0	332	1.081	1.085	50	1.5	2.4
C5	10.6	10.6	328	1.078	1.082	31	2.8	2.4
C6	10.1	10.1	329	1.075	1.079	21	2.4	2.4

[a] Mean reticulocyte count per 100 erythrocytes (n = 3 technical replicates)
[b] Standard deviation of the replicates
b.f. System with the highest level of enrichment

enrichments of reticulocytes. We performed additional enrichments using the hypertonic systems (C1-C6) with different loading volumes (**Figure I.1**). From this we found multiple systems that were capable of attaining enrichments to reticulocytemias over 50%. **Table I.2** details the enrichments for different donors with four different AMPS.

The volume ratio of blood to AMPSs affects both yield and purity of enrichments. We expected that the performance of hypertonic and hypotonic AMPSs would be dependent on the volume ratio of blood and AMPSs. In an isotonic system, we anticipated that this dependence would be negligible since water exchange between polymers and blood cells would be minimal. We found, however, that the volume ratio of blood and AMPSs did affect performance in an isotonic system. A range of volumes of blood (1 mL, 4 mL, and 8 mL) were loaded onto 4 mL of the hypertonic AMPS (C1-C6) (**Figure I.1**).

Dispersal of Plasma Proteins into AMPS. We hypothesized the dependence of enrichments on the volume ratio of blood to AMPS might be due to a slight amount of mixing of plasma which would dilute the phases and would depend on the volume ratio of blood to polymer. We checked the density of the phases after a separation to see if there was a change in the phases. When 2 mL of blood was layered on top of 4 mL of A5, the density of both phases decreased ($\Delta\rho_{top}$ = -0.013 g/cm^3, $\Delta\rho_{bottom}$ = -0.016 g/cm^3); we used isotonic A5 rather than hypertonic AMPS to avoid changes in volume that would result from the cells shrinking or swelling.

If a boundary layer of plasma were to penetrate the top phase with the cells and then mixes with the phase, we would expect to see plasma proteins dispersed in the top phase. To visualize the dispersal of plasma proteins into an AMPS during an experiment—layering blood, introduction into a centrifuge, fractionation by centrifugation, and removal from a centrifuge—

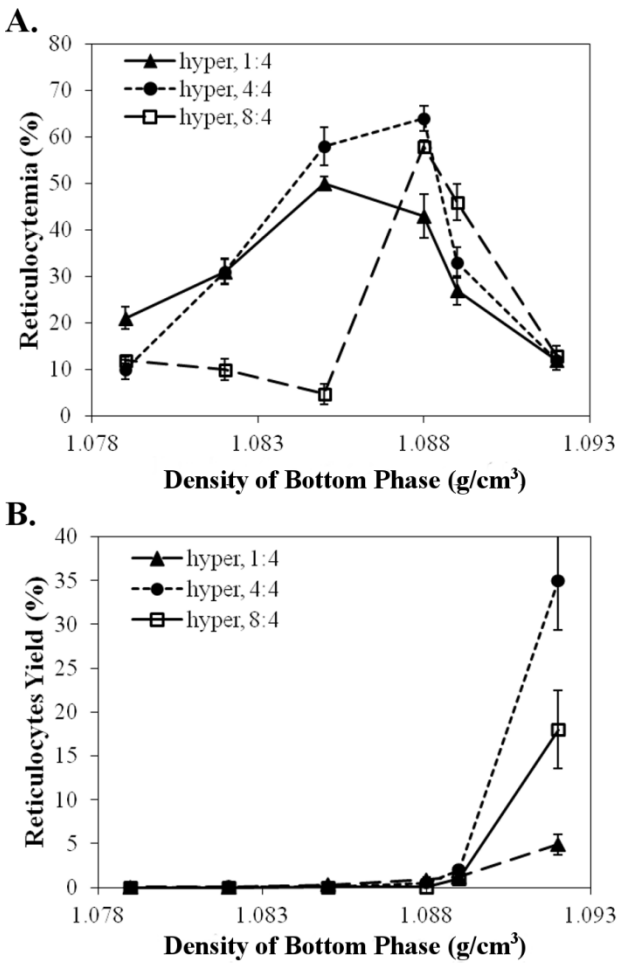

Figure I.1. The enrichment of reticulocytes in hypertonic systems changes with different volume ratios (vol. blood (mL):vol. AMPS (mL)) of blood to AMPS. Both the reticulocytemia and yield show changes. A 4:4 ratio provides the best yield. Several systems provide enrichment to reticulocytemias over 50%.

Table I.2. Performance of AMPS over different individuals.

	Initial	C1 (%)		C2 (%)		B3 (%)		A5 (%)	
Donor	Retic.	Retic.	Yield	Retic.	Yield	Retic.	Yield	Retic.	Yield
A	0.80	19	0.24	28	0.11	35	0.013	35	0.0086
B	0.85	21	0.75	30	0.095	49	0.053	45	0.013
C	1.3	18	2.4	32	1.7	38	0.011	45	0.00079
D	0.83	15	6.0	15	1.7	18	0.0065	15	0.0036
Median	0.84	19	1.6	29	0.89	36	0.012	40	0.0061
Min.	0.80	15	0.24	15	0.095	18	0.0065	15	0.00079
Max.	1.3	21	6.0	32	1.7	49	0.053	45	0.013

we added a fluorescent protein into whole blood as a marker. We prepared fluorescein-labeled bovine serum albumin (FITC-BSA) by following the Thermo Scientific protocol for coupling reactions using fluorescein isothiocyanate. After dialysis against isotonic PBS, the final concentration of FITC-BSA was ~ 7 mg mL^{-1}. We mixed this solution with whole blood at a ratio of 1:9 to create an experimental sample. A control sample was made by mixing PBS with blood at a ratio of 1:9. The blood samples were each layered over dextran–Ficoll AMPS (1 mL blood over 3 mL AMPS). The samples were sedimented by centrifugation at an RCF of 2000 *g* for 100 minutes at 25 °C in an Allegra-6R swinging bucket centrifuge.

We imaged the systems after fractionation using a combination of brightfield and fluorescent techniques (**Figure I.2**). For the fluorescence images, the tubes were kept in a dark box, illuminated with longwave UV light (λ = 365 nm), and imaged using a bandpass filter (500 – 600 nm) in front of the camera. Although the fluorescence intensity is highest in the plasma layer, we observe that some FITC-BSA is present in the top phase of the AMPS. The diffusion length of serum albumin in whole blood over the course of a 100-minute experiment is approximately 5 mm ($D_f \sim 2.1 \times 10^{-10}$ m^2 s^{-1}).[2] The distance between the plasma/top phase boundary and the AMPS interface is 14 mm. Diffusion alone, therefore, cannot account for the presence of FITC-BSA in the top phase of the AMPS. Dilution of the top phase from the mixing of the boundary layer of cells would change the equilibrium of the AMPS, shift the water and polymer contents of the bottom phase, and reduce the bottom phase density. Additional studies could further elucidate the connection between sample volumes and enrichment, but were beyond the scope of this work.

Reticulocyte enrichments scale to 25 mL of blood without a loss in purity. The purity and yield of reticulocytes remain fairly constant as volumes are increased provided that the

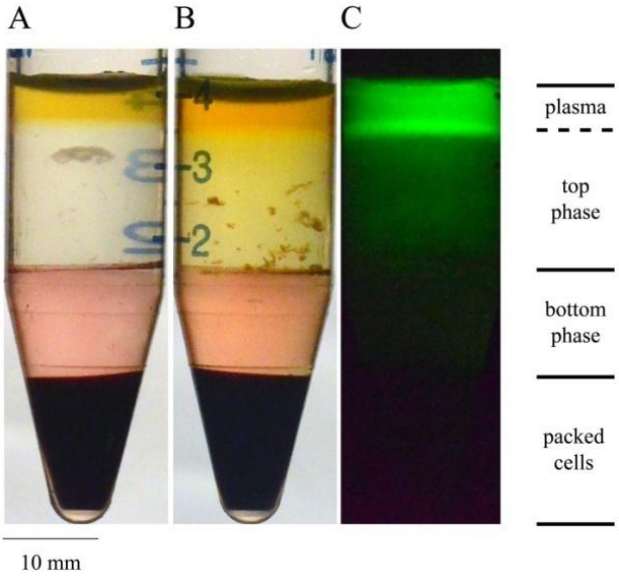

Figure I.2. Dispersion of protein from plasma into AMPS. Brightfield images of whole blood after fractionation by AMPS without (A) and with (B) the addition of 700 µg/mL fluorescein-labeled BSA. A fluorescence image (C) of the tube in (B) after illumination with longwave UV light.

volume ratio of AMPS to blood remains constant (**Figure I.3**). Using the same isotonic dextran–Ficoll AMPS as used in the volume ratio experiments, we performed a series of enrichments on blood from a single donor with volumes of blood ranging from 2 mL to 25 mL. In all cases, a volume ratio of 1:1 between blood and AMPS was used; this ratio provided the best combination of yield and enrichment (**Figures I.1 & I.4**). Both 15 mL and 50 mL conical tubes were used. Interestingly, the yield initially decreased as volume increased. At 6 mL, the results were similar for both the types of tubes used. Above this volume, however, yield and reticulocytemia remained relatively constant.

Pre-enrichment increases the purity of the final enrichment. When using differential centrifugation, naturally pre-enriched blood has a higher final enrichment than normal blood.[3,4] Similarly, we expected that blood pre-enriched for reticulocytes by density would have a higher final enrichment after centrifugation through an AMPS.

Using blood from a single donor with an initial reticulocytemia of 2.2%, we pre-enriched reticulocytes from 100 mL of blood with two different methods: a) differential centrifugation, and b) centrifugation through AMPS C1. The enriched fractions collected had a reticulocytemia of 4.7% and 14%, respectively. The total amount of cells recovered differed as well. We recovered approximately 8 mL of packed cells from differential centrifugation and resuspended them in a volume of 16 mL using homologous plasma recovered from the centrifugation. We only recovered ca. 100 μL of packed cells from AMPS C1. After washing these cells three times in PBS, we resuspended them in a final volume of 3 mL. For the final enrichment, we split each suspension into thirds and layered them over 4 mL of AMPS C1. After centrifugation, we recovered cells from the AMPS interface and washed them three times in PBS. Using flow cytometry, we measured the reticulocytemia of the final enrichments. The results were similar

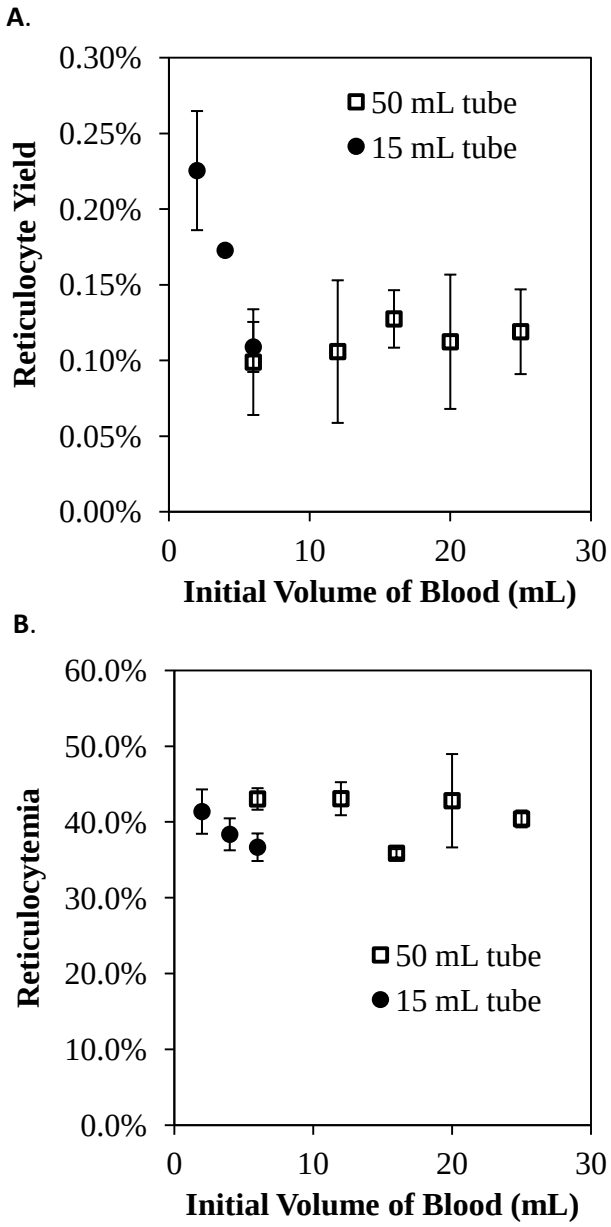

Figure I.3. Reticulocyte enrichment over AMPS C2 was comparable over multiple scales of volume. For both reticulocyte yield (A.) and reticulocytemia (B.), only one datum fell outside one standard deviation of the mean over all volumes, and all data were within two standard deviations of the mean.

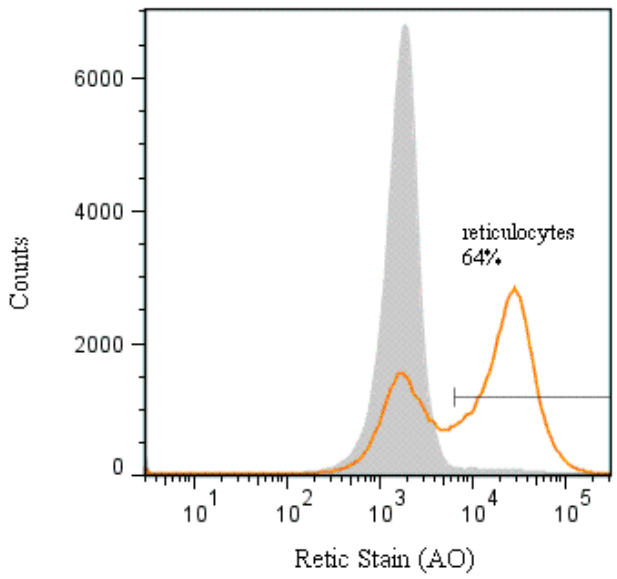

Figure I.4. A 1:1 volume ratio of blood to a hypertonic AMPS provided the maximum enrichment of reticulocytes. Using system C3, we attained a reticulocytemia of 64 ± 3% as measured by flow cytometry. The gray, filled curve shows the blood before enrichment, which had a reticulocytemia of 2.2%. After centrifugation through AMPS, the fraction of cells at the interface is dominated by reticulocytes (orange curve). Acridine orange (AO) preferentially stains the RNA in the reticulocytes, and causes the shift to the right.

for the fraction pre-enriched by differential centrifugation and that pre-enriched by centrifugation through AMPS. Final reticulocytemia was 20% and 21%, respectively.

Osmotic effects on reticulocyte enrichment by density. As discussed in Chapter 3, systems with different osmolalities achieved different yields when final reticulocytemias were similar. Also, different osmolalities had maximum enrichments for different densities of AMPS (**Chapter 3; Figure 3.2**). The effect of osmolality on the density of the cell populations of interest—reticulocytes and mature erythrocytes—may explain the difference in yields.

A cell at osmotic equilibrium with a system has a concentration of solutes, c, and a volume, V. Both the cell and the surrounding environment have a osmolarity: $\phi = \frac{c}{V}$. If the cell is now placed into a hypertonic environment with osmolarity, $\phi' = \phi + \delta\phi$, where $\delta\phi > 0$, then the volume of the cell will change to compensate by losing water. We assume that the concentration of solutes remains fairly constant due to the presence of ion pumps to maintain internal ion concentrations. Although there still may be some solute exchange between the cell and environment, we assume that at least, $\frac{\delta c}{c} \ll \frac{\delta V}{V}$. With this assumption then, the cell volume changes to V', given by Equation 1:

$$V' = \frac{V}{1 + \frac{\delta\phi}{\phi}} \qquad \text{(Equation S1)}$$

This change in volume shifts the density of a cell ($\rho_1 = \frac{m_1}{V_1}$) by changing both the mass and volume. The mass can be split into both dry mass and water mass, $m_1 = m_{1d} + m_{1w}$. The density then shifts as follows:

$$\rho_1^{'} = \frac{m_1^{'}}{V_1^{'}} = \frac{m_1 + \left(V_1^{'} - V_1\right)\rho_w}{\frac{V_1}{1 + \frac{\delta\phi}{\phi}}} \quad \text{(Equation S2)}$$

$$\rho_1^{'} = \rho_1\left(1 + \frac{\delta\phi}{\phi}\right) - \left(\frac{\delta\phi}{\phi}\right)\rho_W \quad \text{(Equation S3)}$$

$$\rho_1^{'} - \rho_w = \left(1 + \frac{\delta\phi}{\phi}\right)(\rho_1 - \rho_w) \quad \text{(Equation S4)}$$

Two different cells (e.g., a reticulocyte and a mature erythrocyte) with a density different of $\Delta\rho = \rho_2 - \rho_1$, will have a new density difference of $\Delta\rho' = \Delta\rho\left(1 + \frac{\delta\phi}{\phi}\right)$. On a population scale, this means that the distance between the two peaks of the density distribution of cells will scale with the osmolality.

Morphology of Cells after Centrifugation through AMPSs. Washing cells was an important step to restore morphology and remove excess polymer. Dextran adsorbs to the surface of cells.[5–7] Repeated washing removes some, but not all of the dextran.[6] Washing cells in an isotonic buffer such as PBS appeared to return them to their physiological volumes; that is, unwashed cells from hypotonic systems appeared swollen when observed by microscopy. After extracting and washing cells from the interface of the AMPSs, we found that both mature erythrocytes and reticulocyte had a similar morphology to fresh blood on thin blood smears (Figure I.5).

We compared the mean corpuscular volume (MCV) and the mean corpuscular hemoglobin (MCH) of RBCs isolated from five random donors before and after separations by AMPS (**Table I.3**). These quantitative results support the hypothesis that sedimentation through the AMPS does not drastically affect the morphology or the contents of cells. Evaluation of the percentage of cells that were hypochromic, hyperchromic, microcytic, and macrocytic revealed

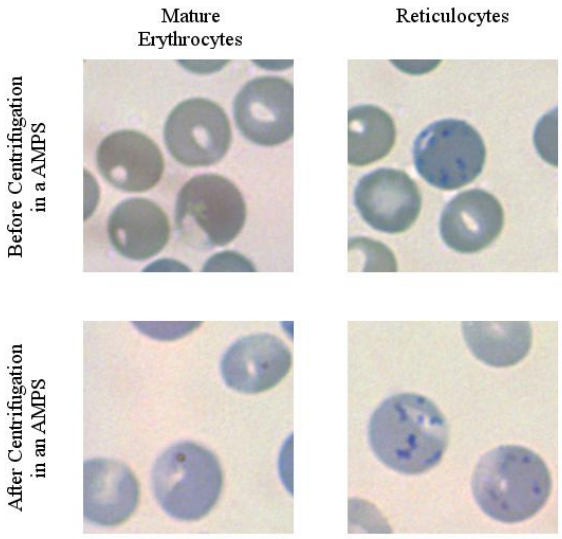

Figure I.5. Morphology of cells after separation using an AMPS. Representative micrographs of mature erythrocytes and reticulocytes before and after centrifugation in an AMPS demonstrate no significant morphological change as a result density-based separation. The blue stained clumps of RNA identify the reticulocytes in the right hand micrographs.

Table I.3. Hematological indices of the size and contents of erythrocytes (RBCs) pre- and post-exposure to an AMPS.

	MCV[a] (fL)		MCH[b] (pg)		% Macro[c]		% Micro[d]		% Hypo[e]		% Hyper[f]	
Donor	Pre	Post	Pre	Post	Pre	Post	Pre	Post	Pre	Post	Pre	Post
A	82	84	27	26	0.0	0.1	1.2	0.8	4.8	12	0.2	0.1
B	92	93	31	30	0.7	0.7	0.2	0.1	0.3	0.4	0.5	0.0
C	90	91	30	30	0.4	0.4	0.3	0.2	1.0	1.5	0.3	0.0
D	94	95	31	31	1.3	1.5	0.3	0.3	0.4	0.7	0.4	0.4
E	85	86	27	26	0.1	0.1	0.9	0.7	7.6	15	0.1	0.0

[a] mean corpuscular volume
[b] mean corpuscular hemoglobin
[c] percentage of erythrocytes that are macrocytic
[d] percentage of erythrocytes that are microcytic
[e] percentage of erythrocytes that are hypochromic
[f] percentage of erythrocytes that are hyperchromic

very little change between the original blood and the cells from the bottom fraction of the AMPS for the latter three indices. There was a slight increase in the percent of hypochromic cells and decrease in the percentage of hyperchromic cells that indicates minor swelling, but the effect is small and could be further reduced by increasing the salt content of the AMPS. Donors A and E had the lowest mean cellular hemoglobin concentration (MCHC) and, hence, had potentially more cells near the threshold of being hypochromic; the effect of a slight swelling would be more pronounced in these two samples.

Parasite Culture. Parasites were maintained *in vitro* in rhesus blood (purchased from the New England Primate Research Center, Southborough, MA) at 2% hematocrit, in RPMI-1640 supplemented with 25mM HEPES, sodium bicarbonate, 50mg/L hypoxanthine, and 0.5% Albumax. Parasitemia of cultures are determined by microscopy. Reticulocytemias for each enriched sample are given in **Table I.4**.

Invasion Assays. For invasion assays, late stage *P. knowlesi* H parasites were purified through magnet columns (MACS Miltenyi Biotec). They were plated at a final parasitemia of 0.5-1% in 150 µl cultures at 2% hematocrit in a 96 well plates. Normal human blood and rhesus blood were used as controls. Each red blood cell type was plated in triplicate. Parasites were incubated overnight to allow re-invasion. Parasitized erythrocyte multiplication rate (PEMR) was calculated by dividing the parasitemia after re-invasion to the initial parasitemia seeded.

Invasion of *P. falciparum*. Even if parasites can invade erythrocytes, mechanical stress from centrifugation or polymers on the surface of cells might reduce the infection rate of erythrocytes. *P. falciparum* 3D7 strain should have a similar invasion rate of erythrocytes regardless of the reticulocyte content. Invasion assays using *P. falciparum* provide an additional control to see whether density centrifugation through AMPS obstructs the invasion of malaria

Table I.4. Reticulocytemia of samples used for invasion assays.

	Matched Reticulocytemia (%)*	
Donor	AMPS[a]	DC-Percoll[b]
1	9.2	9.2
2	21	19
3	21	20
4	5.0	11
5	7.0	7.1
6	5.6	3.5
7	16	20

[a] blood enriched by aqueous multiphase systems (AMPSs)
[b] blood enriched by differential centrifugation followed by centrifugation over layered Percoll
***** reticulocytemia was matched by diluting the system with a greater reticulycemia with normal blood

parasites compared to normal human blood. Enrichment by AMPS did not affect the PEMR for *P. falciparum*. Parasites invaded cells at rates similar to those in normal blood (Figure I.6).

Additional Background

Direct growth of reticulocytes and labeled methods to enrich reticulocytes are not practical for the routine cultivation of malaria. Reticulocytes may be obtained directly from the *in vitro* culture of hematopoietic stem cells (HSCs).[8] This method has been used to culture *P. vivax* at a parasitemia below 0.0013%; access to HSCs remains expensive, and asynchronous erythropoiesis limits reticulocytemia.[9] Blood can be enriched highly for reticulocytes (>90% measured by microscopy) using antibodies that differentiate reticulocytes from mature erythrocytes based on characteristic surface proteins.[10] Recovering undamaged reticulocytes from affinity-based separations is difficult, however, and is expensive for routine use.[11] As a result, attempts to enrich reticulocytes for the cultivation of malaria parasites have focused on label-free methods using the physical properties of these cells (e.g., size and density).[3,4,12]

Density provides a label-free parameter to enrich reticulocytes. Reticulocytes are generally larger in volume than mature erythrocytes and they contain ribosomal RNA; the average density of reticulocytes, thus, is slightly lower than that of mature erythrocytes ($\Delta\rho \approx 0.009$ g/cm^3).[13,14] The reported values of the densities of these two populations differs with the study and the method, but most studies agree that the reticulocyte population is concentrated in the least dense quarter of the distribution of density of erythrocytes.[14,15] Differential centrifugation and centrifugation through a gradient in density are the most common methods to separate these types of cells by density.[3,4,11]

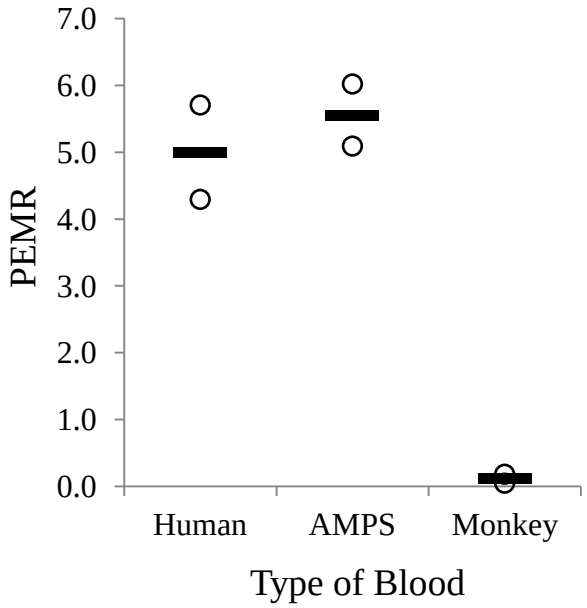

Figure I.6. *P. falciparum* 3D7 strain grows in blood enriched for reticulocytes by AMPS at a rate similar to that at which it grows in normal blood. Blood from a rhesus monkey provides a negative control to demonstrate that the parasite requires suitable host cells for invasion. Open circles depict data from different donors (n = 2) and horizontal bars indicate the mean parasitized erythrocyte multiplication rate (PEMR).

In differential centrifugation, erythrocytes sediment and pack at the bottom of a container; the erythrocytes located at the top of the packed cells have a lower density than those below. As a result, the top quarter of the packed cells contain relatively more reticulocytes than the lower three quarters. Starting with whole blood from normal subjects, differential centrifugation results in an average enrichment of reticulocytes of 2.6%.[4] Using sources of blood with elevated reticulocyte counts (e.g., blood from umbilical cords[16] or from patients with hemochromatosis[3]) can increase the final enrichment obtained from differential centrifugation. Use of these sources is a barrier to the routine use of this method. Cord blood is prohibitively expensive, and the total volume of blood that can be harvested from each cord is limited to an average of 75 mL.[17]

Gradients in density improve the enrichment of reticulocytes by separating reticulocyte-rich fractions and reticulocyte-poor fractions of erythrocytes into visible bands. Percoll—a suspension of colloidal silica stabilized by polyvinylpyrrolidone (PVP)—will form a time-dependent gradient in a centrifuge with an angled rotor. Separations are highly dependent on the centrifugation parameters (e.g., rotor angle, applied relative centrifugal force, acceleration, and time). As a result, reproducibility suffers; initial reports of fractionation of reticulocytes over Percoll gradients achieved a maximum of 78% reticulocytemia in enriched fractions of blood, while average reticulocytemias %.[4,18]

Layered gradients—manually assembled by carefully layering decreasing concentrations of aqueous solutions of a dense solute (e.g., sucrose or arabinogalactan)[11,19]—provide a means to tune the resolution of separations at multiple densities. The boundary between layers provides a location at which cells of specific densities will collect. Such gradients achieve 68%

reticulocytemia in some subjects, but they are time-consuming to assemble and susceptible to mixing and destruction without careful handling.[11]

References

(1) Kratz, A.; Ferraro, M.; Sluss, P. M.; Lewandrowski, K. B. *N. Engl. J. Med.* **2004**, *351*, 1548–1564.

(2) Liu, M.; Nicholson, J. K.; Parkinson, J. A.; Lindon, J. C. *Anal. Chem.* **1997**, *69*, 1504–1509.

(3) Golenda, C. F.; Li, J.; Rosenberg, R. *Proc. Natl. Acad. Sci. U. S. A.* **1997**, *94*, 6786–6791.

(4) Rushing, D.; Vengelen-Tyler, V. *Transfusion* **1987**, *27*, 86–89.

(5) Van Oss, C. J.; Arnold, K.; Coakley, W. T. *Cell Biophys.* **1990**, *17*, 1–10.

(6) Brooks, D. E. *J. Colloid Interface Sci.* **1973**, *43*, 700–713.

(7) Chien, S.; Simchon, S.; Abbott, R. E.; Jan, K.-M. *J. Colloid Interface Sci.* **1977**, *62*, 461–470.

(8) Giarratana, M.-C.; Kobari, L.; Lapillonne, H.; Chalmers, D.; Kiger, L.; Cynober, T.; Marden, M. C.; Wajcman, H.; Douay, L. *Nat. Biotechnol.* **2005**, *23*, 69–74.

(9) Panichakul, T.; Sattabongkot, J.; Chotivanich, K.; Sirichaisinthop, J.; Cui, L.; Udomsangpetch, R. *Int. J. Parasitol.* **2007**, *37*, 1551–1557.

(10) Brun, A.; Gaudernack, G.; Sandberg, S. *Blood* **1990**, *76*, 2397–2403.

(11) Sorette, M. P.; Shiffer, K.; Clark, M. R. *Blood* **1992**, *80*, 249–254.

(12) Andreux, A.; Merino, A.; Renard, M.; Forestier, F.; Cardot, P. *Exp. Hematol.* **1993**, *21*, 326–330.

(13) Key, J. *Arch. Intern. Med.* **1921**, *1882*, 511–549.

(14) Leif, R. C.; Vinograd, J. *Proc. Natl. Acad. Sci. U. S. A.* **1964**, *51*, 520–528.

(15) Haidmayer, R.; Kenner, T.; Hinghofer-Szalkay, H. *Biomed. Tech.* **1980**, *25*, 258–260.

(16) Russell, B.; Suwanarusk, R.; Borlon, C.; Costa, F. T. M.; Chu, C. S.; Rijken, M. J.; Sriprawat, K.; Warter, L.; Koh, E. G. L.; Malleret, B.; Colin, Y.; Bertrand, O.; Adams, J. H.; D'Alessandro, U.; Snounou, G.; Nosten, F.; Rénia, L. *Blood* **2011**, *118*, e74–81.

(17) Hillyer, C. D.; Strauss, R. G.; Luban, N. L. C. *Handbook of Pediatric Transfusion Medicine*; 2004; pp. 295–296.

(18) Branch, D.; Hian, A.; Carlson, F.; Maslow, W.; Petz, L. *Am. J. Clin. Pathol.* **1983**, *80*, 453–458.

(19) Martínez-Salas, E.; Martín, J. A.; Vicente, M. *J. Bacteriol.* **1981**, *147*, 97–100.

Appendix II

Supporting Information

Density-based Separation in Multiphase Systems Provides a Simple Method to Identify Sickle Cell Disease

Ashok A. Kumar, Matthew Patton, Jonathan W. Hennek, S.Y. Ryan Lee, Gaetana D'Alesio-Spina, Xiaoxi Yang, Julie Kanter, Sergey S. Shevkoplyas, Carlo Brugnara, and George M. Whitesides

Materials and Methods

Chemicals. We purchased the following polymers: poly(ethylene glycol) (Sigma-Aldrich; MW = 20000 Da), Ficoll (Sigma-Aldrich; MW = 70000 Da and 400000 Da), dextran (Spectrum Chemical; 500000 Da), and poly(vinyl alcohol) (PVA) (Polysciences; MW = 3000 Da)—formed by hydrolyzing 75% of poly(vinyl acetate). Solutions of AMPS contained the following chemicals: ethylenediaminetetra-acetic acid disodium salt (EDTA) (Sigma-Aldrich), potassium phosphate monobasic (EMD), sodium phosphate dibasic (Mallinkrodt AR), sodium chloride (EMD), $MgCl_2$ (USB), and Nycodenz (Axis-Shield PoC). We used a Hemacolor Stain Kit (Harelco) to stain slides of thin smears of blood. For the nystatin treatment, we purchased the following additional chemicals: nystatin (*Streptomyces noursei*, Calbiochem), choline chloride (Sigma-Aldrich), tris (hydroxymethyl) aminomethane hydrochloride (Tris HCL, Bethesda Research Laboratories), 3-(N-morpholino) propane-sulfonic acid (MOPS, EM Science), potassium chloride (EMD), sucrose (EMD), glucose (Sigma-Aldrich), albumin from bovine serum (Sigma-Aldrich), and sodium phosphate monobasic (Mallinkrodt Chemicals).

Blood Samples. Children's Hospital Boston (CHB) and the Sickle Cell Center of Southern Louisiana (SCCSL) (New Orleans) provided de-identified blood samples with known hemoglobin genotypes. We tested our system on a variety of blood samples that were Hb AA, Hb AS, Hb SS, Hb SC, and Hb $S\beta^+$. The Hb SS samples varied in their Hb F content and their proportion of dense sickled cells. We used de-identified blood from Research Blood Components in Boston for our model sickle blood systems.

At the SCCSL, blood samples were collected into 4 mL Vacutainer tubes (K_2EDTA, BD, Franklin Lakes, NJ) during routine blood draws from patients with informed consent, according to a protocol approved by Tulane University Biomedical IRB. At CHB, blood samples were

collected when clinically indicated and discarded samples were used according to a protocol approved by Children's Hospital Boston IRB.

Three normal controls were obtained from consented volunteers at Harvard University under a protocol approved by the Committee on the Use of Human Subjects at Harvard University.

Materials for Rapid Tests. We purchased the following materials to make our rapid tests: heparinized, polycarbonate microhematocrit tubes (Iris Sample Processing), clay seals (Critoseal, Leica), silicone rubber tubing with an inner diameter of 1.02 mm and an outer diameter of 2.06 mm (Helix Mark, Helix Medical), and five-minute epoxy.

Preparation of AMPS. To prepare each AMPS, we added polymers, buffer salts, and other additives (i.e., Nycodenz and EDTA) in volumetric flasks and added deionized water to attain the final volume. Adjustments to pH and osmolality were made as described in Chapter 4. A vortexer or magnetic stir bar mixed solutions thoroughly.

In our AMPS, we include 5 mM EDTA and 1 mM $MgCl_2$ to help preserve the blood and prevent coagulation. The tubes are also heparinized. We have varied the amount of these additives but we have been unable to completely eliminate the clotting platelets.

Characterization. We measured density with a density meter (DM50, Anton Paar), osmolality with a vapor pressure osmometer (Vapro 5600, Wescor), and pH with a pH meter (Orion 2 Star, Thermo Scientific). Complete blood counts were done on a hematology analyzer (ADVIA 2120, Siemens).

Rapid Test Fabrication. We used a 3D printer (Fortus 250mc, Stratasys) to print a holder to punch reproducible holes in the sides of the microhematocrit tubes. The holder was designed with AutoCAD (AutoDesk). We load each holder with microhematocrit tubes and use

standard metal pushpins (Staples) to punch holes in the sides of the tubes at the prescribed length. We also used fine tipped markers to mark a fixed point on the length of the tubes as fill lines to hold the prescribed volume of the AMPS. After removing the tubes from the holder, we blew out any loose plastic with an air gun. We cut small lengths of silicone tubing (3-5 mm) and slid them over the tubes to cover the holes in their sides. While an AMPS was being stirred by a magnetic stir plate, we used a micropipettor to fill the marked tubes up to the fill lines and then sealed them with either white sealing clay or epoxy. The completed tests were then used on blood samples as described in Chapter 4.

For larger productions, we estimated the costs necessary to cap and more permanently seal the tubes with glue as well as labor, equipment, and packaging costs (**Table II.1**). Time estimates were based on current manufacturing procedures in the laboratory and materials costs were based on the volumes at which we currently purchased materials and chemicals. With these parameters, the cost per test is $0.50. Production in a market with lower labor costs and with bulk chemical prices should reduce this cost.

Nystatin Treatment for Model Sickle System. We created dehydrated erythrocytes using the nystatin loading procedure developed by Canessa.[1] When nystatin is present, the membrane of erythrocytes becomes permeable and the volume of the cell can be set by adjusting the osmolality of the solution with additives like sucrose. Washing to remove the nystatin returns cells to a less permeable membrane while retaining the adjusted volume. Cells were washed five times in a choline wash solution of 150 mM choline chloride, 1 mM $MgCl_2$, and 10 mM Tris HCl and MOPS with a pH adjusted to 7.4 at 4° C. We then exposed the cells to nystatin in a nystatin loading solution containing 10 mM NaCl, 130 mM KCl, and 200 mM sucrose for 20 minutes at 4° C. This solution was spun down and the supernatant removed. We

Table II.1. Itemized cost per test estimated for production.

Item	**Unit Cost**
Polycarbonate capillary tube	$ 0.1000
Critoseal	$ 0.0027
Critocaps	$ 0.0415
Silicone sleeve	$ 0.0079
Glue (Krazy Glue)	$ 0.0033
Polymer solutions	$ 0.0032
Foil-lined Pouch (12 devices/pack)	$ 0.0625
Total Consumable	**$ 0.2211**
Total Manufacturing Equipment & Personnel	**$ 0.2756**
Total Cost	**$ 0.4967**

incubated the cells in loading solution (without nystatin) for 10 minutes at 37° C followed by four washes with the loading solution at the same temperature. Finally, we washed the cells five times in the choline wash solution at 4° C. We suspended packed cells in homologous plasma at the same hematocrit as the original blood and made serial dilutions to attain a range of percentages of dense cells of blood from each donor.

Visual Evaluation of Rapid Tests. Samples from either Children's Hospital Boston or the Sickle Cell Center of Southern Louisiana were coded before being sent for evaluation by the rapid test at Harvard University. The samples were run on both SCD-AMPS-2 and SCD-AMPS-3 in duplicate and evaluated independently by two readers who had been trained on previous prototypes to read tests as positive when a full layer of red cells were present at the bottom of the microhematocrit tube. In instances where the duplicate samples gave different results, a third test was run with the same sample. In instances when the two readers disagreed on a result, a third trained reader evaluated the test independently. The two readers were in accordance on 97% of tests with SCD-AMPS-2 and 86% of tests with SCD-AMPS-3. Tests where the two original readers did not agree did not correlate to false positives or false negatives.

Digital Evaluation of Rapid Tests. To capture comparable digital images of all our rapid tests, we used a digital scanner in transmission mode (Epson Perfection V330 Photo) to record images of up to 12 tubes at a time placed in a plastic grid. We then used custom written Matlab code to process and analyze the images through several steps: i) scanned images were matched to a key image file using image registration and cropped to a standard size, ii) the matched images were cropped at twelve positions into separate image files for each tube, iii) images were converted into the Lab colorspace, iv) the region of interest that contained the bottom of the tube was selected, v) each pixel was evaluated for the intensity of the red color

through a combination of intensity and distance in the Lab space from a training set of red, vi) the scores for all pixels were summed to give a single score for each tube, and vii) the calculated values for each tube were written to a file for further analysis and comparison.

The Lab colorspace is designed to approximate human vision so we chose to use this colorspace over other schemes, such as RGB and CMYK. We then defined a range of acceptable red colors using a training set of sickle cell positive samples and using a weighting scheme to evaluate the distance in the colorspace from the learned red color. We used the "L" component, or lightness, to weight the density of the packed red cells so that darker packed red would count more strongly than a light red that was present when cells were not packed.

Statistical methods. Sensitivity is defined as (# true positives)/(# true positives + # false negatives). Specificity is defined as (# true negatives)/(# true negatives + # false positives). We chose to use Jeffreys confidence intervals because our values were near the upper bounds of 100% sensitivity or specificity.

Experimental Details

AMPS phases for separations. An AMPS with *n* phases has a total of *n+1* interfaces (AMPS/container, *n-1* AMPS phase/phase, and AMPS/air) at which to separate objects. For practical applications where blood is layered on top of an AMPS, and centrifugation is used to separate cells at the interfaces between the phases of the AMPS, the top (AMPS/serum) interface is diffuse and not useful for separations in this application; there are, therefore, *n* sharp interfaces that can concentrate cells.

Erythrocytes have a distribution of densities that is specific to sickle-cell disease. Dense cells present in SCD have a mass density ($\rho \sim 1.12$ g/cm^3) that is higher than the most

dense erythrocytes in healthy individuals (ρ_{max} ~ 1.10 g/cm^3);[2–5,a] the difference in density between these cells makes SCD a strong candidate for a density-based diagnostic test. Not all high density cells in SCD have a sickled shape and some sickled cells may not have a very high density. Nevertheless, the presence of red blood cells with a high density is a well documented characteristic of SCD.[3,6] We refer to this class of dense cells as dense, SCD cells.

The percentage of dense, SCD cells in the blood varies among individuals. Under most conditions, however, the blood of individuals with SCD has 13% (S.D. 8%) dense cells.[7] A notable exception comprises individuals that express a significant amount of fetal hemoglobin (Hb F); in these individuals, sickled cells comprise a smaller proportion of erythrocytes and clinical symptoms are normally milder than others with SCD.[8,9] The lower number of sickled cells may correspond to less dense, SCD cells in these individuals.

Hemoglobin C disease (Hb CC)—much more rare and geographically isolated than SCD[10–13]—also increases the mass density of erythrocytes,[14] and constitutes a potentially confounding interpretation. In Hb CC, the entire distribution of densities of erythrocytes shifts to a slightly higher density; reticulocytes in Hb CC are more dense than those in Hb AA, but the high-density erythrocytes in Hb CC are less dense than the densest cells in Hb SS.[3] In sickle-cell disease, erythrocytes that are not sickled remain at normal densities, and the erythrocytes exist in two populations: a high-density, often sickled, population (~10% of cells) and a lower-density, predominantly normocyte, population, which also comprises reticulocytes and the youngest erythrocytes.[2,4]

[a] Specific values of density vary in the literature and may be dependent on the media (e.g., Percoll, stractan or phthalate esters). The values cited here were found to be consistent in AMPS.

Densities of erythrocytes determine the densities of the phases. A bottom phase, with a density of $\rho \geq 1.120$ g/cm^3, should permit dense, SCD cells ($\rho \geq 1.12$ g/cm^3) to sediment, while creating a barrier to the dense cells of Hb CC blood ($\rho_{max} \sim 1.11$ g/cm^3).[14] Although we were unable to test blood with Hb CC due to the rarity of this blood type in the hemoglobinopathy clinics we worked with, we designed both systems with sufficiently dense bottom phases that future work with Hb CC could be done in areas (e.g., West Africa) with a higher prevalence of this genotype. The top phase must be less dense than low-density erythrocytes, such as reticulocytes ($\rho = 1.085$ g/cm^3), to ensure that all the erythrocytes pack at a well-defined interface. In a three-phase system, a middle phase with a density of $\rho = 1.110$ g/cm^3 will separate the main population of normal erythrocytes from the high-density tail of the distribution of cells. The middle phase of the three-phase system allows us to distinguish subtypes. In the case of Hb AA and Hb SS, we expected the majority of red cells to collect between the top and middle phase. In the case of Hb SC and Hb CC, however, the shift in the density of the population is seen by a dense band of red cells between the middle and bottom phase. Red cells are present below the bottom phase in both Hb SS and Hb SC. The pattern of the red bands at each interface distinguishes these different hemoglobin types (**Chapter 4; Figure 4.1**).

Several other factors could influence density in a way that could affect the performance of our AMPS-based tests. Patients suffering from sickle-cell disease with alpha thalassemia trait and alpha thalassemia may have fewer dense cells;[5] one of our Hb SS samples had alpha thalassemia and it was distinguishable both visually and digitally as Hb SS in our test. Iron deficiency often leads to hypochromic, microcytic anemia;[15] a patient with SCD and iron deficiency anemia may have a more complex distribution of densities of erythrocytes. Testing on

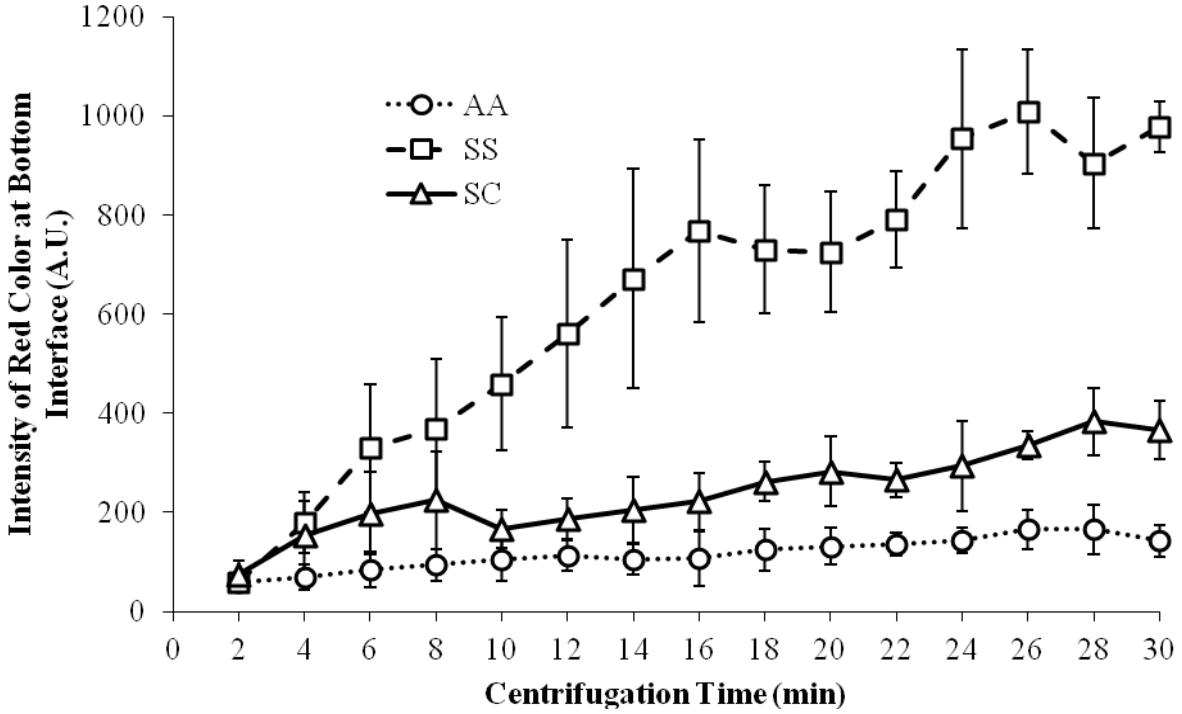

Figure II.1. The intensity of the red color at the bottom interface of the SCD-AMPS-3 system increases with centrifugation time. We evaluated a set of six replicates digitally from samples of Hb AA (AA, n = 4), Hb SS (SS, n = 2), and Hb SC (SC, n = 3) at two minute increments of centrifugation. Error bars depict the average deviation from the mean value of the intensity of the red color from the different subjects. After six minutes, the signal from SCD postive samples (SS and SC) are distinguishable from SCD negative samples (Hb AA). The separation, in general, increases over time. Notably, blood with Hb SS has a significantly higher signal than Hb SC over time.

a larger population that might include patients with these and other concomitant conditions would determine the generality of density as a diagnostic for SCD.

Co-solutes tune the osmolality and density of an AMPS to physiological levels. Any swelling or dehydration of erythrocytes that reduces the separation between the three sub-populations of interest may compromise a diagnostic test based on density. To maintain physiological conditions and prevent changes in volume of the cells, we wanted to maintain an osmolality that was isotonic with blood (~295 mOsm).[16]

Achieving the densities necessary to separate dense cells in SCD with polymers alone is difficult. High concentrations of polymer create viscous and hypertonic environments. For example, a solution of 30% (w/v) dextran (MW = 500 kD) in a phosphate buffered solution has a density of 1.122 g/cm^3 and an osmolality of 336 mOsm. This system would dehydrate normal erythrocytes and could increase their density to be indistinguishable from dense cells from SCD. To generate phases with high density that are isotonic with blood, co-solutes with high densities can be used to increase the density of an AMPS.[17]

Separation over Time. In order to choose the time of centrifugation for our rapid test, we performed a time series experiment with the SCD-AMPS-3 system. Six replicates of the rapid test were loaded with blood (n = 2 with Hb SS, n = 3 with Hb SC, and n = 4 with Hb AA). The tests were subjected to centrifugation for two minutes and then scanned in repeated iterations for a total centrifugation time of 30 minutes. The scanned images were then analyzed for the intensity of the red color at the bottom of each test (**Figure II.1**). After six minutes, both the Hb SS and Hb SC blood begin to collect significantly more red color at the bottom of the tube than the Hb AA blood. This difference gradually increases over time. To take advantage of

this signal amplification without compromising the rapidity of our test, we chose to centrifuge our test for 10 minutes.

Rapid Test Capillary Tube Design. We created two methods to load blood into a sealed tube that was preloaded with AMPS (**Chapter 4; Figure 4.2**). We have described the "hole-in-tube" method in the main text. Briefly, we use a pushpin in a custom-made alignment mold to puncture the side of the plastic capillary tubes at a specific point along the length of the tube to ensure a repeatable volume is added to all tubes. Air, which would otherwise be trapped and block capillary action, escapes through the hole. To prevent blood from escaping through the puncture during centrifugation, we slid a sleeve of silicone rubber over the hole.

The other method, tube-in-tube, relies on the use of a smaller glass capillary tube that fits within the larger, preloaded polycarbonate capillary (**Figure II.2A**). We used the smaller capillary to wick blood into a controlled volume and then introduced the smaller capillary directly into the larger capillary. A small ring of epoxy on the upper portion of the small capillary prevents the small capillary from entering the SCD-AMPS upon centrifugation. This method is fast, but requires some manual dexterity to load the smaller capillary into the larger one.

The tubes hold ~24 µL of liquid in addition to the seal. This provided a constraint to design the volume of our test. Double the volume of blood per test is reserved for loading the sample and then ensuring that once the sample passes into the AMPS, the combined volume is not higher than the hole in the side of the tube—we found that liquid above this level would occasionally leak out, and, if blood was being used, would present a biohazard. Early screening of AMPSs for the sickle test had used a volume ratio of blood to AMPS of 1:3. As we scaled

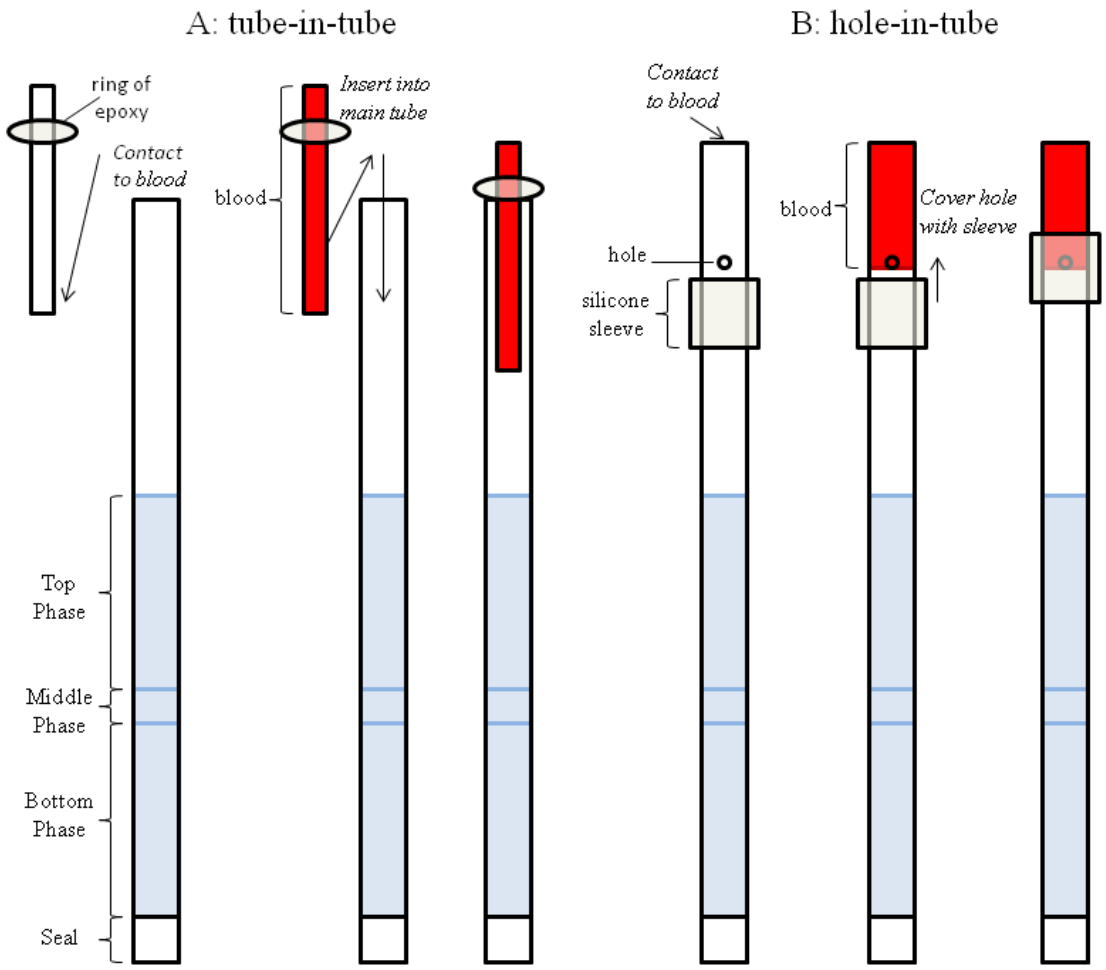

Figure II.2. Two designs to load blood samples into a capillary that has been preloaded with SCD-AMPS-3 and sealed. In the "tube-in-tube" method (A), a small capillary with a ring of epoxy around it fills with blood by capillary action. This small tube can then be loaded into the larger capillary. In the "hole-in-tube" method (B), a small hole allows blood to wick into the prefilled tube. A silicone sleeve prevents the blood from leaking during centrifugation.

down to the rapid test format, we needed to maintain this ratio to maintain a similar performance. Using 14 µL of AMPS and loading 4.7 µL of blood allowed us to satisfy all our constraints.

Fabrication. We used calibrated micropipettors to fill tubes with the specific volume and then used the fill line to measure the distance we used. We used a custom built hole puncher to make repeatable holes (see *Materials and Methods*). By eye and by pipette the volumes filled were similar. From scans, we estimated the distance between the end of the capillary and the far end of the hole to have a coefficient of variance (CV) of less than 2%.

Hematocrit and Packing of Cells. By comparing the volume that the cells occupied in these three regions to the volume of blood loaded, we can estimate hematocrit (**Figure II.3**). We measured the height of the packed cells in each area digitally (ImageJ) and compared it to the length from the hole in the side of the tube to the top of the tube. The low volume of blood used and slight variations in the volumes of the blood and AMPS only allow, however, for a coarse measure of hematocrit (± 10 %). In general, the hematocrit after 10 minutes in the AMPS was an overestimate of the real hematocrit. Additional centrifugation time improved the packing of the cells (**Figure II.4**) and could improve the hematocrit estimation.

Aggregates in Negative Samples. To investigate the white or pink layer that occasionally formed at the bottom of negative samples, we examined the material by optical microscopy. We identified the samples to investigate by using the smaller rapid test format, but we could not extract enough material from these systems to identify the objects under a microscope. We, thus, scaled up the separation to a 1.5 mL Eppendorf tube, while maintaining the same ratio of blood to AMPS and comparable centrifugation parameters. After separation, we used a micropipettor to extract the layer of material below the bottom phase of the AMPS and stained a thin smear of the sample on a glass slide **(Figure II.5).**

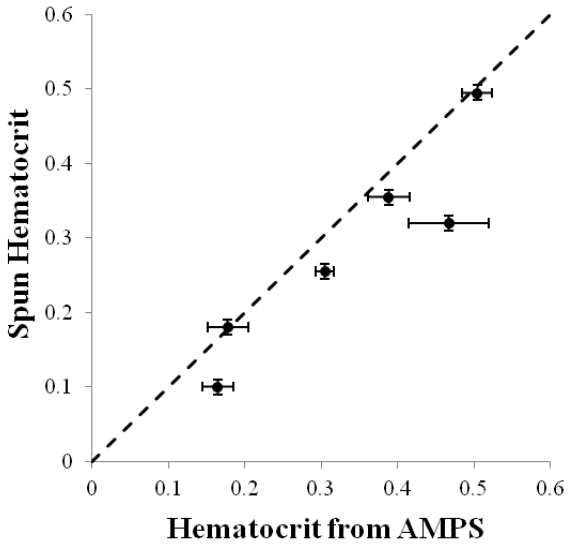

Figure II.3. The hematocrit measured in AMPSs provides an estimate of the spun hematocrit. A range of hematocrits was made by mixing packed cells with homologous plasma. The estimated hematocrit from AMPS is generally a slight overestimate of the real hematocrit because at 10 minutes, the cells are not completely packed.

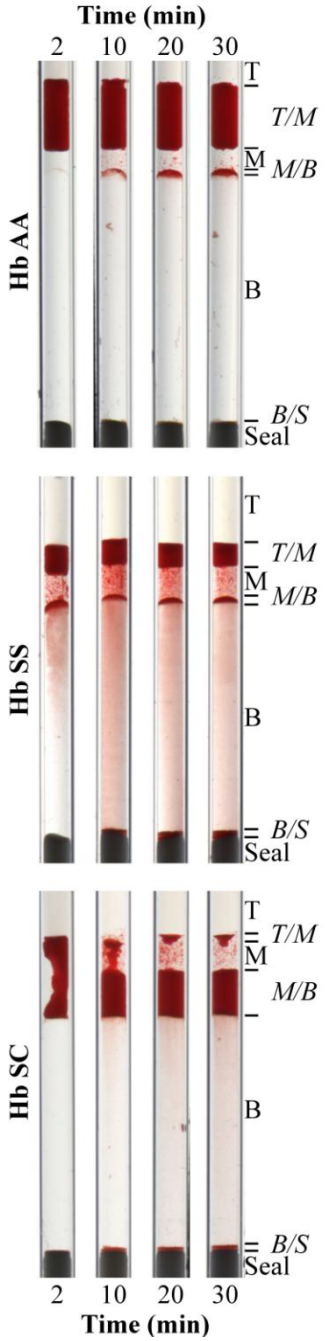

Figure II.4. Additional centrifugation time results in clearer separation of the cells. Some isodense cells remain unchanged after 30 minutes (Hb SS). Hb SC is easily distinguished from Hb SS after 20 minutes. The pack of cells above the white clay seal (dark gray in transmission imaging) increases over time (Hb SS and Hb SC).

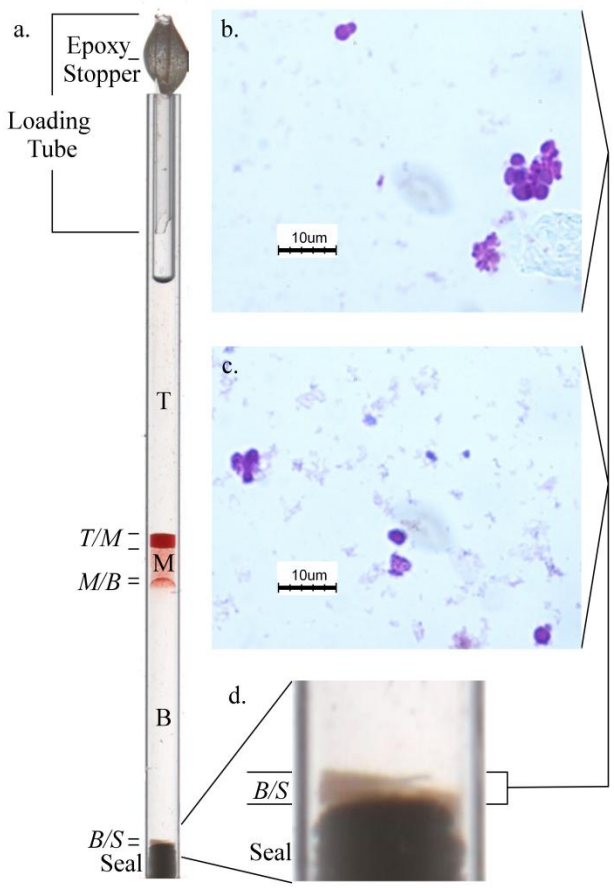

Figure II.5. Example of white pellet found at the bottom of some of the samples from Hb AA subjects. A tube-in-tube version of the SCD-AMPS-3 test is negative for SCD (a.). Although the bottom is not red, there is a substantial gray layer above the above the white clay seal (dark gray in transmission imaging) (*B/S*) (d.). Micrographs (b. and c.) reveal a large number of platelets and cell aggregates.

After centrifugation, we extracted and washed the cells from each interface of the AMPS. We made thin smears stained with Hemacolor (Harelco) to evaluate the morphological distribution of erythrocytes.

Using bright field microscopy we captured a series of images, which we then analyzed with CellProfiler™ (Broad Institute) to quantify the percentage of erythrocytes that were sickled in each interface. We classified a cell as sickled if the aspect ratio of the major axis length over the minor axis length was greater than 2. We found this measure to correlate well with sickled morphologies over several fields of view that we evaluated by eye (**Figure II.6**).

When using blood from a patient with Hb SS with a very low level of sickled cells (0.7%), we were able to visualize the presence of dense cells at the bottom of the SCD-AMPS in both the capillary tubes and the microcentrifuge tubes. The fraction of cells at the bottom phase/seal interface contained 7.3% sickled cells. Over half of the remaining cells appeared crenated and dehydrated, similar to the “holly wreaths” or "holly leaf shapes" that result from deoxygenation of cells with Hb SS.[18–20] Upon entering the SCD-AMPS, the erythrocytes may have deoxygenated. Rapid deoxygenation in Hb SS causes the formation of crenated cells and “holly-wreaths” or "holly leaf shapes" instead of the classic sickle shape.[18–20] Normal erythrocytes in the smears from the bottom fraction may be either cells that have been oxygenated during the washing step and returned to a normal morphology or normal cells that became engulfed by a mass of dense cells and trapped at the bottom of the tube. Interestingly, the cells at the upper and lower liquid/liquid interfaces had 4.4% and 4.7% sickled cells, respectively. These layers, however, did not contain crenated, dehydrated cells. The existence of cells with a high aspect ratio may have been a result of smearing cells from the polymer

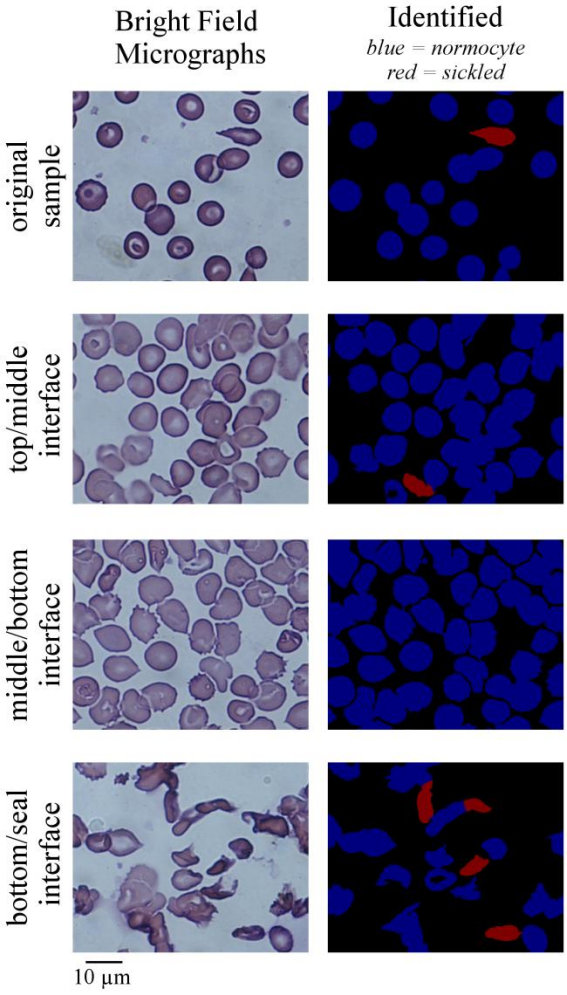

Figure II.6. Micrographs of blood from the different fractions of a sample with Hb SS run on SCD-AMPS-3 test is evaluated digitally to quantify sickling. Identified cells are classified as normocytes (blue) or sickled (red). The cells at the bottom interface (bottom/seal) are markedly more sickled and dehydrated.

solutions, but the higher proportion of cells with high aspect ratios in the bottom layer suggests that there was a higher amount of sickled cells in the bottom population.

Quantification of Dense Cells. To quantify the percentage of dense cells, we evaluated the digital images of the results from the SCD-AMPS-2 tests. Using digital analysis (ImageJ) we measured the height of the packed cells above the seal and the height of the packed cells at the liquid interface. We then calculated the percentage of dense cells for all the samples that had SCD (both Hb SS and Hb SC) (**Table II.2**). Note that in two cases of Hb SS, we did not visually identify a band of red cells at the bottom and the calculated percentage of dense cells in these cases was zero. Of the 21 SCD samples that were tested on SCD-AMPS-2, the average percentage of dense cells was 10%.

Results by Genotype. The sensitivity and specificity values described in Chapter 4 were based on binning all positives (Hb SS and Hb SC) together and all negatives (Hb AA and Hb AS) together. **Table II.3** details the results of visual evaluation of all four genotypes in this study. Five of the six Hb SC samples could be distinguished from Hb SS after evaluating the distribution of cells between the two liquid interfaces in SCD-AMPS-3. All Hb SS samples appeared as expected in **Chapter 4; Figure 4.1;** none of the Hb SS samples appeared with a majority of the red cells at the lower liquid interface.

Nystatin provides a means to create model SCD blood. Testing the diagnostic capabilities of the SCD-AMPS required samples of blood from SCD patients that had not been recently transfused (transfusion reduces the number of dense cells present in a patient's blood). To characterize the limit of detection of our system in a quantitative way we needed model dense cells whose behavior was less subject to change than sickle cells, we created dense erythrocytes

Table II.2. Quantification of the dense cells from the SCD-AMPS-2.

Donor	Genotype	Visual Reading	Dense Cells
1	SS	Positive	21%
2	SS	Positive	15%
3	SS	Positive	8%
4	SS	Positive	16%
5	SS	Positive	14%
6	SS	Positive	10%
7	SS	Positive	12%
8	SS	Positive	12%
9	SS	Positive	15%
10	SS	Positive	11%
11	SS	Positive	8%
12	SS	Positive	13%
13	SS	Positive	10%
14	SS	Negative	0%
15	SS	Negative	0%
16	SC	Positive	8%
17	SC	Positive	8%
18	SC	Positive	10%
19	SC	Positive	4%
20	SC	Positive	9%
21	SC	Positive	8%
Average	--	--	*10%*

Table II.3. Visual evaluation of the SCD-AMPS for sample sizes of *N*.

	SCD-AMPS-3			SCD-AMPS-2		
Sample	***N***	**Positive Rate[a]**	**Negative Rate**	***N***	**Positive Rate[a]**	**Negative Rate**
Hb SS	20	**0.90**	0.10	15	**0.87**	0.13
Hb SC	6	**1.00**	0.00	6	**1.00**	0.00
Hb AA	26	0.15	**0.85**	24	0.04	**0.96**
Hb AS	7	0.00	**1.00**	7	0.00	**1.00**

[a] Rates were calculated by comparing the results from the AMPS test to the known status of the subjects as measured by a gold standard (either Hb electrophoresis or HPLC).

by treating blood with nystatin, and exposing them to hypertonic media.[1] This creates dense, dehydrated cells;[21] we used these cells as a model of dense cells.

We mixed known volumes of these dense cells with untreated blood to simulate SCD blood. The model blood contained small (cell volume < 60 fL) cells (microcytic) with high concentrations of hemoglobin (hyperchromic), similar to sickled cells in SCD; after treatment, the erythrocytes from three blood samples had a mean corpuscular volume ranging from 67.3–71.5 fL, and mean corpuscular hemoglobin content ranging from 39.9–41.5 g dL^{-1}. When we mixed 5% of the treated cells with the original blood, the model samples had a mean corpuscular volume ranging from 81.9–83.9 fL, a mean corpuscular hemoglobin content ranging from 32.4–34.8 g dL^{-1}, and the percent of microcytic erythrocytes ranged from 2.6–3.8%.

Determination of the Limit of Detection Using a Model System for SCD. Using normal blood (n = 3) spiked with dense cells created by the nystatin treatment, we evaluated the bottom of the SCD-AMPS-3 for the presence of red color after 10 minutes of centrifugation. By eye, we could detect the presence of dense cells in normal blood at a concentration of 2% about half the time. At a concentration of 5%, a layer of red covered the bottom of the capillary. Most SCD patients have over 13% dense, SCD cells.[7]

We also imaged the results of each test with a flatbed scanner in transmission mode (Perfection Photo V550, Epson). Image processing in Matlab evaluated the amount of red that had collected at the bottom of each capillary. **Figure II.7** depicts the measured value of the "intensity of red color" in arbitrary units (AU) for the different concentrations of dense cells that were added to the normal blood. We found a good linear fit ($R^2 > 0.995$) to the data with an intercept set at 0. For the digital analysis, we found the limit of detection to be 2.8% dense cells by finding the value of the linear fit that provided a signal that was three standard deviations

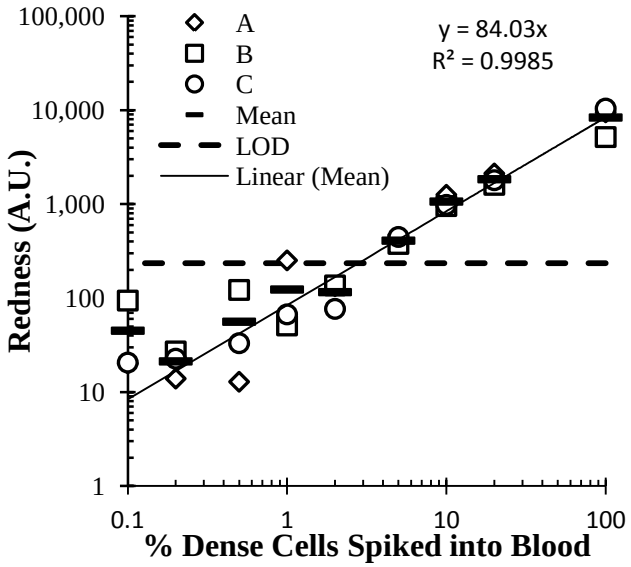

Figure II.7. Measuring the intensity of red color at the bottom of the SCD-AMPS-3 can detect dense erythrocytes in whole blood at a concentration of 5%. Erythrocytes from three donors (A–C) were treated with nystatin to be dense and dehydrated, and then spiked into untreated blood at known concentrations. After centrifugation in a tube containing the SCD-AMPS-3, the tests were scanned and analyzed to quantify the presence of dark red bands below the bottom phase. The limit of detection (dashed line) was established as three standard deviations above the mean measured on normal blood (n = 7).

above the signal from normal blood (n = 7). Below this concentration, it is possible for the digital analysis to confuse results from normal blood and SCD blood; this limit provides the false positives and false negatives that were observed in **Chapter 4; Figure 4.4**.

Alternative Methods to Diagnose SCD at the Point-of-Care. Miligan *et al.* have proposed monitoring hemolysis in non-electrolyte solutions as a means to diagnose sickle-cell disease.[22] Quantifying hemolysis allows them to distinguish some genotypes and may provide a means to monitor certain clinical effects of SCD (**Table II.4**). This test requires an hour of incubation, the use of an expensive tonometer, and optical density measurements; meeting these requirements in a point-of-care setting may be challenging.

The recent development of a paper-based test for SCD may provide an alternative low-cost diagnostic test.[23] This test distinguishes Hb AA, Hb AS, and Hb SS visually by evaluating blood stains on paper after lysing and deoxygenating the hemoglobin (using a method similar to a solubility test). The visual signal can be analyzed by a scanner and correlates to the concentration of Hb S present. Even with the use of the digital analysis, the test is, however, less accurate than the AMPS-based tests at distinguishing individuals with Hb AS (non-disease) and Hb SC (disease); the Hb S concentration in these two genotypes can be very similar. In a person with Hb SC, the presence of Hb C leads to dehydration that induces sickling at a significant level that would not take place in a person with similar levels of Hb S, but with Hb AS.[24]

Distinguishing between Hb SC and Hb AS is clinically important, especially in West Africa where both genes are common. In settings where Hb C is rare, such as eastern and southern Africa, this test could be a quick and inexpensive way to identify and distinguish between sickle-cell trait and disease.

Table II.4. Comparison of methods to detect SCD.

Ref.	Method	Time (min)	Differentiation				Fieldable	Biophysical Indicator	Sample Prep. Free	Instrument Free	Instrument Cost	Unit Cost
			AS /SS	AS /SC	SC /SS	AA /AS						
This work	AMPS	12	✓	✓	✓[a]		✓	✓	✓		$150-1,600	$0.50
[22]	Hemolysis	> 60	✓		✓			✓[b]			~$10,000	NA
[23]	Paper	20	✓	✓[c]	✓	✓	✓				$300-500	$0.07[d]
†	Solubility	5				✓	✓			✓	$0	$3.00
†	HPLC*	> 120	✓	✓	✓	✓					>$60,000	$10.00
†	HE*	> 180	✓	✓	✓	✓					>$10,000	$3.00
†	Genetic	>180	✓	✓	✓	✓					>$20,000	$1.00

[a] specifically, SCD-AMPS-3

[b] under investigation

[c] except in cases where hemoglobin S levels are close

[d] based on cost estimates for a similar paper test [25]

† based on market prices and product literature

* gold standard method

Conventional techniques of separation by density are not suitable for use in field settings. Sequentially layering solutions with decreasing concentrations of a dense solute (e.g., sucrose, Percoll, arabinogalactan) creates a layered gradient in density.[26] These gradients can separate blood into multiple subpopulations of cells of different densities. Layered gradients in density are not practical for use in a point-of-care test for several reasons: i) diffusion-driven homogenization of layers limits the long-term storage of a layered gradient, ii) agitation or mixing destroys a layered gradient, and iii) assembly of a gradient requires careful and tedious layering, and a high level of technical competence.

Centrifugation of blood over mixtures of phthalate esters provides a simpler method to characterize the density profile of blood.[4,27] Mixtures of phthalate esters provide a range of single-density media. Upon centrifugation, blood cells either sink or float in a phthalate solution based on the difference in density between the cells and the solution. The immiscibility of the phthalates and water ensures that cells at the top of the phthalate are packed at an interface (i.e., a water/phthalate interface); cells layered over an aqueous medium would collect in a diffuse boundary between the plasma and the medium. Packing cells is an important characteristic for a separation to provide quantitative information. Comparison of the volume of packed cells above and below a phthalate provides a measure of the distribution of the density of cells. Although simpler to use than layered gradients, phthalate esters are unsuitable for point-of-care use for two reasons: i) they require a temperature-controlled centrifuge,[28] and ii) they cannot distinguish more than two subpopulations of cells in a single system—a necessary ability to differentiate sub-types of SCD by density.

AMPSs combines the best aspects of layered gradients and phthalate esters, while overcoming the principal drawbacks of each. Like layered gradients, AMPSs allow multiple

sub-populations to be separated in a single system. Like phthalate esters, AMPSs concentrate cells at well-defined interfaces and are easy to use. Together, these characteristics allow centrifugation through AMPSs to distinguish blood from patients with SCD from normal blood by density and classify the two main subtypes of the disease.

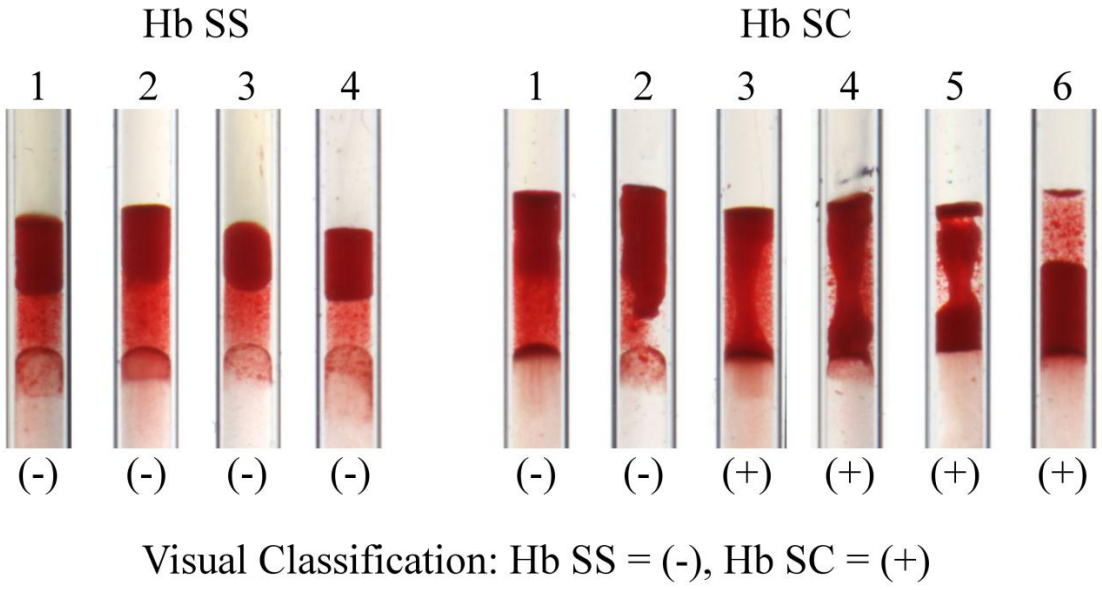

Figure II.8. Examples of the patterns of red cells at the liquid interfaces for Hb SC and Hb SS in the SCD-AMPS-3 system. Four representative examples of the layers of red blood cells from samples with Hb SS show the characteristic pattern of the majority of cells packed at the upper liquid/liquid interface with a thin packed band at the lower liquid/liquid interface. All six samples with Hb SC are shown after 10 minutes of centrifugation. Samples Hb SC-4, 5, and 6 all have red bands at the lower liquid interface that are comparable to or greater than the bands at the upper liquid interface. Sample Hb SC-3 has a significant pack of cells at the lower liquid interface an hour glass shape of red cells between the two liquid interfaces. Sample Hb SC-2 packed to a pattern more similar to Hb SC-3 and 4 after 20 total minutes of centrifugation.

References

(1) Canessa, M.; Brugnara, C.; Cusi, D.; Tosteson, D. C. *J. Gen. Physiol.* **1986**, *87*, 113–142.

(2) Grover, W. H.; Bryan, A. K.; Diez-Silva, M.; Suresh, S.; Higgins, J. M.; Manalis, S. R. *Proc. Natl. Acad. Sci. U. S. A.* **2011**, *108*, 10992–10996.

(3) Fabry, M. E.; Mears, J. G.; Patel, P.; Schaefer-Rego, K.; Carmichael, L. D.; Martinez, G.; Nagel, R. L. *Blood* **1984**, *64*, 1042–1046.

(4) Weems, H. B.; Lessin, Lawrence, S. *Acta Haematol.* **1984**, *71*, 361–370.

(5) Embury, S.; Clark, M. *J. Clin. Invest.* **1984**, *73*, 116–123.

(6) Kaul, D. K.; Fabry, M. E.; Windisch, P.; Baez, S.; Nagel, R. L. *J. Clin. Invest.* **1983**, *72*, 22–31.

(7) Bartolucci, P.; Brugnara, C.; Teixeira-Pinto, A.; Pissard, S.; Moradkhani, K.; Jouault, H.; Galacteros, F. *Blood* **2012**, *120*, 3136–3141.

(8) Akinsheye, I.; Alsultan, A.; Solovieff, N.; Ngo, D.; Baldwin, C. T.; Sebastiani, P.; Chui, D. H. K.; Steinberg, M. H. *Blood* **2011**, *118*, 19–27.

(9) Rees, D. C.; Williams, T. N.; Gladwin, M. T. *Lancet* **2010**, *376*, 2018–2031.

(10) Modell, B. *Bull. World Health Organ.* **2008**, *2008*, 480–487.

(11) Piel, F. B.; Hay, S. I.; Gupta, S.; Weatherall, D. J.; Williams, T. N. *PLoS Med.* **2013**, *10*, e1001484.

(12) Piel, F. B.; Howes, R. E.; Patil, A. P.; Nyangiri, O. A.; Gething, P. W.; Bhatt, S.; Williams, T. N.; Weatherall, D. J.; Hay, S. I. *Sci. Rep.* **2013**, *3*, 1671.

(13) Bunn, H. F.; Forget, B. G. *Hemoglobin--molecular, genetic, and clinical aspects*; W.B. Saunders Co.: Philidelphia, 1986; p. 690.

(14) Fabry, M. E.; Kaul, D. K.; Raventos-Suarez, C.; Chang, H.; Nagel, R. L. *J. Clin. Invest.* **1982**, *70*, 1315–1319.

(15) Brugnara, C. *Clin. Chem.* **2003**, *49*, 1573–1578.

(16) Kratz, A.; Ferraro, M.; Sluss, P. M.; Lewandrowski, K. B. *N. Engl. J. Med.* **2004**, *351*, 1548–1564.

(17) Mace, C. R.; Akbulut, O.; Kumar, A. A.; Shapiro, N. D.; Derda, R.; Patton, M. R.; Whitesides, G. M. *J. Am. Chem. Soc.* **2012**, *134*, 9094–9097.

(18) Horiuchi, K.; Ballas, S. K.; Asakura, T. *Blood* **1988**, *71*, 46–51.

(19) Kaul, D.; Xue, H. *Blood* **1991**, 1353–1361.

(20) Itano, H.; Pauling, L. *Blood* **1949**, 66–68.

(21) Clark, M. R.; Mohandas, N.; Caggiano, V.; Shohet, S. B. *J. Supramol. Struct.* **1978**, *8*, 521–532.

(22) Milligan, C.; Rees, D. C.; Ellory, J. C.; Osei, A.; Browning, J. A.; Hannemann, A.; Gibson, J. S. *J. Physiol.* **2013**, *6*, 1463–1474.

(23) Yang, X.; Kanter, J.; Piety, N. Z. N.; Benton, M. S. M.; Vignes, S. M.; Shevkoplyas, S. S. *Lab Chip* **2013**, *13*, 1464–1467.

(24) Embury, S. H. *Annu. Rev. Med.* **1986**, *37*, 361–376.

(25) Pollock, N. R.; Rolland, J. P.; Kumar, S.; Beattie, P. D.; Jain, S.; Noubary, F.; Wong, V. L.; Pohlmann, R. A.; Ryan, U. S.; Whitesides, G. M. *Sci. Transl. Med.* **2012**, *4*, 152ra129.

(26) Pretlow, T. P. T. G. T. T. *Methods* **1991**, *2*, 183–191.

(27) Shperling, T.; Danon, D. *Exp. Gerontol.* **1990**, *25*, 413–422.

(28) Rodgers, G. P.; Schechter, A. N.; Noguchi, C. T. *J. Lab. Clin. Med.* **1985**, *106*, 30–37.

Appendix III

Supporting Information

Evaluation of a Density-based Rapid Diagnostic Test for Sickle Cell Disease in a Clinical Setting in Zambia

Ashok A. Kumar, Catherine Chunda-Liyoka, Jonathan W. Hennek, Hamakwa Mantina, S.Y. Ryan Lee, Matthew Patton, Pauline Sambo, Silvester Sinyangwe, Chipepo Kankasa, Chifumbe Chintu, Carlo Brugnara, Thomas Stossel, and George M. Whitesides

Materials and Methods

Chemicals. We used the following polymers: poly(ethylene glycol) (Sigma-Aldrich; MW = 20000 Da), Ficoll (Sigma-Aldrich; MW = 70000 Da and 400000 Da), dextran (Spectrum Chemical; 500000 Da), and poly(vinyl alcohol) (PVA) (Polysciences; MW = 3000 Da)—formed by hydrolyzing 75% of poly(vinyl acetate). Solutions of AMPS contained the following chemicals: ethylenediaminetetra-acetic acid disodium salt (EDTA) (Sigma-Aldrich), potassium phosphate monobasic (EMD), sodium phosphate dibasic (Mallinkrodt AR), sodium chloride (EMD), $MgCl_2$ (USB), and Nycodenz (Axis-Shield PoC).

Components. We purchased the following components to assemble our rapid tests: heparinized, polycarbonate microhematocrit tubes (Iris Sample Processing), clay seals (Critoseal, Leica), silicone rubber tubing with an inner diameter of 1.02 mm and an outer diameter of 2.06 mm (Helix Mark, Helix Medical), glue (Krazy Glue), rubber caps (Critocaps, Leica), foil-lined pouches (Vapor-Flex VF48, LPS Industries), and shipping labels (5163, Avery). Templates to punch holes in capillary tubes and meter the volume of polymer to fill were printed in acrylonitrile butadiene styrene (ABS) using a 3D printer (Fortus 400mc, Dimension).

Blood collection used vacutainers (Becton Dickinson) coated with K_2EDTA for 2 mL. Aliquots of the collected blood were transferred to vacutainers with no coating (Becton Dickinson).

Fabrication. Figure III.1 outlines the fabrication of a single test. We puncture a hole in the side of a polycarbonate capillary tube at a prescribed height using a customized holder and push-pin (**Figure III.1**). A silicone sleeve slides over the tube to open or close the hole. Using a pipette, we load a pre-mixed solution of an SCD-MuPS solution into the tube from one end and then seal that end with white sealing clay (Critoseal, Leica).

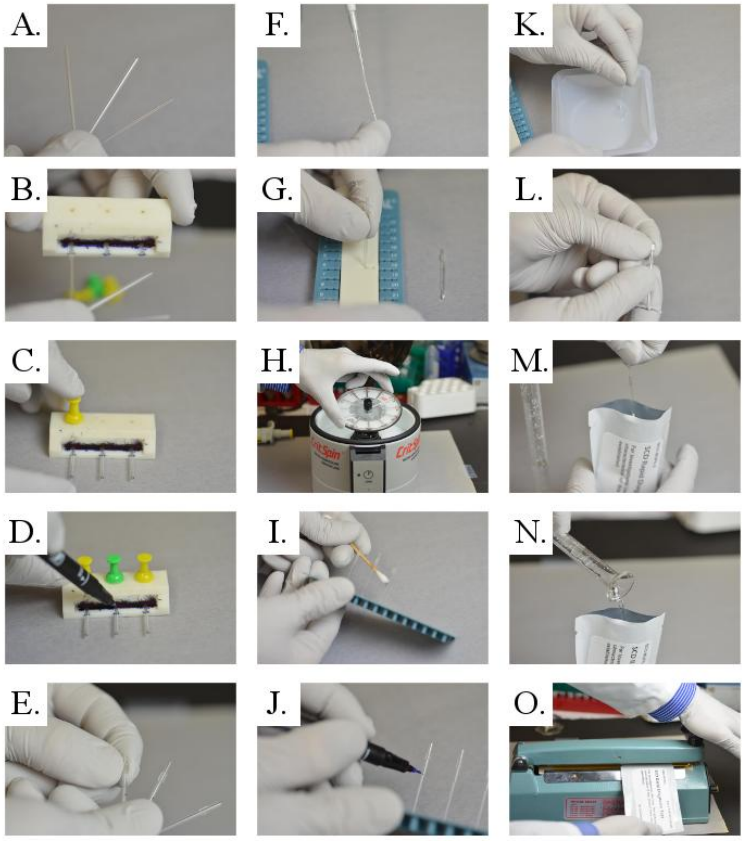

Figure III.1. Schematic of the fabrication of SCD-AMPS tests. Plastic microhematocrit tubes (A) insert into a holder (B) and can then be punctured with a pushpin (C) and metered with a marker (D). After blowing out debris with an airgun, we add a silicone sleeve to cover the hole in the side of the tube (E). We then added a well mixed AMPS solution (F) and seal the bottom of the tube with putty (G). After a quick spin (H), the initial metering mark is removed (I) and replaced with a line to mark the level of the volume of the test (J). We then seal the bottom of the test with glue (K) and cover the open end with a rubber cap (L). A dozen completed tests fit into a foil lined pouch (M). We add 4 mL of water (N) and seal the package (O).

To ensure the sealing clay does not fail during shipping or storage, we dipped the sealed end of the tube in Krazy Glue and allowed the glue to set. After two minutes of centrifugation at 13,000 *g*, the phases of the SCD-MuPS system separated. We used a marker to indicate the highest level of the liquid in the tube at the time of fabrication as a quality control measure that could be checked before use. To reversibly seal the open end of the capillary, we used white rubber capillary covers (Critocaps, Leica).

AMPS were made by weighing out the specified weight of polymer and Nycodenz into a volumetric flask. In this volume, we added a total concentration of 5 mM of Na2EDTA, 2.96 mM of KH_2PO_4 and 9.36 mM of Na_2HPO_4. We added de-ionized water (MilliQ) to dissolve the solutes and bring the solution to the final volume. We then transferred the solutions to bottles and adjusted the pH using small volumes (less than 0.5% of the total volume) of concentrated NaOH and HCl to a final pH of 7.40 ± 0.02 (Orion 2 Star pH meter, Thermo Scientific). We added solid NaCl to the solution to adjust the osmolality to a 295 ± 15 mOsm/kg using a vapor pressure osmometer (Vapro 5600, Wescor). Solutions of AMPS were stored in sealed bottles at 4 °C until the day of use to create rapid tests. We used a U-tube oscillator to measure density (DMA 35A, Anton Paar). All parameters (density, osmolality, and pH) were measured and tested and adjusted to the target ranges before adding the solution to the rapid tests.

Evaluation of Fabrication Variability. Metering a precise volume of blood into the rapid tests is potentially important to create reproducible results. In order to evaluate the effectiveness of our hole in the side of the tube, we scanned (V550, Epson) 48 tubes and used ImageJ to evaluate the distance between the top of the tube and the bottom of the hole that was punched. The coefficient of variance (standard deviation/mean) of the distance was 2%. We then wicked blood into each tube and measured the distance between the top and bottom of the

column of blood using a digital scanner. The coefficient of variance of the volume of blood that was loaded was 4%.

Storage Tests. We tested various methods to seal and package the rapid tests. For a method to seal the open end of the capillary we tried parafilm, tape, various wax seals, and rubber caps (CritoCaps, Leica). Tubes were filled with water and sealed on one end with white putty (CritoSeal, Leica). The other end was then sealed with one of the above-mentioned methods. The mass and volume of the tests were measured and then the tests were put into an oven at 50 °C. Each day for one week, the tests were removed and measured again. At the end of the week, the tubes with the rubber caps had the least loss of volume and were the easiest to remove. We noted moisture and evaporation on the end of the tube that had been sealed with putty. Coating this seal with glue (Krazy Glue) minimized evaporation from this end.

We tested several packaging methods to store the sealed rapid tests. Using an impulse sealer (PFS-200), we sealed tests in plastic pouches modified from freezer bags (ZipLoc), foil-lined modified from food packaging (Lays), and foil-lined pouches from a vendor (LPS Industries). After adding rapid tests to each pouch and sealing them, we weighed the packages and added them to an oven at 50 °C. The pouches were weighed every day for one week. Only the foil lined pouches showed no measureable loss of mass. We chose the pouches from LPS Industries because of cost and availability. Opening the pouches revealed that even though water had not escaped the packaging, it had come out of the rapid tests; a small drop of water was generally found inside the pouch near the tubes. Based on the location, we found that either the glued end had broken or the caps had come off, potentially because of the build-up of pressure.

By adding water to the packaging along with the rapid tests, we created a moist environment. Performing similar stability tests as before revealed no measureable loss of volume

in each of the individual rapid tests stored in the packaging with water. For packages containing 12 rapid tests, we added 4 mL of water.

In order to estimate the effects of long term storage on the SCD-AMPS tests, we packaged 300 rapid tests of SCD-AMPS-2 and SCD-AMPS-3 and stored them at 50 °C for one month. After this time, we let each package equilibrate to room temperature and then removed each rapid test. We removed the cap and used a razor blade to cut the putty seal off of the bottom of the test. Using a micropipette, we then removed the liquid from each of the tests and combined the samples of SCD-AMPS-2 and SCD-AMPS-3 in two separate conical tubes. The solutions were mixed with a vortex mixer and then centrifuged to separate the phases. Aliquots of the top and bottom phase of each system were removed and we measured density, osmolality, and pH. In each of the systems, the osmolality of the systems increased by ~10%. Density in each phase also increased by roughly 0.004 g/cm^3. The pH of SCD-AMPS-2 increased from 7.40 to 7.56 while the pH of SCD-AMPS-3 was fairly stable, changing from 7.39 to 7.42. Some error may have been introduced into this method due to the difficulty in removing the entire polymer solution from the capillary. A method to assess the density in the rapid tests without removing the sample could provide a more accurate measure of density.

The observed increase in both osmolality and density may be the result of a loss of water during long term storage at high temperature. Also, some water may have evaporated inside the rapid test and coated the upper part of the capillary, leaving a more concentrated solution at the bottom of the tube that would have been removed. Centrifuging the tests before use to ensure that all the water has been added back to the solution could reduce this concentration. Increasing the length of the silicone sleeve could also reduce the potential for loss of volume in the tests. Additionally, the sodium heparin coating the capillary tubes may have increased the density and

osmolality of the systems. Although these tests demonstrate the need for further improvement, the observed changes in density are less than the difference in density of normocytes and sickled erythrocytes. With further improvements, SCD-AMPS could provide stable tests stored at room temperature for several months.

Classification of Subjects Based on Results from Hemoglobin Electrophoresis. Most subjects were easily classified based on the results from hemoglobin electrophoresis. No HbC was detected in any of the subjects. Subjects with no detectable HbS were classified as HbAA. Subjects with HbA > 50% and HbS < 50% were classified as HbAS. Patients with no detectable HbA and with detectable HbS were classified as HbSS. HbF was quantified for all subjects where it was detected. Of the over 500 subjects tested, we were then left with 12 subjects that had HbS > 50% but also had detectable HbA. We classified these subjects as positive for SCD for the purposes of the study. All had either elevated reticulocyte counts or low hemoglobin concentrations. HbS concentrations ranged from 54-78%. Based on the CBC results from these subjects, three of the subjects had a microcytic and hypochromic anemia. These 12 subjects may may be SCD patients with HbSβ+ or they may have been transfused. The study was designed to exclude those who had recently been transfused, but due to occasional missing health records and missing information on health records, we relied on self-reporting for patients to identify whether they had received a transfusion in the last four months.

Statistics. Statistical analysis was done using R (http://www.r-project.org). We used Bayesian confidence intervals (Jeffreys prior) for the binary data that was used to make point estimates of sensitivity and specificity. We used two-sided t-tests to test for significant differences between performance of different batches and performance on samples stored for different time intervals.

Human Subjects Research. The Committee on the Use of Human Subjects (CUHS) at Harvard University and the ERES Converge Committee in Lusaka, Zambia each provided IRB approval for the testing of SCD-AMPS at UTH. The survey of rural health workers in Zambia was deemed exempt by CUHS and underwent full IRB review and approval by ERES.

Experimental Details

Detailed Protocol. All subjects were recruited from patients who were already indicated to have a venipuncture. During the clinically indicated venipuncture, an additional 2 mL of blood was collected in an EDTA coated vacutainer and labeled with a study ID number. Nurses interviewed subjects and guardians to fill out a short survey to capture demographic data and patient history. These surveys were used to identify whether subjects should be excluded or included based on the recruitment criteria (see **Chapter 5; Table 5.1** and Chapter 5 for details).

Blood samples were stored in an insulated container with ice packs and transported to the reference laboratory running CBCs and HE. The laboratory technician then checked each sample to ensure it was properly labeled and to see if visible clots had formed. Samples with visible clots were noted and excluded from the study. The laboratory technician aliquoted samples of blood to untreated vacutainers labeled with the same study number and a study staff member then transported these samples to the pediatric laboratory where the rapid tests were run by a second laboratory technician. The laboratory technician running the rapid tests performed the procedure outlined in **Figure III.2**, and made an initial reading using the evaluation levels depicted in **Figure III.3**. A nurse from the study then performed an independent reading. In cases of conflicting readings, a second nurse read the rapid tests. All blood was tested within the amount of time specified by **Table III.1** (i.e., the times specified by the manufacturer of the tests

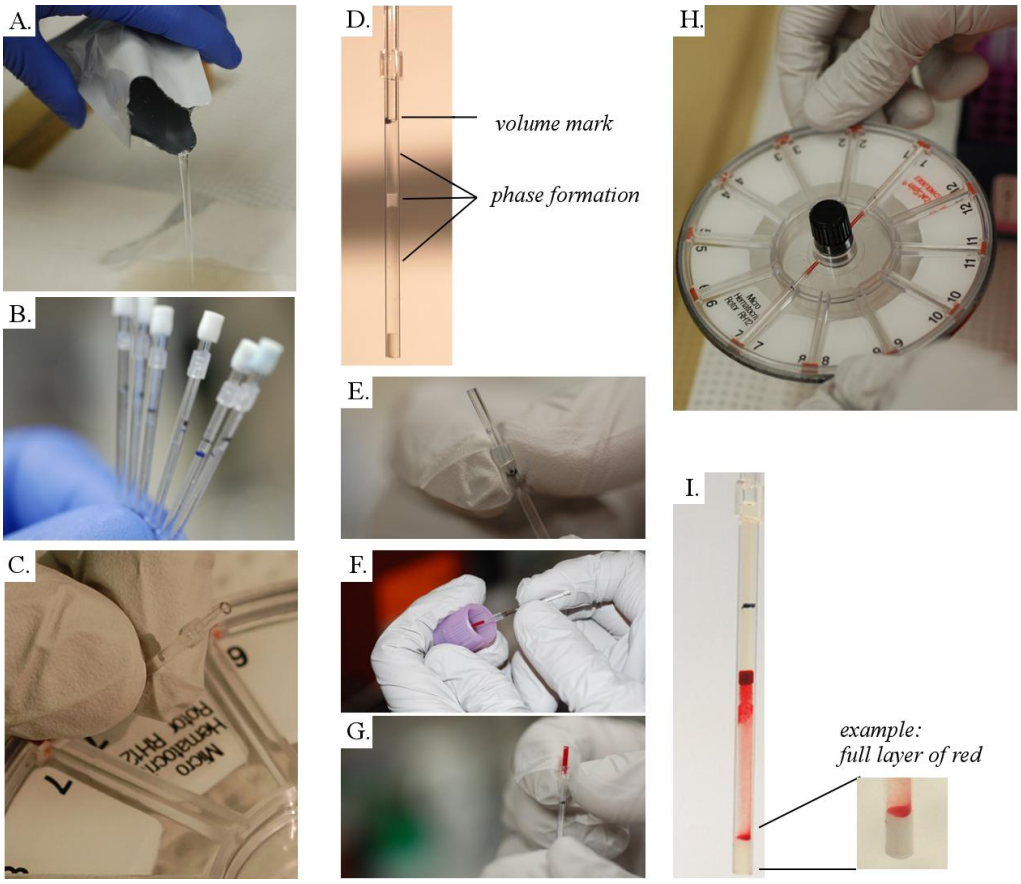

Figure III.2. Process to perform a rapid test for SCD with SCD-AMPS**.** The user opens a packet and pour out the water (A) to retrieve the rapid tests (B). She then removes the rubber cap and centrifuges the test for 2 minutes (C). After checking that the phases have formed and the proper volume of liquid is present (D), the user slides down the silicone sleeve to reveal the punched hole (E) and wicks blood into the test until it reaches the hole (F). The user then slides the sleeve back over the hole (G) and centrifuges the test for 10 minutes (H). The test can then be read by eye (I).

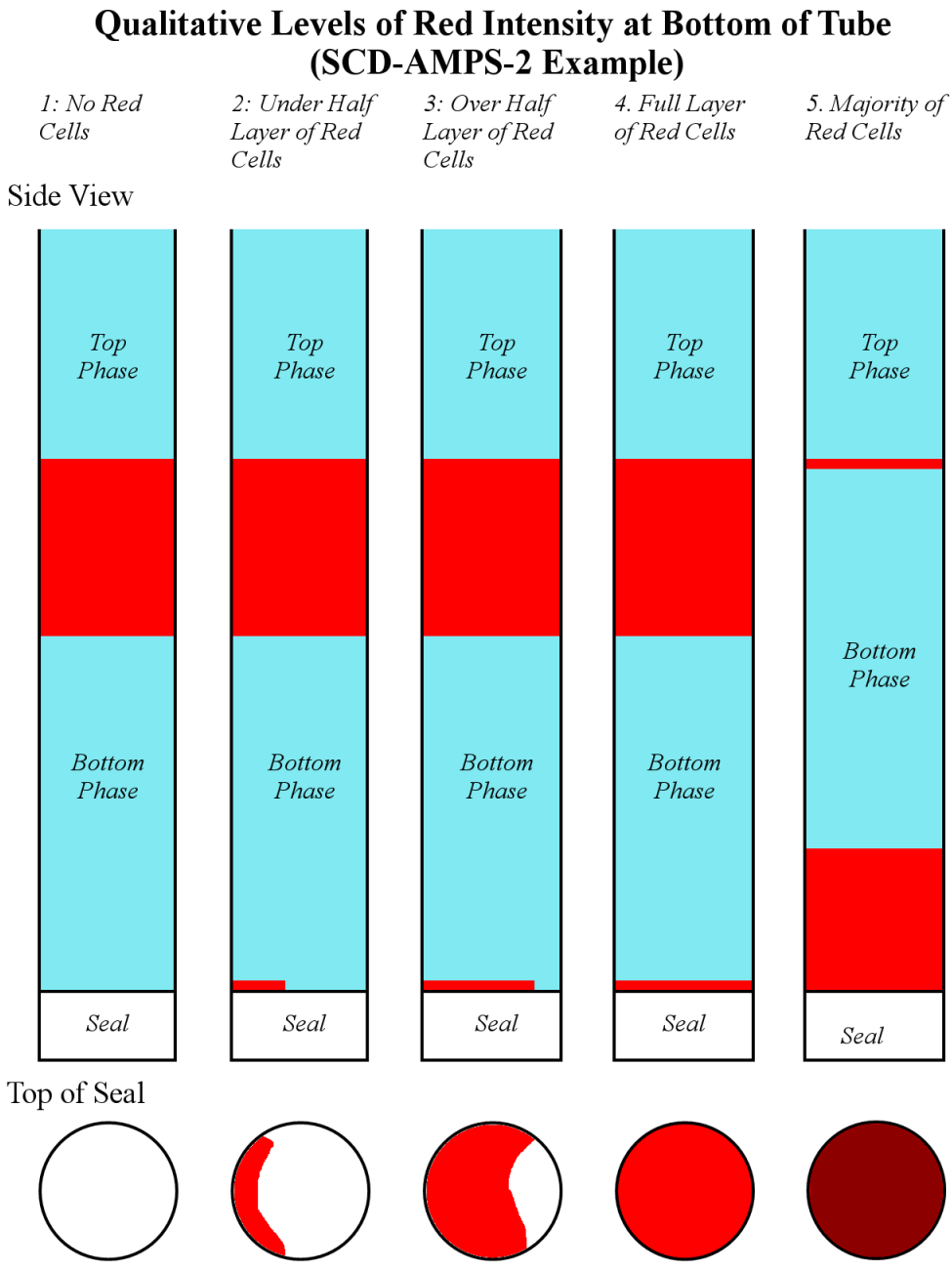

Figure III.3. Schematic representation of the five levels of evaluation of the bottom of an SCD-AMPS test. Levels 1 through 5 correspond to increasing levels of accumulation of red cells at the bottom of the test.

Table III.1. Time cutoffs for testing samples in the study.

Test Method	Maximum Time Before Testing
SCD-AMPS-2; SCD-AMPS-3	48 hours
Hemoglobin Electrophoresis	1 week
Complete Blood Count	4 hours

and equipment). Tests run after the times specified were marked as invalid and excluded from the analysis.

Each laboratory had a form to fill in values for each sample they received including the study number. The original questionnaire and these laboratory forms were collected at the end of each week and entered into a database using a user interface designed with Epi Info (CDC). The database was stored as an encrypted file and transferred to the Harvard team at the end of the study.

Pilot Study. For a pilot study, we recruited 20 participants fitting Subset 1, 11 participants fitting Subset 2, and 6 participants fitting Subset 4. Data from these participants was used to evaluate the recruitment and testing process and is presented separately from the main trial data.

Evaluation of variability in reading tests between expert reader and trained readers. One of the researchers who developed the SCD-AMPS at Harvard University trained a primary reader and three secondary readers at UTH. After an initial one day training, the readers at UTH shadowed the Harvard researcher in interpreting tests during the pilot phase of the study.

Halfway through the study, the researcher from Harvard returned and 100 rapid tests (51 SCD-AMPS-3 and 49 SCD-AMPS-2) were run on anonymous samples. The expert reader, as well as three of the UTH staff, independently read the results of each tests and compared responses. The three UTH staff readings were identical to the expert reader on 82% of the SCD-AMPS-3 and 60% of the SCD-AMPS-2. The difference in reading was generally only one level of redness off (e.g., “full layer of red” vs. “half layer of red”). On average, the UTH readers read tests with slightly higher levels of redness than the readings by the expert reader. This bias

could cause an increase in false positives or decrease false negatives compared to results previously obtained for the SCD-AMPS test (Chapter 4).

Variability in Performance by Batch. During the six months of the study, a total of 5 batches each of SCD-AMPS-2 and SCD-AMPS-3 rapid tests were manufactured at Harvard University and shipped to UTH on ice. Batch 3 took approximately 5 days longer to arrive at UTH after being shipped from Harvard because a fire in the Nairobi airport disrupted international shipping routes. The conditions under which Batch 3 was stored while being held are unknown and, thus, we could not justify exclusion of data from this batch. The divergence in performance of Batch 3 from the other batches, however, does provide some insight into the role that shipping and storage could play in performance. When analyzing the performance of each test as a function of batch, we found large variations (**Chapter 5; Figure 5.4**). Batch 1 showed best discriminative ability with diagnostic accuracies near or above 0.8 for both systems (n = 150). The density of the bottom phases of Batch 1 and 5 for both systems were ~0.002 g/cm^3 less dense than they were for Batches 2-4. **Table III.2** and **Figure III.4** details the characteristics and performance of each batch.

Evaluation of Potentially Confounding Factors.

Clotting: Blood samples in Zambia were collected in EDTA coated tubes. Variability in the total volume of blood drawn may have resulted in some samples receiving more or less than the recommended concentration of EDTA (~5 mM). To test what effect this variation might have, we collected blood from a healthy donor and treated it with different concentrations of EDTA (0 mM, 2.5 mM, 5 mM, and 10 mM). Replicates (n = 3) of each of the treatments were loaded into SCD-AMPS-2 and SCD-AMPS-3 tests and centrifuged for 10 minutes. After centrifugation, we scanned each tube using a transmission scanner (Epson V550) and analyzed

Table III.2. Characterization of each batch of SCD-AMPS used in the study.

Batch	SCD-AMPS	Top Phase			Bottom Phase			Diagnostic Accuracy	95% CI
		Density (g/cm^3)	Osmolality (mOsm/kg)	pH	Density (g/cm^3)	Osmolality (mOsm/kg)	pH		
1	2	1.0776	292	7.37	1.1287	295	7.38	86%	(80,91)
1	3	1.0754	293	7.36	1.1184	305	7.39	81%	(75,87)
2	2	1.0790	293	7.35	1.1310	305	7.35	77%	(69,84)
2	3	1.0787	297	7.44	1.1213	304	7.49	72%	(64,80)
3	2	1.0782	299	7.39	1.1303	NA	NA	69%	(61,76)
3	3	1.0776	301	7.39	1.1208	NA	NA	55%	(47,62)
4	2	1.0788	306	7.40	1.1306	303	NA	66%	(53,78)
4	3	1.0788	294	7.39	1.1204	297	NA	70%	(51,83)
5	2	1.0786	303	7.40	1.1291	305	NA	92%	(80,99)
5	3	1.0771	301	7.40	1.1184	304	NA	68%	(51,83)

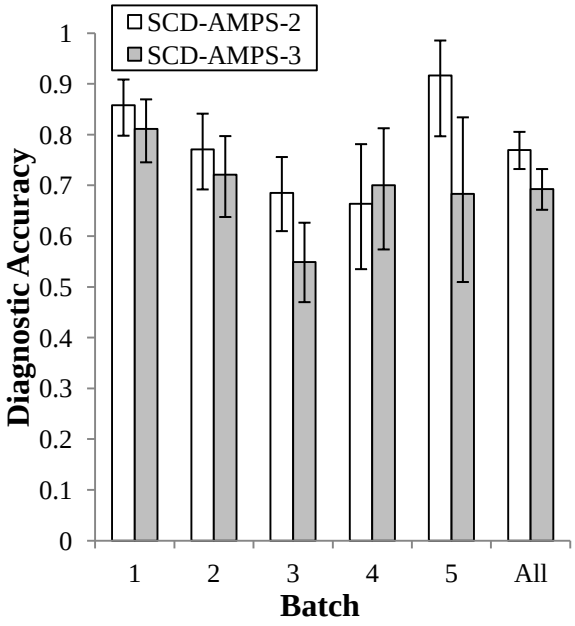

Figure III.4. The performance of the rapid test varied between batches shipped to Zambia. The diagnostic accuracy was calculated for each of the five batches of rapid tests evaluated in Zambia show significant variation for both SCD-AMPS-2 (white) and SCD-AMPS-3 (light gray). Both the combined results (All) and individual batch results (1-5) are shown. Batch 1 showed the good discriminative ability with a diagnostic accuracy over 0.8 (80%) for both tests. Error bars indicate 95% confidence intervals.

the intensity of the red at the bottom of the tube using a method previously described (Chapter 4). The signal from the blood treated with the standard concentration of EDTA (5 mM) was lowest (**Figure III.5**); exposure of blood samples to either too much or too little EDTA could result in some false positives.

Sickle Cell Trait: In solubility tests, people with sickle cell trait (HbAS) are difficult to distinguish from those with SCD (HbSS, HbSC, and other variations). Interestingly, the specificity of SCD-AMPS-2 and SCD-AMPS-3 was similar between those with HbAA and those with HbAS; sickle cell trait is not a major source of false positives for the SCD-AMPS tests (**Table III.3**). If improvements to the quality control of batches and anticoagulants used leads to improved performance, the ability to discriminate HbAS from HbSS could be a significant advantage for SCD-AMPS as way to screen for SCD.

Assets in Rural Health Centers. Sickle cell disease can be managed with the resources available in the two rural health centers that were visited in the Northern Province (**Table III.4**)

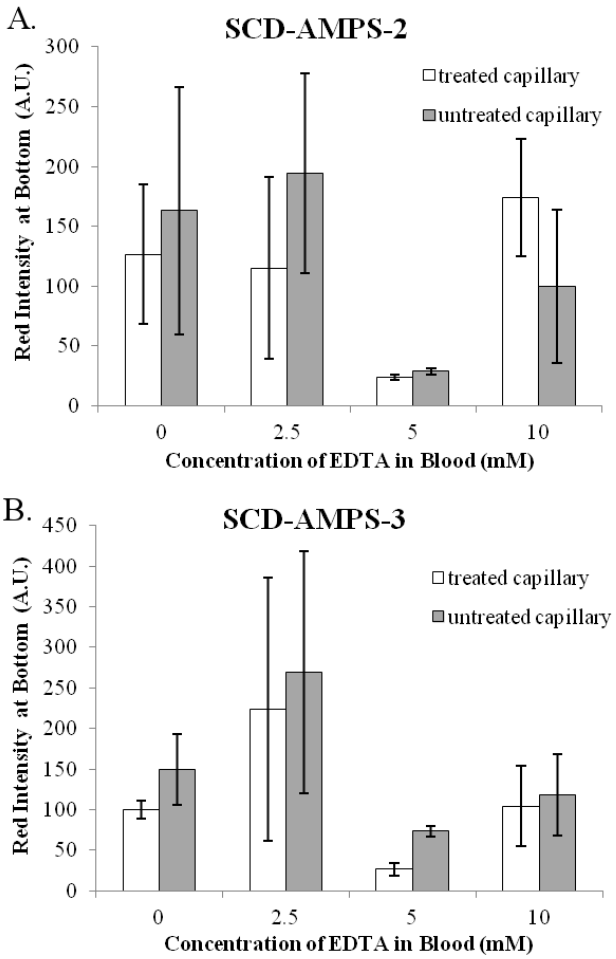

Figure III.5. Digital analysis of the red intensity at the bottom of the SCD-AMPS tests for a normal subject whose blood was treated with different concentrations of anticoagulant (EDTA). Samples were run in standard SCD-AMPS tubes treated with heparin (treated capillary) as well as SCD-AMPS loaded in tubes without any coating (untreated capillary). In all cases, the samples collected in the standard concentration of EDTA (5 mM) showed the least amount of red at the bottom of the tube. Variability in the concentration of anticoagulant during blood collection could be a source of false positives. Error bars represent standard error of the mean of triplicate experiments.

Table III.3. Specificity of SCD-AMPS on HbAA and HbAS (negative samples).

Genotype	Specificity	C.I.
SCD-AMPS-2		
HbAA	60%	(52,68)
HbAS	60%	(45,72)
SCD-AMPS-3		
HbAA	58%	(50,66)
HbAS	66%	(52,78)

Table III.4: Assets at Rural Health Centers to treat SCD.

Interventions for SCD	**Luena**	**Ipusukilo**
Ward with beds	✓	✓
Non-opiate pain killers	✓	✓
Opiates		
Ferrous	✓	✓
Folic acid	✓	✓
Antibiotics	✓	✓
Antimalarials	✓	✓
PCV Vaccine	✓	✓
IV fluids	✓	✓
Transfusions		

Appendix IV

Aqueous Multiphase Systems of Polymers and Surfactants Provide Self-Assembling Step-Gradients in Density

Charles R. Mace, Ozge Akbulut, Ashok A. Kumar, Nathan D. Shapiro, Ratmir Derda, Matthew R. Patton, and George M. Whitesides

Reprinted with permission from *J. Am. Chem. Soc.* **2012**, *134*, 9094-9097

JACS
JOURNAL OF THE AMERICAN CHEMICAL SOCIETY

Communication

pubs.acs.org/JACS

Aqueous Multiphase Systems of Polymers and Surfactants Provide Self-Assembling Step-Gradients in Density

Charles R. Mace,[†] Ozge Akbulut,[†] Ashok A. Kumar,[‡] Nathan D. Shapiro,[†] Ratmir Derda,[†] Matthew R. Patton,[†] and George M. Whitesides*[,†,§]

[†]Department of Chemistry & Chemical Biology, [‡]School of Engineering and Applied Sciences, and [§]Wyss Institute for Biologically Inspired Engineering, Harvard University, Cambridge, Massachusetts 02138, United States

Supporting Information

ABSTRACT: This Communication demonstrates the generation of over 300 phase-separated systems—ranging from two to six phases—from mixtures of aqueous solutions of polymers and surfactants. These aqueous multiphase systems (MuPSs) form self-assembling, thermodynamically stable step-gradients in density using a common solvent, water. The steps in density between phases of a MuPS can be very small ($\Delta\rho \approx 0.001$ g/cm^3), do not change over time, and can be tuned by the addition of co-solutes. We use two sets of similar objects, glass beads and pellets of different formulations of Nylon, to demonstrate the ability of MuPSs to separate mixtures of objects by differences in density. The stable interfaces between phases facilitate the convenient collection of species after separation. These results suggest that the stable, sharp step-gradients in density provided by MuPSs can enable new classes of fractionations and separations based on density.

All matter has density, and density can be used to differentiate sub-populations of complex mixtures. Separations based on differences in density have applications in fields as varied as archeology (e.g., fossils),[1] forensics (e.g., trace materials transferred by contact),[2] and hematology (e.g., cells in blood).[3] Two sub-populations of different densities in a mixture can be separated by a liquid medium that provides a step in density (e.g., a sink/float assay). Separating multiple sub-populations based on density may require multiple liquids and steps. One method to prepare fluid systems having multiple layers with different densities is to overlay miscible solutions of a solute in a common solvent (e.g., sucrose or polysucrose in water) in increments of increasing concentration.[4] This approach is not ideal because the profiles of density that are produced by this method are not sharp and change as the components diffuse. Self-assembling, thermodynamically stable, molecularly sharp step-gradients in density would offer new approaches to separations based on density.

When mixed, many aqueous solutions of polymers, surfactants, and salts form insoluble phases. Common examples of such two-component mixtures (aqueous two-phase systems, ATPSs) are solutions of poly(ethylene glycol) (PEG) and Ficoll (a polysucrose),[5] dextran (a polyglucose) and Ficoll,[6] or PEG and Triton (a surfactant).[7] The two phases of those ATPSs order spontaneously according to density and provide three stable interfaces—air/phase I, phase I/phase II, phase II/container—for the collection of species based on density. The interfacial surface energy between the phases of an ATPS is astonishingly low (100 nJ/m^2–100 μJ/m^2)[8] due to the use of water as the common solvent for the system. A low interfacial surface energy minimizes the effect of the interface on the equilibrium position of an object within an ATPS (Supporting Information (SI)). Furthermore, using water as the common solvent in phase-separated systems enables the investigation of biological mixtures.[9]

Systems that generate more than two phases in a common solvent would provide additional interfaces and enable the collection of more than three populations that differ in density. Step-gradients in density produced by phase separation are superior to systems based on concentration gradients: (i) They have distinct (sharp on the molecular scale) steps in density at phase boundaries. (ii) The composition and properties of the phase-separated layers do not change with time. (iii) The difference in densities between adjacent phases can be very small ($\Delta\rho \approx 0.001$ g/cm^3). (iv) They can be prepared well in advance of their use and stored until needed. (v) They re-form spontaneously if perturbed or agitated. Stable, sharp step-gradients in density thus provide the basis for new types of fractionations, classifications, and separations.

This Communication demonstrates the use of immiscible mixtures of aqueous solutions of polymers and surfactants to generate multiple thermodynamically stable steps in density through phase separation. We describe a library of 311 new aqueous multiphase systems (MuPSs), ranging from two to six phases. These systems can be used to generate self-assembling step-gradients in density. Each phase of a MuPS contains multiple solutes: the immiscible phases of a MuPS are not solutions of single components but mixtures of components, and the net composition of each phase determines its density. The densities of the phases of MuPSs can also be adjusted using water-soluble additives (e.g., salts) and water-miscible solvents (e.g., D_2O). We demonstrate the use of MuPSs in density-based applications using two model systems: a mixture of six glass beads in a five-phase system, and a mixture of four different formulations of Nylon in a three-phase system.

We investigated 23 polymers and 11 surfactants for their ability to induce phase separation in aqueous solutions (Table S1). The criteria for selection were (i) commercial availability

Received: April 2, 2012
Published: May 17, 2012

dx.doi.org/10.1021/ja303183z | J. Am. Chem. Soc. 2012, 134, 9094–9097

(to make them conveniently available to users), (ii) low cost (< $2/g; we required multigram quantities to complete preliminary miscibility assays), (iii) solubility in water at pH ~7 (to limit the number of parameters for this initial screen), and (iv) chemical diversity (to provide a range of potentially useful functionality). Several types of polymers and surfactants did not satisfy our criteria for selection, and we did not include them in our screen for MuPSs. For instance, we did not include polypeptides (high cost) or linear polyethyleneimine (PEI; low solubility in water ~pH 7). Branched PEI, however, is more soluble and was included in the screen. We focused on compositional diversity. We did not investigate the effect of temperature on phase separation nor systematically examine the influence of molecular weight or branching of the polymers on the properties of the MuPSs; others have studied these effects in the context of ATPSs.[5,6,10]

The densities of the phases of MuPSs can be adjusted by changing the concentrations of the polymers or the surfactants that are used to generate them.[6] These densities can be tuned further by incorporating co-solutes into MuPSs (here, D_2O and CsBr). We chose to investigate D_2O instead of other water-miscible solvents (e.g., ethanol) because D_2O—as an isotope of water—does not affect the solubility of polymers or surfactants (SI). It provides a maximum 11% increase in the density of an aqueous solution and is relatively inexpensive for solutions that are not highly enriched isotopically (<$0.35/mL for a solution with 70% D_2O enrichment). We used CsBr as an additive to increase the densities of the phases of MuPSs. We selected this salt for five reasons: (i) Polymers with coordinating functional groups (e.g., poly(methacrylic acid); PMAA) may chelate multivalent cations and precipitate; they do not, however, chelate monovalent cations like Cs^+. (ii) CsBr is commercially available and inexpensive. (iii) Solutions of CsBr span a range of densities that is useful for biological separations (the density of a 1 M CsBr solution is 1.161 g/cm^3). (iv) CsBr is very soluble in water at room temperature (>5 M). (v) Solutions of CsBr at high concentrations are transparent at visible wavelengths.

We prepared every two-component combination of the 34 polymers and surfactants we selected for this screen (561 mixtures in total; Figure 1). For each combination, we thoroughly mixed equal volumes of two selected stock solutions of a polymer or a surfactant by vortexing for 30 s to allow the components of each phase to reach their equilibrium concentrations. Mixtures of immiscible solutions form emulsions and thus appear turbid. If these emulsions are left to equilibrate under ambient conditions, separation of the phases into distinct layers occurs over the course of minutes to days; the time required depends on the differences in density and viscosity of the phases ($\Delta\rho \approx 0.001-0.100$ g/cm^3; $\Delta\eta \approx 1-1000$ cP). To accelerate phase separation, we subjected the emulsions to centrifugation: typically, complete separation is observed after <5 min at 2000*g*.

A visually discernible interface characterized those two-component mixtures that separated into discrete phases (i.e., formed an ATPS); miscible mixtures produced homogeneous solutions. A number of mixtures formed either gels or precipitates; these systems are not immediately useful in density-based applications, and we did not consider them further. We confirmed that phase separation occurs for a number of previously characterized ATPSs and identified 91 previously unreported systems (Table S2). These new ATPSs include systems produced from mixtures of two polymers, one polymer and one surfactant, or two surfactants.

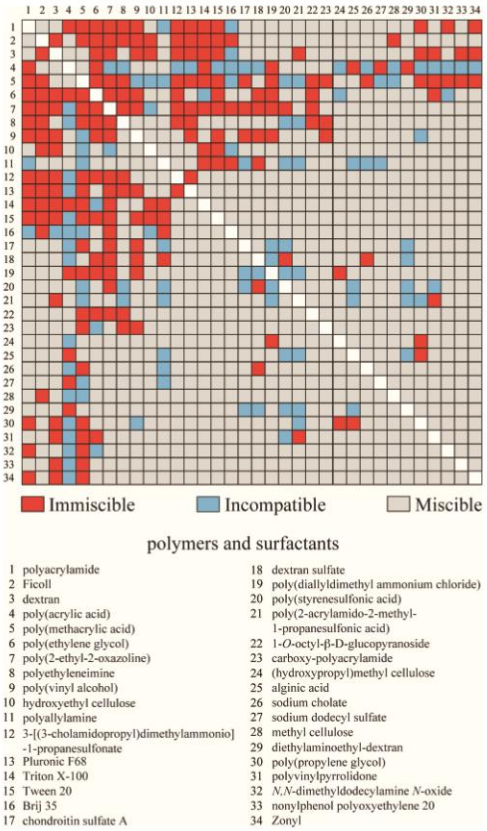

Figure 1. Phase separation in two-component mixtures of aqueous solutions of polymers and surfactants. Two-component mixtures of 23 aqueous polymer solutions and 11 aqueous surfactant solutions (561 mixtures in total) produced three outcomes: no phase separation (*miscible*, gray), formation of a precipitate or gel (*incompatible*, blue), or phase separation (*immiscible*, red).

We wrote an algorithm using Matlab (SI) that used the results of the two-component screen to predict the multi-component mixtures that would produce multiple phases. For example, if mixtures of solutes A/B, B/C, and A/C each result in two-phase systems, then we expected a mixture of solutes A/B/C to produce a three-phase system.[6] Using this approach, we predicted the existence of MuPSs with as many as six phases from combinations of solutes used in the two-component miscibility screen. Based on the ATPSs listed in Table S2, the algorithm predicted 247 systems with three or more phases. We were able to prepare 221 of these systems, included five six-phase MuPSs (details in Tables S3–S6). Prior to this study, only one of the three-phase systems that we found had been described in the literature.[11] Including new ATPSs identified from our two-component screen, we have discovered 311

mixtures of aqueous solutions of polymers or surfactants that result in phase separation.

Each phase of an ATPS contains water and some amount of both solutes used to form the ATPS.[8] We expected each phase of a MuPS would contain a mixture of solutes as well, and the evaluation of a five-phase MuPS by ^{1}H NMR spectroscopy confirmed this hypothesis (SI). Each phase of a MuPS can be described by the solute that exists at the highest concentration in the phase (e.g., a PMAA-rich phase).

To demonstrate the use of MuPSs in density-based applications, we added a group of six density standard beads to an emulsion of an aqueous solution containing 6.4% (w/v) PEG, 5.6% (w/v) poly(2-ethyl-2-oxazoline) (PEOZ), 9.0% (w/v) poly(vinyl alcohol) (PVA), 4.8% (w/v) dextran, and 6.4% (w/v) Ficoll (Table S8). This emulsion behaved as a sink/float medium for the added density standard beads: three beads floated and three beads sank (Figure 2). Upon centrifugation,

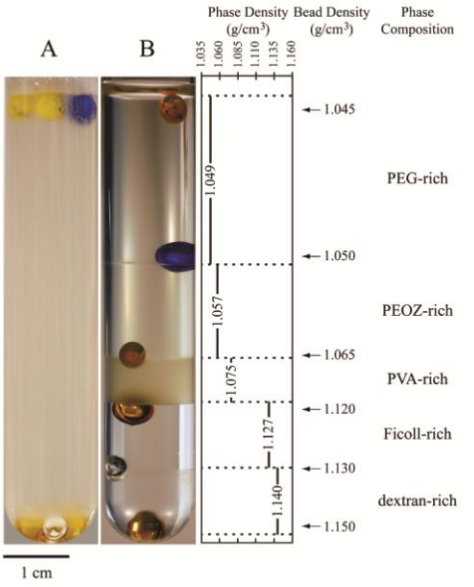

Figure 2. Preparation and demonstration of MuPSs in density-based separations. We prepared a five-phase MuPS by mixing aqueous solutions of PEG, PEOZ, PVA, dextran, and Ficoll. We added a set of six density standard beads to this mixture: three beads floated and three beads sank in the emulsified aqueous medium (A). The mixture of polymers separated into five phases upon centrifugation, and each bead sedimented under the applied centrifugal field until it reached an interface whose densities straddled the density of the bead (B).

this mixture produced a five-phase MuPS, and the beads sedimented to positions based on their densities: one at each of the four interfaces between the five phases, one at the interface between air and the top phase, and one at the interface between the bottom phase and the container. The position of the center of mass of the bead at an interface gives additional information about its density (SI).

We reproduced this separation using an identical MuPS that we prepared prior to the addition of beads rather than *in situ*. After 12 months at room temperature, the step-gradient in density produced by this MuPS remained unchanged, and we were able to reproduce the bead separation experiments successfully after this prolonged storage period. This stability is, of course, entirely different from that observed in layered solutions of sucrose of different concentrations.

Co-solutes and co-solvents can be added to MuPSs to tune the densities of the phases. We prepared a series of two-phase MuPSs that contained 10% (w/v) PEOZ and 15% (w/v) PEG in aqueous solutions that contained H_2O/D_2O ranging from 100% H_2O to 70% D_2O/30% H_2O. Each MuPS had identical polymer compositions and differed only in the total concentration of D_2O. After phase separation by centrifugation, we measured the densities of isolated samples of each phase (Figure 3A). The relationship between the concentration of

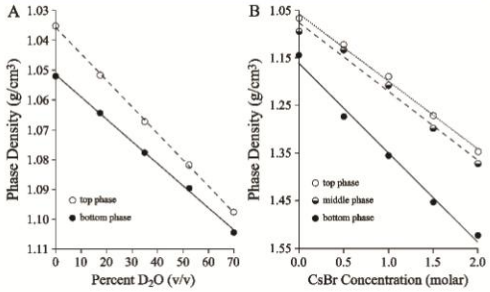

Figure 3. Tuning the density of the phases of MuPSs with additives. A two-phase MuPS was prepared from mixtures of PEG and PEOZ in aqueous solutions with a range of isotopic purity (0–70% D_2O by volume) (A). A three-phase MuPS was prepared from mixtures of PEG, PEI, and PMAA in aqueous solutions that included CsBr over a range of concentrations of salt (B). In both cases, the densities of the phases increased linearly with the concentration of the additive.

D_2O added to the mixture of polymers and the density of each phase was linear ($R^2 > 0.998$), but the slopes of the linear fit to each set of data were not equal: 9×10^{-4} and 7×10^{-4} g/cm^3/%D_2O for the top and bottom phases, respectively. These results are consistent with the observation that the concentrations of water differ between phases of ATPSs.[6] The phase with lower water content will incorporate less *total* D_2O at equal concentrations, and the density of this phase will thus increase at a lower rate compared to the density of a phase with higher water content (SI).

We also examined the addition of water-soluble salts as a method to increase the densities of the phases of a MuPS. We prepared a series of three-phase MuPSs that contained 11.7% (w/v) PEG, 8.3% (w/v) PEI, and 10.7% (w/v) PMAA and included up to 2.0 M CsBr. Although CsBr is soluble in water at concentrations >5.0 M, the presence of high concentrations of polymers in solution lowered the solubility of the salt to ~2.0 M. The relationship between the concentration of salt added to the MuPSs and the density of each phase was linear, but the slopes were not equal (Figure 3B). Using LiBr instead of CsBr produced a similar result but with lower densities at equal concentrations of salt (Figure S3).

For the three-phase system with added CsBr, we used ^{1}H NMR to quantify the concentrations of water and polymer in each phase and to calculate the amount of salt in each phase (Figure S4). As expected, CsBr is not distributed equally among

the three phases; the phase to which CsBr partitions preferentially—in this case, the bottom phase—increases in density more than the other phases.

The ability to tune the densities of the phases of MuPSs using a number of methods—changing the combinations of solutes, changing the concentrations of solutes, or adding co-solutes—provides options to identify compositions of systems that are useful for separations. For example, we prepared a three-phase MuPS from a mixture of 10% (w/v) Ficoll, 13.3% (w/v) PEOZ, and 10% (v/v) Brij 35 and tuned the density of this system by adding 25.5% (v/v) D_2O. Following centrifugation, this system separated four different formulations of Nylon—Nylon 12 (ρ = 1.032 g/cm^3), Nylon 6 (ρ = 1.057 g/cm^3), Nylon 6/66 (ρ = 1.120 g/cm^3), and Nylon 6/12 (ρ = 1.147 g/cm^3)—by differences in their densities (Figure 4). In

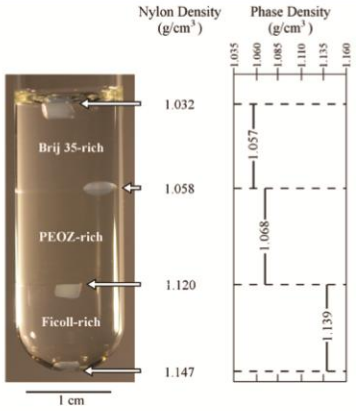

Figure 4. Separation of Nylon beads based on density using a MuPS. We prepared a three-phase MuPS from a mixture of aqueous solutions of Ficoll, PEOZ, and Brij 35. The water used to prepare this MuPS contained ~25.5% (v/v) D_2O. We used this MuPS to separate four formulations of Nylon based on density.

the analogous three-phase system containing 100% H_2O, however, the separation of Nylon species was incomplete: two Nylon beads (Nylon 6 and Nylon 6/66) were captured at the same interface between the middle and the bottom phases. The addition of D_2O to the MuPS increased the densities of the phases to appropriate values for separation of the Nylon species (Figure S6).

Density, as a common property of all matter, often serves as a convenient and efficient marker for the differentiation and separation of species from mixtures. MuPSs provide a means to produce self-assembling, thermodynamically stable step-gradients in density; these systems should find use in separations and analyses based on density. MuPSs can be prepared by mixing immiscible aqueous solutions of polymers and surfactants.

The number of immiscible components used to produce the system determines the final number of phases and, therefore, the number of interfaces: a MuPS with N phases has N+1 interfaces, and each interface is capable of isolating species based on density. Herein, we describe a library of over 300 MuPSs that range from two to six phases and demonstrate that the steps in density produced by MuPSs can be tuned by incorporating water-miscible additives (e.g., co-solvents or co-solutes).

Unlike the step-gradients in density produced by layered media, the interfaces between the layers of a MuPS are sharp on a molecular scale and stable. Species collected at sharp interfaces are easier to visualize, separate, and isolate. MuPSs enable the creation of small steps in density ($\Delta\rho \approx 0.001$ g/cm^3) that remain stable because the composition and properties of the phase-separated layers do not change with time. This characteristic makes MuPSs useful when the storage and long-term stability of the separation media are important. Although multi-solvent systems can also produce stable, immiscible phases, only MuPSs can be used to separate objects that are compatible with a single solvent. Specifically, the use of water as the common solvent should enable the separation and analysis of multiple sub-populations from complex biological mixtures (e.g., cells from whole blood) based on density.

■ ASSOCIATED CONTENT

Supporting Information

Detailed materials and methods, description of ordering of solutes in two-component mixtures, description of algorithm to predict MuPSs, tables of MuPSs, and quantification of ^{1}H NMR experiments. This material is available free of charge via the Internet at http://pubs.acs.org.

■ AUTHOR INFORMATION

Corresponding Author

gwhitesides@gmwgroup.harvard.edu

Notes

The authors declare no competing financial interest.

■ ACKNOWLEDGMENTS

This work was supported by the Bill and Melinda Gates Foundation under award no. OPP1016360. A.A.K. acknowledges financial support from the Office of Naval Research through the NDSEG fellowship program.

■ REFERENCES

(1) Munsternan, D.; Kerstholt, S. *Rev. Palaeobot. Palyno.* **1996**, *91*, 417.
(2) Petraco, N.; Kubic, T. *J. Forensic Sci.* **2000**, *45*, 872.
(3) English, D.; Andersen, B. R. *J. Immunol. Methods* **1974**, *5*, 249.
(4) Glinski, W.; Gershwin, M. E.; Budman, D. R.; Steinberg, A. D. *Clin. Exp. Immunol.* **1976**, *26*, 228.
(5) Albertsson, P.-Å. *Biochim. Biophys. Acta* **1958**, *27*, 378.
(6) Albertsson, P.-Å. *Partition of Cell Particles and Macromolecules*; Wiley Interscience: New York, 1986.
(7) Yamazaki, M.; Ohsika, M.; Ito, T. *Biochim. Biophys. Acta* **1991**, *1063*, 175.
(8) Hatti-Kaul, R. *Mol. Biotechnol.* **2001**, *19*, 269.
(9) (a) Fisher, D. *Biochem. J.* **1981**, *196*, 1. (b) Lutwyche, P.; Norris-Jones, R.; Brooks, D. E. *Appl. Environ. Microb.* **1995**, *61*, 3251. (c) Kamei, D. T.; Liu, C.-L.; Haase-Pettingell, C.; King, J. A.; Wang, D. I. C.; Blankschtein, D. *Biotechnol. Bioeng.* **2002**, *78*, 190. (d) Frampton, J. P.; Lai, D.; Sriram, H.; Takayama, S. *Biomed. Microdevices* **2011**, *13*, 1043.
(10) (a) Albertsson, P.-Å.; Cajarville, A.; Brooks, D. E.; Tjerneld, F. *Biochim. Biophys. Acta* **1987**, *926*, 87. (b) Johansson, H.; Karlström, G.; Tjerneld, F.; Haynes, C. *J. Chromatogr. B* **1998**, *711*, 3.
(11) (a) Albertsson, P.-Å. *Biochemistry* **1973**, *12*, 2525. (b) Ruan, K.; Wang, B.-H.; Xiao, J.-X.; Tan, J.-N. *J. Disper. Sci. Technol.* **2006**, *27*, 927.

Supporting Information

Aqueous Multiphase Systems of Polymers and Surfactants Provide Self-Assembling Step-Gradients in Density

Charles R. Mace[1], Ozge Akbulut[1], Ashok A. Kumar[2], Nathan D. Shapiro[1], Ratmir Derda[1], Matthew R. Patton[1], and George M. Whitesides[1,3*]

[1]Department of Chemistry & Chemical Biology, Harvard University, 12 Oxford St., Cambridge, MA 02138, United States,

[2]School of Engineering and Applied Sciences, Harvard University, 29 Oxford St., Cambridge, MA 02138, United States, and

[3]Wyss Institute for Biologically Inspired Engineering, Harvard University, 60 Oxford St., Cambridge, MA 02138, United States

[*]Corresponding author: gwhitesides@gmwgroup.harvard.edu

Materials and Methods

Materials. The following chemicals were purchased from Sigma-Aldrich: alginic acid sodium salt, chondroitin sulfate A, dextran sulfate sodium salt, Ficoll, (hydroxypropyl)methyl cellulose, poly(2-acrylamido-2-methyl-1-propanesulfonic acid), poly(2-ethyl-2-oxazoline), polyacrylamide, poly(diallyldimethyl ammonium chloride), poly(ethylene glycol), polyethyleneimine, poly(methacrylic acid sodium salt), poly(propylene glycol), polyvinylpyrrolidone, Brij 35, 3-[(3-cholamidopropyl)dimethylammonio]-1-propanesulfonate (CHAPS), cetyl trimethylammonium bromide (CTAB), Pluronic F68, sodium cholate, Tween 20, Triton X-100, Zonyl, lithium bromide (LiBr), cesium bromide (CsBr) and benzene-1,2-disulfonic acid dipotassium salt. The following chemicals were purchased from Polysciences: poly(acrylic acid), poly(allylamine hydrochloride), poly(styrenesulfonic acid sodium salt), and poly(vinyl alcohol). Dextran was purchased from Spectrum Chemical. Diethylaminoethyl-dextran hydrochloride was purchased from MP Biomedicals. Carboxy-modified polyacrylamide, hydroxyethyl cellulose, methyl cellulose were purchased from Scientific Polymer Products. 1-*O*-octyl-β-D-glucopyranoside was purchased from Calbiochem. *N*,*N*-dimethyldodecylamine *N*-oxide was purchased from Fluka. Sodium dodecyl sulfate was purchased from J.T. Baker. All polymers were used without further purification.

We purchased a series of glass density standard floats ("beads") from American Density Materials, the densities of which spanned 1.0400 g/cm^3 to 1.1500 g/cm^3. The vendor certified that the density of each bead was calibrated to ± 0.0002 g/cm^3 at 23 °C. We purchased pellets of four different formulations of nylon (i.e., Nylon 6, Nylon 12, Nylon 6/12, and Nylon 6/66) from Sigma Aldrich. The pellets were irregularly shaped with dimensions on the order of 2–5 mm. The densities of the Nylon formulations were determined by magnetic levitation (*vida infra*).

Preparation and Characterization of Stock Solutions. We prepared stock solutions of polymers in Milli-Q water (pH 5.5) at high concentrations, between 1–50% (w/v) or 1–50% (v/v) without adding salts or titrating the pH. We characterized the density of each stock solution (Table S1) using an oscillating U-tube densitometer (Anton Paar DM35N). Each measurement requires approximately 800 μL. The viscosities of the stock solutions of some polymers were too viscous to be analyzed directly by the densitometer (e.g., polyacrylamide and poly(2-acrylamido-2-methyl-1-propanesulfonic acid)). We calculated these densities by measuring the densities of three lower concentrations and determining the linear fit to the data.

Experimental Details

Phase Separation in Two-Component Mixtures of Aqueous Solutions of Polymers and Surfactants. To perform the initial two-component immiscibility screens, we added equal volumes (150 μL) of each polymer or surfactant solution in Table S1 into a microcentrifuge tube, we vortexed the tube for 30 seconds to thoroughly mix the solutions, and we accelerated phase-separation by centrifugation at 2000*g* for five minutes in a VWR Galaxy Mini centrifuge. In some cases, although each experiment began with equal volumes of stock solutions, we observed that the final aqueous two-phase system (ATPS) was characterized by phases with unequal volumes. This is a well-understood phenomenon that results when the initial concentrations of the system are near the node of the tie-line that characterizes the phase diagram of the system.[1] From our investigation of 34 polymers and surfactants, we identified a number of unreported ATPSs and confirmed those that have been previously described by others (Table S2).

Table S1. Properties of the aqueous stock solutions of polymers and surfactants: average molecular weight (Da), concentration (% w/v or % v/v), and density (g/cm^3). An asterisk (*) refers to densities that were calculated, rather than measured.

	polymer or surfactant	avg. MW (Da)	concentration	density (g/cm^3)
1	polyacrylamide	10,000	40% (w/v)	* 1.149
2	Ficoll	400,000	40% (w/v)	1.130
3	dextran	500,000	30% (w/v)	1.101
4	poly(acrylic acid)	450,000	10% (w/v)	1.035
5	poly(methacrylic acid)	5,000	40% (w/v)	1.279
6	poly(ethylene glycol)	20,000	40% (w/v)	1.069
7	poly(2-ethyl-2-oxazoline)	200,000	35% (w/v)	1.059
8	polyethyleneimine	25,000	30% (w/v)	1.037
9	poly(vinyl alcohol)	3,000	10% (w/v)	1.022
10	hydroxyethyl cellulose	90,000	2% (w/v)	1.004
11	polyallylamine	60,000	20% (w/v)	1.052
12	CHAPS	614	25% (w/v)	1.042
13	Pluronic F68	8,400	44% (w/v)	1.049
14	Triton X-100	625	20% (w/v)	1.017
15	Tween 20	1,228	45% (v/v)	1.067
16	Brij 35	1,198	30% (v/v)	1.025
17	chondroitin sulfate A	25,000	10% (w/v)	1.044
18	dextran sulfate	500,000	20% (w/v)	1.103
19	poly(diallyldimethyl lammonium chloride)	400,000	20% (w/v)	1.044
20	poly(styrenesulfonic acid)	75,000	30% (w/v)	1.100
21	poly(2-acrylamido-2-methyl-1-propanesulfonic acid)	2,000,000	15% (w/v)	* 1.042
22	1-*O*-Octyl-β-D-glucopyranoside	292	10% (w/v)	1.011
23	carboxy-polyacrylamide	200,000	6% (w/v)	1.018
24	(hydroxypropyl)methyl cellulose	10,000	2% (w/v)	1.003
25	alginic acid	240,000	2% (w/v)	1.010
26	sodium cholate	408	43% (w/v)	0.997
27	sodium dodecyl sulfate	288	35% (w/v)	0.998
28	methyl cellulose	86,000	1% (w/v)	1.001
29	diethylaminoethyl-dextran	500,000	10% (w/v)	1.028
30	poly(propylene glycol)	425	40% (w/v)	1.029
31	polyvinylpyrrolidone	55,000	20% (w/v)	1.038
32	*N,N*-dimethyldodecylamine *N*-oxide	229	24% (w/v)	1.123
33	nonylphenol polyoxyethylene (20)	13,420	40% (v/v)	1.035
34	Zonyl	N/A	50% (v/v)	1.037

Table S2. List of new and previously reported ATPS found by this study.

	Previously Reported ATPS		REF
1	dextran	Ficoll	2
6	dextran	poly(ethylene glycol)	3
3	dextran	poly(propylene glycol)	3
7	dextran	poly(vinyl alcohol)	3
2	dextran	polyvinylpyrrolidone	3
4	dextran	Triton X-100	4
5	dextran	Tween 20	4
8	dextran sulfate	poly(ethylene glycol)	2
9	dextran sulfate	poly(styrenesulfonic acid)	5
10	Ficoll	poly(ethylene glycol)	2
11	hydroxyethyl cellulose	Triton X-100	6
12	poly(acrylic acid)	poly(ethylene glycol)	7
15	poly(ethylene glycol)	poly(vinyl alcohol)	3
13	poly(ethylene glycol)	polyvinylpyrrolidone	3
14	poly(ethylene glycol)	Tween 20	4

	New ATPS	
16	1-*O*-octyl-β-D-glucopyranoside	poly(2-ethyl-2-oxazoline)
17	1-*O*-octyl-β-D-glucopyranoside	poly(ethylene glycol)
18	1-*O*-octyl-β-D-glucopyranoside	poly(methacrylic acid)
19	1-*O*-octyl-β-D-glucopyranoside	polyethyleneimine
20	alginic acid	poly(acrylic acid)
21	alginic acid	poly(propylene glycol)
22	Brij 35	Ficoll
23	Brij 35	poly(2-ethyl-2-oxazoline)
24	Brij 35	polyallylamine
25	carboxy-polyacrylamide	poly(methacrylic acid)
26	carboxy-polyacrylamide	poly(vinyl alcohol)
27	carboxy-polyacrylamide	polyethyleneimine
28	CHAPS	dextran
29	CHAPS	Ficoll
30	CHAPS	Pluronic F68
31	CHAPS	poly(2-ethyl-2-oxazoline)
32	CHAPS	poly(ethylene glycol)
33	CHAPS	poly(methacrylic acid)
34	CHAPS	polyacrylamide
35	CHAPS	polyethyleneimine
36	chondroitin sulfate A	poly(2-ethyl-2-oxazoline)
37	chondroitin sulfate A	poly(methacrylic acid)
38	chondroitin sulfate A	poly(vinyl alcohol)
39	dextran	hydroxyethyl cellulose
40	dextran	nonylphenol polyoxyethylene (20)
41	dextran	Pluronic F68
42	dextran	poly(2-ethyl-2-oxazoline)
43	dextran	poly(2-acrylamido-2-methyl-1-propanesulfonic acid)
44	dextran	Zonyl
45	dextran sulfate	poly(2-ethyl-2-oxazoline)
46	dextran sulfate	poly(vinyl alcohol)

Table S2, cont.

	New ATPS	
47	dextran sulfate	polyallylamine
48	dextran sulfate	sodium cholate
49	diethylaminoethyl-dextran	poly(acrylic acid)
50	Ficoll	methyl cellulose
51	Ficoll	Pluronic F68
52	Ficoll	poly(2-ethyl-2-oxazoline)
53	Ficoll	poly(methacrylic acid)
54	Ficoll	poly(vinyl alcohol)
55	Ficoll	polyethyleneimine
56	Ficoll	Triton X-100
57	Ficoll	Tween 20
58	hydroxyethyl cellulose	Ficoll
59	hydroxyethyl cellulose	Tween 20
60	(hydroxypropyl)methyl cellulose	poly(diallyldimethyl ammonium chloride
61	(hydroxypropyl)methyl cellulose	poly(propylene glycol)
62	*N*,*N*-dimethyldodecylamine *N*-oxide	poly(methacrylic acid)
63	*N*,*N*-dimethyldodecylamine *N*-oxide	polyacrylamide
64	nonylphenol polyoxyethylene (20)	poly(methacrylic acid)
65	Pluronic F68	poly(2-ethyl-2-oxazoline)
66	Pluronic F68	poly(methacrylic acid)
67	Pluronic F68	poly(vinyl alcohol)
68	Pluronic F68	polyacrylamide
69	Pluronic F68	polyethyleneimine
70	poly(2-acrylamido-2-methyl-1-propanesulfonic acid)	polyvinylpyrrolidone
71	poly(2-ethyl-2-oxazoline)	poly(diallyldimethyl ammonium chloride
72	poly(2-ethyl-2-oxazoline)	poly(ethylene glycol)
73	poly(2-ethyl-2-oxazoline)	poly(methacrylic acid)
74	poly(2-ethyl-2-oxazoline)	poly(styrenesulfonic acid)
75	poly(2-ethyl-2-oxazoline)	poly(vinyl alcohol)
76	poly(2-ethyl-2-oxazoline)	polyacrylamide
77	poly(2-ethyl-2-oxazoline)	polyethyleneimine
78	poly(2-ethyl-2-oxazoline)	Triton X-100
79	poly(2-ethyl-2-oxazoline)	Tween 20
80	poly(acrylic acid)	poly(diallyldimethyl ammonium chloride
81	poly(acrylic acid)	polyacrylamide
82	poly(acrylic acid)	sodium dodecyl sulfate
83	poly(acrylic acid)	Triton X-100
84	poly(diallyldimethyl ammonium chloride	poly(ethylene glycol)
85	poly(diallyldimethyl ammonium chloride	poly(methacrylic acid)
86	poly(diallyldimethyl ammonium chloride	poly(vinyl alcohol)
87	poly(ethylene glycol)	poly(methacrylic acid)
88	poly(ethylene glycol)	polyacrylamide
89	poly(ethylene glycol)	polyethyleneimine
90	poly(methacrylic acid)	poly(propylene glycol)
91	poly(methacrylic acid)	polyacrylamide
92	poly(methacrylic acid)	polyethyleneimine
93	poly(methacrylic acid)	polyvinylpyrrolidone
94	poly(methacrylic acid)	sodium cholate
95	poly(methacrylic acid)	Triton X-100

Table S2, cont.

	New ATPS	
96	poly(methacrylic acid)	Tween 20
97	poly(methacrylic acid)	Zonyl
98	poly(propylene glycol)	polyacrylamide
99	poly(vinyl alcohol)	Tween 20
100	polyacrylamide	poly(vinyl alcohol)
101	polyacrylamide	polyethyleneimine
102	polyacrylamide	Triton X-100
103	polyacrylamide	Tween 20
104	polyacrylamide	Zonyl
105	polyallylamine	Triton X-100
106	polyallylamine	Tween 20

There are several notable exceptions to our screen: we did not investigate kosmotropic salt solutions (e.g., ammonium sulfate) that are known to form ATPS with poly(ethylene glycol),[8] and we did not supplement the aqueous solutions with sodium chloride or other salts that are known to facilitate polymer–polymer phase separation.[9] Furthermore, we observed that several additional polymers were either only sparingly soluble or did not phase separate with the solutes listed above. These included xanthan gum, chitosan, gelatin, linear polyethyleneimine, poly(N-isopropylpolyacrylamide), and a fourth generation hyperbranched bis-MPA polyester-64-hydroxyl dendrimer. Sodium carboxymethyl cellulose and total Yeast RNA (as a polyphosphate source), while soluble, did not phase separate with any of the chemicals listed in Table S1.

Clustering of Two-Phase Systems. Flory-Huggins Theory has been used to describe phase separation in several aqueous two-phase systems.[10] The Flory interaction parameters are dependent on the specific polymers and solvent used. The relationship between key variables, such as temperature and molecular weight, is deeply embedded in the free energy equations; general intuition about which conditions lead to phase separation is difficult to establish without either rigorous computation over several parameters or many simplifying assumptions.[11]

While establishing a general set of solubility parameters for aqueous solutions is beyond the scope of this work, we suggest an ordering system that is both based on solubility and consistent within the set of chemicals that we include in this screen. We assigned a 34-component vector to each of the twenty-three polymers and eleven surfactants, which comprised arbitrary values that we used to characterize the result of each two-component mixture: '0' for mixtures that resulted in homogeneous solutions (miscible), '1' for mixtures that resulted in a precipitate or a gel (incompatible), and '2' for mixtures that resulted in phase separation (immiscible). For example, the matrix for poly(vinyl alcohol), M_{PVA}, and Brij 35, M_{B35}, are:

M_{PVA} = [1 0 0 2 2 2 2 2 2 2 2 0 0 1 0 0 0 0 0 0 2 0 0 0 0 2 0 0 0 2 0 0 0 0]

M_{B35} = [1 1 0 2 0 1 2 1 0 0 0 0 0 0 0 0 0 0 2 0 0 0 1 0 0 0 0 0 0 0 0 0 0 0 0]

In this 34-dimensional space, we can compare the miscibility profiles of clusters of polymers by analyzing the Euclidean distances between vectors. By this method, larger distances between vectors describe polymers that are likely to be components of phase-separated systems within this series, while shorter distances imply miscibility. We ordered the polymers in our ATPS matrix according to these vector distances (Figure S1). Using this approach to ordering, we identified several patterns based on similarities in miscibility in two-component mixtures: neutral polysaccharides (numbers *2* and *3*), acrylic acids (*4* and *5*), sulfated polysaccharides (*17* and *18*), sulfonic acids (*20* and *21*), and some non-fluorinated surfactants (numbers *12–16*) can be clustered by patterns of miscibility. Other species that might be expected to cluster, such as the cellulose derivatives (numbers *10, 24, 28*), have dissimilar patterns of miscibility.

Algorithm for the Prediction of Multiphase Systems. Albertsson observed, in many cases, that sets of mutually immiscible polymers that formed ATPS could be used to generate systems with more than two phases.[2] Applying this principle, we used our list of ATPS to generate a list of systems with more than two phases. For example, we predicted that a combination of solutes A, B and C would produce a three-phase system if two-component combinations of these solutes (i.e., [A B], [A C], and [B C]) phase separate. We developed an algorithm to generate a list of all possible systems of *N* phases given all possible systems of *N-1* phases. For example, we examine a set of component polymers A, B, C, and D. For each candidate multiphase system, there are *N* unique combinations of *N-1* components (i.e., for each

Figure S1. Results of two-component mixtures of aqueous solutions of polymers and surfactants: "miscible" (grey) corresponds to mixtures that produced no phase separation, "incompatible" (blue) corresponds to mixtures that generated a precipitate or a gel, and "immiscible" (red) corresponds to mixtures that resulted in phase separation between the two solutions. The polymers are ordered according to the distances between the vectors that describe their miscibility within this series, from top to bottom with decreasing distance (i.e., increasing similarity), and are illustrated by a miscibility similarity tree.

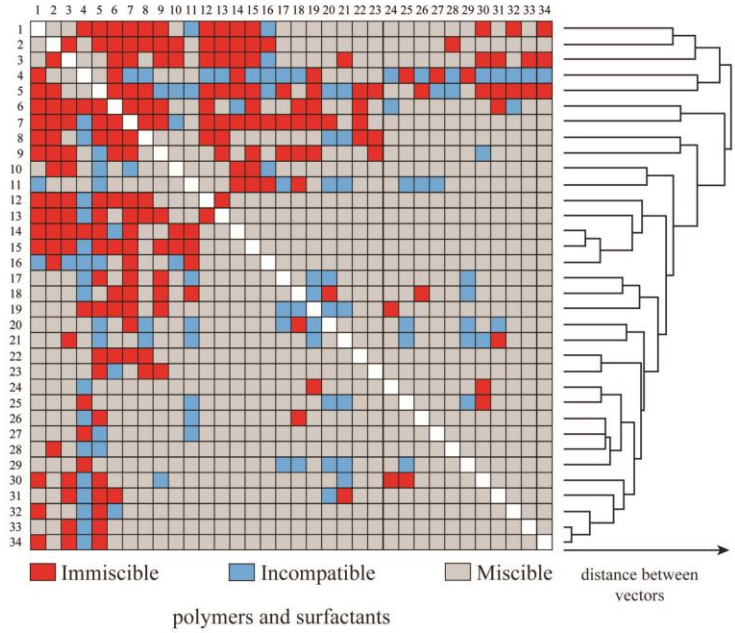

1 polyacrylamide
2 Ficoll
3 dextran
4 poly(acrylic acid)
5 poly(methacrylic acid)
6 poly(ethylene glycol)
7 poly(2-ethyl-2-oxazoline)
8 polyethyleneimine
9 poly(vinyl alcohol)
10 hydroxyethyl cellulose
11 polyallylamine
12 3-[(3-cholamidopropyl)dimethylammonio] -1-propanesulfonate
13 Pluronic F68
14 Triton X-100
15 Tween 20
16 Brij 35
17 chondroitin sulfate A
18 dextran sulfate
19 poly(diallyldimethyl ammonium chloride)
20 poly(styrenesulfonic acid)
21 poly(2-acrylamido-2-methyl-1-propanesulfonic acid)
22 1-*O*-octyl-β-D-glucopyranoside
23 carboxy-polyacrylamide
24 (hydroxypropyl)methyl cellulose
25 alginic acid
26 sodium cholate
27 sodium dodecyl sulfate
28 methyl cellulose
29 diethylaminoethyl-dextran
30 poly(propylene glycol)
31 polyvinylpyrrolidone
32 *N*,*N*-dimethyldodecylamine *N*-oxide
33 nonylphenol polyoxyethylene 20
34 Zonyl

four-phase system there should be *four* three-phase systems). [A B], [A C], and [B C] are the combinations for the candidate [A B C], and [A B], [A D], and [B D] are the combinations for the candidate [A B D]. If the *N* combinations formed a subset of the known systems of *N-1* phases, the candidate system was labeled as a predicted system until all candidates were evaluated and a complete list of predicted systems was formed. In this example, if combinations [A B], [A C], [B C], and [A D] were observed experimentally, but [B D] was not observed, then, [A B C] is a predicted system, and [A B D] is not a predicted system. We applied this algorithm to our list of systems of two phases to predict multiphase systems. We then iteratively applied the algorithm to the predicted multiphase systems until we could not generate a higher order system. In this way, we predicted systems composed of up to six phases based on our initial screen of two-component mixtures.

Aqueous Multiphase Systems of Polymers and Surfactants. We investigated each multiphase system predicted by our algorithm systematically. We were able to generate 112 of the 122 predicted three-phase MuPSs (Table S3), 73 of the 87 predicted four-phase MuPSs (Table S4), 31 of the 33 predicted five-phase MuPSs (Table S5), and all 5 of the predicted six-phase MuPSs (Table S6).

We added equal volumes (150 μL) of the solutions of each component (unless otherwise noted) to a microcentrifuge tube, vortexed the mixture for 30 seconds, and accelerated phase separation by centrifugation for 5 minutes at 16000*g* (VWR Galaxy 1816). For several predicted MuPSs, we observed that phase separation only occurred following the increase of the concentration of a polymer component used with respect to the other polymers (e.g., three-phase system #36 required twice the volume of the hydroxyethyl cellulose solution (300 μL), which increased the overall concentration of this solute in the MuPS mixture). Since phase separation

Table S3. List of prepared three-phase MuPSs. A reference accompanies the previously reported system that we confirmed. Components that were not added at equal volumes are noted by the factor of the increase (i.e., **[2X]** for twice the volume of each of the other components).

	Three-Phase MuPSs			REF
1	1-*O*-Octyl-β-D-glucopyranoside	poly(2-ethyl-2-oxazoline)	poly(ethylene glycol)	
2	1-*O*-Octyl-β-D-glucopyranoside	poly(2-ethyl-2-oxazoline)	poly(methacrylic acid)	
3	1-*O*-Octyl-β-D-glucopyranoside	poly(2-ethyl-2-oxazoline)	polyethyleneimine	
4	1-*O*-Octyl-β-D-glucopyranoside	poly(ethylene glycol)	poly(methacrylic acid)	
5	1-*O*-Octyl-β-D-glucopyranoside	poly(ethylene glycol)	polyethyleneimine	
6	1-*O*-Octyl-β-D-glucopyranoside	poly(methacrylic acid)	polyethyleneimine	
7	Brij 35	Ficoll	poly(2-ethyl-2-oxazoline)	
8	carboxy-polyacrylamide	poly(methacrylic acid)	polyethyleneimine	
9	CHAPS	dextran	Ficoll	
10	CHAPS	dextran	Pluronic F68	
11	CHAPS	dextran	poly(2-ethyl-2-oxazoline)	
12	CHAPS	dextran	poly(ethylene glycol)	
13	CHAPS	Ficoll	Pluronic F68	
14	CHAPS	Ficoll	poly(2-ethyl-2-oxazoline)	
15	CHAPS	Ficoll	poly(ethylene glycol)	
16	CHAPS	Ficoll	poly(methacrylic acid)	
17	CHAPS	Ficoll	polyethyleneimine	
18	CHAPS	Pluronic F68	poly(2-ethyl-2-oxazoline)	
19	CHAPS	Pluronic F68	poly(methacrylic acid)	
20	CHAPS	Pluronic F68	polyacrylamide	
21	CHAPS	Pluronic F68	polyethyleneimine	
22	CHAPS	poly(2-ethyl-2-oxazoline)	poly(ethylene glycol)	
23	CHAPS	poly(2-ethyl-2-oxazoline)	poly(methacrylic acid)	
24	CHAPS	poly(2-ethyl-2-oxazoline)	polyacrylamide	
25	CHAPS	poly(2-ethyl-2-oxazoline)	polyethyleneimine	
26	CHAPS	poly(ethylene glycol)	poly(methacrylic acid)	
27	CHAPS	poly(ethylene glycol)	polyacrylamide	
28	CHAPS	poly(ethylene glycol)	polyethyleneimine	
29	CHAPS	poly(methacrylic acid)	polyacrylamide	
30	CHAPS	poly(methacrylic acid)	polyethyleneimine	
31	CHAPS	polyacrylamide	polyethyleneimine	
32	chondroitin sulfate A	poly(2-ethyl-2-oxazoline)	poly(methacrylic acid)	
33	chondroitin sulfate A	poly(2-ethyl-2-oxazoline)	poly(vinyl alcohol)	
34	dextran sulfate	poly(2-ethyl-2-oxazoline)	poly(vinyl alcohol)	
35	dextran sulfate	poly(ethylene glycol)	poly(vinyl alcohol)	
36	dextran	Ficoll	hydroxyethyl cellulose **[2X]**	
37	dextran	Ficoll	Pluronic F68	
38	dextran	Ficoll	poly(2-ethyl-2-oxazoline)	
39	dextran	Ficoll	poly(ethylene glycol)	2
40	dextran	Ficoll	poly(vinyl alcohol)	
41	dextran	Ficoll	Triton X-100	
42	dextran	Ficoll	Tween 20	

Table S3, cont.

	Three-Phase MuPSs			REF
43	dextran	hydroxyethyl cellulose	Triton X-100	
44	dextran	hydroxyethyl cellulose	Tween 20	
45	dextran	Pluronic F68	poly(2-ethyl-2-oxazoline)	
46	dextran	Pluronic F68	poly(vinyl alcohol)	
47	dextran	poly(2-acrylamido-2-methyl-1-propanesulfonic acid) **[2X]**	polyvinylpyrrolidone	
48	dextran	poly(2-ethyl-2-oxazoline)	poly(ethylene glycol)	
49	dextran	poly(2-ethyl-2-oxazoline)	poly(vinyl alcohol)	
50	dextran	poly(2-ethyl-2-oxazoline)	Triton X-100	
51	dextran	poly(2-ethyl-2-oxazoline)	Tween 20	
52	dextran	poly(ethylene glycol)	poly(vinyl alcohol)	
53	dextran	poly(ethylene glycol)	polyvinylpyrrolidone	
54	dextran	poly(ethylene glycol)	Tween 20	
55	dextran	poly(vinyl alcohol)	Tween 20	
56	Ficoll	hydroxyethyl cellulose	Triton X-100	
57	Ficoll	hydroxyethyl cellulose	Tween 20	
58	Ficoll	Pluronic F68	poly(2-ethyl-2-oxazoline)	
59	Ficoll	Pluronic F68	poly(methacrylic acid)	
60	Ficoll	Pluronic F68	poly(vinyl alcohol)	
61	Ficoll	Pluronic F68	polyethyleneimine	
62	Ficoll	poly(2-ethyl-2-oxazoline)	poly(ethylene glycol)	
63	Ficoll	poly(2-ethyl-2-oxazoline)	poly(methacrylic acid)	
64	Ficoll	poly(2-ethyl-2-oxazoline)	poly(vinyl alcohol)	
65	Ficoll	poly(2-ethyl-2-oxazoline)	polyethyleneimine	
66	Ficoll	poly(2-ethyl-2-oxazoline)	Triton X-100	
67	Ficoll	poly(2-ethyl-2-oxazoline)	Tween 20	
68	Ficoll	poly(ethylene glycol)	poly(methacrylic acid)	
69	Ficoll	poly(ethylene glycol)	poly(vinyl alcohol)	
70	Ficoll	poly(ethylene glycol)	polyethyleneimine	
71	Ficoll	poly(ethylene glycol)	Tween 20	
72	Ficoll	poly(methacrylic acid)	polyethyleneimine	
73	Ficoll	poly(methacrylic acid)	Triton X-100	
74	Ficoll	poly(methacrylic acid)	Tween 20	
75	Ficoll	poly(vinyl alcohol)	Tween 20	
76	*N,N*-dimethyldodecylamine *N*-oxide	poly(methacrylic acid)	polyacrylamide	
77	Pluronic F68	poly(2-ethyl-2-oxazoline)	poly(methacrylic acid)	
78	Pluronic F68	poly(2-ethyl-2-oxazoline)	polyacrylamide	
79	Pluronic F68	poly(2-ethyl-2-oxazoline)	polyethyleneimine	
80	Pluronic F68	poly(methacrylic acid)	polyacrylamide	
81	Pluronic F68	poly(methacrylic acid)	polyethyleneimine	
82	Pluronic F68	poly(vinyl alcohol)	polyacrylamide	
83	Pluronic F68	polyacrylamide	polyethyleneimine	
84	poly(2-ethyl-2-oxazoline)	poly(ethylene glycol)	poly(methacrylic acid)	
85	poly(2-ethyl-2-oxazoline)	poly(ethylene glycol)	poly(vinyl alcohol)	
86	poly(2-ethyl-2-oxazoline)	poly(ethylene glycol)	polyacrylamide	
87	poly(2-ethyl-2-oxazoline)	poly(ethylene glycol)	polyethyleneimine **[2X]**	
88	poly(2-ethyl-2-oxazoline)	poly(ethylene glycol)	Tween 20	
89	poly(2-ethyl-2-oxazoline)	poly(methacrylic acid)	polyacrylamide	
90	poly(2-ethyl-2-oxazoline)	poly(methacrylic acid)	polyethyleneimine	

Table S3, cont.

	Three-Phase MuPSs			REF
91	poly(2-ethyl-2-oxazoline)	poly(methacrylic acid)	Tween 20	
92	poly(2-ethyl-2-oxazoline)	poly(vinyl alcohol)	Pluronic F68	
93	poly(2-ethyl-2-oxazoline)	poly(vinyl alcohol)	polyacrylamide	
94	poly(2-ethyl-2-oxazoline)	poly(vinyl alcohol)	Tween 20	
95	poly(2-ethyl-2-oxazoline)	polyacrylamide	polyethyleneimine	
96	poly(2-ethyl-2-oxazoline)	polyacrylamide	Triton X-100	
97	poly(2-ethyl-2-oxazoline)	polyacrylamide	Tween 20	
98	poly(acrylic acid) **[2X]**	poly(ethylene glycol)	polyacrylamide **[2X]**	
99	poly(ethylene glycol)	poly(methacrylic acid)	polyacrylamide	
100	poly(ethylene glycol)	poly(methacrylic acid)	polyethyleneimine	
101	poly(ethylene glycol)	poly(methacrylic acid)	polyvinylpyrrolidone	
102	poly(ethylene glycol)	poly(methacrylic acid)	Tween 20	
103	poly(ethylene glycol)	poly(vinyl alcohol)	polyacrylamide	
104	poly(ethylene glycol)	poly(vinyl alcohol)	Tween 20	
105	poly(ethylene glycol)	polyacrylamide	polyethyleneimine	
106	poly(ethylene glycol)	polyacrylamide	Tween 20	
107	poly(methacrylic acid)	poly(propylene glycol)	polyacrylamide	
108	poly(methacrylic acid)	polyacrylamide	polyethyleneimine	
109	poly(methacrylic acid)	polyacrylamide	Triton X-100	
110	poly(methacrylic acid)	polyacrylamide	Tween 20	
111	poly(methacrylic acid)	polyacrylamide	Zonyl	
112	poly(vinyl alcohol)	polyacrylamide	Tween 20	

Table S4. List of prepared four-phase MuPSs. Components that were not added at equal volumes are noted by the factor of the increase (i.e., **[2X]** for twice the volume of each of the other components).

	Four-Phase MuPSs			
1	1-*O*-Octyl-β-D-glucopyranoside	poly(2-ethyl-2-oxazoline)	poly(ethylene glycol)	polyethyleneimine
2	CHAPS	dextran	Ficoll	Pluronic F68
3	CHAPS **[2X]**	dextran	Ficoll	poly(ethylene glycol)
4	CHAPS	dextran	Pluronic F68	poly(2-ethyl-2-oxazoline)
5	CHAPS	dextran	poly(2-ethyl-2-oxazoline)	poly(ethylene glycol)
6	CHAPS	Ficoll	Pluronic F68	poly(methacrylic acid)
7	CHAPS	Ficoll	Pluronic F68	polyethyleneimine
8	CHAPS **[2X]**	Ficoll	poly(2-ethyl-2-oxazoline)	poly(ethylene glycol)
9	CHAPS	Ficoll	poly(2-ethyl-2-oxazoline)	poly(methacrylic acid)
10	CHAPS **[2X]**	Ficoll	poly(2-ethyl-2-oxazoline)	polyethyleneimine
11	CHAPS	Ficoll	poly(ethylene glycol)	poly(methacrylic acid)
12	CHAPS	Ficoll	poly(ethylene glycol)	polyethyleneimine
13	CHAPS	Ficoll	poly(methacrylic acid)	polyethyleneimine
14	CHAPS **[2X]**	Pluronic F68	poly(2-ethyl-2-oxazoline)	poly(methacrylic acid)
15	CHAPS	Pluronic F68	poly(2-ethyl-2-oxazoline)	polyethyleneimine
16	CHAPS	Pluronic F68	poly(methacrylic acid)	polyacrylamide
17	CHAPS	Pluronic F68	poly(methacrylic acid)	polyethyleneimine
18	CHAPS	Pluronic F68	polyacrylamide	polyethyleneimine
19	CHAPS **[2X]**	poly(2-ethyl-2-oxazoline)	poly(ethylene glycol)	poly(methacrylic acid)
20	CHAPS	poly(2-ethyl-2-oxazoline)	poly(ethylene glycol)	polyacrylamide
21	CHAPS	poly(2-ethyl-2-oxazoline)	poly(ethylene glycol)	polyethyleneimine
22	CHAPS	poly(2-ethyl-2-oxazoline)	poly(methacrylic acid)	polyacrylamide
23	CHAPS **[2X]**	poly(2-ethyl-2-oxazoline)	polyacrylamide	polyethyleneimine
24	CHAPS	poly(ethylene glycol)	poly(methacrylic acid)	polyacrylamide
25	CHAPS	poly(ethylene glycol)	poly(methacrylic acid)	polyethyleneimine
26	CHAPS	poly(ethylene glycol)	polyacrylamide	polyethyleneimine
27	CHAPS	poly(methacrylic acid)	polyacrylamide	polyethyleneimine
28	dextran	Ficoll	hydroxyethyl cellulose	Triton X-100
29	dextran	Ficoll	hydroxyethyl cellulose	Tween 20
30	dextran	Ficoll	Pluronic F68	poly(2-ethyl-2-oxazoline)
31	dextran	Ficoll	Pluronic F68	poly(vinyl alcohol)
32	dextran	Ficoll	poly(2-ethyl-2-oxazoline)	poly(ethylene glycol)
33	dextran	Ficoll	poly(2-ethyl-2-oxazoline)	poly(vinyl alcohol)
34	dextran	Ficoll	poly(2-ethyl-2-oxazoline)	Tween 20
35	dextran	Ficoll	poly(ethylene glycol)	poly(vinyl alcohol)
36	dextran	Ficoll	poly(ethylene glycol)	Tween 20
37	dextran	Ficoll	poly(vinyl alcohol)	Tween 20
38	dextran	Pluronic F68	poly(2-ethyl-2-oxazoline)	poly(vinyl alcohol)
39	dextran	poly(2-ethyl-2-oxazoline)	poly(ethylene glycol)	poly(vinyl alcohol)
40	dextran	poly(2-ethyl-2-oxazoline)	poly(ethylene glycol)	Tween 20
41	dextran	poly(ethylene glycol)	poly(vinyl alcohol)	Tween 20
42	dextran sulfate	poly(2-ethyl-2-oxazoline)	poly(ethylene glycol)	poly(vinyl alcohol)
43	Ficoll	Pluronic F68	poly(2-ethyl-2-oxazoline)	poly(methacrylic acid)
44	Ficoll	Pluronic F68	poly(2-ethyl-2-oxazoline)	poly(vinyl alcohol)
45	Ficoll	Pluronic F68	poly(2-ethyl-2-oxazoline)	polyethyleneimine
46	Ficoll	Pluronic F68	poly(methacrylic acid)	polyethyleneimine
47	Ficoll	poly(2-ethyl-2-oxazoline)	poly(ethylene glycol)	poly(methacrylic acid)

Table S4, cont.

	Four-Phase MuPSs			
48	Ficoll	poly(2-ethyl-2-oxazoline)	poly(ethylene glycol)	poly(vinyl alcohol)
49	Ficoll	poly(2-ethyl-2-oxazoline)	poly(ethylene glycol)	Tween 20
50	Ficoll	poly(2-ethyl-2-oxazoline)	poly(methacrylic acid)	polyethyleneimine
51	Ficoll	poly(2-ethyl-2-oxazoline)	poly(methacrylic acid)	Tween 20
52	Ficoll	poly(2-ethyl-2-oxazoline)	poly(vinyl alcohol)	Tween 20
53	Ficoll	poly(ethylene glycol)	poly(methacrylic acid)	polyethyleneimine
54	Ficoll	poly(ethylene glycol)	poly(methacrylic acid)	Tween 20
55	Ficoll	poly(ethylene glycol)	poly(vinyl alcohol)	Tween 20
56	Pluronic F68	poly(2-ethyl-2-oxazoline)	poly(methacrylic acid)	polyacrylamide
57	Pluronic F68 **[2X]**	poly(2-ethyl-2-oxazoline)	poly(methacrylic acid)	polyethyleneimine
58	Pluronic F68	poly(2-ethyl-2-oxazoline)	poly(vinyl alcohol)	polyacrylamide
59	Pluronic F68	poly(2-ethyl-2-oxazoline)	polyacrylamide	polyethyleneimine
60	Pluronic F68	poly(methacrylic acid)	polyacrylamide	polyethyleneimine
61	poly(2-ethyl-2-oxazoline)	poly(ethylene glycol)	poly(methacrylic acid)	polyacrylamide
62	poly(2-ethyl-2-oxazoline)	poly(ethylene glycol)	poly(methacrylic acid)	polyethyleneimine
63	poly(2-ethyl-2-oxazoline)	poly(ethylene glycol)	poly(methacrylic acid)	Tween 20
64	poly(2-ethyl-2-oxazoline)	poly(ethylene glycol)	poly(vinyl alcohol)	polyacrylamide
65	poly(2-ethyl-2-oxazoline)	poly(ethylene glycol)	polyacrylamide	polyethyleneimine
66	poly(2-ethyl-2-oxazoline)	poly(ethylene glycol)	polyacrylamide	Tween 20
67	poly(2-ethyl-2-oxazoline)	poly(methacrylic acid)	polyacrylamide	polyethyleneimine
68	poly(2-ethyl-2-oxazoline)	poly(methacrylic acid)	polyacrylamide	Triton X-100
69	poly(2-ethyl-2-oxazoline)	poly(methacrylic acid)	polyacrylamide	Tween 20
70	poly(2-ethyl-2-oxazoline)	poly(vinyl alcohol)	polyacrylamide	Tween 20
71	poly(ethylene glycol)	poly(methacrylic acid)	polyacrylamide	polyethyleneimine
72	poly(ethylene glycol)	poly(methacrylic acid)	polyacrylamide	Tween 20
73	poly(ethylene glycol)	poly(vinyl alcohol)	polyacrylamide	Tween 20

Table S5. List of prepared five-phase MuPSs. Components that were not added at equal volumes are noted by the factor of the increase (i.e., **[2X]** for twice the volume of each of the other components). A sixth phase formed in System 14 (noted with an *) after sitting for over two hours at ambient conditions.

			Five-Phase MuPSs		
1	CHAPS	dextran	Ficoll	Pluronic F68	poly(2-ethyl-2-oxazoline)
2	CHAPS	dextran	Ficoll	poly(2-ethyl-2-oxazoline)	poly(ethylene glycol)
3	CHAPS	Ficoll	Pluronic F68	poly(2-ethyl-2-oxazoline)	poly(methacrylic acid)
4	CHAPS	Ficoll	Pluronic F68	poly(2-ethyl-2-oxazoline)	polyethyleneimine
5	CHAPS **[2X]**	Ficoll	Pluronic F68	poly(methacrylic acid)	polyethyleneimine
6	CHAPS	Ficoll	poly(2-ethyl-2-oxazoline)	poly(ethylene glycol)	poly(methacrylic acid)
7	CHAPS	Ficoll	poly(2-ethyl-2-oxazoline)	poly(ethylene glycol)	polyethyleneimine
8	CHAPS	Ficoll	poly(2-ethyl-2-oxazoline)	poly(methacrylic acid)	polyethyleneimine
9	CHAPS **[2X]**	Ficoll	poly(ethylene glycol)	poly(methacrylic acid)	polyethyleneimine
10	CHAPS	Pluronic F68	poly(2-ethyl-2-oxazoline)	poly(methacrylic acid)	polyacrylamide
11	CHAPS	Pluronic F68	poly(2-ethyl-2-oxazoline)	poly(methacrylic acid)	polyethyleneimine
12	CHAPS	Pluronic F68	poly(2-ethyl-2-oxazoline)	polyacrylamide	polyethyleneimine
13	CHAPS	Pluronic F68	poly(methacrylic acid)	polyacrylamide	polyethyleneimine
14*	CHAPS	poly(2-ethyl-2-oxazoline)	poly(ethylene glycol)	polyacrylamide	polyethyleneimine
15	CHAPS	poly(2-ethyl-2-oxazoline)	poly(ethylene glycol)	poly(methacrylic acid)	polyacrylamide
16	CHAPS	poly(2-ethyl-2-oxazoline)	poly(ethylene glycol)	poly(methacrylic acid)	polyethyleneimine
17	CHAPS	poly(2-ethyl-2-oxazoline)	poly(methacrylic acid)	polyacrylamide	polyethyleneimine
18	CHAPS	poly(ethylene glycol)	poly(methacrylic acid)	polyacrylamide	polyethyleneimine
19	dextran	Ficoll	Pluronic F68	poly(2-ethyl-2-oxazoline)	poly(vinyl alcohol)
20	dextran	Ficoll	poly(2-ethyl-2-oxazoline)	poly(ethylene glycol)	poly(vinyl alcohol)
21	dextran	Ficoll	poly(2-ethyl-2-oxazoline)	poly(ethylene glycol)	Tween 20
22	dextran	Ficoll	poly(2-ethyl-2-oxazoline)	poly(vinyl alcohol)	Tween 20
23	dextran	Ficoll	poly(ethylene glycol)	poly(vinyl alcohol)	Tween 20
24	dextran	poly(2-ethyl-2-oxazoline)	poly(ethylene glycol)	poly(vinyl alcohol)	Tween 20
25	Ficoll	Pluronic F68	poly(2-ethyl-2-oxazoline)	poly(methacrylic acid)	polyethyleneimine
26	Ficoll	poly(2-ethyl-2-oxazoline)	poly(ethylene glycol)	poly(methacrylic acid)	polyethyleneimine
27	Ficoll	poly(2-ethyl-2-oxazoline)	poly(ethylene glycol)	poly(methacrylic acid)	Tween 20
28	Ficoll	poly(2-ethyl-2-oxazoline)	poly(ethylene glycol)	poly(vinyl alcohol)	Tween 20
29	poly(2-ethyl-2-oxazoline)	poly(ethylene glycol)	poly(methacrylic acid)	polyacrylamide	polyethyleneimine
30	poly(2-ethyl-2-oxazoline)	poly(ethylene glycol)	poly(methacrylic acid)	polyacrylamide	Tween 20
31	poly(2-ethyl-2-oxazoline)	poly(ethylene glycol)	poly(vinyl alcohol)	polyacrylamide	Tween 20

Table S6. List of prepared six-phase MuPSs. Components that were not added at equal volumes are noted by the factor of the increase (i.e., **[2X]** for twice the volume of each of the other components).

Six-Phase MuPSs				
1	2	3	4	5
CHAPS **[2X]**	CHAPS **[2X]**	CHAPS	CHAPS	dextran
Ficoll	Ficoll	Pluronic F68	poly(2-ethyl-2-oxazoline)	Ficoll
Pluronic F68	poly(2-ethyl-2-oxazoline)	poly(2-ethyl-2-oxazoline)	poly(ethylene glycol)	poly(2-ethyl-2-oxazoline)
poly(2-ethyl-2-oxazoline)	poly(ethylene glycol)	poly(methacrylic acid)	poly(methacrylic acid)	poly(ethylene glycol)
poly(methacrylic acid)	poly(methacrylic acid)	polyacrylamide	polyacrylamide	poly(vinyl alcohol)
polyethyleneimine	polyethyleneimine	polyethyleneimine	polyethyleneimine	Tween 20

is a function of concentration, this is not an unexpected result. Interestingly, there were several ATPSs that did not combine to produce MuPSs; for example, a carboxy-polyacrylamide–poly(vinyl alcohol)–poly(methacrylic acid) mixture results in the precipitation of some polymers even though each of the three precursor two-component mixtures were immiscible. If the concentration of a component was less than the concentration required to induce phase separation with other components in the system, the result would be a MuPS with fewer phases than anticipated. This result is likely dependent on individual solutes and combinations of solutes. Failed attempts at producing MuPSs typically resulted in a system comprising one fewer layer than anticipated; these systems are listed in Table S7. In one case (Table S5, #14), a mixture of five components—originally five phases after centrifugation—formed six phases with well-defined interfaces after sitting at ambient conditions for over two hours. One component could be the primary constituent of two different phases if micelles are formed and the phases differ in the concentrations of micelles.[12]

Characterization of Layers (i.e., phases) of Multiphase Systems: Density and Composition. We used oscillating U-tube densitometry to measure the final densities of each layer of a MuPS after phase separation. We performed experiments in plastic 15-mL conical tubes because we could pierce the side of the tube with a needle at the specific site of a desired layer in order to remove a sample by syringe. Since the densitometer requires roughly 750 μL of sample to completely fill the U-tube, we used 1–5 mL of stock solutions of solutes to ensure that we could isolate an adequate volume of pure solution after phase separation.

The phase diagrams of aqueous two-phase systems are characterized by a binodal curve and tie-lines.[1] The binodal curve delineates the concentrations where it is either thermodynamically favorable for the two-component mixture to form a homogeneous solution or

Table S7. List of three-phase, four-phase, and five-phase MuPSs that we could not prepare experimentally, but were predicted by our algorithm.

	Multiphase Systems				
1	dextran sulfate	poly(2-ethyl-2-oxazoline)	poly(ethylene glycol)		
2	dextran sulfate	poly(2-ethyl-2-oxazoline)	poly(styrenesulfonic acid)		
3	poly(2-ethyl-2-oxazoline)	poly(diallyldimethyl ammonium chloride	poly(ethylene glycol)		
4	poly(2-ethyl-2-oxazoline)	poly(diallyldimethyl ammonium chloride	poly(methacrylic acid)		
5	poly(2-ethyl-2-oxazoline)	poly(diallyldimethyl ammonium chloride	poly(vinyl alcohol)		
6	poly(2-ethyl-2-oxazoline)	poly(methacrylic acid)	Triton X-100		
7	poly(acrylic acid)	poly(diallyldimethyl ammonium chloride	poly(ethylene glycol)		
8	poly(acrylic acid)	polyacrylamide	Triton X-100		
9	poly(diallyldimethyl ammonium chloride	poly(ethylene glycol)	poly(methacrylic acid)		
10	poly(diallyldimethyl ammonium chloride	poly(ethylene glycol)	poly(vinyl alcohol)		
11	1-*O*-Octyl-β-D-glucopyranoside	poly(2-ethyl-2-oxazoline)	poly(ethylene glycol)	poly(methacrylic acid)	
12	1-*O*-Octyl-β-D-glucopyranoside	poly(2-ethyl-2-oxazoline)	poly(methacrylic acid)	polyethyleneimine	
13	1-*O*-Octyl-β-D-glucopyranoside	poly(ethylene glycol)	poly(methacrylic acid)	polyethyleneimine	
14	CHAPS	dextran	Ficoll	poly(2-ethyl-2-oxazoline)	
15	CHAPS	Ficoll	Pluronic F68	poly(2-ethyl-2-oxazoline)	
16	CHAPS	Pluronic F68	poly(2-ethyl-2-oxazoline)	polyacrylamide	
17	CHAPS	poly(2-ethyl-2-oxazoline)	poly(methacrylic acid)	polyethyleneimine	
18	dextran	Ficoll	poly(2-ethyl-2-oxazoline)	Triton X-100	
19	dextran	poly(2-ethyl-2-oxazoline)	poly(vinyl alcohol)	Tween 20	
20	Ficoll	poly(2-ethyl-2-oxazoline)	poly(ethylene glycol)	polyethyleneimine	
21	Ficoll	poly(2-ethyl-2-oxazoline)	poly(methacrylic acid)	Triton X-100	
22	poly(2-ethyl-2-oxazoline)	poly(ethylene glycol)	poly(vinyl alcohol)	Tween 20	
23	poly(diallyldimethyl ammonium chloride	poly(2-ethyl-2-oxazoline)	poly(ethylene glycol)	poly(methacrylic acid)	
24	poly(diallyldimethyl ammonium chloride	poly(2-ethyl-2-oxazoline)	poly(ethylene glycol)	poly(vinyl alcohol)	
25	1-*O*-Octyl-β-D-glucopyranoside	poly(2-ethyl-2-oxazoline)	poly(ethylene glycol)	poly(methacrylic acid)	polyethyleneimine
26	Pluronic F68	poly(2-ethyl-2-oxazoline)	poly(methacrylic acid)	polyacrylamide	polyethyleneimine

to phase separate. The shape of the binodal is defined by a set of parallel tie-lines, which connect nodes along the binodal. Different points along a tie-line correspond to systems that differ in total composition and volume ratio, but equivalent final concentrations of solutes.

It is apparent from these phase diagrams that, while conditions exist for the formation of separate phases, each layer of an ATPS is a heterogeneous mixture of both components (i.e., a polyacrylamide–polyethyleneimine mixture produces *polyacrylamide-rich* and *polyethyleneimine-rich* phases). Mixtures composed of three or more mutually immiscible solutes should behave similarly, where each layer of a MuPS could contain multiple solutes. Higher dimensional phase diagrams characterizing the behavior of mixtures that lead to a MuPS from several linked ATPS would explain why the initial conditions used in our screen (e.g., concentration and volume) resulted in either (i) phase separation or (ii) the formation of fewer phases than anticipated. We chose to survey the final layer compositions of MuPSs by density and by ^{1}H-NMR spectroscopy in order to support this premise. For the ^{1}H-NMR experiments, 200 μL samples of each phase and of each stock solution were diluted in D_2O containing a known concentration (70 mg/mL) of the NMR internal standard benzene-1,2-disulfonic acid dipotassium salt. Comparisons of the peak integrations (relative to the internal standard) in the ^{1}H-NMR spectra of the stock solutions and the samples from each phase provided estimates of the concentration of each polymer in each phase (Table S8).

Density-Based Separation Using MuPSs. We prepared a five-phase MuPS from a mixture of poly(vinyl alcohol), poly(2-ethyl-2-oxazoline), poly(ethylene glycol), Ficoll, and dextran (Table S9). While we utilized poly(2-ethyl-2-oxazoline) with an average molecular weight of 200,000 Da for screening phase separation, we observed that a shorter chain polymer

Table S8. Measured densities and compositions of each phase of a five-phase MuPS generated from a mixture containing 6.4% (w/v) poly(ethylene glycol) (PEG), 5.6% (w/v) poly(2-ethyl-2-oxazoline) (PEOZ), 9.0% (w/v) poly(vinyl alcohol) (PVA), 4.8% (w/v) dextran, and 6.4% (w/v) Ficoll.

Phase	Density (g/cm^3)	Final Solute Concentration (w/v)				
		PEG	PEOZ	PVA	Ficoll	dextran
1 (top)	1.049	16	1.4	0.4	< 1	< 1
2	1.057	0.6	19	3.2	< 1	< 1
3	1.075	0.4	9.2	10	< 1	< 1
4	1.127	< 1	< 1	< 1	39	< 1
5 (bottom)	1.140	< 1	< 1	< 1	< 1	36

Table S9. List of polymers and conditions used to create a five-phase MuPS for separating density standard beads based on density.

Polymer	avg. MW (Da)	stock % (w/v)	volume added (mL)	total % (w/v)
poly(vinyl alcohol)	3,000	25	4.5	9.0
poly(2-ethyl-2-oxazoline)	50,000	35	2.0	5.6
poly(ethylene glycol)	20,000	40	2.0	6.4
Ficoll	400,000	40	2.0	6.4
dextran	500,000	30	2.0	4.8

with an average molecular weight of 50,000 Da had an identical ATPS miscibility profile to the longer polymer, but its mixtures were characterized by different binodal curves (data not shown). Complete phase separation occurred after centrifugation in a swinging bucket rotor at 3200*g* (Sorvall RT6000B) for 90 minutes. We removed aliquots of each layer and measured their densities by oscillating U-tube densitometry. From least dense to most dense (i.e., top to bottom), the layer densities were 1.049 g/cm^3, 1.057 g/cm^3, 1.075 g/cm^3, 1.127 g/cm^3, and 1.140 g/cm^3. As an alternative to the method we describe in the manuscript, we introduced six density standard beads (American Density Materials) to an identical pre-formed MuPS and sedimented them through the gradient in density in a swinging bucket centrifuge at 1000*g* for 15 minutes. Each of the six beads (densities of 1.0450 g/cm^3, 1.0500 g/cm^3, 1.0650 g/cm^3, 1.1200 g/cm^3, 1.1300 g/cm^3, and 1.1500 g/cm^3 ± 0.0002 g/cm^3) sedimented to a position within the MuPS based on their densities: one at either each of the four interfaces between the five phases, one at the interface between air and the top phase, and one at the interface between the bottom phase and the container.

Position of the Bead at the Interface. The position of the center of mass of the bead at an interface gives additional information about the density of the bead; this position is a function of the difference in buoyant density between the bead and each of the adjacent phases, the magnitude of the interfacial surface tension, and the contact angle of the phases with the surface of the bead.[13] Ignoring slight differences in wetting, if the buoyant density of the bead is equal to the average of the densities of the two phases that meet at the interface, the center of mass of the bead will lie at the interface. If, however, the density of the bead is different than the average, the center of mass will lie above or below the interface. For example, in the five-phase system shown in Figure 2, the center of mass of a bead with a density of 1.050 g/cm^3 is above the

interface between the PEG-rich phase (ρ = 1.049 g/cm^3) and the PEOZ-rich phase (ρ = 1.057 g/cm^3).

Limits to Separations Based on Density. As noted in the manuscript, the interfacial surface energy between the phases of ATPSs is very low, and we expect this characteristic to be true of MuPSs with more than two phases. Interfacial surface energy, however, does provide an inherent limit on the ability of such systems to separate objects by density. A simple dimensional analsysis reveals the relationship between interfacial surface energy, an objects' size, density, and the relative centrifugal force under which a separation is carried out. To a first approximation, the gravitational energy required to remove an object of characteristic size R from an interface will be: $E_g = \Delta\rho R^4 \cdot RCF$, where $\Delta\rho$ is the difference in density between the object and the phase below the interface and RCF is the relative centrifugal force in units of g's. The interfacial surface energy will be: $E_s = \gamma R^2$, where γ is the interfacial surface energy between the phases. When these two energies are of the same order of magnitude, density alone will not determine whether an object remains at an interface. Using these equations we can estimate the minimum size of a particle that could be separated with density (Equation S1).

$$R_{\min} = \sqrt{\frac{\gamma}{RCF \cdot \Delta\rho}} \qquad \text{(S1)}$$

For a desired resolution in density, $\Delta\rho$, we can increase the centrifuge speed to overcome interfacial surface energy effects and separate small objects. For example, even with γ as high as 5 μJ/m^2, micron-sized objects can be separated to a density resolution of 0.05 g/cm^3 if an RCF greater than 10000g is appplied.

Separation of Micron-Sized Particles Based on Density Using MuPSs. We demonstrated this effect—increasing RCF to account for interfacial surface energy effects on

small objects—by separating particles with equal sizes (d = 2.8 μm) but a difference in density: polystyrene microspheres (ρ = 1.05 g/cm^3) and Dynabeads (ρ = 1.14 g/cm^3). We added a suspension containing ~250000 particles (polystyrene, Dynabeads, or a mixture of particle types) in water into a plastic capillary that contained a poly(ethylene glycol)–Ficoll ATPS prepared from a 1:1 mixture of 15% (w/v) poly(ethylene glycol) and 20% (w/v) Ficoll (ρ_{top} = 1.025 g/cm^3, ρ_{bottom} = 1.074 g/cm^3). After two minutes of centrifugation at 13700g in a microhematocrit centrifuge (CritSpinStatSpin; Iris Sample Processing, Inc.), (i) polystyrene particles sedimented through the top phase and concentrated at the interface between phases, (ii) the denser Dynabeads passed through both phases and concentrated at the interface between the bottom phase and the container, and (iii) a mixture of both types of beads sedimented by density independently, resulting in homogenous populations at separate interfaces (Figure S2).

Tuning the Densities of Phases in MuPSs Using D_2O. We prepared stock solutions of 20% (w/v) poly(2-ethyl-2-oxazoline) and 30% (w/v) poly(ethylene glycol) in aqueous solutions containing 100% H_2O to 70% D_2O/30% H_2O. We generated a series of two-phase MuPSs from mixtures of these solutions. After phase separation by centrifugation (five minutes at 2000g), we used an oscillating U-tube densitometer (Anton Paar DMA 35) to measure the densities of isolated samples of each phase. In addition, from the two-phase system containing only H_2O, we diluted 200 μL samples of each phase in a solution of D_2O (99.9% D) containing a known concentration (70 mg/mL) of the NMR internal standard benzene-1,2-disulfonic acid dipotassium salt. We measured the concentration of H_2O in each phase using ^{1}H-NMR. The top phase consisted of 69% H_2O (v/v), while the bottom phase contained only 57% H_2O (v/v). The ratio of these percentages (69/57 = 1.21) is nearly identical, within experimental error, to the

Figure S2. Density-based separation of particles using a MuPS. The density step produced by a poly(ethylene glycol)–Ficoll MuPS selectively filters particles of equivalent size (d = 2.8 μm) based on their differences in density. We added ~250000 particles to a microhematocrit tube containing the MuPS. After centrifugation, the density step produced by the MuPS separated solutions containing: (A) superparamagnetic microspheres only (Dynabeads (Dy); ρ = 1.14 g/cm^3), (B) polystyrene only (PS; ρ = 1.05 g/cm^3), and (C) a mixture of Dynabeads and polystyrene (Dy/PS).

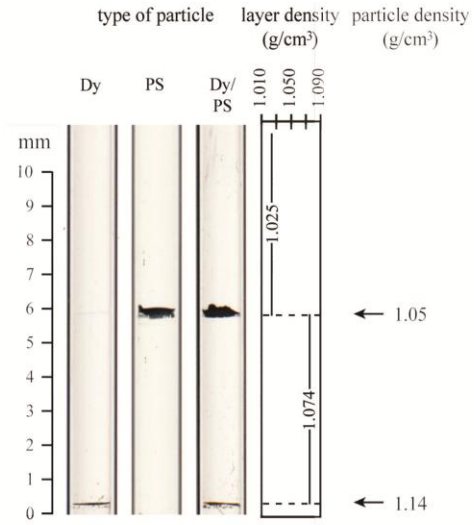

ratio of slopes obtained in the graph of density versus the % D_2O added to the system ($8.85\times10^{-4}/(7.43\times10^{-4}) = 1.19$). These data are consistent with the hypothesis that adding D_2O to a MuPS will increase the density of each phase at a rate that is dependent on the amount of water in that phase.

Tuning the Densities of Phases in MuPSs Using Salts. We used two alkali bromide salts, LiBr and CsBr, as additives to MuPSs. Both alkali bromide salts should have similar characteristics when added to MuPSs (e.g., optical transparency and solubility), but their densities should be different at equal concentrations (e.g., densities of LiBr and CsBr solutions at 1 M are 1.055 g/cm^3 and 1.161 g/cm^3, respectively). We prepared a series of three-phase MuPSs from mixtures equal volumes of 35% (w/v) poly(ethylene glycol), 25% (w/v) polyethyleneimine, and 32% (w/v) poly(methacrylic acid) that also included LiBr or CsBr at a concentration from 0.0 M to 2.0 M. After phase separation, we removed samples from each phase and measured their densities using densitometry. Similar to the trends in Figure 3 with CsBr, the densities of the phases increased linearly with the addition of LiBr (Figure S3).

In addition, we diluted samples (of known volume) of each phase in a solution of D_2O (99.9% D) containing a known concentration (70 mg/mL) of the NMR internal standard benzene-1,2-disulfonic acid dipotassium salt. We measured the concentration of H_2O and of each polymer in each phase using ^{1}H-NMR, and calculated the percentage of salt in each phase by subtraction. This procedure results in relatively large errors in the calculated concentration of CsBr, but still provides data that demonstrate the expected trends. Figure S4 demonstrates that the relative amount of CsBr in each phase (i.e., the partitioning of CsBr between the phases) is constant over the measured concentrations of CsBr.

Figure S3. A three-phase MuPS was prepared from mixtures of PEG, PEI, and PMAA in aqueous solutions that included LiBr over a range of concentrations of salts. The densities of the phases increased linearly with the concentration of the added LiBr.

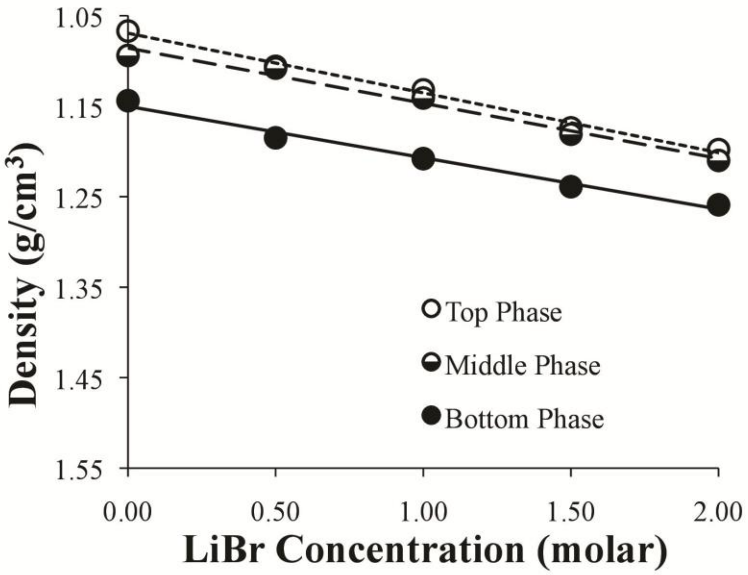

Figure S4. Partitioning of CsBr between each phase of a three-phase system consisting of mixtures of equal volumes of 35% (w/v) poly(ethylene glycol), 25% (w/v) polyethyleneimine, and 32% (w/v) poly(methacrylic acid). The amount of CsBr in each layer of this three phase system is not the same; the preferential partitioning of CsBr to the bottom phase is, however, consistent.

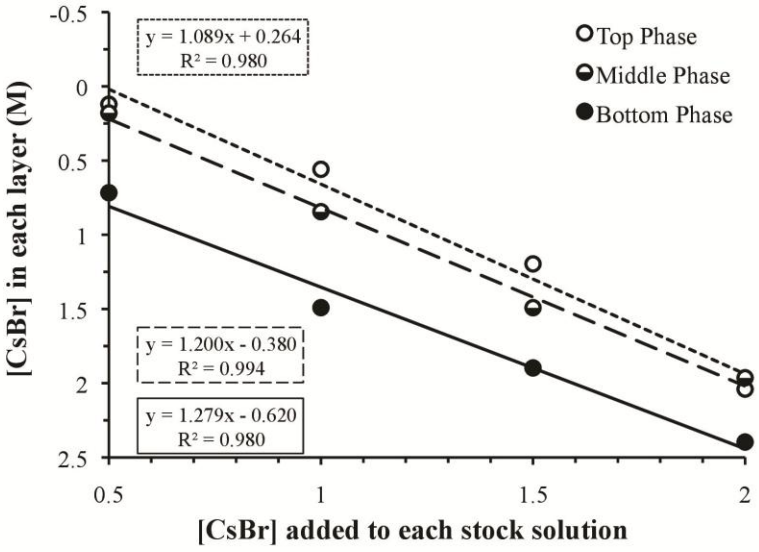

Tuning the Densities of Phases in MuPSs Using Methanol. We evaluated the use of methanol as a co-solvent to decrease the density of phases. We prepared a four phase MuPS consisting of 12% (v/v) Tween-20, 6% (w/v) poly(ethylene glycol), 9% (w/v) poly(2-ethyl-2-oxazoline), and 5% (w/v) polyacrylamide with a range of methanol concentrations (0–20% (v/v)). All phases showed a decrease in density with the addition of methanol. The top three phases fit to lines ($R^2 > 0.99$), but the polyacrylamide-rich bottom phase did not ($R^2 < 0.80$); the density of that phase saturated near a methanol concentration of 10% (v/v) (Figure S5). To avoid this non-linearity, we did not use methanol or similar organic solvents (e.g., ethanol) to tune the densities of MuPSs in this study.

Use of Magnetic Levitation in Measurements of Density. In order to design a MuPS that can separate materials in a mixture based on density, the densities of each material must be known. Unfortunately, the density of a material provided by a manufacturer may not always be accurate. We used magnetic levitation (MagLev) to measure the densities of pellets of four different formulations of Nylon. The MagLev technique has been described in detail elsewhere.[14,15] Briefly, MagLev involves placing diamagnetic samples into a container filled with a paramagnetic fluid, which is then placed into an apparatus comprising two permanent magnets with like poles opposed that are held apart at a fixed distance. The vertical position of the sample within the paramagnetic medium (i.e., "the levitation height") correlates with its density. The resolution of a density measurement by MagLev—and the range of densities of objects that can be levitated within a single paramagnetic medium—is related to the magnetic susceptibility of the paramagnetic medium, and, therefore, the concentration of the paramagnetic

Figure S5. Non-linear effects of the addition of methanol on the density of phases of MuPSs. A four-phase MuPS consisting of 12% (v/v) Tween-20, 6% (w/v) poly(ethylene glycol), 9% (w/v) poly(2-ethyl-2-oxazoline), and 5% (w/v) polyacrylamide was prepared in water with a range of methanol concentrations (0 – 20% (v/v)). Although the addition of methanol reduced the density of the phases of MuPS, the effect on the density of the polyacrylamide-rich bottom phase were non-linear.

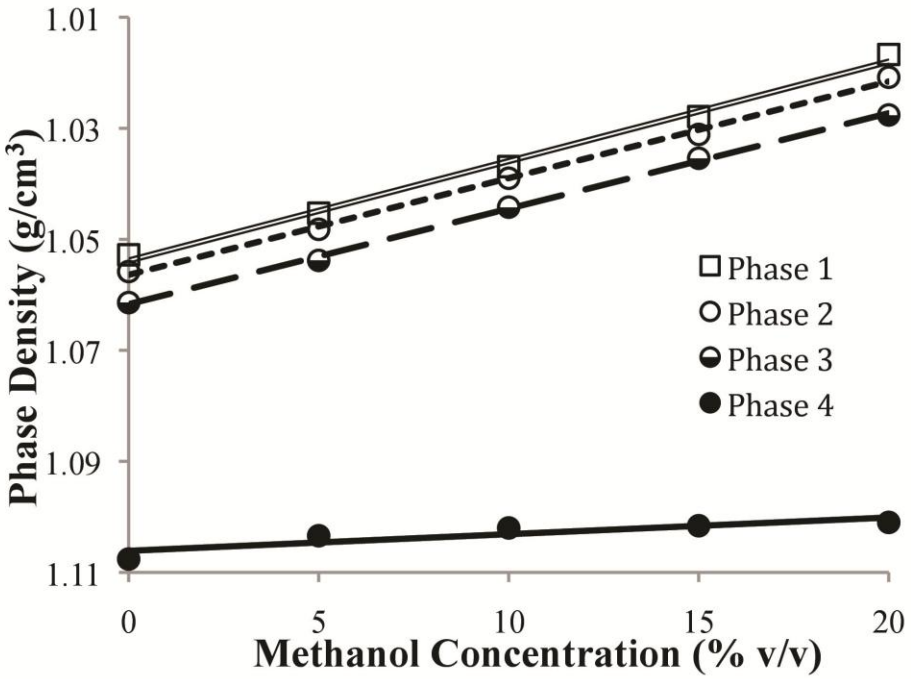

salt dissolved into the medium. To measure the densities of Nylon pellets, we used aqueous solutions of $MnCl_2$ at 0.5 M and 1.0 M. The range of densities available for analysis at 0.5 M $MnCl_2$ is 1.016 – 1.087 g/cm^3, and the range of densities available for analysis at 1.0 M $MnCl_2$ is 1.031 – 1.173 g/cm^3. The accuracies of these measurements are ± 0.001 g/cm^3 and ± 0.002 g/cm^3, respectively. We used density standard beads with densities of 1.0500 g/cm^3 and 1.1000 g/cm^3 to calibrate these two levitation media. Table S10 compares the densities measured by MagLev to those provided by the manufacturer in the product information sheet.

Separation of Nylon Beads. To separate the four different formulations of nylon by density, we used a three-phase MuPS. We mixed stock solutions of 40% (w/v) poly(2-ethyl-2-oxazoline), 30% (v/v) Brij 35, and 30% (w/v) Ficoll at equal volumes to produce a three phase system. The poly(2-ethyl-2-oxazoline) and the Brij 35 were both in 100% H_2O. We made the Ficoll in solutions of varied isotopic purity, from 100% H_2O to 30% H_2O and 70% D_2O—contributing a total concentration of up to 25.5% D_2O (v/v) when mixed in equal volumes with the other solutions. The final D_2O content was measured by ^{1}H-NMR spectroscopy. The densities of the phases increased linearly as more D_2O was added (Figure S6A). At 0% H_2O, the phase densities were not in the right range to separate four formulations of Nylon (i.e., Nylon 6, Nylon 12, Nylon 6/12, and Nylon 6/66) (Figure S6B). By tuning the density with D_2O, we were able to identify a system capable of separating all four formulations of Nylon: a the three-phase MuPS that used the stock solution of Ficoll mixed in 30% H_2O and 70% D_2O (for a final estimated concentration of D_2O of 25.5%) (Figure S5C).

Table S10. Densities of Nylon pellets. We compare the values as provided by the manufacturer (Sigma-Aldrich) to those we measure by magnetic levitation (MagLev).

	Densities (g/cm^3)	
Pellet Type	**Manufacturer**	**MagLev**
Nylon 12	1.01	1.032
Nylon 6/12	1.3	1.058
Nylon 6/66	1.3	1.120
Nylon 6	1.084	1.147

Figure S6. Tuning density of a three-phase MuPS with D_2O to separate different formulations of nylon. The MuPS was formed with a final concentration of 13.3% (w/v) poly(2-ethyl-2-oxazoline), 10% (v/v) Brij 35, and 10% (w/v) Ficoll in solutions with varying isotopic purity of water. The densities of the phases increased linearly as the concentration of D_2O increased (A). The horizontal lines depict the densities of Nylon 12, Nylon 6/12, Nylon 6/66, and Nylon 6. At 0% D_2O, nylon 6 and nylon 6/66 both reside at the same interface at the bottom of the system (B). By increasing the D_2O concentration, we reached a regime where the four different formulations of nylon collect at separate interfaces (C).

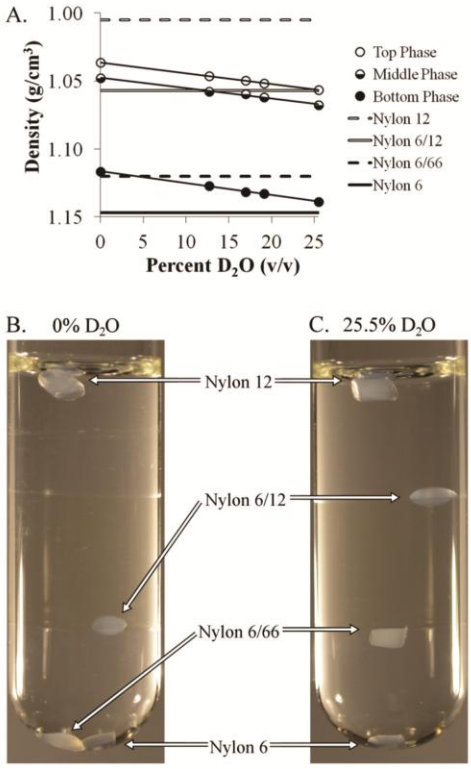
A.
1.00
1.05
1.10
1.15
Density (g/cm³)
0
5
10
15
20
25
Percent D2O (v/v)
Top Phase
Middle Phase
Bottom Phase
Nylon 12
Nylon 6/12
Nylon 6/66
Nylon 6
B. 0% D2O
C. 25.5% D2O
Nylon 12
Nylon 6/12
Nylon 6/66
Nylon 6

References

(1) Albertsson, P.-Å. *Biochem. Pharmacol.* **1961**, *5*, 351–358.
(2) Albertsson, P.-Å. *Partition of Cell Particles and Macromolecules*; Wiley Interscience: New York, 1986.
(3) Albertsson, P.-Å. *Biochim. Biophys. Acta* **1958**, *27*, 378–395.
(4) Sivars, U.; Tjerneld, F. *Biochim. Biophys. Acta* **2000**, *1474*, 133–146.
(5) Piculell, L.; Lindman, B. *Adv. Colloid Interface Sci.*. **1992**, *41,* 149–178.
(6) Robb, I. D.; Williams, P. A.; Warren, P.; Tanaka, R. *J. Chem. Soc. Faraday Trans.* **1995**, *91*, 3901–3906.
(7) Saravanan, S.; Reena, J. A.; Rao, J. R.; Murugesan, T.; Nair, B. U. *J. Chem. Eng. Data* **2006**, *51*, 1246–1249.
(8) Gao, Y.-L.; Peng, Q.-H.; Li, Z.-C.; Li, Y.-G. *Fluid Phase Equilibr.* **1991**, *63*, 173–182.
(9) Eisenberg, H.; Felsenfeld, G. *J. Mol. Bio.* **1967**, *30*, 17–37.
(10) Brooks, D. E.; Sharp, K. A.; Fisher, D. In *Partitioning in Aqueous Two-Phase Systems*; Brooks, D. E., Fisher, D., Eds.; Academic Press: Orlando, FL, 1985.
(11) Johansson, H.; Karlström, G.; Tjerneld, F.; Haynes, C. *J. Chromatogr. B* **1998**, *711*, 3–17.
(12) Kamei, D.T.; Liu, C.-L.; Haase-Pettingell, C.; King, J.A.; Wang, D.I.C.; Blankschtein, D. *Biotechnol. Bioeng.* **2002**, *78*, 190–202.
(13) Rapacchietta, A. V.; Neumann, A. W. *J. Colloid Interface Sci.* **1977**, *59*, 555–567.
(14) Mirica, K. A.; Phillips, S. T.; Shevkoplyas, S. S.; Whitesides, G. M. *J. Am. Chem. Soc.* **2008**, *130*, 17678–17680.
(15) Mirica, K. A.; Shevkoplyas, S. S.; Phillips, S. T.; Gupta, M.; Whitesides, G. M. *J. Am. Chem. Soc.* **2009**, *131*, 10049–10058.

Appendix V

Separation of Nanoparticles in Aqueous Multiphase Systems through Centrifugation

Ozge Akbulut, Charles R. Mace, Ramses V. Martinez, Ashok A. Kumar, Zhihong Nie, Matthew R. Patton, and George M. Whitesides

Reprinted with permission from *Nano Lett.* **2012**, *12*, 4060-4064

NANO LETTERS

Letter

pubs.acs.org/NanoLett

Separation of Nanoparticles in Aqueous Multiphase Systems through Centrifugation

Ozge Akbulut,[†] Charles R. Mace,[†] Ramses V. Martinez,[†] Ashok A. Kumar,[‡] Zhihong Nie,[†] Matthew R. Patton,[†] and George M. Whitesides*[,†,§,∥]

[†]Departments of Chemistry and Chemical Biology, Harvard University, 12 Oxford Street, Cambridge, Massachusetts 02138, United States

[‡]School of Engineering and Applied Sciences, Harvard University, 29 Oxford Street, Cambridge, Massachusetts 02138, United States

[§]Wyss Institute for Biologically Inspired Engineering, Harvard University, 60 Oxford Street, Cambridge, Massachusetts 02138, United States

[∥]Kavli Institute for Bionano Science and Technology, Harvard University, 29 Oxford Street, Cambridge, Massachusetts 02138, United States

Supporting Information

ABSTRACT: This paper demonstrates the use of aqueous multiphase systems (MuPSs) as media for rate-zonal centrifugation to separate nanoparticles of different shapes and sizes. The properties of MuPSs do not change with time or during centrifugation; this stability facilitates sample collection after separation. A three-phase system demonstrates the separation of the reaction products (nanorods, nanospheres, and large particles) of a synthesis of gold nanorods, and enriches the nanorods from 48 to 99% in less than ten minutes using a benchtop centrifuge.

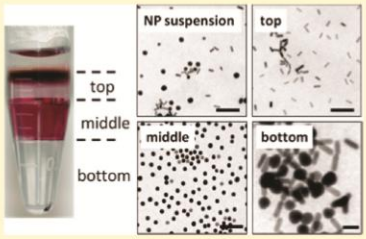

KEYWORDS: *Centrifugation, nanoparticles, separation, polymers, multiphase systems*

Exploiting the potential of nanoparticles in applications in self-assembly, electronics, diagnostics, and sensing[1,2] may require monodisperse populations. Many syntheses of nanoparticles produce polydisperse mixtures[3,4] and techniques to enrich populations according to size, shape, and/or composition are useful. This paper describes a new technique for separating gold nanoparticles according to their rate of migration through a viscous medium under centrifugal force.

Gold nanorods are potentially useful in diagnostic applications due to their unique optical properties such as tunable plasmonic fields.[5,6] They can support a longitudinal surface plasmon with a strong extinction peak in the red end of the visible or the near-infrared region of the spectrum; this characteristic suggests the use of gold nanorods as labels in biological imaging.[7] The resonant wavelength of nanorods depends on their size and aspect ratio.[8] Common preparations of gold nanorods, for example, those generated by the seed-mediated synthesis, produce a variety of shapes.[8] Spheres, rather than rods, may comprise 5−20% (w/w) of the gold nanoparticles formed in a representative synthesis.[9] To establish the relationship between shape and optical properties of gold nanorods and to examine the use of nanorods in technological applications, it would be convenient to have subpopulations of a mixture produced by a reaction easily accessible.

Methods for the Separation of Nanorods. Sedimentation by centrifugation in the solvent used for the reaction (e.g., water or toluene) is a straightforward method to collect the reaction products generated in syntheses of gold nanorods.[10] Multiple rounds of centrifugation are, however, usually necessary to separate byproducts from rods.[11,12] Other techniques used to separate monodisperse nanorods from mixtures are either time-consuming (e.g., size exclusion chromatography)[13] or require secondary chemical modification of the nanoparticles (e.g., gel electrophoresis).[14]

The hydrodynamic behavior of particles depends upon their shape and size (Supporting Information, eqs 1−4). Geometric differences can be used to sort particles dynamically in a medium that has a lower density than the density of the particles (e.g., ρ_{Au} = 19.3 g/cm^3 and ρ_{media} = 1.0−1.4 g/cm^3 for aqueous solutions of sucrose). Viscosity amplifies the spatial separation between two particles with differences in hydrodynamic behavior.

Rate-zonal centrifugation uses the differences in hydrodynamic behavior to separate objects.[15−20] In this technique, the medium of separation consists of zones of different

Received: April 17, 2012
Revised: May 23, 2012
Published: June 5, 2012

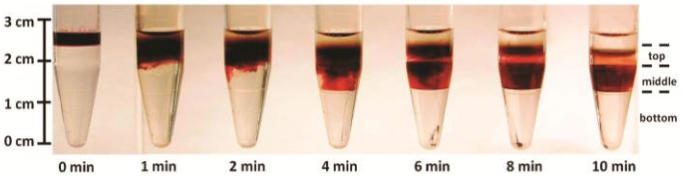

Figure 1. The evolution of the penetration of nanoparticles into an aqueous three-phase system composed of Brij 35 (8.7% v/v), PEOZ (10% w/v), and Ficoll (11.7% w/v) with time during centrifugation at 16 000*g*. The solvent of the suspension of nanoparticles (i.e., water) stayed as a clarified layer on top of the system, small nanorods (i.e., the desired product) penetrated slightly into the top phase, small nanospheres migrated to the middle phase, and large particles of both shapes sedimented to the bottom.

Table 1. Quantification of Separation of Nanoparticles Using an Aqueous Three-Phase System (MuPS)[a]

layer of MuPS	ρ (g/cm^3)	η (cP)	θ_{NS}[b]	θ_{NR}[c]	NS diameter (nm)	NR length (nm)	NR thickness (nm)
top	1.031	30.8	0.008	0.991	N.A.	36 ± 4	11 ± 1
middle	1.045	541.9	0.992	0.007	25 ± 2	N.A.	N.A.
bottom	1.112	139.0	0.4	0.6	244 ± 36	289 ± 27	100 ± 9

[a]We include the densities (ρ, g/cm^3) and viscosities (η, cP) of each phase of this three-phase system composed of Brij 35 (8.7% v/v), PEOZ (10% w/v) and Ficoll (11.7% w/v). We designated entries whose counts of particles were less than five per field of view N.A. (not applicable). [b]NS is the abbreviation for nanospheres. [c]NR is the abbreviation for nanorods. [d]The number fraction of nanoparticles (θ), which is defined as the ratio of the counts of number of nanoparticles of certain shape to the total count of nanoparticles in each layer.

viscosity. These zones are prepared by layering solutions of a single chemical in a common medium (e.g., solutions of Ficoll or sucrose in water) at different concentrations. The use of multiple zones, rather than a single one, is intended to facilitate sample collection and improve enrichment in hydrodynamic separation by localizing bands of nanoparticles to narrow regions. The boundaries between the layers of different viscosities are, however, not thermodynamically stable; they are disrupted easily by convection created during acceleration/deceleration of the centrifuge and by diffusion of boundaries during centrifugation. These instabilities make it more difficult to collect separated populations cleanly. Separation by rate-zonal centrifugation, therefore, could benefit from a medium of centrifugation with sharp, well-defined, and stable interfaces between zones of different density and/or viscosity.

The Use of Aqueous Multiphase Systems (MuPSs) as Media of Separation for Rate-Zonal Centrifugation. This paper describes a new approach to size- and shape-dependent separation of nanoparticles through rate-zonal centrifugation using MuPSs as separation media. We use this method to separate the reaction product (nanorods) and byproducts (nanospheres and bigger particles) of a synthesis of gold nanorods.

Aqueous MuPSs are phase-separated mixtures of water-soluble polymers and/or surfactants.[21] Upon separation in a gravitational field (slow) or through centrifugation (more rapid), the phases of MuPSs order according to their densities. These phases are characterized by different physical properties, such as (importantly for rate-zonal separations) viscosity.

The physical properties of the phases of a MuPS (e.g., viscosity, refractive index, ionic strength) do not necessarily correlate with density. For example, a three-phase MuPS composed of Brij 35 (a nonionic poly(ethylene oxide)-based surfactant), poly(2-ethyl-2-oxazoline) (PEOZ), and Ficoll (a polysucrose) has a highly viscous middle phase bordered by phases with lower viscosities (cf., Table 1). The ability to design and generate stacked, distinct fluid phases based on a common solvent (e.g., water) with viscosities chosen to give the best results in hydrodynamic separation is the basis of the method of separating nanoparticles described here.

We have previously described the separation of objects based on their density by localization at the interfaces between the phases of MuPSs; this method can be described as "equilibrium density separation".[21] Here, we use rate-zonal centrifugation through the phases of a MuPS, which have different viscosities, to separate objects with identical densities but with different hydrodynamic behaviors.

Compared to layered but miscible media, MuPSs offer five advantages: (i) the phases (i.e., the layers) of MuPSs are thermodynamically stable; (ii) the sharp interfaces between the phases facilitate the collection of samples after separation; (iii) the viscosities of each phase can be controlled independently of density; (iv) the MuPSs can be prepared in advance of use and stored; and (v) the MuPSs reform readily by centrifugation if disrupted. Isolating objects in different zones, where each zone is at equilibrium and separated by an interface, simplifies the recovery of enriched species.

MuPSs are versatile and easy to tune for specific separations.[21] In layered miscible media, the viscosity and density of each zone correlate closely and cannot be decoupled from each other. In MuPSs, it is possible to access a range of viscosities for a given density by using different combinations (e.g., different chemicals, or different molecular weights of the same polymer) of solutes that phase separate. (cf., Supporting Information, Tables S1 and S2). Because of this tunability and inherent stability, MuPSs offer a valuable addition to the tools that can be used in hydrodynamic separations.

Synthesis of Nanoparticles. We used a seeded-growth method developed by Nikoobakht and El-Sayed,[22] with minor modifications, to synthesize gold nanoparticles with an aspect ratio of approximately 4:1. It is possible to produce nanorods with a higher aspect ratio (18:1),[23] but a smaller aspect ratio better demonstrates the sensitivity of our approach to hydrodynamic separation of objects based on shape; the difference in sedimentation rates between a sphere and a rod increases in proportion to the aspect ratio (Supporting Information, eqs 3 and 4).

We concentrated as-synthesized nanoparticles produced in this method 20-fold by centrifugation of the reaction medium at 16 000*g* for 10 min. The concentrated solution contained 48% rods and 52% spheres. The length of the rods was in the range of 32−355 nm and the thickness of rods was in the range of 8−125 nm; the diameter of spheres was in the range of 18−265 nm. We refer to this concentrated solution as "the suspension of nanoparticles".

Characterization of Populations of Nanoparticles. UV−vis spectroscopy allowed the characterization of the populations of nanoparticles, both before and after separation, by quantifying the plasmonic absorption bands of their solutions. The wavelengths absorbed by gold nanoparticles depend on their size and shape.[24] For these wavelengths (400−1100 nm), the polymers and surfactants of the MuPSs we used in this work are transparent and do not contribute to the measured absorbance. Transmission electron microscopy (TEM) on these samples characterized the size and shape of the nanoparticles of each layer and allowed statistical analysis of the distribution of sizes and shapes of the isolated population. We used $n > 1000$ particles for each population.

Selection of Parameters and Medium of Separation. The speed and quality of separation of two objects by rate-zonal centrifugation depends, in general, on the speed of centrifugation and the variables that determine the sedimentation coefficients of the objects (eqs 1 and 2 in Supporting Information). Additional considerations exist when working with MuPSs because of the existence of multiple phases and interfaces; appropriate centrifugation parameters must be chosen to prevent the interfaces from trapping nanoparticles (eq 8 in Supporting Information).

Finally, the nanoparticles must be compatible with all the phases of the MuPS used for separation. For our application, we selected a MuPS that was compatible with cetyl trimethylammonium bromide (CTAB)-stabilized gold nanoparticles. We eliminated from consideration the systems comprising charged polymers and surfactants (e.g., poly(methacrylic acid), polyallylamine, poly(acrylic acid), poly(diallyldimethyl ammonium chloride), polyethyleneimine, and 3-[(3-cholamidopropyl)dimethylammonio]-1-propanesulfonate). Upon interaction with CTAB-stabilized gold nanoparticles, these systems formed gel-like structures and precipitated the nanoparticles from the solution (data not shown). Nonionic chemicals such as dextran, Ficoll (a polysucrose), poly(ethylene glycol) (PEG), poly(2-ethyl-2-oxazoline) (PEOZ), poly(vinyl alcohol) (PVA), Brij 35, and Pluronic F68 (a poly(ethylene oxide)-poly(propylene oxide) copolymer-based surfactant) were compatible with nanoparticles.

The large library of aqueous polymers and surfactants that form MuPSs offers a wide range of systems with different viscosities and densities that can be used as media in separations.[21] We investigated three-phase systems for this study to capture three main populations of the synthesis of nanorods that we use: small nanorods, small nanospheres, and bigger particles.

Determining the Viscosity of the Top Phase for the Separation of Nanoparticles. We designed a MuPS with a top phase (lowest density) that had a sufficiently high viscosity to delay the penetration of nanorods into the MuPS until the nanospheres, which have larger sedimentation velocities, migrated into the middle phase.

A solution containing a high percentage of nanorods should appear brown, while a solution containing mostly nanospheres should appear pink/red.[3] We evaluated the separation of these species by observing the formation of a narrow brown band of nanorods on top of a single-phase polymer system and the sedimentation of this band into the medium (i.e., a rate-dependent separation of nanoparticles in a homogeneous medium). For this evaluation, we first examined dilutions of solutions of PEOZ (MW = 200 000 g/mol). When the concentration of PEOZ in a solution is varied from 4% (w/v) to 35% (w/v), the viscosity of the solution covers a wide range (from 4 to 1100 cP, respectively) while its density increases by only 6% (Supporting Information, Table S3).

We layered a suspension of nanoparticles (100 μL) onto solutions of PEOZ (1 mL). We then sedimented the nanoparticles through these single-phase systems by centrifugation at 16 000*g* for different intervals of time (2−8 min) to determine the relationship between the effectiveness of separation and the viscosity of the layer (Supporting Information, Figure S1).

Viscosities greater than 65 cP were too high for the effective separation of nanorods and nanospheres into distinct populations within 8 min (i.e., we did not observe the formation of separate bands). In a solution with a viscosity of 19 cP, the nanorods started to penetrate into the system in less than 4 min (Supporting Information, Figure S1). Considering that the suspension of nanoparticles we use is polydisperse (i.e., we expect a continuum in penetration distance without clear boundaries between different sizes of particles), it is crucial for our method to delay the penetration of nanorods into the system until the band of nanorods is free of nanospheres. On the basis of these experiments, we concluded that a range for the viscosity of the top phase of a MuPS between 20 and 65 cP would produce an optimal separation. This conclusion was also supported by our attempts to separate populations of nanoparticles in two different systems (i) a two-phase system composed of PEG (20% w/v) and 1-*O*-octyl-β-D-glycopyranoside (5% w/v), with a low viscosity top phase (3.9 cP), and (ii) a three-phase system composed of PEG (13.3% w/v), dextran (10% w/v), and PEOZ (11.7% w/v) with a high viscosity top phase (69 cP). In the former case, the nanoparticles penetrated into the system without forming bands. In the latter case, even the larger particles could not advance into the middle phase in less than ten minutes of centrifugation at 16 000*g* (Supporting Information, Figure S3).

Separation of Reaction Products of a Nanorod Synthesis. We prepared a series of three-phase MuPSs and measured the viscosity of each phase in order to evaluate their suitability as centrifugation media for enrichment of gold nanorods. The three phases of a MuPS should have viscosities that allow the three subpopulations of interest (i.e., nanorods, nanospheres, and larger particles) to be separated within 10 min of centrifugation. The top phase should retain the nanorods, which have the smallest sedimentation coefficient of the three subpopulations, while allowing the other populations to pass through within this time. The middle phase should be viscous enough to capture nanospheres while allowing the larger particles to pass to the bottom phase. Of the MuPSs that we tested, we obtained the best enrichment of gold nanorods in a three-phase system composed of Brij 35 (8.7% v/v), PEOZ (10% w/v) and Ficoll (11.7% w/v) (Figure 1). The properties (density, ρ, and viscosity, η) of this system were (i) ρ_{top} = 1.031 g/cm^3, η_{top} = 31 cP; (ii) ρ_{middle} = 1.045 g/cm^3,

dx.doi.org/10.1021/nl301452x | *Nano Lett.* 2012, 12, 4060−4064

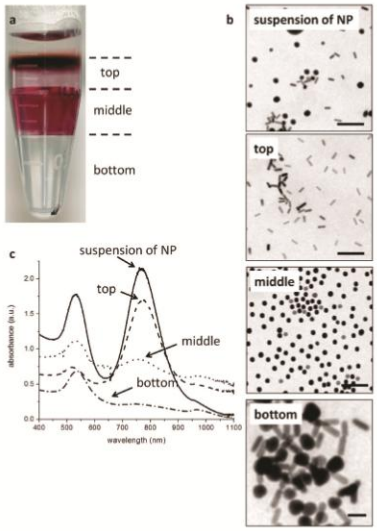

Figure 2. (a) Image of an aqueous three-phase system composed of Brij 35 (8.7% v/v), PEOZ (10% w/v), and Ficoll (11.7% w/v) after sedimenting the reaction products of a gold nanoparticle synthesis for 8 min at 16 000*g*. The properties of the phases of this system are (i) ρ_{top}= 1.031 g/cm^3, η_{top}= 30.8 cP; (ii) ρ_{middle}= 1.045 g/cm^3, η_{middle}= 541.9 cP; (iii) ρ_{bottom}= 1.112 g/cm^3, η_{top}= 139.0 cP. (b) TEM images of suspension of nanoparticles (suspension of NP) and samples collected from the layers as shown in (a). The scale bar in each image corresponds to 200 nm.

η_{middle} = 542 cP; and (iii) ρ_{bottom} = 1.112 g/cm^3, η_{bottom} = 139 cP.

We layered the suspension of nanoparticles on this three-phase system and centrifuged these systems at 16 000*g* for 1−10 minutes. The effect of time on the penetration of particles into this MuPS was monitored by eye and quantified using spectroscopy and transmission electron microscopy (TEM). Figure 1 shows an example of penetration of nanoparticles into this MuPS. During centrifugation, the small nanorods were enriched in the top phase of the MuPS and formed a brown band. The penetration of small nanospheres into the middle phase was visualized by the color change of this phase from transparent to red. After the complete migration of nanoparticles from the solution (i.e., suspension of nanoparticles) that was layered onto the MuPS, this solution appears as a transparent band at the top the MuPS. In this system, it took a 25 nm diameter sphere 3−4 min at 16 000*g* to migrate through the top phase and to begin to penetrate the middle phase. A nanorod (l = 36 nm, d = 11 nm) would sediment about four times more slowly than a sphere (Supporting Information, eqs 3 and 4), hence requiring 12− 16 min to travel through the top phase of the MuPS under these conditions. On the basis of these estimates, we expect optimal separation to require between 5−10 min of centrifugation.

We used a fixed angle benchtop centrifuge (VWR 1816) without temperature control to demonstrate simplicity of our method. We found reasonable agreement between the theoretical predictions and experimental results. The nanoparticles travel approximately three times more rapidly in the system that we use than predicted by theoretical calculations using eqs 2−4 (Supporting Information). We attribute this difference to the heating of the sample during centrifugation. This heating leads to a corresponding decrease in viscosity of the phases (the viscosity of the top phase drops from 31 to 12 cP with an increase from 22 to 28 °C after 8 min of centrifugation at 16 000*g* in the centrifuge that we use).

We quantified the efficiency of the separation of nanoparticles by an aqueous three-phase system using TEM and UV−vis spectroscopy (Figure 2). In the top phase, nanorods were enriched to 99% (from 48% in the suspension of nanoparticles) and the average length and thickness of the nanorods was 36 ± 4 and 11 ± 1 nm, respectively. The amount of nanorods of similar size in other layers was less than 1%; these values demonstrate that the method we use here is highly shape- and size-dependent. Similarly, the middle phase contained 99% nanospheres with average diameters 25 ± 2 nm, indicating a decrease in polydispersity (Table 1).

In conclusion, we have developed a method using thermodynamically stable phases of liquids as separation media that offers an improvement for a known technique, rate-zonal centrifugation. Phase-separated media overcome the difficulties associated with conventional media (e.g., layered systems) such as the collection of samples after enrichment and the lack of stability over time. We expect this stability to be useful to enhance the separation of other objects such as proteins and DNA, where long periods of ultracentrifugation are typically necessary. In addition, the robustness of interfaces of the phase-separated systems allows scaling of the separations such that larger amounts of purified materials can be obtained by using bigger containers.

■ ASSOCIATED CONTENT

Supporting Information

Characterization methods, pictures of time-dependent penetration of nanoparticles into other aqueous MuPSs under centrifugation, tables of viscosity and density of solutions of polymers and surfactants, and viscosities of different solutions with similar density. This material is available free of charge via the Internet at http://pubs.acs.org.

■ AUTHOR INFORMATION

Corresponding Author

*E-mail: gwhitesides@gmwgroup.harvard.edu.

Notes

The authors declare no competing financial interest.

■ ACKNOWLEDGMENTS

This work was supported by the Bill and Melinda Gates Foundation (award number OPP1016360) and by a subcontract from a Department of Energy award to Northwestern University (DE-SC0000989).This work was performed in part using the facilities of the Center for Nanoscale Systems (CNS), a member of the National Nanotechnology Infrastructure Network (NNIN), which is supported by the National Science Foundation under NSF (award number ECS-0335765). CNS is part of the Faculty of Arts and Sciences at Harvard University. O.A. thanks Professor Osman Bakr of KAUST for fruitful discussions. R.V.M. acknowledges funding by the FP7 People program under the project Marie Curie IOF-275148. A.A.K. acknowledges financial support from the Office of Naval Research through the NDSEG fellowship program. The authors

thank Professor David Weitz and the Weitz group for the use of their rheometry facilities, and Ms. Felice Frankel for her valuable advice on photography.

■ REFERENCES

(1) Jiang, W.; Kim, B. Y. S.; Rutka, J. T.; Chan, W. C. W. *Nat. Nanotechnol.* **2008**, *3*, 145−150.
(2) Narayanan, R.; El-Sayed, M. *Nano Lett.* **2004**, *4*, 1343−1348.
(3) Murphy, C. J.; Sau, T. K.; Gole, A. M.; Orendorff, C. J.; Gao, Jinxin; Gou, L.; Hunyadi, S. E.; Li, T. *J. Phys. Chem. B* **2005**, *109*, 13857−13870.
(4) Adair, J. H.; Suvaci, E. *Curr. Opin. Colloid Interface Sci.* **2000**, *5*, 160−167.
(5) Lee, K.-S.; El-Sayed, M. A. *J. Phys. Chem. B* **2005**, *109*, 20331−20338.
(6) Alekseeva, A. V.; Bogatyrev, V. A.; Dykman, L. A.; Khlebtsov, B. N.; Trachuk, L. A.; Melnikov, A. G.; Khlebtsov, N. G. *Appl. Opt.* **2005**, *44*, 6285−6295.
(7) Jain, P. K.; Lee, K. S.; El-Sayed, I. H.; El-Sayed, M. A. *J. Phys. Chem. B* **2006**, *110*, 7238−7248.
(8) Huang, X.; Neretina, S.; El-Sayed, M. A. *Adv. Mater.* **2009**, *21*, 4880−4910.
(9) Jana, N. R.; Gearheart, L.; Murphy, C. J. *Adv. Mater.* **2001**, *13*, 1389−1393.
(10) Sharma, V.; Park, K.; Srinivasarao, M. *Proc. Natl. Acad. Sci. U.S.A.* **2009**, *106*, 4981−4985.
(11) Khanal, B. P.; Zubarev, E. R. *J. Am. Chem. Soc.* **2008**, *130*, 12634−12635.
(12) Kim, F.; Song, J. H.; Yang, P. *J. Am. Chem. Soc.* **2002**, *124*, 14316−14317.
(13) Wei, G.-T.; Liu, F.-K.; Wang, C. R. C. *Anal. Chem.* **1999**, *71*, 2085−2091.
(14) Hanauer, M.; Pierrat, S.; Zins, I.; Lotz, A.; Sonnichsen, C. *Nano Lett.* **2007**, *7*, 2881−2885.
(15) Xiong, B.; Cheng, J.; Qiao, Y.; Zhou, R.; He, Y.; Yeung, E. S. *J. Chromatogr. A* **2011**, *1218*, 3823−3829.
(16) Bai, L.; Ma, X.; Liu, J.; Sun, X.; Zhao, D.; Evans, D. G. *J. Am. Chem. Soc.* **2010**, *132*, 2333−2337.
(17) Sun, X.; Tabakman, S. M.; Seo, W.-S.; Zhang, L.; Zhang, G.; Sherlock, Sarah; Bai, L.; Da, H. *Angew. Chem., Int. Ed.* **2009**, *48*, 939−942.
(18) Qiu, P.; Mao, C. *Adv. Mater.* **2011**, *23*, 4880−4885.
(19) Chen, G.; Wang, Y.; Tan, L. H.; Yang, M.; Tan, L. S.; Chen, Y.; Chen, H. *J. Am. Chem. Soc.* **2009**, *131*, 4218−4219.
(20) Tyler, T. P.; Henry, A.-I.; Duyne, R. P. V.; Hersam, M. C. *J. Phys. Chem. Lett.* **2011**, *2*, 218−222.
(21) Mace, C. R.; Akbulut, O.; Kumar, A. A.; Shapiro, N. D.; Derda, R.; Patton, M. R.; Whitesides, G. M. *J. Am. Chem. Soc.* **2012**, *134*, 9094−9097.
(22) Nikoobakht, B.; El-Sayed, M. A. *Chem. Mater.* **2003**, *15*, 1957−1962.
(23) Jana, N. R.; Gearheart, L.; Murphy, C. J. *J. Phys. Chem. B* **2001**, *105*, 4065−4067.
(24) Jain, P. K.; Lee, K. S.; El-Sayed, I. H.; El-Sayed, M. A. *J. Phys. Chem. B* **2006**, *110*, 7238−7248.

Supporting Information

Separation of Nanoparticles in Aqueous Multiphase Systems through Centrifugation

Ozge Akbulut[1], Charles R. Mace[1], Ramses V. Martinez[1], Ashok A. Kumar[2], Zhihong Nie[1], Matthew R. Patton[1], and George M. Whitesides[1,3,4*]

[1]Departments of Chemistry & Chemical Biology, Harvard University, 12 Oxford Street, Cambridge, MA 02138, United States

[2]School of Engineering and Applied Sciences, Harvard University, 29 Oxford Street, Cambridge, MA 02138, United States

[3]Wyss Institute for Biologically Inspired Engineering, Harvard University, 60 Oxford Street, Cambridge, MA 02138, United States

[4]Kavli Institute for Bionano Science and Technology, Harvard University, 29 Oxford Street, Cambridge, MA 02138, United States

[*] Corresponding author email: gwhitesides@gmwgroup.harvard.edu

Materials and Methods

Chemicals. Brij 35 (MW= ~1,200 g/mol), 3-[(3-cholamidopropyl) dimethylammonio]-1-propanesulfonate (CHAPS), cetyl trimethylammonium bromide (CTAB), chloroauric acid, silver nitrate, ascorbic acid, sodium borohydride, Ficoll (MW= 400,000) g/mol, poly(2-ethyl-2-oxazoline) (PEOZ) (MW=200,000 g/mol), polyacrylamide (MW=10,000 g/mol), poly(diallyldimethylammonium chloride) (MW=400,000 g/mol), poly(ethylene glycol) (PEG) (MW=20,000 g/mol), polyethyleneimine (PEI) (MW=25,000 g/mol), poly(methacrylic acid sodium salt) (MW=5,000 g/mol), polyvinylpyrrolidone (PVP) (MW=55,000 g/mol) and Pluronic F68 were purchased from Sigma-Aldrich. Poly(acrylic acid) (MW= 450,000 g/mol), poly(allylamine hydrochloride) (MW=60,000 g/mol), and poly(vinyl alcohol) (MW= 3,000 g/mol) were obtained from Polysciences. Dextran (MW= 500,000 g/mol) was purchased from Spectrum Chemical. 1-*O*-octyl-β-D-glucopyranoside was purchased from Calbiochem. Sodium dodecyl sulfate was purchased from J.T. Baker. All chemicals were used without further purification. We used Milli-Q water at pH 5.5 throughout the experiments.

Preparations of the Aqueous Multiphase Systems (MuPSs). We prepared stock solutions of polymers and surfactants in water without adding salts or adjusting the pH. We then mixed the appropriate volumes of these solutions by vortexing for thirty seconds and centrifuged the mixtures at 2,000*g* for five minutes to obtain phase separation.

Measurements of Density. We determined the density of each stock solution and phase via oscillating U-tube densitometry (Anton Paar DM35N).

UV-Vis Spectroscopy. UV-Vis spectroscopy was performed on a Hewlett Packard 8453 Spectrophotometer. After separating nanoparticles in an aqueous MuPS through centrifugation, we collected 60 μL of sample from each layer, and directly analyzed these samples in the

spectrophotometer without dilution. For the measurement of the sediment, almost the entire supernatant was removed by pipetting before resuspending the sediment in a 100 μL of a 10 mg/mL CTAB solution.

Transmission Electron Microscopy (TEM). TEM was performed on a JEOL 2100; we used Lacey Formvar/Carbon, 300-mesh, copper TEM grids (Ted Pella, Inc.). For TEM on samples from the top and middle phases, we diluted 50 μL of sample from each phase by adding 150 μL of DI water, centrifuged the solutions at 16,000*g* for ten minutes, and collected 20 μL of concentrated sample from the bottom of tube. We put 2μL of this concentrated solution onto a TEM grid and allowed it to evaporate at ambient conditions. To analyze the particles that sedimented to the bottom of the tube after separation, we decanted almost the entire solution. We suspended the sediment in 50 μL 10 mg/mL CTAB solution, deposited 2 μL of this solution onto a TEM grid, and allowed it to evaporate at ambient conditions.

Statistics on Populations of Nanoparticles. We measured the sizes of nanoparticles and counted them by analyzing ten bright field TEM images with even illumination from each solution layer using Image J software (National Institute of Health, USA). The analyzed images were chosen to be as representative of the layer as possible. We collected data from ~1000 particles/layer and calculated their average size; we estimated our error by taking the standard deviation of the sizes measured.

Rheometry. The rheometry measurements were carried out on a AR2-G2 stress-controlled rheometer (TA Instruments) at room temperature in the shear-rate range of 1/10 to 1/200 (1/s) at room temperature with a geometry cone/plate 1° 40 mm (part no:S#987620). The viscosity over this range of shear-rates was constant within the sensitivity of the instrument

implying that shear-thinning and shear-thickening effects are minimal for the polymers and surfactants used. The viscosities listed in Table S1 were measured at a shear-rate of 1/100 (1/s).

Experimental Details

Hydrodynamic Behavior of Objects with Different Shapes in a Viscous Medium. In order to separate objects by shape and size, we exploited the differences in viscous drag that objects experience during centrifugation. The concept is best exemplified by the ratio of the sedimentation coefficients of two different shapes. The sedimentation coefficient S (s) is defined by eqn. 1, with v_T (cm/s) as the terminal velocity of the object in the medium and a (cm/s^2) as the acceleration provided by gravity or centrifugation:

$$S = \frac{v_T}{a} \qquad (1)$$

Using Stokes' Law, the sedimentation coefficient for a sphere S_s (s) can be found by eqn. 2, where η (P; g/(cm s)) is the viscosity of the medium, d_H (cm) is the diameter of the sphere and ρ_p (g/cm^3) and ρ_l (g/cm^3) are the densities of the object and the liquid medium, respectively:

$$S_s = \frac{1}{18} {d_H}^2 \frac{(\rho_p - \rho_l)}{\eta} \qquad (2)$$

This equation can be modified to account for arbitrary shapes (eqn. 3), where f/f_o is the frictional coefficient of an arbitrary shape, and usually estimated numerically. The term d_H (cm) is the diameter of a sphere of equivalent volume to the object:

$$S = \frac{1}{18} \left(\frac{f}{f_0}\right)^{-1} {d_H}^2 \frac{(\rho_p - \rho_l)}{\eta} \qquad (3)$$

Hubbard and Douglas calculated the frictional coefficient for a rod with a diameter, d (cm), and a length, l (cm), to be equivalent to eqn. 4 (valid for $0 < l/d < 8$):[1]

$$\frac{f}{f_0} = 0.55\left(\frac{l}{d}\right)^{-1/3}\left(1 + 0.869\left(\frac{l}{d}\right)^{0.76}\right) \qquad (4)$$

Guidelines to Select a MuPS to Separate Nanoparticles by Rate-Zonal Centrifugation. Separations by rate-zonal centrifugation rely on the differences in the hydrodynamic behavior of objects under centrifugal force—the sedimentation ratio of two objects must be different than 1. For two objects to sediment through a medium, their densities (ρ_1 and ρ_2) must each be greater than that of the medium (ρ_l). When using a MuPS to perform rate-zonal centrifugation, we must also take into account the interfacial surface energies between phases. The interfacial surface energy of a two phase MuPS, or any aqueous two-phase system, is quite small (γ, 100 nJ/m^2 to mJ/m^2).[2] For nanoparticles moving through a MuPS, these seemingly small interfacial energies can pose a non-trivial barrier for continued sedimentation. This energy barrier can be overcome with the appropriate choice of object densities (ρ_p), relative centrifugal force (RCF), and particle sizes (d_H). We use a simplified comparison of energies to determine the relationship between these variables to ensure that the gravitational energy (E_g) is significantly greater than the surface energy (E_s).

$$\frac{E_g}{E_S} > 10 \qquad (5)$$

To a first approximation, the energies can be written as follows:

$$E_g \approx (\rho_p - \rho_l) RCF \times g\, {d_H}^4 \qquad (6)$$

$$E_S \approx \gamma {d_H}^2 \qquad (7)$$

For densities in units g/cm^3, g in units of m/s^2, sizes in units of nm, and interfacial surface energies in units of mJ/m^2, we assume that the density of the medium is 1, that the gravitational

constant is 10, and that the interfacial surface energy is 0.0001. Incorporating these assumptions into eqn.'s 6 and 7, we can re-write eqn. 5:

$$(\rho_p - 1) RCF\, {d_H}^2 > 10^{-8} \qquad (8)$$

We can use this equation to estimate the speed of centrifugation required for gold nanoparticles. For example, the RCF must be greater than 8,800*g* for a 25-nm (diameter) gold nanosphere (d_{gold} = 19.3 g/cm^3) in order to overcome the effect of the interfacial surface energy. We chose to use 16,000*g* (achievable in a benchtop centrifuge) to ensure that we were well above the limit and also to reduce the time required to separate the objects. The RCF is inversely related to the time required for an object to sediment a fixed distance for a given viscosity.

Synthesis of Nanoparticles. We synthesized gold nanorods according to the seeded growth method developed by Nikoobakht and El-Sayed[3] with minor modifications. We prepared a seed solution by mixing cethyl trimethylammonium bromide (CTAB) solution (2.5 mL, 0.20 M) with 1.5 mL of 1.0 mM $HAuCl_4$. We vigorously stirred this solution and then quickly added 0.60 mL of ice-cold 0.010 M $NaBH_4$ and immediately observed the formation of a brownish-yellow color. The seed solution continued to be stirred for another two minutes and was then kept at 25 °C for thirty minutes for aging. We prepared the growth solution by mixing 50 mL of a 0.2 M CTAB solution with 5 mL of an aqueous 5 mM $HAuCl_4$ solution, 2.8 mL of an aqueous 4 mM $AgNO_3$ solution, and 40 mL of water. Following the addition of 1 mL of an aqueous 0.8 M solution of ascorbic acid, this dark yellow solution turned colorless. Finally, we added 1 mL of an aged seed solution of nanoparticles to the growth solution at 27–30 °C. The color of the solution gradually changed within ten to twenty minutes. The growth medium was kept at constant temperature (27–30 °C) for twenty hours.

After synthesizing gold nanoparticles, we concentrated the products in the reaction solution 20-fold to create a stock solution by centrifuging the total reaction volume for five minutes at 16,000*g* and collecting the concentrated solution of nanoparticles in the bottom by a pipette. This concentrated solution is referred as "suspension of the nanoparticles" in the main text.

Table S1. The viscosities of different solutes with densities 1.038 ± 0.001 g/cm^3 (± 0.2%).

solutes	concentration (% w/v)	density (g/cm^3)	viscosity (cP)
CHAPS	24.2	1.037	2.1
PVP	20	1.038	7.4
PEG	25	1.037	29.8
Pluronic F68	35	1.039	30.0
PEOZ	24	1.039	175.0
PEI	30	1.037	302.5

Table S2. Properties of the aqueous stock solutions of polymers and surfactants that are used in this study: average molecular weight (g/mol), concentration (% w/v or % v/v), density (g/cm^3) and viscosity (cP).

	Polymer	avg. MW (g/mol)	concentration	density (g/cm^3)[4]	viscosity (cP)
1	poly(methacrylic acid)	5,000	40 (% w/v)	1.279	684.6
2	poly(vinyl alcohol)	3,000	10 (% w/v)	1.022	111.3
3	poly(ethylene glycol)	20,000	40 (% w/v)	1.069	284.5
4	dextran	500,000	30 (% w/v)	1.101	1071.0
5	Ficoll	400,000	40 (% w/v)	1.130	480.0
6	poly(diallyldimethylammonium chloride)	400,000	20 (% w/v)	1.044	112.6
7	polyethyleneimine	25,000	30 (% w/v)	1.037	302.5
8	polyallylamine	60,000	20 (% w/v)	1.052	23.7
9	Brij 35	~1,198	30 (% v/v)	1.025	378.0
10	1-*O*-octyl-β-D-glucopyranoside	292	10 (% w/v)	1.011	2.7
11	Pluronic F68	~8,400	44 (% w/v)	1.049	30.0
12	CHAPS	614	25 (% w/v)	1.042	4.7

Table S3. The densities (g/cm^3) and viscosities (cP) of dilutions of PEOZ.

dilutions of PEOZ (% w/v)	density (g/cm^3)	viscosity (cP)
35	1.059	1100.0
24	1.039	193.0
17.5	1.028	65.1
12	1.017	19.1
8	1.012	10.8
4	1.004	2.5

Figure S1. Time-dependent penetration of nanoparticles into solutions of PEOZ with different densities and viscosities. In each column, we varied the concentration of PEOZ (35%, 17.5 %, 12%, and 4% (w/v), respectively), while the rows correspond to different time intervals during centrifugation

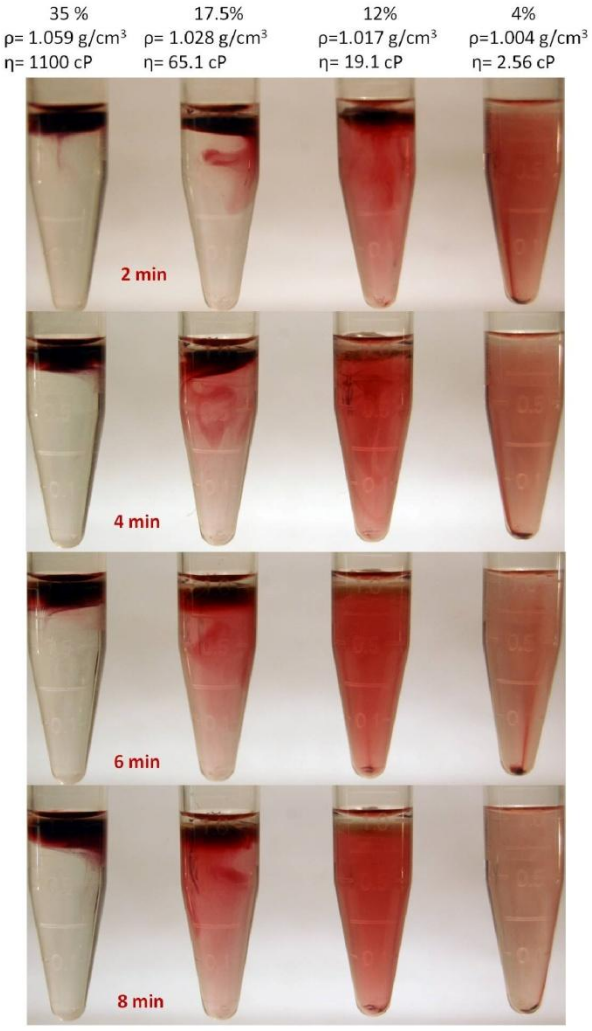

Figure S2. Evaluation of aqueous multiphase systems with different viscosities for the top phase. (a) Picture of a two-phase system composed of 1-*O*-octyl-β-D-glucopyranoside (5% w/v) and PEG (20% w/v). The tube on the left shows the system after overlaying the stock solution on top; the tube on the right shows the system after centrifugation at 16,000*g* for two minutes. The viscosity of the top phase of this system is 3.9 cP. (b) Picture of the three-phase system composed of PEG (13.3% w/v), PEOZ (11.7% w/v) and dextran (10% w/v). The tube on the left shows the system after overlaying the stock solution on top; the tube on the right shows the system after centrifugation at 16,000*g* for eight minutes. The viscosity of the top phase of this system is 69 cP.

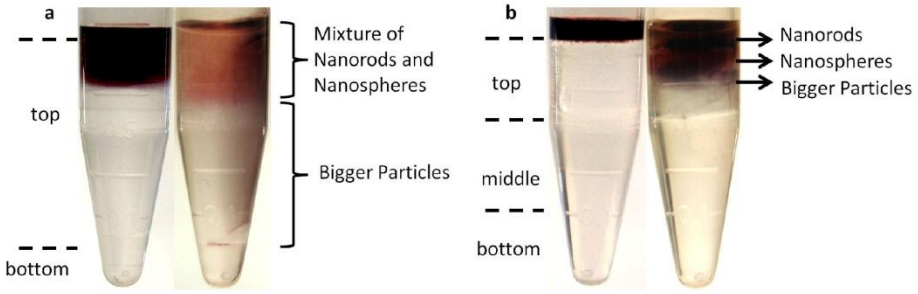

References

1. Hubbard, J. B.; Douglas, J. F. *Phys. Rev. E* **1993,** 47, R2983–R2986.
2. Hatti-Kaul, R. *Biotechnol.* **2001,** 19, 269–277.
3. Nikoobakht, B.; El-Sayed, M. A. *Chem. Mater.* **2003,** 15, 1957–1962.
4. Mace, C. R.; Akbulut, O.; Kumar, A. A.; Shapiro, N. D.; Derda, R.; Patton, M. R.; Whitesides, G. M. *J. Am. Chem. Soc.* **2012**, 134, 9094−9097.

Appendix VI

Using Magnetic Levitation to Separate Mixtures of Crystal Polymorphs

Manza B. J. Atkinson, David K. Bwambok, Jie Chen, Prashant D. Chopade, Martin M. Thuo, Charles R. Mace, Katherine A. Mirica, Ashok A. Kumar, Allan S. Myerson, and George M. Whitesides

Reprinted with permission from *Angew. Chemie Int. Ed.* **2013**, *52*, 10208-10211

Crystal Polymorphs Hot Paper

DOI: 10.1002/anie.201305549

Using Magnetic Levitation to Separate Mixtures of Crystal Polymorphs**

Manza B. J. Atkinson, David K. Bwambok, Jie Chen, Prashant D. Chopade, Martin M. Thuo, Charles R. Mace, Katherine A. Mirica, Ashok A. Kumar, Allan S. Myerson, and George M. Whitesides**

The crystallization of an organic compound can produce a mixture of crystalline solids with different solid-state structures (polymorphs).[1] No convenient method now exists to separate crystals of a single polymorph from a mixture of crystals of different polymorphs. Of the physical properties that might be used to separate polymorphs,[1a] density is attractive for two reasons: 1) Different packings of molecules in a crystal often result in different densities for polymorphs;[1a,2] 2) Separations by density do not destroy the crystals.

Magnetic levitation (MagLev) is a simple system that provides a continuous apparent density gradient in which to measure density and separate objects.[3] MagLev can distinguish small differences in the density ($\Delta\rho = 0.01$–$0.0001\ g\,cm^{-3}$, depending on the type of the experiment) of diamagnetic objects.[4] Although several methods to separate crystals by density exist,[5] MagLev offers four advantages: 1) it separates multiple populations in a single step, 2) it quantifies the density of each population, 3) it is applicable to small crystals (100 μm size), and 4) it provides seed crystals for large-scale crystallization. We used MagLev to separate mixtures of polymorphs of four compounds: 5-methyl-2-[(2-nitrophenyl)amino]-3-thiophenecarbonitrile (ROY) **1**, sulfathiazole **2**, carbamazepine **3**, and *trans*-cinnamic acid **4** (Scheme 1).

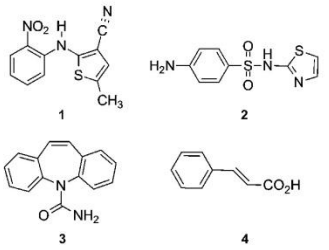

Scheme 1. Chemical formulas of compounds analyzed in this study: 1) 5-methyl-2-[(2-nitrophenyl)amino]-3-thiophenecarbonitrile (ROY) **1**, 2) sulfathiazole **2**, 3) carbamazepine **3**, and 4) *trans*-cinnamic acid **4**.

A survey of the Cambridge Structural Database indicates that 3.1–3.5% of the compounds submitted crystallize in different polymorphic forms.[6] A review by Stahly indicated that of 245 small-molecule pharmaceuticals, approximately 90% showed evidence of multiple crystalline and noncrystalline forms, with approximately half of these exhibiting polymorphism.[7] Mixtures of polymorphs are problematic when desired properties depend on a single polymorph.[8] Examples of properties influenced by crystal form include solubility and dissolution rate (which impacts bioavailability in pharmaceuticals),[1b,8] the color of pigments[9] and dyes,[10] and sensitivity towards detonation in explosives.[11]

Methods to obtain single polymorphs from mixtures of polymorphic crystals include selective nucleation,[12] interconversion,[13] isolation based on differences in physical properties,[14] and luck. Success in controlling the kinetics of crystal nucleation and growth in polymorphic systems is limited and largely empirical.[15] Interconversion of polymorphs is restricted to methods that produce thermodynamically stable forms.[8] Separations based on differences in morphology,[16] melting points,[17] or other physical properties can be tedious. Density is, however, a physical property closely linked to molecular packing—the process that forms polymorphs—and provides a means to identify and separate polymorphs.[18] Differences in density between polymorphs may be small ($\Delta\rho \leq 0.01\ g\,cm^{-3}$), and rarely exceed five

[*] Dr. M. B. J. Atkinson, Dr. D. K. Bwambok, Dr. M. M. Thuo, Dr. C. R. Mace, Dr. K. A. Mirica, A. A. Kumar, Prof. Dr. G. M. Whitesides
Department of Chemistry and Chemical Biology
Harvard University
12 Oxford Street, Cambridge, MA 02138 (USA)
E-mail: gwhitesides@gmwgroup.harvard.edu
Dr. J. Chen, Dr. P. D. Chopade, Prof. Dr. A. S. Myerson
Department of Chemical Engineering
Massachusetts Institute of Technology
77 Massachusetts Ave, Cambridge, MA 02139 (USA)
E-mail: myerson@mit.edu

[**] The work at Harvard was supported by the Department of Energy, Office of Basic Energy Sciences, Division of Materials Sciences and Engineering under award no ER45852. D.K.B., C.R.M., K.A.M., and A.A.K. wish to acknowledge the Bill and Melinda Gates Foundation, award no 51308 for salary support. We would like to thank Dr. Shao-Liang Zheng of the Harvard Center for Crystallographic Studies for assistance with X-ray diffraction, Jack Alvarenga of the Wyss Institute for Biologically Inspired Engineering at Harvard University for support with Raman Spectroscopy, Dr. Steve Morin and Dr. Joshua Lessing for equipment, Dr. Phillip W. Snyder, Dr. Nathan Shapiro, and Dr. Rafael Luna of Luna Scientific Storytelling for discussions. A.A.K. acknowledges support from the Office of Naval Research through the NDSEG fellowship program.

Supporting information for this article is available on the WWW under http://dx.doi.org/10.1002/anie.201305549.

percent.[18] For example, for the compound ROY **1**, the density of form R is 1.438 $g\,cm^{-3}$, while that of the form OP is 1.435 $g\,cm^{-3}$ as calculated from X-ray diffraction (XRD).[19] Methods that separate crystals by density must be able to resolve these small differences.

One of the simplest ways to separate polymorphs by density is the sink–float method.[20] In a fluid with a density between that of two known polymorphs, one type floats while the other sinks. This method can, thus, only separate two crystal forms at once. Steps in density provide multiple bins to separate mixtures,[21] but these systems work best when the density of the objects to be separated is known. A continuous gradient can separate multiple subpopulations with high resolution. The generality of a method based on continuous gradients is helpful when separating polymorphs, because differences in density between crystal forms can be small and precise densities are not known a priori; continuous gradients are, however, often technically demanding to form and to manipulate.

To demonstrate the use of MagLev to separate crystal polymorphs, we used the four compounds in Scheme 1. We selected them for four reasons: 1) Each compound exhibits polymorphism. 2) The density and structure of each crystal form has been characterized by single-crystal XRD, and the densities measured by MagLev can be compared to values calculated from crystal structures. 3) The polymorphs have different shapes, which makes their visual identification straightforward.[22] 4) These crystals have densities in the most convenient working range of MagLev (0.8–2.0 $g\,cm^{-3}$).[3a]

We have described the MagLev device and procedures in detail elsewhere.[3a] Briefly, two permanent magnets (NdFeB; 5 cm × 5 cm × 2.5 cm) with like poles facing at a distance of 4.5 cm, generates a linear gradient in the magnetic field with a minimum in the field located at the vertical midpoint between the magnets ($d/2$; Figure 1). When suspended in a solution containing paramagnetic ions and placed between the magnets, a diamagnetic object will levitate at a height, h (m), where the gravitational (F_g) and magnetic forces (F_m) acting on it are balanced [Eq. (1)].[3a]

$$h = \frac{(\rho_s - \rho_m) g \mu_0 d^2}{(\chi_s - \chi_m) 4 B_0^2} + \frac{d}{2} \quad (1)$$

In this equation, ρ_m ($kg\,m^{-3}$) is the density of the paramagnetic medium, ρ_s ($kg\,m^{-3}$) is the density of the levitating sample, g is the acceleration due to gravity ($m\,s^{-2}$), χ_m and χ_s (both unitless) are the magnetic susceptibilities of the paramagnetic medium and the suspended sample, respectively, μ_0 ($T\,m\,A^{-1}$) is the magnetic permeability of free space, and B_0 (T) is the magnetic field strength at the surface of the magnet.

We crystallized each compound as a mixture of polymorphs (see Supporting Information for details). Approximately 0.5 mg of the mixture of crystals was placed into a cuvette filled with an aqueous solution of manganese(II) chloride ($MnCl_2$), and the container was placed between the magnets. The densities and magnetic susceptibilities of the paramagnetic solutions were adjusted empirically (concentrations were in the range 0.7–3.0 M) to achieve levitation, and to allow separation of the crystals by density (see Supporting Information for details). To minimize the adhesion of air bubbles to the surface of the crystals, we added 1% Tween 20 to the paramagnetic solution, introduced the crystals, and degassed and sonicated the mixture. Polymorphs required seconds to minutes to reach their equilibrium levitation heights, h, once placed in the MagLev device (Figure 2).

The average density of the crystals calculated using MagLev ($n = 7$) correlate well with that obtained using

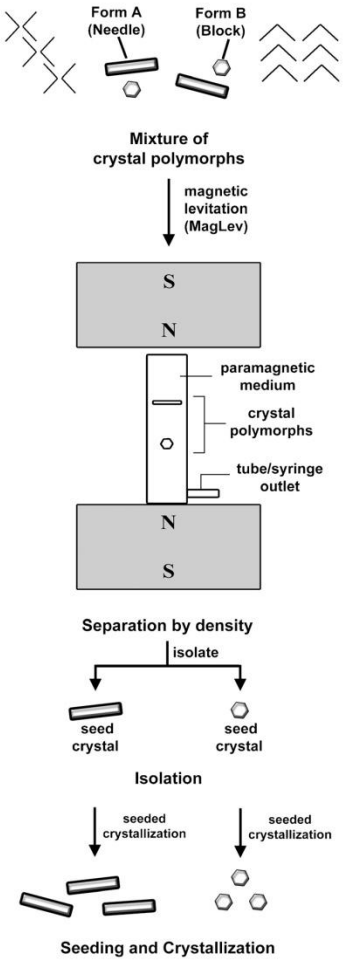

Figure 1. Separation, isolation, and seeding of crystal forms using MagLev, for a polymorphic system that crystallizes as Form A (needles) and Form B (blocks). The compound adopts different structural orientations in Form A and B. MagLev enables separation and isolation of these two crystal forms by their difference in density and enables the subsequent use of these forms to seed crystallizations of single polymorphs.

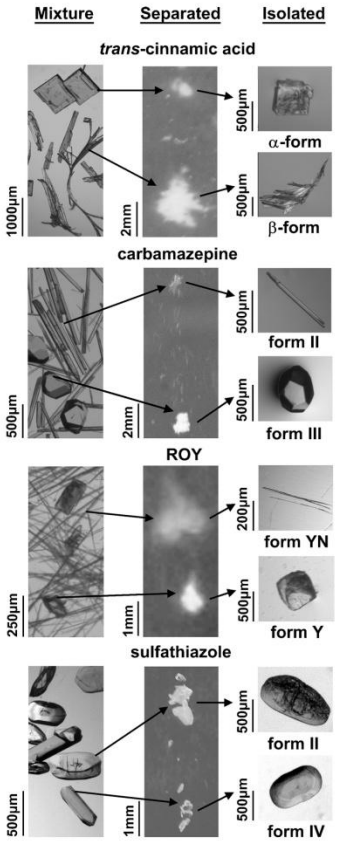

Figure 2. Photographs showing mixtures of crystal polymorphs (left), their separation using MagLev levitating at their respective equilibrium heights (middle), and their isolated forms (right). A mixture of α (top; $\rho = 1.251 \pm 0.006\ g\,cm^{-3}$) and β (bottom; $\rho = 1.268 \pm 0.005\ g\,cm^{-3}$) polymorphs of *trans*-cinnamic acid **4** are separated in MagLev using an aqueous solution of 0.7 M $MnCl_2$, 0.9 M $ZnCl_2$, 0.8 mL glycerine, 1% Tween 20. A mixture of form YN (top; $\rho = 1.419 \pm 0.010\ g\,cm^{-3}$), form Y (bottom; $\rho = 1.450 \pm 0.010\ g\,cm^{-3}$) of ROY **1** is separated in MagLev using an aqueous solution of 3.0 M $MnCl_2$, 0.5 M $ZnCl_2$, 1% Tween 20. A mixture of form II (top; $\rho = 1.541 \pm 0.001\ g\,cm^{-3}$) and form IV (bottom; $\rho = 1.580 \pm 0.001\ g\,cm^{-3}$) of sulfathiazole **2** is separated in MagLev using an aqueous solution of 0.965 M $MnCl_2$, 4.19 M $ZnCl_2$, 1% Tween 20. A mixture of form II (top; $\rho = 1.271 \pm 0.004\ g\,cm^{-3}$) and form III (bottom; $\rho = 1.320 \pm 0.004\ g\,cm^{-3}$) of carbamazepine **3** is separated in MagLev using an aqueous solution of 2 M $MnCl_2$, 1 M $ZnCl_2$, 1% Tween 20.

XRD (Figure 3) with an R^2 value of 0.993. For example, sulfathiazole **2** gives these densities ($g\,cm^{-3}$): form II, 1.541 ± 0.001 (MagLev) and 1.546[23] (XRD); form IV, 1.580 ± 0.001 (MagLev) and 1.600[23] (XRD). The difference in density between the crystal forms determined by MagLev and XRD are $\Delta\rho = 0.005\ g\,cm^{-3}$ for form II and $\Delta\rho = 0.02\ g\,cm^{-3}$ for form IV.

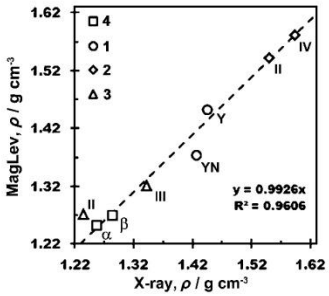

Figure 3. Comparison of the densities of crystal polymorphs measured using MagLev ($n = 7$) and estimated from XRD. The error bars are smaller than the data points and are not shown for clarity.

After separation of the polymorphs by density using MagLev, we isolated samples of each form to use as seeds for selective nucleation. We used two syringes—each coupled to the container by tubing—to withdraw crystals levitating at specific locations (see Supporting Information for details). The crystal structure of each isolate was confirmed using XRD. The unit cell parameters were collected for seven crystals from each isolation container and compared with unit cell parameters from seven random crystals collected before being placed in the paramagnetic media. No difference in crystal form was observed among parameters of the unit cells of the crystals before and after separation. Given that the isolated crystals maintained their form, we demonstrated their utility as seeds for further crystallization using form Y of ROY **1** and form II of sulfathiazole **2** (see Supporting Information for details).

MagLev is the first convenient technique capable of separating crystal polymorphs. This capability is useful in isolating seed crystals for crystallization,[24] identifying the presence of multiple crystalline forms,[25] and separating mixtures of crystal forms when crystal morphologies and/or shapes are visually indistinguishable. This technique is also applicable for separations of other crystal types that include pseudopolymorphs (e.g. solvates) and chiral systems (see Supporting Information). We expect this approach to be useful for separations of minerals and other crystalline materials (e.g. cocrystals).[26]

MagLev has two useful characteristics for separating mixtures of crystal polymorphs: 1) The separation of crystals (with dimensions of approximately $250 \times 30 \times 30\ \mu m$ for the smallest needles; approximately $50 \times 50 \times 50\ \mu m$ for the smallest irregular-shaped crystals, prisms, trapezoids) is automated and rapid. Upon introduction into the MagLev device, suspended crystals equilibrate to their equilibrium positions in seconds to minutes. 2) It enables simultaneous identification, separation, and isolation of polymorphs by density. The densities obtained can conveniently be compared with densities estimated by XRD.

MagLev also has limitations as a method for separating crystal polymorphs by density: 1) There is no single best levitation medium for all crystals. Each crystal system may require a different paramagnetic medium (in terms of the

concentrations of paramagnetic and diamagnetic ions). 2) The crystal may be soluble in a particular paramagnetic medium. The rate of dissolution of the crystal in the medium is dependent upon the solubility and surface area of the crystal. The potential for dissolution requires that the crystals separate within the timescale of the experiment. In the experiments summarized in Figure 2, the crystals (by qualitative observation) seemed stable in suspension for periods ranging from a minimum of one hour (forms II and IV of **2**) to three days (form Y of **1**). In addition, there was no apparent color change in the solution and/or of the crystals that suggested coordination of the organic compound with manganese ions. 3) Crystals smaller than about 5 μm in diameter remain dispersed as a result of Brownian motion, and do not localize at a well-defined equilibrium levitation height.

MagLev can make separating and isolating polymorphs for seeding more straightforward than existing methods, even in situations when the desired crystals cannot be separated manually and where the presence of multiple polymorphs may not be obvious.

Received: June 27, 2013
Published online: August 12, 2013

Keywords: crystal growth · crystal polymorphs · density · magnetic properties · paramagnetic solution

[1] a) J. Bernstein, *Polymorphism in Molecular Crystals*, Oxford University Press, Oxford, **2002**; b) *Polymorphism: In the Pharmaceutical Industry*, (Ed.: R. Hilfiker), Wiley-VCH, Weinheim, **2006**.

[2] G. Desiraju, J. J. Vittal, A. Ramanan, *Crystal Engineering: A Textbook*, World Scientific, Singapore, **2011**.

[3] a) K. A. Mirica, S. S. Shevkoplyas, S. T. Phillips, M. Gupta, G. M. Whitesides, *J. Am. Chem. Soc.* **2009**, *131*, 10049–10058; b) A. Winkleman, R. Perez-Castillejos, K. L. Gudiksen, S. T. Phillips, M. Prentiss, G. M. Whitesides, *Anal. Chem.* **2007**, *79*, 6542–6550; c) N. D. Shapiro, S. Soh, K. A. Mirica, G. M. Whitesides, *Anal. Chem.* **2012**, *84*, 6166–6172.

[4] a) K. A. Mirica, S. T. Phillips, S. S. Shevkoplyas, G. M. Whitesides, *J. Am. Chem. Soc.* **2008**, *130*, 17678–17680; b) K. A. Mirica, S. T. Phillips, C. R. Mace, G. M. Whitesides, *J. Agric. Food Chem.* **2010**, *58*, 6565–6569; c) F. Ilievski, K. A. Mirica, A. K. Ellerbee, G. M. Whitesides, *Soft Matter* **2011**, *7*, 9113–9118; d) N. D. Shapiro, K. A. Mirica, S. Soh, S. T. Phillips, O. Taran, C. R. Mace, S. S. Shevkoplyas, G. M. Whitesides, *J. Am. Chem. Soc.* **2012**, *134*, 5637–5646.

[5] T. D. Keene, D. J. Price, C. J. Kepert, *Dalton Trans.* **2011**, *40*, 7122–7126.

[6] a) F. Allen, *Acta Crystallogr. Sect. B* **2002**, *58*, 380–388; b) J. Bernstein, *Cryst. Growth Des.* **2011**, *11*, 632–650.

[7] G. P. Stahly, *Cryst. Growth Des.* **2007**, *7*, 1007–1026.

[8] a) J. Bernstein, R. J. Davey, J.-O. Henck, *Angew. Chem.* **1999**, *111*, 3646–3669; *Angew. Chem. Int. Ed.* **1999**, *38*, 3440–3461; b) A. Y. Lee, D. Erdemir, A. S. Myerson, *Annu. Rev. Chem. Biomol. Eng.* **2011**, *2*, 259–280.

[9] a) K. Hunger, *Rev. Prog. Color. Relat. Top.* **1999**, *29*, 71–84; b) M. U. Schmidt, D. W. M. Hofmann, C. Buchsbaum, H. J. Metz, *Angew. Chem.* **2006**, *118*, 1335–1340; *Angew. Chem. Int. Ed.* **2006**, *45*, 1313–1317.

[10] a) M. C. Etter, R. B. Kress, J. Bernstein, D. J. Cash, *J. Am. Chem. Soc.* **1984**, *106*, 6921–6927; b) D. E. Cohen, J. B. Benedict, B. Morlan, D. T. Chiu, B. Kahr, *Cryst. Growth Des.* **2007**, *7*, 492–495.

[11] a) M. F. Foltz, C. L. Coon, F. Garcia, A. L. Nichols, *Propellants Explos. Pyrotech.* **1994**, *19*, 19–25; b) F. P. A. Fabbiani, C. R. Pulham, *Chem. Soc. Rev.* **2006**, *35*, 932–942.

[12] D. Erdemir, A. Y. Lee, A. S. Myerson, *Acc. Chem. Res.* **2009**, *42*, 621–629.

[13] J. D. Dunitz, J. Bernstein, *Acc. Chem. Res.* **1995**, *28*, 193–200.

[14] D. Mangin, F. Puel, S. Veesler, *Org. Process Res. Dev.* **2009**, *13*, 1241–1253.

[15] J. A. Zerkowski, J. C. MacDonald, G. M. Whitesides, *Chem. Mater.* **1997**, *9*, 1933–1941.

[16] J. Thun, L. Seyfarth, C. Butterhof, J. Senker, R. E. Dinnebier, J. Breu, *Cryst. Growth Des.* **2009**, *9*, 2435–2441.

[17] D. Das, L. J. Barbour, *J. Am. Chem. Soc.* **2008**, *130*, 14032–14033.

[18] A. Gavezzotti, G. Filippini, *J. Am. Chem. Soc.* **1995**, *117*, 12299–12305.

[19] S. Chen, I. A. Guzei, L. Yu, *J. Am. Chem. Soc.* **2005**, *127*, 9881–9885.

[20] O. K. Farha, K. L. Mulfort, A. M. Thorsness, J. T. Hupp, *J. Am. Chem. Soc.* **2008**, *130*, 8598–8599.

[21] a) C. R. Mace, O. Akbulut, A. A. Kumar, N. D. Shapiro, R. Derda, M. R. Patton, G. M. Whitesides, *J. Am. Chem. Soc.* **2012**, *134*, 9094–9097; b) O. Akbulut, C. R. Mace, R. V. Martinez, A. A. Kumar, Z. Nie, M. R. Patton, G. M. Whitesides, *Nano Lett.* **2012**, *12*, 4060–4064.

[22] R. C. Kelly, N. Rodríguez-Hornedo, *Org. Process Res. Dev.* **2009**, *13*, 1291–1300.

[23] P. McArdle, Y. Hu, A. Lyons, R. Dark, *CrystEngComm* **2010**, *12*, 3119–3125.

[24] W. Beckmann, *Org. Process Res. Dev.* **2000**, *4*, 372–383.

[25] a) A. J. Alvarez, A. Singh, A. S. Myerson, *Cryst. Growth Des.* **2009**, *9*, 4181–4188; b) D. E. Braun, P. G. Karamertzanis, J.-B. Arlin, A. J. Florence, V. Kahlenberg, D. A. Tocher, U. J. Griesser, S. L. Price, *Cryst. Growth Des.* **2010**, *10*, 210–220.

[26] a) M. B. J. Atkinson, S. V. Santhana Mariappan, D.-K. Bučar, J. Baltrusaitisa, T. Friščić, N. G. Sinad, L. R. MacGillivray, *Proc. Natl. Acad. Sci. USA* **2011**, *108*, 10974–10979; b) M. B. J. Atkinson, I. Halasz, D.-K. Bučar, R. E. Dinnebier, S. V. Santhana Mariappan, A. N. Sokolov, L. R. MacGillivray, *Chem. Commun.* **2011**, *47*, 236–238.

Angewandte Chemie
Eine Zeitschrift der Gesellschaft Deutscher Chemiker

Supporting Information

69451 Weinheim, Germany

Using Magnetic Levitation to Separate Mixtures of Crystal Polymorphs**

Manza B. J. Atkinson, David K. Bwambok, Jie Chen, Prashant D. Chopade, Martin M. Thuo, Charles R. Mace, Katherine A. Mirica, Ashok A. Kumar, Allan S. Myerson, and George M. Whitesides**

anie_201305549_sm_miscellaneous_information.pdf

Supporting Information

1. Materials

Sulfathiazole **2** was purchased from TCI America. Carbamazepine **3** was purchased from VWR International (Pittsburgh, PA). Compounds 5-methyl-2-[(2-nitrophenyl)amino]-3-thiophenecarbonitrile (ROY) **1**, trans-cinnamic acid **4**, and ibuprofen (S- and R,S- forms) **5** were purchased from Sigma Aldrich Company (St. Louis, MO). All compounds were used as received. All solvents used in this study were purchased from Sigma Aldrich Company (St. Louis, MO) and used as received.

The NdFeB magnets (5 cm × 5 cm × 2.5 cm) were purchased from K&J Magnetics (www.kjmagnetics.com) and aligned on top of one another 4.5 cm apart within aluminum blocks. Calibrated density standards (±0.0002 g cm^{-3} at 23°C) were purchased from American Density Materials (Stauton, VA; www.densitymaterials.com). Spherical polymer samples were purchased from McMaster-Carr (www.mcmaster.com). Polystyrene microspheres with precisely defined radii were supplied by Duke Scientific Corporation (www.dukescientific.com), Polysciences, Inc. (www.polysciences.com), and Spherotech (www.spherotech.com). All other samples and reagents were purchased from Sigma Aldrich (Atlanta, GA) and used without further purification.

Crystals of diffraction quality were characterized using single crystal X-ray diffraction, while crystals of poor diffraction quality, or a size too small for single crystal X-ray were characterized using Raman spectroscopy or powder X-ray diffraction (PXRD). Crystal data were collected on an APEX II DUO CCD diffractometer and an APEX II CCD diffractometer using MoK_α radiation ($\lambda = 0.7107$ Å) at 100K. Raman spectra were obtained using a Raman

Microprobe (Kaiser Optical Systems), equipped with a diode laser as the excitation source at 785 nm, an optical light microscope (Leica), and a CCD camera. Images of crystals were taken using a Zeiss SteREO Discovery V8 microscope.

2. Polymorphism

Polymorphs can have differences in the following properties: density, ρ;[1] morphology; melting point;[2] stability;[3] solubility;[4] color;[5] sensitivity to detonation;[6] solid-state reactivity;[7] absorptivity;[8] electrical conductivity;[9] magnetic susceptibility;[10] tendency to charge triboelectrically;[11] flowability;[12] agglomeration;[13] tableting,[14] hygroscopicity,[15] and index of refraction.[9a,16]

Polymorphism is of particular interest in the pharmaceutical industry. Drugs made from different polymorphic forms of the same active ingredient can vary in stability, solubility and dissolution rate and thus bioavailability. A well-known example of a drug that exhibits polymorphism is Ritonavir, a protease inhibitor. The appearance of a second, less soluble polymorph of Ritonavir resulted in the need to reformulate the drug two years after it was launched.[17]

3. Methods

3.1. Preparation of crystal polymorphs

Y and YN polymorphs of ROY. ROY (0.040 g) was dissolved in 1 mL of isopropanol and allowed to crystallize at room temperature. Yellow needles and prisms formed rapidly over a period of three to five minutes. For seeding experiments, single crystals of form Y isolated from MagLev, were placed in a solution containing 20 mg of ROY dissolved in 3 mL of ethanol (200

proof) after hot filtration. Product crystals were left to crystallize upon cooling to room temperature for a period of 24 hours.

Polymorphs II and IV of sulfathiazole. Sulfathiazole, (0.020 g) was dissolved in 2.5 mL of ethanol and left to crystallize upon cooling of solvent at room temperature. Crystals formed over a period of twenty-four hours. For seeding experiments, single crystals of form II isolated from MagLev, were placed in a solution containing 20 mg of sulfathiazole dissolved in 2 mL of nitromethane after hot filtration. Product crystals were left to crystallize upon cooling to room temperature for a period of one hour.

α- and β- forms of trans-cinnamic acid. trans-Cinnamic acid (0.250 g) was dissolved in 1 mL of ethanol (200 proof), and left to crystallize at room temperature. Curved needles and blocks formed over a period of five minutes.

Polymorphs II and III of carbamazepine. Carbamazepine (0.020 g) was dissolved in 3 mL of toluene, and left to crystallize at room temperature. Long needles and prisms formed over a period of twenty-four hours.

R,S-Ibuprofen. Single crystals of RS-Ibuprofen were prepared by dissolving 40 mg of solid in 2 mL of ethanol. The solution was allowed to evaporate at room temperature to afford single crystals of the racemate.

S-Ibuprofen. Single crystals of S-Ibuprofen were prepared by gently heating 1 g of solid in 0.5 mL of diethyl ether in a closed 1.8 mL vial on a hot plate. The solution was then left on the hot plate, and crystallization occurred as the plate cooled to room temperature.

Figure S1. a) Molecular structure of ibuprofen. b) Photographs of single crystals of R,S-Ibuprofen and S-Ibuprofen levitating in an aqueous 0.55 M $MnCl_2$ solution containing 0.25 M sucrose and 1.0% Tween 20.

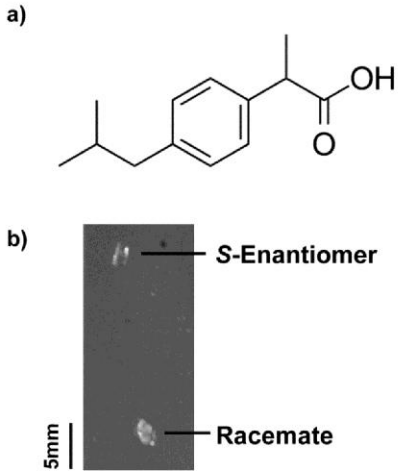

3.2. MagLev Apparatus

Figure S2. Photographs of components for isolating crystal polymorphs. a) A plastic cuvette composed of polymethyl methacrylate (PMMA). Holes of either 3/16" or 5/8" diameter were drilled approximately 2 mm from the bottom of the cuvette. Silicone rubber tubing is cut in 3 inch pieces and placed inside the holes of the cuvette. Five-minute epoxy is used to seal the tubing and cuvette. Luer locks are placed at the end of the tubes. Plastic syringes are connected to the Luer locks for extraction of the fluid. b) A cuvette holder made of transparent acrylic polymer. The acrylic block has a slit for the cuvette to slide into the center and a nylon screw to further secure the cuvette from moving. c) Complete assembly that includes syringes mounted on a microscopy stage.

a)

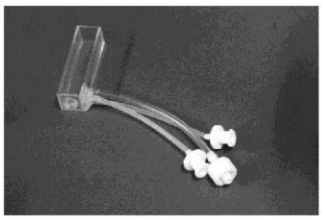

b)

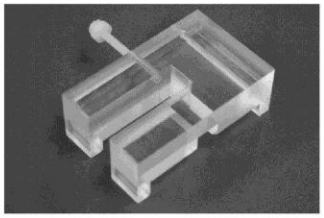

c)

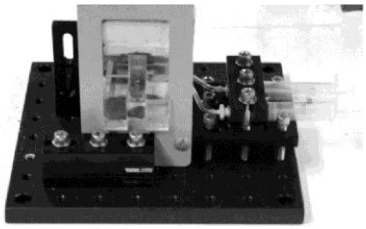

Figure S3. Isolating crystal polymorphs. (i) A syringe is used to withdraw the paramagnetic medium and the more dense population of crystals suspended within. (ii) As the first population of crystals from the paramagnetic medium is being removed, the less dense moves with the meniscus toward the bottom of the cuvette. The syringes were disconnected from the tubes and the contents were ejected into an empty container.

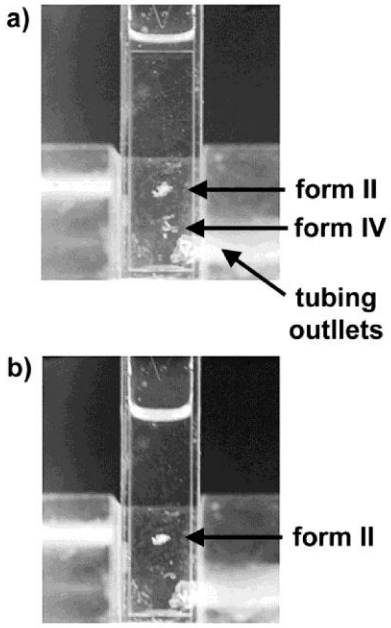

Figure S4. Photographs of seed crystals isolated from MagLev and products of seeded crystallizations of form Y of ROY **1**, and form II of sulfathiazole, **2**. The product of form Y of ROY increases in size (~2x). The product crystals of sulfathiazole (form II), show nucleation on the surface of the seed crystals.

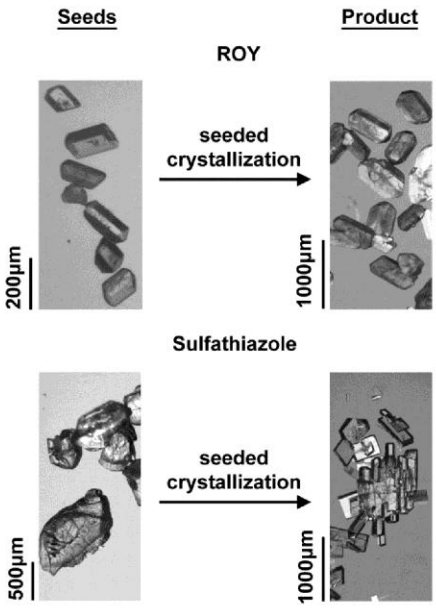

4. X-ray Crystallographic Information

Single crystals were taken from each experiment before and after levitation. The unit cell dimensions of each crystal were collected and used to confirm the polymorphic form. Equation 2 is used to determine if the unit cell parameters are significantly different before and after MagLev, where Δ is the difference between the two parameters and σ_1 is the standard uncertainty of the unit cell parameter of a crystal before levitation and σ_2 is the standard uncertainty of the

$$\frac{\Delta}{\sqrt{\sigma_1^2 + \sigma_2^2}} \geq 3 \qquad (2)$$

unit cell parameter of a crystal after levitation.[18] If the difference (Δ) between the unit cell parameters from Eq.(2), is more than three times the standard uncertainty of the difference, than the two unit cells are significantly different. In contrast, if the difference (Δ) between the unit cell parameters is less than three times the standard uncertainty of the difference, than the two unit cells are not significantly different. The density of the solids were calculated by incorporating the values obtained from the unit cell data into equation 3 as shown below, where ρ is the density (g cm^{-3}), M is the mass of a mole of molecules (kg), N_A is Avogadro's number, V is

$$\rho = \frac{MN_A}{V^3 Z} \qquad (3)$$

the volume of the unit cell (cm^3), and Z is the number of molecules per unit cell.[18]

4.1. X-ray Crystallographic Tables

Table S1. Unit cell values obtained from literature and average unit cell values from single crystal x-ray crystallography of seven crystals before levitation and after levitation in the paramagnetic medium. Quantitative differences between the average unit cell parameters before and after levitation are calculated by using the 3σ rule as calculated from equation 2. No value is significantly different owing to the fact that no value for each parameter is greater than three.

Compound	Form	Unit Cell Experiment	a	b	c	α	β	γ	V (Å^3)
1	Y	Literature	8.5001(8)	16.413(2)	8.5371(5)	90	91.767(7)	90	1190.5(4)
		Before MagLev	8.494(7)	16.08(1)	8.501(6)	90	91.36(3)	90	1161(2)
		After MagLev	8.477(6)	16.036(7)	8.486(4)	90	91.28(3)	90	1153(1)
		3σ test value	2.064	2.699	1.82	N/A	1.835	N/A	2.36
2	II	Literature	8.235(4)	8.550(4)	15.558(8)	90	93.67(1)	90	1093.181
		Before MagLev	8.195(4)	8.48(5)	15.45(1)	90	94.17(4)	90	1078(1)
		After MagLev	8.20(2)	8.56(1)	15.56(8)	90	94.3(2)	90	1090(8)
		3σ test value	0.5008	1.391	1.354	N/A	0.5942	N/A	1.409
	IV	Literature	10.774(1)	8.467(1)	11.367(1)	90	91.65(1)	90	1036.507
		Before MagLev	10.78(1)	8.480(2)	11.395(4)	90	91.62(2)	90	1041(1)
		After MagLev	10.81(1)	8.498(9)	11.41(1)	90	91.75(5)	90	1048(3)
		3σ test value	1.469	1.797	1.342	N/A	2.278	N/A	1.639
3	II	Literature	35.454(3)	35.454(3)	5.253(1)	90	90	120	5718.321
		Before MagLev	35.20(4)	35.20(4)	5.176(5)	90	90	120	5555(18)
		After MagLev	35.27(7)	35.27(7)	5.17(1)	90	90	120	5579(34)
		3σ test value	0.8747	0.8747	0.02111	N/A	N/A	N/A	0.03969
	III	Literature	7.534(1)	11.150(2)	13.917(3)	90	92.94(4)	N/A	1167.546
		Before MagLev	7.505(4)	11.06(5)	13.79(1)	90	92.96(4)	90	1143(1)
		After MagLev	7.53(2)	11.091(1)	13.82(8)	90	92.9(2)	90	1153(8)
		3σ test value	0.5008	1.391	0.9902	N/A	0.5942	N/A	1.409
4	α	Literature	5.582(2)	17.671(4)	7.735(2)	90	96.49(2)	90	758.087
		Before MagLev	5.547(9)	17.51(3)	7.70(1)	90	96.24(1)	90	743(4)
		After MagLev	5.557(8)	17.55(1)	7.73(1)	90	96.29(8)	90	749(3)
		3σ test value	0.7457	1.038	1.036	N/A	0.5726	N/A	0.9869

4.2. Raman Spectra

Figure S5. Raman spectra before and after MagLev showing the characteristic stretches of a) form YN of ROY, b) β-trans-cinnamic acid, and (c) S- and RS-Ibuprofen. The characteristic Raman shifts are similar before and after levitation showing that the polymorphs have the same form before and after MagLev.

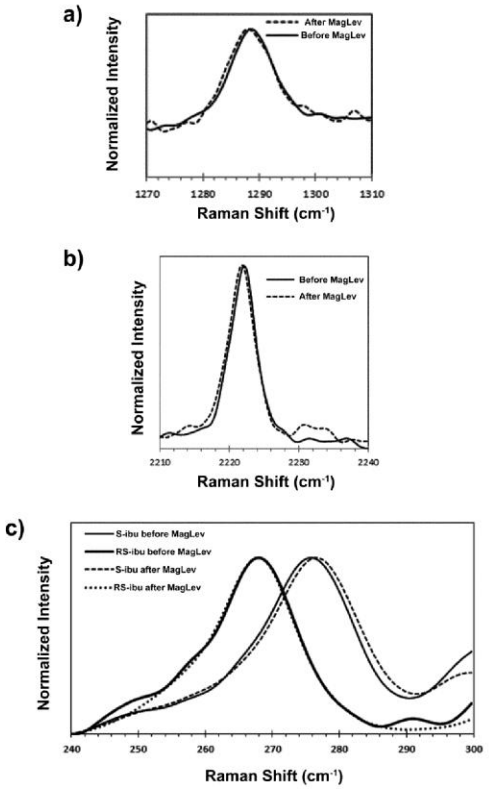

4.3. Powder X-ray diffraction

Figure S6. Powder X-ray diffraction patterns of trans-cinnamic acid (signature peaks are highlighted with an asterisk, *). a) The experimental PXRD of the β-polymorph (needle-like plates) of trans-cinnamic acid. b) The simulated PXRD pattern of β-polymorph of trans-cinnamic acid. The β-polymorph is confirmed as evidenced by the simulated pattern that matches with the experimental.

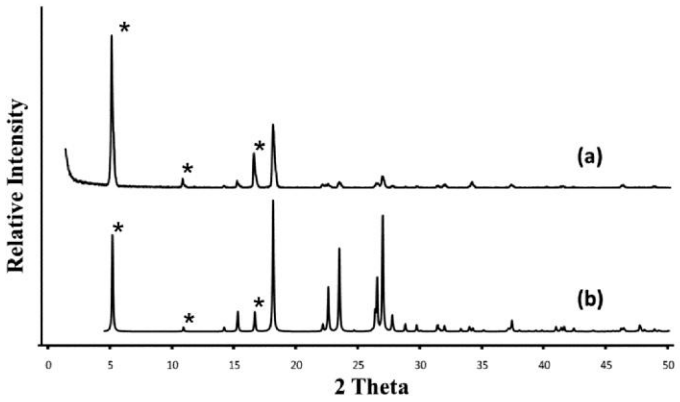

4.4. Densities calculated from X-ray and MagLev

Table S2. Average values (calculated from seven independent measurements) and the uncertainty in measurement of density of all solids. We calculated the densities of the crystals using calibration curves determined from levitation heights using density standards (i.e. glass, polymer beads) as previously reported.[19]

Compound	Form	ρ (g/cm^3) X-ray	ρ (g/cm^3) MagLev
ROY	YN	1.428[20]	1.372±0.020
	Y	1.447[20]	1.450±0.006
sulfathiazole	II	1.546[21]	1.541±0.004
	IV	1.600[21]	1.580±0.004
trans-cinnamic acid	α	1.265[22]	1.251±0.006
	β	1.286[23]	1.268±0.006
carbamazepine	II	1.235[24]	1.271±0.004
	III	1.343[25]	1.320±0.004
ibuprofen	S	1.099[26]	1.091±0.001
	R,S	1.119[27]	1.108±0.001

References

[1] A. Gavezzotti, G. Filippini, J. Am. Chem. Soc. **1995**, 117, 12299-12305.

[2] D. Giron, Thermochim. Acta **1995**, 248, 1-59.

[3] L. Yu, J. Pharm. Sci. **1995**, 84, 966-974.

[4] a) J. Bauer, S. Spanton, R. Henry, J. Quick, W. Dziki, W. Porter, J. Morris, Pharm. Res. **2001**, 18, 859-866; b) L.-F. Huang, W.-Q. Tong, Adv. Drug Delivery Rev. **2004**, 56, 321-334.

[5] a) L. Yu, J. Phys. Chem. A **2001**, 106, 544-550; b) L. Yu, Acc. Chem. Res. **2010**, 43, 1257-1266.

[6] R. M. Vrcelj, H. G. Gallagher, J. N. Sherwood, J. Am. Chem. Soc. **2001**, 123, 2291-2295.

[7] a) M. D. Cohen, G. M. J. Schmidt, F. I. Sonntag, J. Chem. Soc. **1964**, 2000-2013; b) T. Friščić, L. R. MacGillivray, Chem. Commun. **2009**, 773-775. c) M. B. J. Atkinson, A. N. Sokolov, D.-K. Bučar, S. V. S. Mariappan, M. T. Mwangi, M. C. Tiedman, L. R. MacGillivray, Photochem. Photobiol. Sci. **2011**, 10, 1384-1386.

[8] P. Li, I. W. Chen, J. E. Penner-Hahn, Phys. Rev. B: Condens. Matter **1993**, 48, 10063-10073.

[9] a) G. Barbarella, M. Zambianchi, L. Antolini, P. Ostoja, P. Maccagnani, A. Bongini, E. A. Marseglia, E. Tedesco, G. Gigli, R. Cingolani, J. Am. Chem. Soc. **1999**, 121, 8920-

8926; b) T. Siegrist, C. Kloc, J. H. Schön, B. Batlogg, R. C. Haddon, S. Berg, G. A. Thomas, Angew. Chem. Int. Ed. **2001**, 40, 1732-1736.
[10] R. A. Heintz, H. Zhao, X. Ouyang, G. Grandinetti, J. Cowen, K. R. Dunbar, Inorg. Chem. **1998**, 38, 144-156.
[11] S. Airaksinen, M. Karjalainen, E. Räsänen, J. Rantanen, J. Yliruusi, Int. J. Pharm. **2004**, 276, 129-141.
[12] A. Nokhodchi, M. Maghsoodi, D. Hassan-Zadeh, M. Barzegar-Jalali, Powder Technol. **2007**, 175, 73-81.
[13] a) Y. Kawashima, T. Niwa, H. Takeuchi, T. Hino, Y. Itoh, S. Furuyama, J. Pharm. Sci. **1991**, 80, 472-478; b) A. Angermann, J. Töpfer, J. Mater. Sci. **2008**, 43, 5123-5130.
[14] C. Sun, D. W. Grant, Pharm. Res. **2001**, 18, 274-280.
[15] V. Niederwanger, F. Gozzo, U. J. Griesser, J. Pharm. Sci. **2009**, 98, 1064-1074.
[16] a) Y.-n. Xu, W. Y. Ching, Phys. Rev. B: Condens. Matter **1991**, 44, 11048-11059; b) H. S. Nalwa, T. Saito, A. Kakuta, T. Iwayanagi, J. Phys. Chem. **1993**, 97, 10515-10517; c) M. Brinkmann, G. Gadret, M. Muccini, C. Taliani, N. Masciocchi, A. Sironi, J. Am. Chem. Soc. **2000**, 122, 5147-5157.
[17] a) S. R. Chemburkar, J. Bauer, K. Deming, H. Spiwek, K. Patel, J. Morris, R. Henry, S. Spanton, W. Dziki, W. Porter, J. Quick, P. Bauer, J. Donaubauer, B. A. Narayanan, M. Soldani, D. Riley, K. McFarland, Org. Process Res. Dev. **2000**, 4, 413-417; b) J. Bauer, S. Spanton, R. Henry, J. Quick, W. Dziki, W. Porter, J. Morris, Pharmaceut Res **2001**, 18, 859-866.
[18] W. Clegg, A. J. Blake, R. O. Gould, P. Main, Crystal Structure Analysis: Principles and Practice, **2002**.
[19] K. A. Mirica, S. S. Shevkoplyas, S. T. Phillips, M. Gupta, G. M. Whitesides, J. Am. Chem. Soc. **2009**, 131, 10049-10058.
[20] G. A. Stephenson, T. B. Borchardt, S. R. Byrn, J. Bowyer, C. A. Bunnell, S. V. Snorek, L. Yu, J. Pharm. Sci. **1995**, 84, 1385-1386.
[21] P. McArdle, Y. Hu, A. Lyons, R. Dark, CrystEngComm **2010**, 12, 3119-3125.
[22] T.-J. Hsieh, C.-C. Su, C.-Y. Chen, C.-H. Liou, L.-H. Lu, J. Mol. Struct. **2005**, 741, 193-199.
[23] G. M. J. Schmidt, J. Chem. Soc. **1964**, 2014-2021.
[24] M. M. J. Lowes, M. R. Caira, A. P. Lotter, J. G. D. Van Watt, J. Pharm. Sci. **1987**, 76, 744-752.
[25] a) J. N. Lisgarten, R. A. Palmer, J. W. Saldanha, J. Chem. Crystallogr. **1989**, 19, 641-649; b) V. L. Himes, A. D. Mighell, W. H. De Camp, Acta Crystallogr., Sect. B: Struct. Sci **1981**, 37, 2242-2245.
[26] A. A. Freer, J. M. Bunyan, N. Shankland, D. B. Sheen, Acta Crystallogr., Sect. C: Cryst. Struct. Commun. **1993**, 49, 1378-1380.
[27] J. F. Cryst. Struct. Commun.McConnell, Cryst. Struct. Commun. **1974**, 3, 73-75.

Appendix VII

A Universal Mobile Electrochemical Detector Designed for Use in Resource-Limited Applications

Alex Nemiroski,[1] Dionysios C. Christodouleas,[1] Jonathan W. Hennek,[1] Ashok A. Kumar,[2] E. Jane Maxwell,[1] Maria Teresa Fernández-Abedul,[3] and George M. Whitesides[1,4,5]

[1] Department of Chemistry & Chemical Biology, Harvard University, Cambridge, MA 02138

[2] School of Engineering and Applied Science, Harvard University, Cambridge, MA 02138

[3] Departamento de Química Física y Analítica, Universidad de Oviedo, Asturias, Spain

[4] Wyss Institute for Biologically Inspired Engineering, Harvard University, Cambridge, MA 02138 USA

[5] The Kavli Insitute for Bionano Science, Harvard University, Cambridge, MA 02138 USA

Submitted to *Proc. Natl. Acad. Sci. U.S.A.*

ABSTRACT

This article describes an inexpensive, hand-held device that couples the most common forms of electrochemical analysis directly to "the cloud" using any mobile phone, for use in resource-limited settings. The device is designed to operate with a wide range of electrode formats, can perform on-board mixing of samples by vibration, and transmits data over voice using audio—an approach that guarantees broad compatibility with any available mobile phone (from low-end phones to smartphones) or cellular network (2, 3, or 4G). The electrochemical methods that we demonstrate enable quantitative, broadly applicable, and inexpensive sensing with flexibility based on a wide variety of important electroanalytical techniques (chronoamperometry, cyclic voltammetry, differential pulse voltammetry, square-wave voltammetry, and potentiometry), each with different uses. Four applications demonstrate the analytical performance of the device: these involve the detection of i) glucose in blood for personal health, ii) trace heavy metals—lead, cadmium, and zinc—in water for in-field environmental monitoring, iii) sodium in urine for clinical analysis, and iv) a malarial antigen, *Plasmodium falciparum* histidine-rich protein 2 (*Pf*HRP2), for clinical research. The combination of these electrochemical capabilities in an affordable, hand-held format that is compatible with any mobile phone or network worldwide guarantees that sophisticated diagnostic testing can be performed by users with a broad spectrum of needs, resources, and levels of technical expertise.

SIGNIFICANCE STATEMENT

The ability to perform electrochemical testing in the field, and in resource-limited environments, and to transmit data automatically to "the cloud" can enable a broad spectrum of analyses useful for personal and public health, clinical analysis, food safety, and environmental monitoring. Although the developed world has many options for analysis and web connection, the developing world, however, does not have broad access to either the expensive equipment necessary to perform these tests, or the advanced technologies required for network connectivity. To overcome these limitations, we have developed a simple, affordable, handheld device that can perform all the most common electrochemical analyses, and transmit the results of testing to the cloud with any phone, over any network, anywhere in the world.

INTRODUCTION

Electrochemistry provides a broad array of quantitative methods for detecting important analytes (e.g. proteins, nucleic acids, metabolites, metals) for personal and public health, clinical analysis, food and water quality, and environmental monitoring (1, 2). Although useful in a variety of settings, these methods—with the very important exception of glucometers for monitoring blood glucose (3, 4)—are generally limited to well-resourced laboratories run by skilled personnel. If simplified and made inexpensive, however, these versatile methods could become broadly applicable tools in the hands of healthcare workers, clinicians, farmers, and military personnel who need accurate and quantitative results in the field, especially in resource-limited settings. Furthermore, if results of testing were directly linked to "the cloud" through available mobile technology, expertise (and archiving of information) could be geographically decoupled from the site of testing. To enable electrochemical measurements to be performed and communicated in any setting, a useful technology must be: i) able to perform complete electrochemical analyses while remaining low in cost, simple to operate, and as independent of infrastructure as possible, and ii) compatible with *any* generation of mobile telecommunications technology, including the low-end phones and 2G networks that continue to dominate communications in much of the developing world.

The parallel development of two successful technologies—mobile health (mHealth) and point-of-care (POC) diagnostics—is broadly agreed to provide two convergent paths towards a potential solution, although, practically, technical and conceptual connections between them are weak (5, 6). mHealth is the general term given to medical and health-related information technologies that depend on mobile wireless communication for connectivity. Although these networks and devices can capture information relevant to health (and other problems involving

chemical and biological sensing) and transmit it globally over the web, they typically do not have the capability to collect data directly, and rely, instead, on (error-prone) entry of data by the user, either alphanumerically or through images. Conversely, while POC diagnostics (e.g. lateral flow immunoassays, urinalysis dipsticks, and hand-held glucometers) provide examples of simple, inexpensive devices that enable minimally trained users to perform chemical testing, these devices are typically limited in function and cannot connect easily to networks for mHealth.

Many devices are now being explored that attempt to connect mHealth with POC testing. Because these systems have been developed in, and often implicitly targeted towards, the developed world, they typically require: i) smartphones; ii) custom applications (“apps"); iii) third or fourth generation (3G/4G) data networks; iv) proprietary connectors for sophisticated sensors that interface with diagnostic tests; and v), in some cases, a substantial level of technical sophistication (7-12). As such, these first-generation hybrid mHealth/POC devices are often too expensive, too restricted to a single type of phone, too limited in function, and too reliant on advanced mobile telecommunication technology to be practically applicable in resource-limited settings where 3G/4G networks and smartphones are still not widely used. Although mobile connectivity has spread rapidly across the world, low-end mobile phones and second-generation (2G) networks dominate the telecommunications infrastructure (especially in rural areas) in the developing world (7, 13-16), and will continue to do so for the foreseeable future (Figure VII.S5). This lack of advanced mobile technologies in much of the developing world, coupled with myriad operating systems, generations of software, and types of connecting ports amongst all mobile phones presents a major challenge to any device that requires a specific phone or application to communicate the results of testing.

To provide a system that combines broad flexibility in electrochemical capability with connectivity to the web through widely available technology, we have developed a low-cost (~$25),

handheld device that i) performs all of the most common electrochemical methods; ii) interfaces with a variety of commercially available electrodes; iii) provides on-board vibration to mix samples when necessary; and iv) is simple to operate. For communication of data, we have exploited the ubiquity of the hands-free audio port, a nearly universal interface to mobile phones, and designed a protocol to transmit digital data over a live voice connection. This approach guarantees that i) any phone can function as a modem to link the results of testing to a remote facility through any available mobile network (2, 3, or 4G), and that ii) the device does not require any specific software application, operating system, or connector (beyond an audio cable).

We refer to our device as a universal-mobile-electrochemical-detector (uMED) because of i) its universal compatibility with mobile technology, ii) the broad range of electrochemical techniques that it can perform, including various forms of amperometry, coulometry, voltammetry (e.g. cyclic, differential-pulse, square-wave), and potentiometry, and iii) its broad compatibility with different commercial available and paper-based electrodes. Figures VII.1a-b shows the uMED connected to a low-end mobile phone, and sketches the flow of information that links an in-field measurement to a remote facility.

We demonstrate the electrochemical capabilities of the uMED by first comparing the performance of each implemented mode of sensing to a commercial electrochemical analyzer. We then test the uMED in four representative applications: i) as a personal diagnostic device for the detection of glucose in blood, ii) for in-field testing of water quality by detection of heavy metals, and iii) as a low-cost, clinical analyzer for detection of electrolytes, and iv) to perform an electrochemical enzyme-linked immunosorbant assay (ELISA) for the detection of an antigen diagnostic of malaria. We also demonstrate the transmission of POC data by audio through a low-end mobile phone to a remote computer.

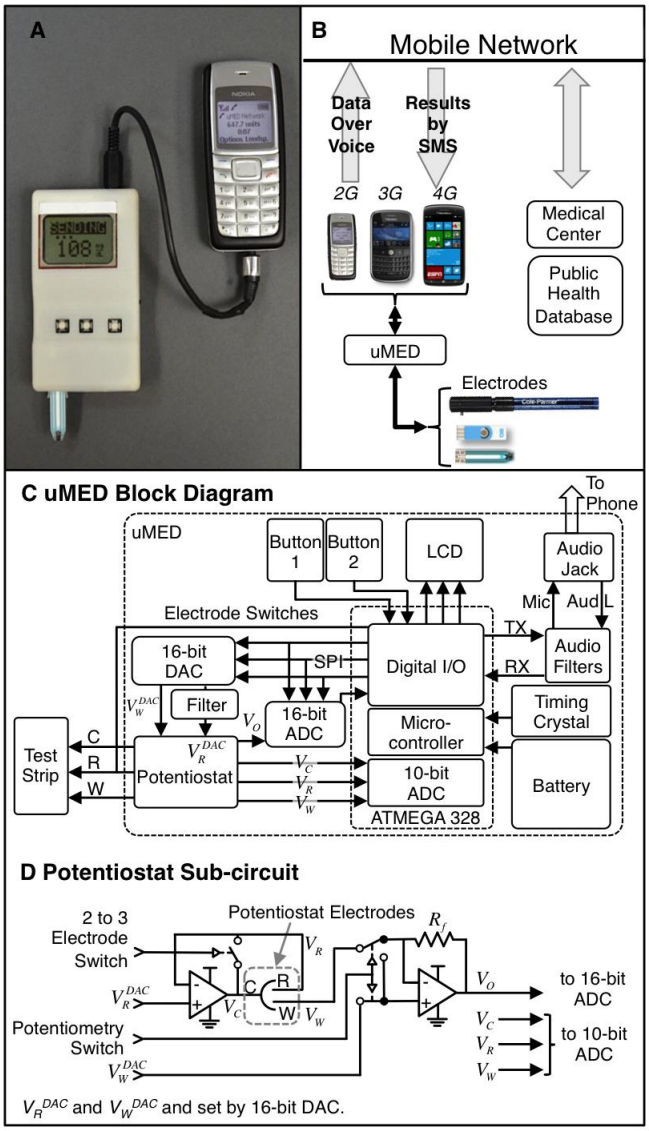

Figure VII.1: Details of the physical and network connections to and design of the uMED. (**A**) An image of the uMED interfaced to a commercial test-strip for data acquisition, and to a low-end mobile phone through a standard audio cable for transmission of data over voice. (**B**) A schematic of the connections and flow of data from the electrodes, through the uMED, to the remote medical back end. (**C**) A block diagram of the hardware and interconnections of the device. (**D**) The circuit design for the reconfigurable potentiostat.

EXPERIMENTAL DESIGN

Design of the uMED

Briefly, the device includes: i) a custom-made, three-electrode potentiostat, formed from two operational amplifiers, to perform electrochemical measurements; ii) three digital switches to reconFigure VII.the potentiostat between two- and three- electrode operation and between amperometric or potentiometric measurement, iii) a small vibration motor to mix fluid samples; iv) a dual-channel, 16-bit, digital-to-analog (DAC) converter to set the potentials of the reference electrode (RE) and working electrode (WE); v) a single-channel, 16-bit analog-to-digital (ADC) converter to sample data at high resolution; vi) a pair of sockets to interface with various electrodes; vii) a liquid crystal display (LCD) and three buttons to interface with the user; viii) an audio port to communicate data; ix) a microcontroller to operate the device; x) a serial port to program the microcontroller; xi) a 3.7-V lithium polymer battery to supply power to the device; and xii) a pair of 3.3-V voltage regulators to supply voltage independently to the digital (microprocessor) and analog (potentiostat and DAC) portions of the circuit. We chose the Atmega328 (Atmel) 8-bit microcontroller for its compatibility with the popular Arduino development environment and its many, programmable channels for input and output. We used a common 2.5-mm, 4-conductor audio cable to connect to the audio port of a mobile phone. Figure VII.1 shows a block diagram and circuit schematic that describes the electronic design of the device. We include part numbers and further technical details in the SI.

Modes of Electrochemical Detection

We designed the uMED to mimic the simplicity of a glucometer (whose acceptance by users worldwide is well tested) and the versatility of a bench-top potentiostat. The uMED can

perform (but is not limited to) the following five important types of electroanalytical techniques: i) cyclic voltammetry (CV), ii) chronoamperometry, iii) differential pulse voltammetry (DPV), iv) square wave voltammetry (SWV), and v) potentiometry. Each pulse sequence is stored in the device; when the user selects the appropriate mode using a button, the uMED acquires and computes data automatically without further input from the user. Depending on the selected mode, the microcontroller sets the potentiostat to measure current in a two-electrode (chronoamperometry) or three-electrode (CV, SWV, DPV) configuration, or voltage (potentiometry) in a two-electrode configuration. Figure VII.2 shows the time and voltage sequences implemented for the different types of measurements, and, when appropriate, the expected transient behavior of the measured current.

For **CV** (Figure VII.2a), the uMED sweeps the potential E applied between the RE and WE linearly from E_1 to E_2 (and back again), and measures the current I consumed by the electrochemical cell. Steps in voltage E_{step}, each held for a duration t_{step}, form a staircase ramp with a scan-rate E_{step}/t_{step}.

For **chronoamperometry**, the uMED applies a potential E between the counter electrode (CE) and WE for a fixed duration and measures the transient current I. Figure VII.2b shows an example of this pulse sequence in context of a specific application (glucometry). To improve the signal-to-noise ratio, the uMED i) begins the measurement at the point where the Faradaic current is dominant to reduce the effect of the initially large, non-Faradaic, capacitive current that is not related to the concentration of the analyte, and then ii) averages I over a fixed length of time Δt to decrease the influence of noise (which arises primarily from electrochemical and thermal fluctuations) by a factor of $\sqrt{\Delta t}$.

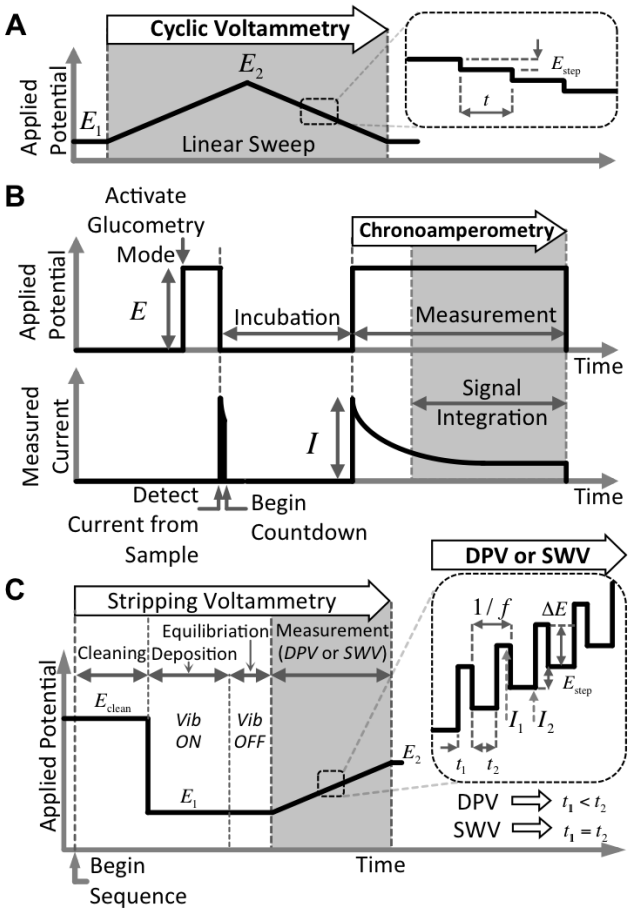

Figure VII.2: Examples of the timed sequence of applied potentials and measurement for a sample of possible pulse sequences. (**A**) Cyclic voltammetry. (**B**) Chronoamperometry in the context of glucometery. (**C**) SWV and DPV in the context of ASV.

For **DPV** and **SWV**, the uMED measures the current generated in the electrochemical cell during a series of regular voltage pulses applied between the RE and WE. Figure VII.2c shows an example of these pulse sequences used in context of a specific application (anodic stripping voltammetry, ASV). This pulse train has a peak-to-peak height ΔE, frequency $f = (t_1 + t_2)^{-1}$ (where t_1 is the pulse duration and t_2 is the time between pulses), and is superimposed on a linear sweep from E_1 to E_2. In these differential techniques, the device records the currents I_1 and I_2 immediately before a change in the applied voltage (i.e. at end of the pulse).

For **potentiometry**, the uMED measures the constant voltage *E* generated by the electrochemical species. To prevent destabilization of *E*, the uMED incorporates operational amplifiers with a high input impedance (~10^{12} Ω) that limit the current flowing during measurement to < 0.1 pA.

Electrochemical Characterization

To compare the performance of the uMED to that of a commercial, bench top electrochemical analyzer we used both devices to perform a series of five test measurements for each type of pulse sequence; i) **CV** on a solution of ferricyanide/ferrocyanide redox couple (linear sweep from $E_1 = -0.5\ V$ to $E_2 = 0.5$ V with $E_{step} = 2.5$ mV and a scan-rate of 50 mV/s); ii) **chronoamperometry** on a solution of ferrocyanide ions ($E = 0.5$ V for 30 s); iii) **SWV** ($E_1 = -0.2$ V, $E_2 = 0.6$ V, $f = 10$ Hz, $\Delta E = 50$ mV, $E_{step} = 4$ mV) and iv) **DPV** $E_1 = -0.2$ V, $E_2 = 0.6$ V, $f = 10$ Hz, $\Delta E = 140$ mV, $E_{step} = 7$ mV) on solutions of 1-naphthol, which we adapted from previous literature (2, 17, 18); and iv) **potentiometry** on solutions of sodium and potassium ions.

Electrochemical Applications

We used the device in four real applications that involve the detection of: i) glucose in blood by chronoamperometry ii) heavy metals in water by square wave ASV (SWASV), iii) sodium in urine by potentiometry, and iv) the malarial antigen *Plasmodium falciparum* histidine-rich protein 2 (*Pf*HRP2) through a sandwich, electrochemical ELISA using chronoamperometry for the detection step.

For these measurements, we used commercial glucose test strips, screen-printed electrodes (SPEs), and ion-selective electrodes (ISEs) to evaluate the performance of our device, ensure proper calibration, and determine the limits of detection in all modes of measurement. These electrodes are readily available, and guarantee that the device is immediately applicable to real-world testing. For cost-sensitive applications in the developing world, we would also expect to use inexpensive test strips made of paper of other materials (5, 6, 19-22).

Detection of Glucose in Blood. For the detection of blood glucose by chronoamperometry, we used glucose test strips (TrueTrak, CVS) and real blood samples (Meter Trax Control, Biorad). For each measurement, we selected glucometry from the uMED menu, inserted the test strip, and applied a droplet of blood (~5 µL, a volume easily obtained from a fingerprick) to the test strip. Application of the sample triggered the chronoamperometry sequence (Figure VII.2b), which began with an incubation period of 5 s at $E = 0$ followed by a measurement period of 10 s at $E = 0.5$ V. The uMED sampled the output signal at 8 Hz and digitally averaged the transient signal over the last $t = 5$ s of the measurement.

Detection of Heavy Metals in Water. For the detection of heavy metals (Zn(II), Cd(II) and Pb(II) by SWASV we used SPEs (DRP110-CNT, DropSens) that had three electrodes: i) a WE consisting of carbon ink modified by carbon nanotubes (23), ii) a CE consisting of carbon ink, and iii) a RE consisting of Ag/AgCl ink. This procedure requires a four-step pulse sequence (Figure

VII.2c) that we adapted from Nie et al. (7, 13-16, 19): i) Cleaning: A positive potential ($E_{clean} = 0.5\ \text{V}, 120\ \text{s}$) applied to the WE oxidizes any impurities from the electrode surface in order to prepare it for the measurement: ii) Deposition: A negative potential ($E_1 = -1.4\ \text{V}, 120\ \text{s}$) applied to the WE causes metal ions in solution to reduce onto the electrode surface, if the potential is more negative than the reduction potential of the metal. The solution must be agitated during this step so that the rate of deposition is not limited by the rate of diffusion: iii) Equilibration: The potential maintained at E_1 with no agitation for a short time (30 s) ensures equilibration of the solution: iv) Measurement: SWASV (SWV sequence from E_1 to $E_2 = -0.1$ V, at $\Delta E = 50$ mV, $E_{step} = 5$ mV, $f = 20$ Hz) causes the metals deposited on the electrode surface to re-oxidize and re-dissolve into the solution. The re-oxidation occurs when the potential at the WE matches the oxidation potential of the metal, so that the measured current exhibits a different peak for each metal species.

In ASV, agitation is necessary to facilitate the deposition of the ions onto the electrode. To eliminate the need for magnetic stirring in an electrochemical cell (a configuration that would add cost and complexity) we, instead, incorporated a small vibration motor (similar to one found in a mobile phone) into the uMED to mix the droplet on the SPE and enhance the depositions of ions onto the WE during the cleaning and deposition phases. The uMED applies 3.3 V to the motor to vibrate the sample at 530 Hz. This approach enabled us to perform a full measurement by: i) mixing an 80-µL droplet of aqueous sample containing the metal ions with a 20-µL droplet of the reagent solution, on top of the SPE, and then ii) activating the uMED to execute the fully automatic SWASV sequence in which the uMED mixes the sample, applies the pulse sequence, extracts the peak heights of all elements found, and displays the extracted data to the user.

Detection of Sodium in Urine. To detect sodium in urine by potentiometry, we used an ion-selective electrode (ISE, K27504-30, Cole-Palmer). We prepared a series of urine samples with

different levels of sodium from standard urine samples (Liquicheck Urine Chemistry Control, Biorad) that adjusted to pH ~ 9.5 using 4-M NH_4OH. To perform the measurement, we dipped the ISE into each sample, and recorded the potential difference between the RE and the WE. This voltage typically stabilized over a period of 0.5 – 10 min, with longer times required for lower concentrations.

Detection of Malaria. To perform a malaria immunoassay, we used chronoamperometry to measure the concentration of *Pf*HRP2 through a sandwich ELISA that we augmented for electrochemical detection (7, 13-16). The detecting antibody was conjugated to horseradish peroxidase (HRP), which oxidized 3,3',5,5'-tetramethylbenzidine (TMB), a widely used chromogenic substrate. We performed this reaction in a 96-well-plate and then pipetted a drop of solution onto a commercial SPE (DRP110-CNT, DropSens). The uMED detected the oxidized product by performing chronoamperometry for 20 s at $\Delta E = 0.2$ V, and sampling the output signal at 20 Hz, digitally averaged the transient signal over the last t = 8 s of the measurement. We include more details for all measurements in the Supporting Information.

Acquisition and Transmission of Data

Local Acquisition. The uMED contains enough memory (32 kilobytes) to store approximately ten different pulse sequences, the code that operates other functions of the device, and approximately 500 16-bit data points for on-board analysis. The device can, therefore, automatically perform the basic analysis and baseline corrections that are necessary to extract the concentration of an analyte from the raw data, display the measured concentration on the screen, and, if necessary, (using the method described in the next section) upload the information to a remote facility, without user intervention. To analyze the raw data directly, we interfaced a personal computer to the serial

port of the uMED through a serial-to-USB converter (FT232RL, FTDI) and used a custom application in MATLAB (Mathworks) to acquire and display the received data.

Telecommunication. The cellular voice-channel is particularly susceptible to signal interruption by burst noise and distortion by voice codecs that render analog modulation inappropriate for transmission of numeric data, such as concentrations of analytes or patient identification numbers. It is, therefore, simpler to transmit these data by digital modulation that can be supplemented with error detection or correction. We implemented a basic frequency-shift keying (FSK) protocol to transmit digital data over the audio channel of a mobile phone during a live connection. Since mobile phones are designed to transmit audio frequency signals in the range of 500 to 3300 Hz (24), we divided the available bandwidth in the voice channel into a band for the data (f = 500 to 1400 Hz) and a band for the header (f > 1500 Hz). We further subdivided the data band into ten, 100-Hz intervals, each corresponding to a single transmitted integer (0 – 9). We also incorporated a 10-bit binary cyclic-redundancy check (CRC), which is an error-detecting code that allows the validation of uncorrupted data by the receiving computer and is particularly effective at detecting the kinds of burst errors associated with the mobile voice channel (7, 14).

A pair of standard, 3.5-mm TRRS stereo connectors and a corresponding four-conductor audio cable provided an interface between the uMED and the audio port of a mobile phone. For our experiments, we chose a low-end phone from the Nokia 1100 series (1112) as it is still among one of the most widely used in developing countries (8, 25, 26). We used the stereo and microphone channels of the mobile phone to transmit and receive FSK signals to and from the device. We developed a custom application in MATLAB to establish a live voice link, through the VoIP application Skype (Microsoft, Redmond WA), between the mobile phone and a remote personal computer. This application received and decoded the FSK-based data, and sent an SMS-message to

back the mobile phone with contents relevant to the data it had received. Figure VII.S3 shows the flow of data in this network.

RESULTS

Device Overview.

The bill of materials for uMED was ~$25 (Table VII.S2), and the range of electrochemical measurements that we could perform were primarily limited by: i) the practical range of applied voltages (±2 V); ii) the sample-rate of the ADC (800 Hz); iii) the resolution of the DAC (0.05 mV); and iv) the electronic noise floor ($0.5\ \mathrm{nA_{rms}}$). Within these limitations, the uMED can perform the most common electrochemical measurements.

Device Performance.

To test the performance of the device, we compared the results obtained using our device to those obtained by a commercial electrochemical analyzer. Figure VII.3 shows the five types of electrochemical measurements that we implemented. For *CV* (Figure VII.3a), ferricyanide/ferrocyanide provided a well-understood model electroactive system, as it is the most common redox couple used for probing the performance of modified electrodes. For *chronoamperometry* (Figure VII.3b), ferrocyanide provided a model electroactive compound for chronoamperometric detection, as it is one of the most common electrochemical mediators that can be detected by amperometric methods. For *SWV* and *DPV* (Figure VII.3c), 1-naphthol provided a common substrate used in electrochemical ELISA. For each measurement we performed the same analysis on the uMED and a commercial potentiostat (AutoLab PGSTAT12, Metrohm) using the same solutions and batches of test strips. For *potentiometry*, sodium and potassium ions are common, clinically relevant electrolytes that we compared to a commercial ion-selective electrode over their physiological range of concentrations.

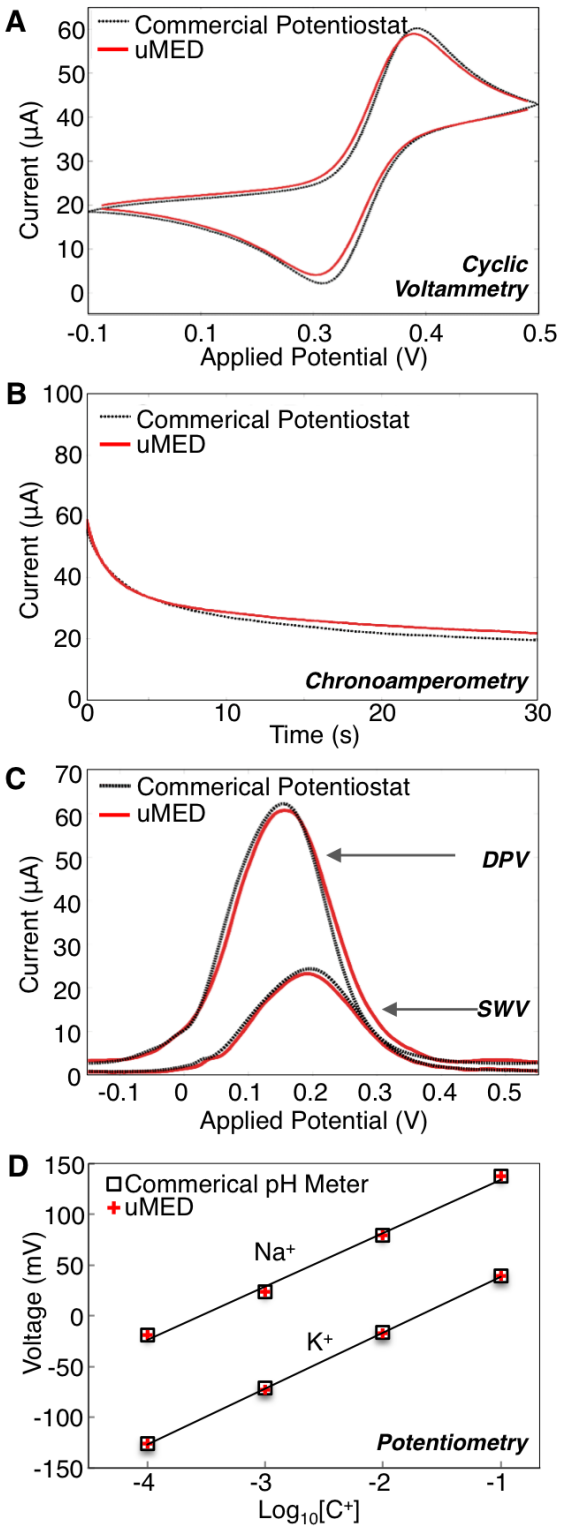

Figure VII.3: (**A**) A cyclic voltammagram of 2.5-m*M* ferricyanide/ferrocyanide in 0.1-M KCl**.** (**B**) A plot of the measured current versus time for chronoamperometry performed on 1-mM ferrocyanide in 0.1-M KCl. (**C**) Differential-pulse and square-wave voltammagrams of 1-mM 1-naphthol in 100-mM tris, 100-mM NaCl. (**D**) Detection of $[K^+]$ and $[Na^+]$ with potentiometry in an ionic strength adjuster.

Detection of Glucose by Chronoamperometry

Self-testing of blood glucose using a glucometer and disposable test strips is the most commonly performed point-of-care measurement globally. To test the performance of the uMED to function as a personal glucometer we used both a commercial glucometer (TrueTrak, CVS) and the uMED to measure the concentration of blood glucose in a series of real blood samples (Figure VII.4). Within the physiological range of 50 – 500 mg/dL, the uMED displayed a linear relationship relative to the values measured by the glucometer on the same samples. We also found that, that average relative standard deviation (5%) was better than most commercial glucometers (5–20%), and well within the performance criteria set out by the U.S. Food and Drug Administration (3).

Detection of heavy metals in water by SWASV

Lead and cadmium are among the most common toxic heavy metals found in water supplies, and zinc is an essential micronutrient. These metal ions can be simultaneously detected by ASV. We chose SWASV to detect Zn(II), Cd(II) and Pb(II) in water samples because this method provides higher sensitivity than, and better discrimination between, metals with similar redox potentials than DPV or linear sweep voltammetry. We implemented a three-electrode SWASV measurement sequence for detection of heavy metals following the timing previously described. To calculate the concentration of analyte, the uMED performed a baseline correction, calculated the difference between the maximum and minimum current measured, and subtracted the value of the blank (measured on the same SPE). Figure VII.4b shows a calibration plot for detection of lead, performed with commercial SPEs. Based on these data, we determined a detection limit of 4.0 μg/L, which is less than the minimum of 10 μg/L imposed by the World Health Organization (WHO) (27). We also verified the ability of the device to detect Cd, Zn, and Pb simultaneously. Figure VII.4b shows the

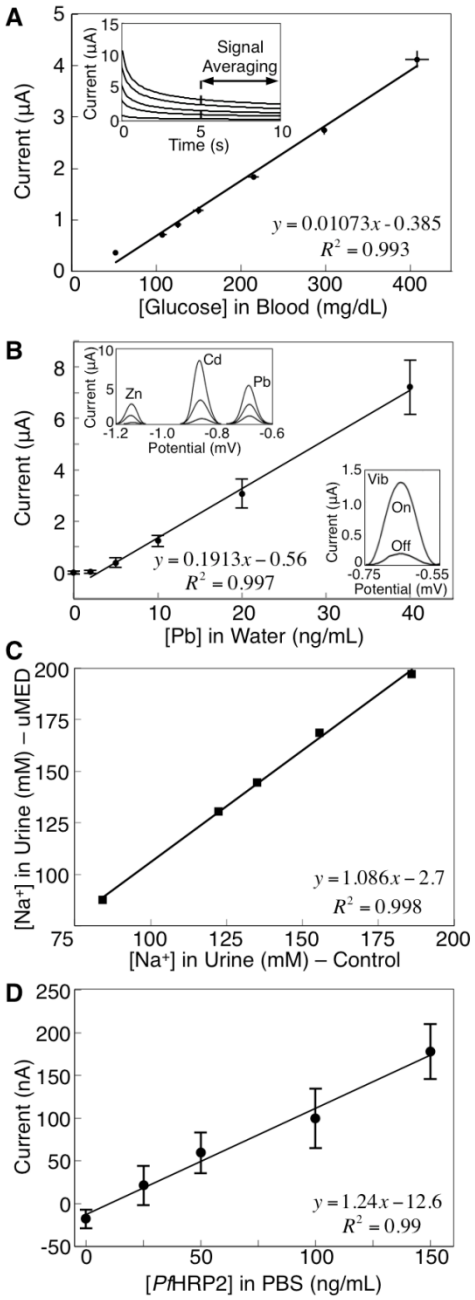

Figure VII.4: (**A**) A calibration plot of current versus concentration of glucose in assayed samples of human blood measured by chronoamperometry. **Inset:** A plot of the transient current for five representative concentrations of glucose (107, 150, 215, 298, and 408 mg/dL). (**B**) A calibration plot of the peak current versus the concentration of lead measured by SWASV. **Upper Inset:** The simultaneous detection of three heavy metals (Zn, Cd, and Pb) at three concentrations (5, 10, and 20 μg/L). **Lower Inset**: A comparison of the peak height for a 10-ng/mL solution of lead with and without the use of vibration during deposition. (**C**) Detection of Na^+ in assayed human urine control samples measured by potentiometry. (**D**) A calibration plot of the current versus the concentration of *Pf*HRP2 in PBS (1x). In all cases, the error bars indicate the standard deviation of n = 7 independent measurements.

resolved current peaks for various concentrations of these metals; we performed an indepedant baseline correction on each peak.

Detection of Sodium in Urine by Potentiometry

Sodium content in urine is often used to evaluate the amount of fluid within the blood vessels or the overall balance of electrolytes within the body (28) This test may be used when conditions such as hyponatremia (low sodium levels in the body) are suspected (29-31). We calibrated the potentiometric response of the uMED using standard solutions of sodium in an ionic strength adjustment buffer (4 M NH_4Cl with 4 M NH_4OH), and then applied that calibration to a series of urine control samples (Figure VII.4C). The systematic error of the measured concentrations (~8%) falls within the certified range of the assayed urine samples (±14%).

Electrochemical ELISA for detection of Malaria

ELISA is a sensitive technique often used for the detection of specific proteins. Although quantification of the enzymatically amplified product in an ELISA generally relies on optical measurements of absorbance, this biological recognition process can also be measured electrochemically (32-35). To demonstrate the capability to perform electrochemical ELISA in a research or clinical setting, we measured the concentration of the malarial antigen *Pf*HRP2 in a sandwich electrochemical ELISA. The quantification of *Pf*HRP2 is important because the antigen correlates with the parasite load in the body (36). Chronoamperometric measurements performed by the uMED show a linear response for concentrations of *Pf*HRP2 in the clinically relevant range of 0 – 150 ng/mL (37). In this proof-of-principle experiment, the limit of detection was 20 ng/mL.

Measurement and Remote Transmission of Results with a Low-End Mobile Phone

We demonstrated the complete capabilities of our system by measuring the concentration of glucose in a sample of blood from a single user and reporting the result to a remote computer through a low-end mobile phone. Figure VII.5 shows the result of a typical reporting sequence. We also performed an analysis of the effect of noise and latency of the voice channel on the delivery of FSK-based packets (Fig S4). Briefly, we found that, with our algorithm, the optimal tone length is ~34 ms (29 symbols per second), which allows the successful delivery of ~1.4 data packets per second at an effective throughput of 31 bits per second. We believe that this data rate is sufficient for the transmission of the results of POC testing (it requires, on average, only 2 s to send a value and receive an acknowledgement of receipt.

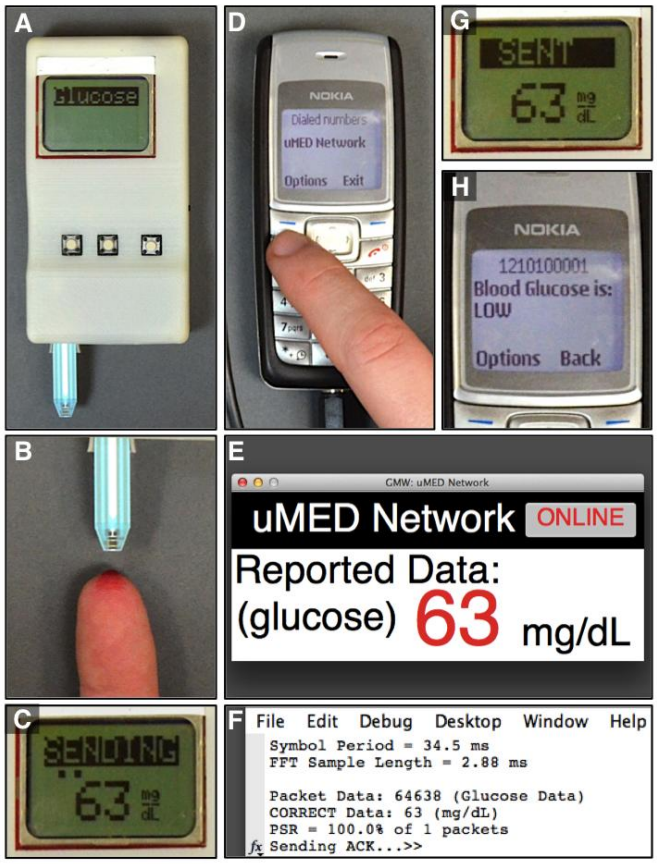

Figure VII.5: A demonstration of the uMED network in operation. **(A, B)** The local user made a blood-glucose measurement with the uMED. (**C**) Upon completion, the device automatically began to transmit repeated packets of data (series of tones) corresponding to value of the measurement. (**D**) The user then connected the device to a mobile phone and placed a call to a remote Skype-in number. (**E**, **F**) The remote user recorded the data packet, onto a laptop computer, as a stream of audio received through Skype, to a Matlab-based application for data acquisition. This application automatically: (i) extracted the data from the recorded audio; (ii) verified that the received data was uncorrupted; (iii) displayed the data to the user; (iv) sent a tone of acknowledgement signifying the receipt of an uncorrupted packet of data; and (v) sent an SMS message to the local user containing a diagnosis. (**G**) The local user's uMED received the acknowledgement, which triggered the device to cease transmission and to update the displayed text from "SENDING.." to "SENT". (**H**) Finally, the local user received an SMS message to their mobile phone signifying that the measured concentration of blood-glucose was "low". In principle, this upload process can also be performed on a batch of data collected throughout the day.

DISCUSSION

Electrochemical detection is a very attractive method to perform simple, in-field testing for many reasons. i) In contrast to technologies based on optical sensing, the signal measured by the electrochemical test is not affected by the color of the sample, the lighting conditions, or the presence of particulate matter. ii) The measured current or voltage can be transformed into a numeric output by simple electronics and the results of testing can be made "user-blind" in order to eliminate user bias, or provide security if privacy is a concern. iii) Electrochemical sensors can be used to detect a range of important analytes using different pulse-sequences, while the required electronics can be assembled at low cost without sacrificing this versatility.

The popularity and applicability of hand-held glucometers demonstrates the advantages of electrochemical detection in POC setting. We and others have demonstrated that glucometers can quantify analytes other than glucose—such as lactate, cholesterol and ethanol (20), cocaine, adenosine, and uranium (38) or a specific DNA aptamer (39). It is, however, impractical to adapt a commercial hand-held glucometer for the detection of a broader range of analytes because it is engineered to perform a single task, is not designed to be particularly sensitive, and cannot perform scanning or multi-step measurements, such as voltammetry.

To perform a broad variety of electrochemical measurements requires the design of a custom potentiostat. Recently, Rowe et al. (40) demonstrated that a low-cost (~$80) potentiostat can be assembled from off-the-shelf components and programmed to perform a variety of electrochemical pulse sequences. This device, however, is designed for bench top applications: it requires a personal computer and USB connection for operation, full-size expensive electrodes to perform measurements, a magnetic stirrer for mixing of samples, and glassware to handle a large sample volume. In another paper, Lillehoj et al. (10) demonstrated a similar type of potentiostat

coupled to a smartphone, although it could only perform chronoamperometry, and required a sophisticated microfluidic device to handle the sample.

Here, we aim to solve a greater challenge: can a low-cost device provide a nearly "universal solution" by overcoming the challenges of performing field-based electrochemical analyses in any resource-limited setting. To qualify as a "universal solution", we have designed the uMED to be, i) capable of performing a variety of complete and accurate analyses, ii) simple enough to be used by untrained users, iii) require a minimum of resources, iv) be able to acquire, process, display, and transmit data automatically, v) be reprogrammable to accommodate new assays, sequences, or standards, vi) be applicable in the field using available technology, and most importantly, and v) be compatible with any phone and network.

The variety of important pulse sequences that the uMED can perform—including amperometry, coulometry, voltammetry, and potentiometry—is comparable to an expensive ($1k – $50k), commercial, bench-top potentiostat; for all pulse sequences the performance of the uMED matched that of the commercial comparison. Differences between the commercial device and uMED were primarily caused by variations between test strips and electrochemical fluctuations during measurements, and not by differences in the performance of the electronics.

These common electrochemical pulse sequences enable a broad range of quantitative applications. *CV*, for example, is the most widely used technique for acquiring information about electrochemical properties (e.g. redox potentials) of the species in the reaction mixture and of the electrode surface (41, 42) or, in some cases, to is used to assay analytes (43). *Chronoamperometry* is one of most common techniques for monitoring an enzymatic reaction that produces a redox-active species, such that the measured current correlates to the concentration of the redox species. This technique can be used for the determination of metabolites (20), proteins, or other biomolecules

when coupled with electrochemical ELISA (2, 35). *DPV* and *SWV* are more sensitive than CV and chronoamperometry because they use differential sampling to reduce the influence of non-Faradaic currents, and are therefore used when low limits of detection are required. They are also the primary techniques used to detect trace amounts of heavy metals (44), and can also be used for immunoassays in which a tracer antibody is labeled with an enzyme (e.g. electrochemical ELISA), metal nanoparticle, or quantum dot (2, 44). *Potentiometry* with ion-selective electrodes is widely used for the detection of electrolytes (e.g., Na^+, K^+, Cl^-, and NH_4^+) (45). Potentiometry is also used to detect biomarkers for liver function, such as blood urea nitrogen (BUN) and creatinine, by converting urea and creatinine into ammonium ions that can be detected by an ammonium-selective electrode (46).

We have also demonstrated the applicability of the uMED in a variety of important applications and contexts. The uMED detected blood glucose in real blood samples with a linearity and precision equivalent to that of a commercial hand-held glucometer. In water samples, the uMED provided a comparable limit of detection to other portable electrochemical detectors for heavy metals (47); this result indicated that this device can enable a broad spectrum of users—from concerned citizens to budget-constrained municipalities—to perform in-field agricultural or environmental monitoring of water quality. The uMED also measured the sodium content in urine samples with acceptable accuracy over the clinically relevant range - an indication that this device can be used for commonly performed clinical tests for electrolytes. The vast and fast-growing field of ion-selective electrodes also provides many opportunities to couple new electrodes with the uMED device to measure diverse analytes (48). The use of the uMED device for electrochemical ELISAs could benefit researchers studying diseases such as malaria, as well as aid in the development of high sensitivity diagnostics. The approach can also be generalized to

many other assays without significant modification of the protocol because we selected the commonly used substrate TMB for HRP-based systems.

The use of commercially available screen-printed electrodes and test strips ensures reproducibility, guarantees that the device is useful immediately, and reduces the required-sample volume to a single droplet. In principle, the device is also compatible with other low cost technologies that can give comparable performance, such as electrochemical microfluidic paper analytic devices (EμPADs) that we and others have developed, (19-21, 49, 50).

The compatibility of the uMED with the popular Arduino development environment makes it extremely simple to reprogram the device to alter or add pulse sequences, and may extend the use of the device to educational contexts as well. The voltage range, sensitivity, accuracy, and speed (e.g. for dielectric spectroscopy) can all be improved with simple modifications to the system and without significantly affecting the design or cost of the device. The addition of an optical detector and/or source, in principle, would enable electro-chemiluminesence, fluorometry, spectrophotometry, etc. While the throughput of audio data over voice that we achieved was acceptable for low data-rate POC applications, if necessary, it can be increased substantially by implementing more sophisticated error correction and adding a dedicated tone generator (51).

Mobile phone and network compatibility remains a challenge for all current hybrid mHealth/POC devices because each is typically developed to operate with a specific smartphone that requires custom applications. Nearly 2.8 billion people however, continue to use low-end phones (62% of worldwide users of mobile phones), and, although the use of smartphones is rising rapidly, it is projected that by 2017 nearly 2.6 billion mobile subscribers will remain without a smartphone (52). A majority of these low-end phones are, and will be, used in low- to middle- income countries such as those found in Sub-Saharan Africa as well as Brazil, Russia, India, China, and Indonesia.

These regions alone will account for nearly two billion of the users of low-end phones by 2017 (Figure VII.S5). Furthermore, although some non-smartphones (feature-phones) may have limited Internet access via 3G, it is impractical to develop compatibility with all the hundreds of variations of software applications, operating systems, types of data ports, and cellular networks. It is clear that compatibility with low-end phones and 2G networks, especially in resource-limited applications, will be a requirement for years to come.

We have designed the uMED to perform electrochemical analyses entirely in a handheld, stand-alone format (that is, without a mobile phone), and to require only a mobile phone to transmit data. There are a number of benefits to this approach: i) the uMED does not depend on the mobile phone for power, and can last for months to years on a single battery charge (smartphones, by contrast, have notoriously short battery lives); ii) the uMED can be used by someone who does not own a mobile phone to collect data; and iii) the uMED does not depend on any particular type of phone. Our approach to transmit diagnostic data by audio-based frequency shift keying i) is compatible with any phone (from low-end phones to smartphones); ii) is compatible with all generations of cellular networks (2G-4G); iii) does not require any phone-based applications to operate; and iii) guarantees, in combination with our choice of error-detecting code, that uncorrupted data can be uploaded to "the cloud".

CONCLUSION

The uMED is an inexpensive, versatile tool that links all the most common electrochemical methods with the telecommunication technology most widely available across the globe. The unique combination of capabilities of the uMED enables sensitive and quantitative analysis in resource limited settings by: i) eliminating the need for expensive laboratory *equipment* (such as a commercial potentiostat, pH meter, glassware, or a magnetic stirrer); ii) reducing the need for expensive or

limited *resources* (such as reagents or blood samples) by reducing the sample volume to a single droplet (~10 – 100 μL, depending on the application) on a test strip or SPE; iii) enabling remote *expertise*, monitoring, or archiving to be provided using *any* available mobile technology; and iv) minimizing the *training* required to perform sophisticated electrochemical analyses by using appropriate design to make the system as simple as possible. All that is required is to insert the strip, select the test, apply the sample, and place a phone call.

ACKNOWLEDGEMENTS

This work was funded in part by Bill and Melinda Gates Foundation, under award No. 51308, which provided salary support for A.N., J.H., and A.A.K., and an award from the Defense Threat Reduction Agency (DTRA) and the Lawrence Livermore National Laboratory, No. B603629, which provided salary support for D.C. A.A.K. was also supported by the NSF Graduate Research Fellowship Program. E.J.M was supported by a postdoctoral fellowship from the Natural Sciences and Engineering Research Council of Canada (NSERC-PDF). M.T.F.A. was supported by an award from Ministerio de Economía y Competitividad Español (MINECO, old MICINN), No. CTQ2011-25814.

REFERENCES

1. Maxwell EJ, Mazzeo AD, Whitesides GM (2013) Paper-based electroanalytical devices for accessible diagnostic testing. *MRS Bull* 38:309–314.

2. Chikkaveeraiah BV, Bhirde AA, Morgan NY, Eden HS, Chen X (2012) Electrochemical Immunosensors for Detection of Cancer Protein Biomarkers. *ACS Nano* 6:6546–6561.

3. Tonyushkina K, Nichols JH (2009) Glucose Meters: A Review of Technical Challenges to Obtaining Accurate Results. *J Diabetes Sci Technol* 3:971–980.

4. Freckmann G et al. (2012) System accuracy evaluation of 43 blood glucose monitoring systems for self-monitoring of blood glucose according to DIN EN ISO 15197. *J Diabetes Sci Technol* 6:1060–1075.

5. Kahn JG, Yang JS, Kahn JS (2010) "Mobile" health needs and opportunities in developing countries. *Health Affairs* 29:252–258.

6. Chin CD, Chin SY, Laksanasopin T, Sia SK (2013) Low-Cost Microdevices for Point-of-Care Testing. *Point-of-Care Diagnostics on a Chip*, eds Issadore D, Westervelt RM (Springer), pp 3–21.

7. Estrin D, Sim I (2010) Open mHealth Architecture: An Engine for Health Care Innovation. *Science* 330:759–760.

8. Lee D-S, Jeon BG, Ihm C, Park J-K, Jung MY (2010) A simple and smart telemedicine device for developing regions: a pocket-sized colorimetric reader. *Lab Chip* 11:120.

9. Liu L, Liu J (2011) Biomedical sensor technologies on the platform of mobile phones. *Front Mech Eng* 6:160–175.

10. Lillehoj PB, Huang M-C, Truong N, Ho C-M (2013) Rapid electrochemical detection on a mobile phone. *Lab Chip* 13:2950–2955.

11. Chin CD et al. (2013) Mobile Device for Disease Diagnosis and Data Tracking in Resource-Limited Settings. *Clin Chem* 59:629–640.

12. Delaney JL, Doeven EH, Harsant AJ, Hogan CF (2013) Use of a mobile phone for potentiostatic control with low cost paper-based microfluidic sensors. *Anal Chim Acta* 790:56–60.

13. Noedl H et al. (2005) Simple histidine-rich protein 2 double-site sandwich enzyme-linked immunosorbent assay for use in malaria drug sensitivity testing. *Antimicrob Agents Chemother* 49:3575–3577.

14. Stigge M, Plötz H, Müller W, Redlich J-P (2006) Reversing CRC—Theory and Practice. *Humboldt-University Berlin, Public Report*.

15. Kaplan WA (2006) Can the ubiquitous power of mobile phones be used to improve health outcomes in developing countries? *Global Health* 2:9.

16. Vodafone (2005) Africa: The Impact of mobile phones. *The Vodafone Policy Paper Series* 2.

17. Centi S, Laschi S, Fránek M, Mascini M (2005) A disposable immunomagnetic electrochemical sensor based on functionalised magnetic beads and carbon-based screen-printed electrodes (SPCEs) for the detection of polychlorinated biphenyls (PCBs). *Anal Chim Acta* 538:205–212.

18. Chatrathi MP, Wang J, Collins GE (2007) Sandwich electrochemical immunoassay for the detection of Staphylococcal enterotoxin B based on immobilized thiolated antibodies. *Biosens Bioelectron* 22:2932–2938.

19. Nie ZZ et al. (2010) Electrochemical sensing in paper-based microfluidic devices. *Lab Chip* 10:477–483.

20. Nie ZZ, Deiss FF, Liu XX, Akbulut OO, Whitesides GMG (2010) Integration of paper-based microfluidic devices with commercial electrochemical readers. *Lab Chip* 10:3163–3169.

21. Liu H, Crooks RM (2012) Paper-based electrochemical sensing platform with integral battery and electrochromic read-out. *Anal Chem* 84:2528–2532.

22. Liu H, Xiang Y, Lu Y, Crooks RM (2012) Aptamer-Based Origami Paper Analytical Device for Electrochemical Detection of Adenosine. *Angew Chem Int Ed* 51:6925–6928.

23. Fernández-Abedul MT, Costa-García A (2007) Carbon nanotubes (CNTs)-based electroanalysis. *Anal Bioanal Chem* 390:293–298.

24. Rodman J (2003) The effect of bandwidth on speech intelligibility. *White paper, POLYCOM Inc, USA*.

25. Ledgard JM (2011) Digital Africa. *The Economist: Intelligent Life*. Available at: http://moreintelligentlife.com/content/ideas/jm-ledgard/digital-africa?page=full [Accessed May 25, 2013].

26. Mudanyali O et al. (2012) Integrated rapid-diagnostic-test reader platform on a cellphone. *Lab Chip* 12:2678.

27. World Health Organization (WHO) (2011) Guidelines for drinking-water quality 4th edition. *Geneva, Switzerland*.

28. Kamel KS, Ethier JH, Richardson RMA, Bear RA, Halperin ML (1990) Urine Electrolytes and Osmolality: When and How to Use Them. *Am J Nephrol* 10:89–102.

29. Milionis HJ, Liamis GL, Elisaf MS (2002) The hyponatremic patient: a systematic approach to laboratory diagnosis. *Can Med Assoc J* 166:1056–1062.

30. McPherson RA, Pincus MR (2011) *Henry's Clinical Diagnosis and Management by Laboratory Methods, 22/e* (Elsevier Health Sciences).

31. DeVita MV, Michelis MF (1993) Perturbations in sodium balance. Hyponatremia and hypernatremia. *Clin Lab Med* 13:135–148–148.

32. Lee A-C et al. (2008) Sensitive Electrochemical Detection of Horseradish Peroxidase at Disposable Screen-Printed Carbon Electrode. *Electroanalysis* 20:2040–2046.

33. Yi J et al. (2012) Development of an electrochemical immunoassay for detection of gatifloxacin in swine urine. *J Zhejiang Univ Sci B* 13:118–125.

34. Fanjul-Bolado P, González-García MB, Costa-García A (2005) Amperometric detection in TMB/HRP-based assays. *Anal Bioanal Chem* 382:297–302.

35. Pyun JC, Lee HH, Lee CS (2001) Application of an amperometric detector to the conventional enzyme-immunoassay (EIA). *Sens Actuators B Chem* 78:232–236.

36. Dondorp AM et al. (2005) Estimation of the total parasite biomass in acute falciparum malaria from plasma PfHRP2. *PLoS medicine* 2:e204.

37. Kifude CM et al. (2008) Enzyme-Linked Immunosorbent Assay for Detection of Plasmodium falciparum Histidine-Rich Protein 2 in Blood, Plasma, and Serum. *Clin Vaccine Immunol* 15:1012–1018.

38. Xiang Y, Lu Y (2011) Using personal glucose meters and functional DNA sensors to quantify a variety of analytical targets. *Nat Chem* 3:697–703.

39. Xiang Y, Lu Y (2012) Using Commercially Available Personal Glucose Meters for Portable Quantification of DNA. *Anal Chem* 84:1975–1980.

40. Rowe AA et al. (2011) CheapStat: An Open-Source, "Do-It-Yourself" Potentiostat for Analytical and Educational Applications. *PLoS ONE* 6:e23783.

41. Huang K-J, Niu D-J, Xie W-Z, Wang W A disposable electrochemical immunosensor for carcinoembryonic antigen based on nano-Au/multi-walled carbon nanotubes–chitosans nanocomposite film modified glassy carbon electrode. *Anal Chim Acta* 659:102–108.

42. Etienne M, Guillemin Y, Grosso D, Walcarius A (2012) Electrochemical approaches for the fabrication and/or characterization of pure and hybrid templated mesoporous oxide thin films: a review. *Anal Bioanal Chem* 405:1497–1512.

43. Saurina J, Hernández-Cassou S, Saurina J, Fàbregas E, Alegret S (1999) Determination of tryptophan in feed samples by cyclic voltammetry and multivariate calibration methods. *Analyst* 124:733–737.

44. Chen A, Shah B (2013) Electrochemical sensing and biosensing based on square wave voltammetry. *Anal Methods* 5:2158.

45. Dimeski G, Badrick T, John AS (2010) Ion Selective Electrodes (ISEs) and interferences—A review. *Clinica Chimica Acta* 411:309–317.

46. Lad U, Khokhar S, Kale GM (2008) Electrochemical Creatinine Biosensors. *Anal Chem* 80:7910–7917.

47. Yantasee W et al. (2007) Electrochemical sensors for the detection of lead and other toxic heavy metals: the next generation of personal exposure biomonitors. *Environ Health Perspect* 115:1683–1690.

48. Bühlmann P, Chen LD (2012) Ion-Selective Electrodes With Ionophore-Doped Sensing Membranes. *Supramolecular Chemistry: From Molecules to Nanomaterials*, eds Steed JW, Gale PA (Wiley & Sons).

49. Dungchai W, Chailapakul O, Henry CS (2009) Electrochemical Detection for Paper-Based Microfluidics. *Anal Chem* 81:5821–5826.

50. Lan W-J et al. (2013) Paper-based electroanalytical devices with an integrated, stable reference electrode. *Lab Chip* 13:4103–4108.

51. Dhananjay A et al. (2010) Hermes: data transmission over unknown voice channels. *Proceedings of the sixteenth annual international conference on Mobile computing and networking*:113–124.

52. eMarketer, Inc. (2014) Smartphone Users Worldwide Will Total 1.75 Billion in 2014. *eMarketercom*. Available at: http://www.emarketer.com/Article/Smartphone-Users-Worldwide-Will-Total-175-Billion-2014/1010536 [Accessed March 9, 2014].

Supporting Information for

A Universal Mobile Electrochemical Detector Designed for Use in Resource-Limited Applications

Alex Nemiroski[a], Dionysios C. Christodouleas[a], Jonathan W. Hennek[a], Ashok A. Kumar[b], E. Jane Maxwell[a], Maria Teresa Fernández-Abedul[c], and George M. Whitesides[a,d,e]

[a] Department of Chemistry & Chemical Biology, Harvard University, Cambridge, MA 02138
[b] School of Engineering and Applied Science, Harvard University, Cambridge, MA 02138
[c] Departamento de Química Física y Analítica, Universidad de Oviedo, Asturias, Spain
[d] Wyss Institute for Biologically Inspired Engineering, Harvard University, Cambridge, MA 02138 USA
[e] The Kavli Insitute for Bionano Science, Harvard University, Cambridge, MA 02138 USA

Corresponding author: George M. Whitesides (gwhitesides@gmwgroup.harvard.edu)

EXPERIMENTAL

Device Design and fabrication

We used the microcontroller to sample and compute data acquired from the potentiostat, to encode and decode frequency-modulated data, and to display a graphical user interface (GUI) on the LCD. We configured six digital input/output channels to operate the external DAC, ADC, and LCD over a serial peripheral interface (SPI) protocol, and one digital output channel to transmit data over audio by frequency shift keying (FSK). We configured four analog input channels to sample the voltages associated with the potentiostat, one analog input channel to receive data over audio, and three digital input channels to detect the states of the buttons.

Device Fabrication

We mounted these electronics on a custom-made printed circuit board (Advanced Circuits) and housed all components in a plastic case that we fabricated by 3D-printing (Fortus 250mc, Stratasys). The assembled device measured 56 mm x 106 mm x 18mm and weighed 63 g. The bill of materials was $25 (not counting the case, and assuming a purchase volume of at least 1000 components each). We show the circuit schematic in Figure VII.S1 and the bill of materials in Table VII.S2.

Design of the Potentiostat

Together with a feedback resistor R_f, the op-amp controlling the working electrode formed a transimpedance amplifier (TIA), converting the current I into an output voltage $V_O = V_W - IR_f$ while maintaining the working electrode at V_W, set by the DAC. The feedback resistance R_f set the sensitivity of the system. We chose $R_f = 8\ k\Omega$ for all measurements, and suitable DC offsets for all electrodes in order to place the desired measurements in the range of the potentiostat.

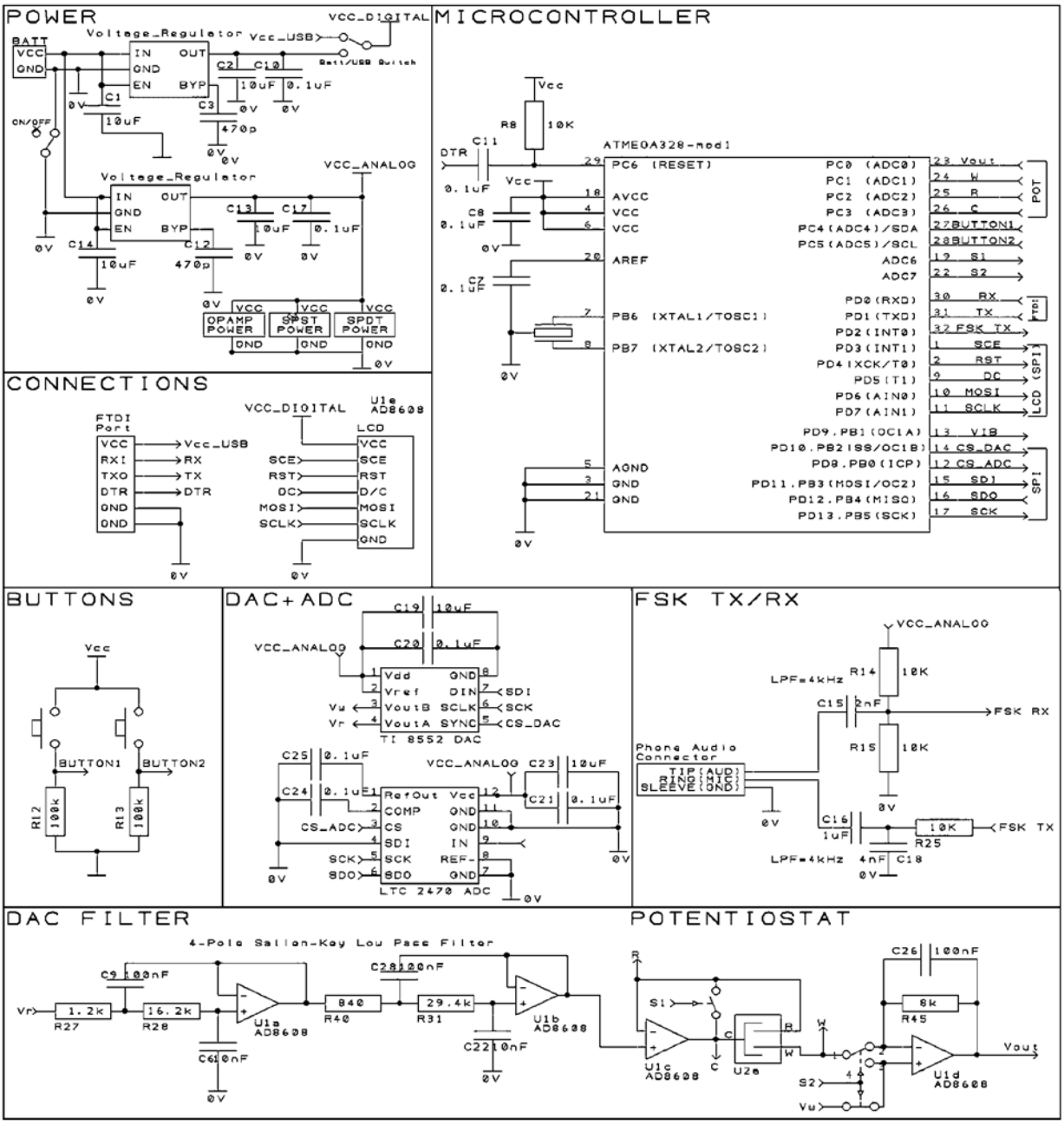

Figure VII.S1: Full Circuit Diagram for uMED.

Description	Part No	Quant.	Price Ea.	Total	Vendor
JST Right-Angle Connector	455-1719-ND	1	$0.07	$0.07	Digikey
Polymer Li-Ion Cell (3.7V, 210mAh)	PL-651628-2C	1	$2.65	$2.65	BatterySpace
IC LDO Regulator (3.3V, SOT23-5)	576-1259-1-ND	2	$0.39	$0.78	Digikey
Microcontroller (ATMEGA328P)	455-1719-ND	1	$1.77	$1.77	Digikey
2.5 mm 4 Conn Audio Jack (SMD)	CP1-42534SJTR-ND	1	$0.39	$0.39	Digikey
AD8608 Quad R-R Opamp	AD8608ARUZ-ND	1	$1.96	$1.96	Digikey
DAC8552 16-bit DAC (Dual Channel)	296-20676-1-ND	1	$3.99	$3.99	Digikey
LTC2470 16-bit ADC (Single Channel)	52R9827	1	$2.37	$2.37	Newark
Graphic LCD 84x48 - Nokia 5110	SKU091069	1	$2.83	$2.83	Banggood
Resonator 8.00 MHz Ceramic (SMD)	490-1195-1-ND	1	$0.25	$0.25	Digikey
Resistor: 0603	*n/a*	11	$0.00	$0.02	Digikey
Capacitor: 0402 (<= 0.1 uF) Ceramic	*n/a*	18	$0.00	$0.03	Digikey
Capacitor 0402 (1uF) Ceramic	587-1231-1-ND	1	$0.01	$0.01	Digikey
Capacitor 0805 (10uF) Ceramic	587-1300-1-ND	4	$0.01	$0.06	Digikey
Capacitor 1206 (10uF) Tantalum	495-2174-1-ND	2	$0.04	$0.08	Digikey
Analog Switch SPST (Dual Channel)	MAX4643	1	$1.01	$1.01	Mouser
Analog Switch SPDT (Single Channel)	MAX4644	1	$0.86	$0.86	Mouser
Vibration Motor, Flat Coin	28821-ND	1	$3.99	$3.99	Digikey
PCB	*custom*	1	$1.03	$1.03	4PCB
			TOTAL	**$24.15**	

Table VII.S2: Bill of Materials for the uMED. For the price, we quote for >1000 units.

To set V_R and V_W, we chose a two-channel, 16-bit DAC (DAC8552, Texas Instruments) programmed by the popular 3-wire SPI protocol. The smallest potential step required in our applications was ~5 mV, and since the nonlinearity of most DACs is within a few least-significant bits (LSB), the 16-bit resolution provided us with sufficient voltage resolution (3.3 V / 2^{16} ~ 0.05 mV) to ensure that any non-idealities in the voltage generation were at most a few percent of the smallest voltage steps. We updated the output of the DAC at a rate ~2 kHz although, in principle, the system could support rates up to ~20 kHz if necessary. To sample the output signal with high resolution, we also incorporated a 16-bit ADC. With its required 1.25-V reference, this ADC provided us with a resolution of 1.25 V / 2^{16} ~ 20 μV, although the practical minimum voltage that we could resolve was limited by the voltage noise of $\sim 40\ \mu V_{rms}$, as measured by the ADC, which for $R_f = 8\ k\Omega$, corresponded to a current resolution of $\sim 5\ nA_{rms}$. For most measurements, however, we averaged the signal over 5 seconds (100 consecutive data points) to reduce the electronic noise to $\sim 0.5\ nA_{rms}$. We found, in all cases, that the electrochemical noise was substantially (10 – 100x) greater than the electronic noise. Therefore, for all pulse sequences, we also configured the uMED to apply a 30-point smoothing function on all traces automatically to reduce the electrochemical noise. After the uMED performed these various forms of signal averaging automatically, it then extracted a concentration by comparing to a saved calibration or sent the acquired values to a PC for further analysis.

Acquisition of Data

To evaluate the performance of the device, however, we needed to extract the raw data from the device. We interfaced with and collected raw data from the uMED by connecting a personal computer to the serial port of the uMED through a serial-to-USB converter (FT232RL, FTDI). We developed a custom application in MATLAB (Mathworks, Natick MA) to acquire, convert, and

display raw data received over USB from the uMED. Once we calibrated the uMED for chronoamperometry, SWASV, and potentiometry, we programmed the microcontroller to perform these measurements (e.g. signal averaging, baseline correction, peak extraction) automatically, without an external computer.

Network Connection, Packet Structure, and Error Correction

Figure VII.S3 shows a flow of data from a POC measurement to a remote facility. We employed a simple packet structure with two sections: i) a header to identify the type of measurement being transmitted (glucose, lead, sodium, or malaria) and ii) a body to store the numeric data, modified by the CRC. The header contained a single 50-ms tone that identified whether the data being transmitted corresponded to glucose (f = 1600 Hz), lead (f = 1700 Hz), sodium (f = 1800 Hz), or malaria (f = 1900 Hz). The body contained an integer-valued, base-10 representation of the concentration of a single measured analyte, encoded with the CRC. We encoded each integer in the sequence by a 50-ms tone at a frequency corresponding to the integer value. Since the ATmega328 can only output digital signals, we represented data as a sequence of square wave tones and passed the output through a passive, low-pass filter to attenuate all but the lowest-order, sinusoidal harmonic. In our implementation, we used a 10-bit CRC (0b1000000001) that enables detection of errors for sent values up to $2^{10} = 1024$. For larger values, it would be necessary to use a longer CRC for to reliably detect errors.

Power Consumption

The total number of measurements N the uMED can perform on a single battery charge can be calculated by

$$N = \frac{Q_{BATT}}{\langle I \rangle \cdot T}, \quad (1)$$

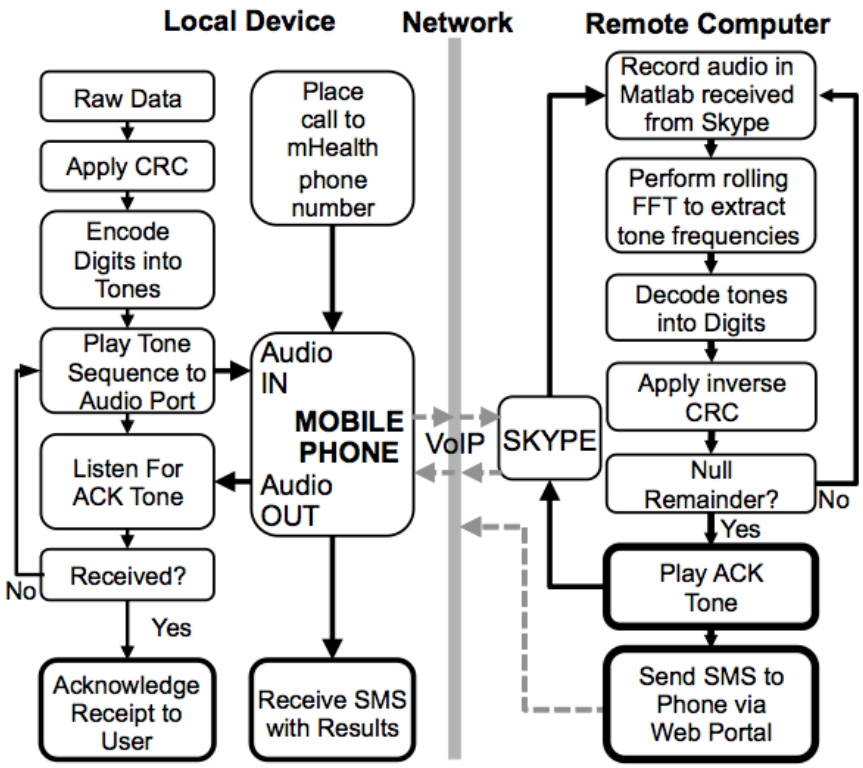

Figure VII.S3: A flow chart describing the sequence of operations involved establishing error-free communication over a mobile voice network between the uMED and a remote computer. We developed a custom application in MATLAB to i) sample the audio stream received by VoIP, ii) analyze and identify the frequency content of each packet, iii) convert the sequence of tones into a corresponding sequence of integers, iv) identify the type of measurement, v) verify the integrity of the received data with a CRC, and if error-free, vi) log and display the data to the remote user, vi) play an acknowledgement (ACK) tone (5 s, 500 Hz) to the VoIP application, and vii) send the decoded value, or a diagnostic interpretation, to the local user's mobile phone in the form of a text message over short messaging service (SMS), sent through the web-portal of the chosen mobile carrier (here, AT&T). We configured the uMED to send packets continuously until it received an ACK from the remote computer and, upon receipt, to cease the transmission of data packets and display a message informing the user.

where Q_{BATT} is the battery lifetime, $\langle I \rangle$ is the average current consumption, and T is the total time spent in operation. The rechargeable, 3.7-V lithium-polymer battery (PL-651628-2C, AA Portable Power Corp) that we used had a lifetime $Q_{BATT} = 210$ mAH. The uMED consumed $\langle I_{stby} \rangle = 10$ mA during standby (no measurement). The current consumption during measurements ranged from $\langle I_{gluc} \rangle = 11$ mA for glucometry ($T_{gluc} = 20$ s) to $\langle I_{ASV} \rangle = 24$ mA for ASV ($T_{ASV} = 280$ s), for which the power consumption was dominated by the vibration motor used for mixing. For an initially fully charged battery, these values indicate that the uMED can perform a maximum of $N_{gluc} \sim 3440$ glucose measurements or $N_{ASV} \sim 110$ ASV measurements before depletion. Depending on which measurements are performed and the frequency of use, the uMED can, therefore, last from one to several months before needing to be recharged.

MATERIALS AND METHODS

Chemical Reagents

All chemicals were used without further purification. For evaluating the performance of the different electrochemical pulse sequences we used potassium ferrocyanide, potassium ferricyanide, 1-napthol, sodium chloride, and potassium chloride purchased from Sigma-Aldrich. For detection of heavy metals we used sodium chloride (NaCl, 99.999%), sodium acetate Trace SELECTA (99.999%), water trace SELECT Ultra (AGS reagent), bismuth standard for AAS (999 ± 4 mg/L), cadmium standard for ICP (1000 ± 2 mg/L), zinc standard for ICP (1000 ± 2 mg/L), and lead standard solution for ICP/OCP (10.127 ppm) purchased from Sigma-Aldrich. For detection of recombinant *Pf*HRP2 (PIP001 from AbD Serotec) we used 96-well plates (Costar 3590) from Corning, anti-*Plasmodium falciparum* antibody (ab9206) and anti-*Plasmodium falciparum* horseradish peroxidase conjugate detection antibody (ab30384) from Abcam, bovine serum

albumin (BSA), and Tween-20 from Sigma-Aldrich, and Ultra TMB-ELISA from ThermoScientific. For the determination of glucose in assayed blood samples and the determination of sodium in assayed urine samples we used the Liquicheck Urine Chemistry Control Levels 1 and 2 (LOT 64360) and Trilevel minipole control Meter Trax Control (LOT 92510) from BioRad.

Materials and Instrumentation

For evaluation of chronoamperometry, cyclic voltammetry, SWV, and DPV we used unmodified screen-printed carbon electrodes (DRP110) from DropSens. For potentiometry we used ion-selective electrodes for sodium (K27504-30) and potassium (WU-27504-26) purchased from Cole-Palmer. For detection of glucose we used commercial test strips (TRUEtrack, Nipro Diagnostics). For SWASV and chronoamperometric detection of *Pf*HRP2 we used carbon nanotube-modified SPEs (DRP110-CNT) from DropSens, for enhanced sensitivity.

Measurement Procedure

For measurement of glucose we used a new test strip for each measurement. For detection of heavy metals, we measured the entire dilution series (6 samples, including the blank) on a single SPE in order of increasing concentration. We performed seven replicates of this series of measurements, each with a new SPE. We conditioned each new SPE by first performing a full sequence on a sample with no metal ions to ensure the electrode was free of any contaminants that could be removed by sampling conditions. After the cleaning step of each measurement, we rinsed the electrode with ultrapure DI water and dried with N_2. For detection of malaria, we measured the entire dilution series (5 samples, including the blank) on a single SPE in order of increasing concentration. We performed seven replicates of this series of measurements, each with a new SPE. Before taking measurements with a new electrode, we performed chronoamperometry at $E = 0.2$ V for 40 s on a solution of

PBS to ensure the electrode was free of any contaminants that could be removed by sampling conditions. Each SPE was rinsed with PBS and dried with N_2 between each measurement.

Glucometry

The glucose test strips that we use have a pair of electrodes (WE and CE) defined by carbon ink, and all of the necessary reagents (e.g., enzymes and electrochemical mediator) pre-stored on the test strip. A typical hand-held glucometer uses a two-electrode (counter and working) potentiostat to apply a simple voltage sequence that consists of an incubation period at zero applied voltage, followed by a measurement period at a fixed applied voltage (typically $E = 0.5$ V). The glucose oxidase (an enzyme) present in the test strip converts glucose (the analyte) and potassium ferricyanide (an electrochemical mediator) to gluconic acid and potassium ferrocyanide, the oxidation of which can be measured by chronoamperometry. We adapted this type of sequence and programmed the uMED to first apply $E = 0.5$ V to test for the presence of the sample in the reaction zone (Figure VII.2b). With the test strip inserted, but no sample present, there were no mobile ions to carry charge (current) between the electrodes. When we placed a sample on the test strip, the presence of ions in the solution gave sufficient conductivity to the test zone that it could be measured as current.

Detection of Heavy Metals by SWASV

To test the device for detection of metals (Zn(II), Cd(II) and Pb(II)) in water samples we first prepared a solution containing all the necessary reagents: 2 mg/L of bismuth ions as a co-deposition agent in a solution of 0.5-M acetic acid, 0.5-M sodium acetate, and 0.25-M sodium chloride. Next we prepared a series of sample solutions of Zn, Cd, and Pb ions (blank and 2 – 40 μg/L each) in water. To measure the concentration of these ions, we mixed 20 μL of the reagent solution with 80 μL of

the sample solution on the top of the SPE and activated the uMED to perform the SWASV sequence automatically.

Malaria Immunoassay by with Chronoamperometric Detection

Preparation of the 96-well plates was performed following the procedure by Noedl *et al.* (1-3). We coated high-binding 96 well plates with 100 µl of 1.0-µg/mL solution of anti-*Plasmodium falciparum* antibody in PBS (1x). The plates were sealed and incubated overnight at 4 °C after which the supernatant was discarded and the wells were incubated with 200 µL/well of 2% bovine serum album (BSA) in PBS for 2 hrs. After washing three times in 0.05% Tween-20 PBS, the plates were sealed and stored at -20 °C until use. Recombinant *Pf*HRP-2 was diluted in PBS to the desired concentration (0 - 200 ng/ml) and 100 µL was added to each well followed by 1 h incubation at RT. The wells were washed three times with PBS-Tween solution before the addition of 100 µL anti-*Plasmodium falciparum* horseradish peroxidase conjugate detection antibody at a concentration of 0.5 µg/ml in a solution of PBS with 2% BSA and 1% Tween-20. After 1 h incubation at RT, wells were washed in PBS-Tween solution three times. The final washing solution was left in the well until just before the addition of 100 µL of Ultra TMB-ELISA. The TMB solution incubated at RT for 2 min. in the dark before the reaction was stopped with 50 µL of 10% sulfuric acid (v/v). A 75-µL drop was immediately placed on the SPE. Chronoamperometry was performed at E = 0.2 V for 20 s. The potential used for amperometry was selected by first performing at CV scan from E_1 = 0 V to E_2 = 0.7 V at a scan-rate of 0.03 V/s step size of E_{step} = 2.5 mV. The position of the oxidation and reduction peaks is highly dependent of the pH of the system. We chose E = 0.2 V to ensure that reduction can be completed with minimal contribution from oxidation.

We programmed the uMED to automatically check whether the output current followed the expected chronoamperometric sequence (monotonically increasing and reaching a stable plateau after ~ 20 s) by automatically discarding any sequences for which $\mathrm{I(t-5s)-I(t)} < -0.043\ V$ (a value that we determined empirically) for any time t. This process is similar to the way a hand-held glucometer displays an error message when the chronoamperometric sequence yields data that is not consistent with the expected transient behavior.

Verification of Packet Structure and Data Throughput

It is important that physiological, medical, and environmental data received by a remote computer be correct. Our choice of CRC error detection guarantees that any three-digit value can be determined to be completely error free after transmission. This reliability, however, does not prevent corrupt data from arriving at the destination, effectively slowing down the transmission rate to the time it takes to deliver a correct packet of data. The rate at which packets are corrupted depends on the quality of the data channel and the method of decoding used. Figure VII.S4a-c shows a frequency-modulated packet with a randomly chosen value, its frequency spectrum, and its decoded value. We sent the data from the uMED, through a Nokia 1112, over the AT&T voice network, and received it with through a custom MATLAB application via Skype on a remote personal computer. We sampled the data at 44.1 kHz, and performed a rolling Fast Fourier Transform to analyze the frequency content of the packet and decode the sequence of integers. We characterized the effect of errors during transmission on the average throughput of data by determining the packet success rate (*PSR*) by

$$\mathrm{PSR} = \frac{\#\ \text{uncorrupted packets}}{\#\ \text{sent packets}}, \qquad (1)$$

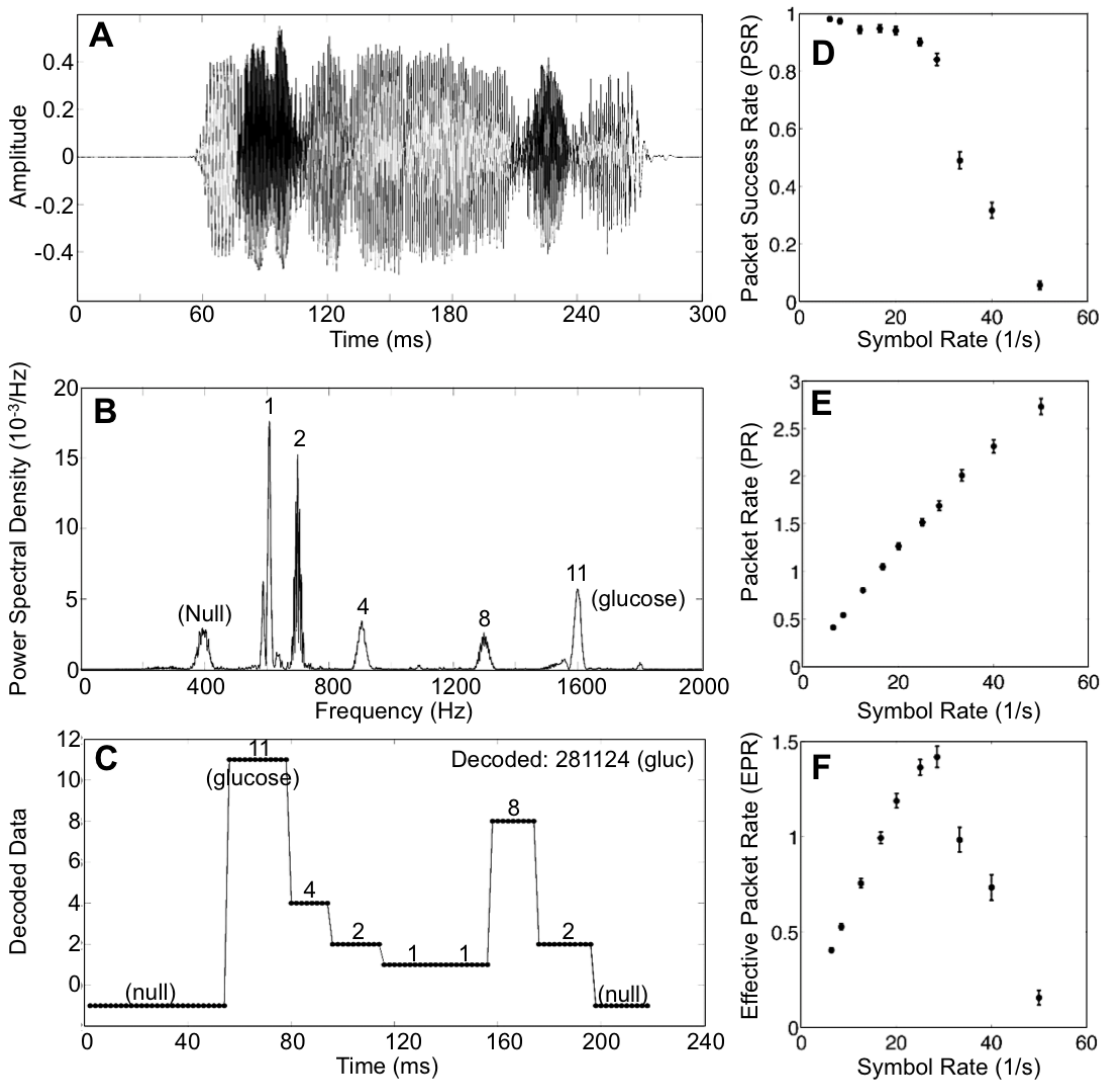

Figure VII.S4: An example of a successfully transmitted packet and an analysis data throughput versus symbol rate. We encoded the randomly chosen value 274 mg/dL of glucose (encoded as 2-8-1-1-2-4-11 after CRC; the 11 corresponds to glucose) and transmitted it over an active voice connection. (**A**) The audio signal received by the DAQ application. (**B**) An FFT of the entire packet demonstrating the presence of seven distinct frequency signals and the values to which they correspond. (**C**) The decoded packet containing the sequence (read in reverse) 2-8-1-1-2-4-11, which, after removing the CRC value, decodes to the value 274-11, or 274 mg/dL of glucose. (**D**) The overall PSR versus the symbol rate. (**E**) The PR versus the symbol rate. (**F**) The EPR versus the symbol rate (EPR = PSR · PR). The optimal EPR = 1.4 packets/s occurred at 29 symbols/s. The error bars in (D) signify the standard error of the mean $\varepsilon_{\mathrm{PSR}} = \sqrt{\frac{\mathrm{PSR}(1-\mathrm{PSR})}{\mathrm{N}}}$, where p is the packet success rate, and $\mathrm{N} = 300$. The error bars in (B) are propagated from (A) by $\varepsilon_{\mathrm{EPR}} = \sqrt{\left(\frac{\partial \mathrm{EPR}}{\partial \mathrm{PSR}}\varepsilon_{\mathrm{PSR}}\right)^2 + \left(\frac{\partial \mathrm{EPR}}{\partial \mathrm{PR}}\varepsilon_{\mathrm{PR}}\right)^2}$, where $\varepsilon_{\mathrm{PR}}$ is the measured standard deviation in PR.

and the effective packet rate (*EPR*) by $\mathrm{EPR} = \mathrm{PSR} \cdot \mathrm{PR}$, where PR is the raw packet rate (packets / s). The *EPR* quantifies the average rate at which correct packets are received, and signifies the average throughput of uncorrupted data.

Figure VII.S4d-f shows how the PSR and EPR depend on the symbol rate—the rate at which individual digits are transmitted. We characterized the PSR and its effect on the EPR by i) establishing a live connection to a remote computer through a mobile phone, ii) sending a sequence of packets containing random numeric data, encoded by CRC, from the uMED to the remote computer, and iii) comparing the received packets with the sent packets to determine the fraction of corrupted packets. We found that the PSR was constant around 98% at low symbol rates, but increased dramatically above 25 symbols/s, where the symbols begin to be too short to be properly identified with a simple FFT due to the distortion present in the voice channel. We found that the EPR is maximized at 29 symbols/s, indicating an optimal tradeoff between PER and the PR. Each packet consisted of average of six digits of CRC-encoded, numeric data (20 bits)— including three digits of underlying numeric data (10 bits)—and header (2 bits). At the maximal EPR (1.4 packets/s), the effective bitrate of CRC-encoded data and header was 31 bits per second (bps) and the effective bitrate of the underlying data and header was 17 bps.

Although we used a binary header, there was enough bandwidth to signify up to 16 different identifiers (4 bits), which would increase the effective bit rates by 3 bps each. We never identified an instance where the CRC failed to properly discriminate between corrupted and uncorrupted packets of data. When receiving data from a user, the remote computer responds with an ACK as soon as it receives a single uncorrupted packet. The signal delay between the user and the remote computer can vary depending on signal strength and other factors, but is usually approximately 0.5 seconds. We

found that at the optimal EPR, the median time a user had to wait for an ACK after beginning to send data was 2.2 seconds.

Mobile phone usage in the developing world

We compiled data on mobile phone usage for Brazil (1, 3-6), Russia (4-9), India (7-10), China (10, 11), Indonesia (11), SSA (2, 12) and present the data in Figure VII.S5.

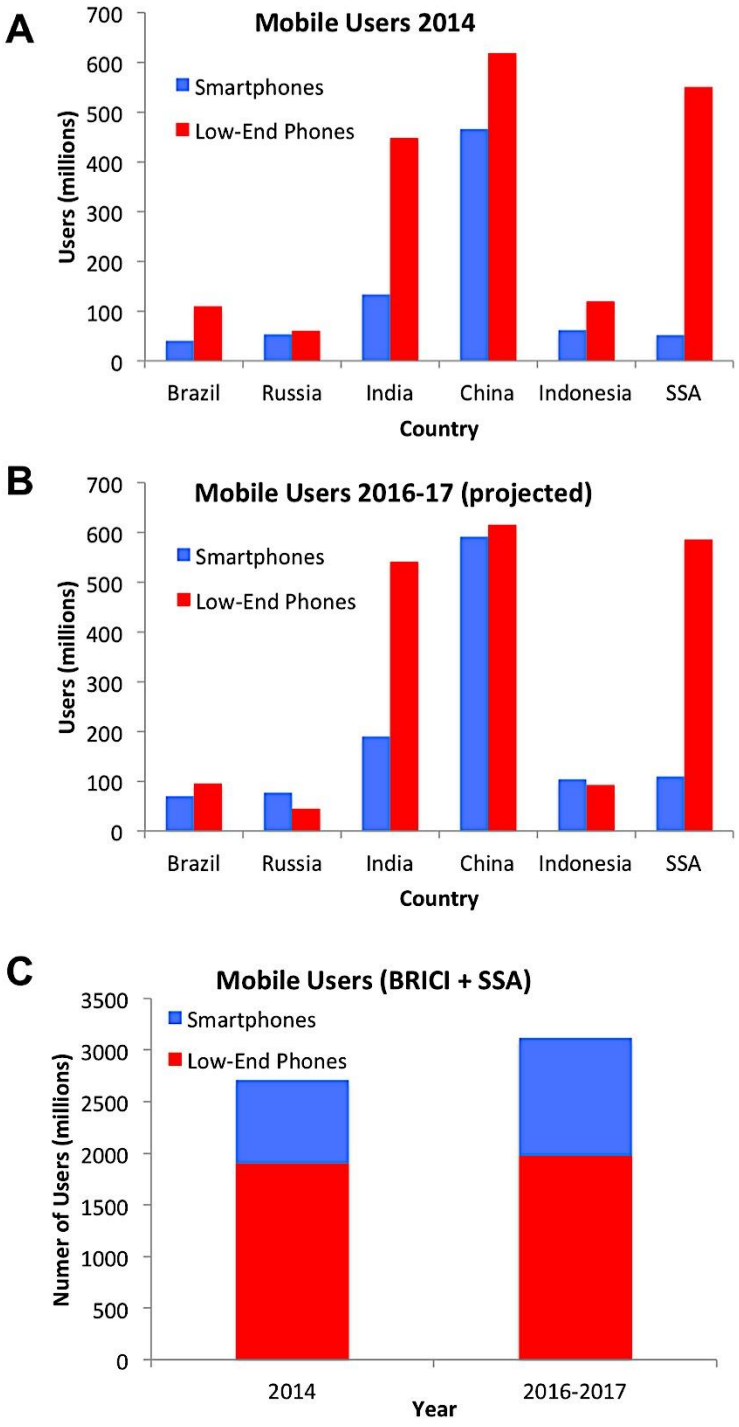

Figure VII.S5: Comparison of relative usage of smartphones vs. non-smartphones (low-end phones) in Brazil, Russia, India, China, Indonesia, and Sub-Saharan Africa (SSA) in (**A**) 2014 and (**B**) 2016-2017 (projected), and (**C**) combined.

SUPPORTING REFERENCES

1. eMarketer, Inc. (2013) Mobile Rivals PCs for Brazil's Internet Audience. *eMarketercom*. Available at: http://www.emarketer.com/Article/Mobile-Rivals-PCs-Brazilrsquos-Internet-Audience/1010311 [Accessed March 9, 2014].

2. Noedl H et al. (2005) Simple histidine-rich protein 2 double-site sandwich enzyme-linked immunosorbent assay for use in malaria drug sensitivity testing. *Antimicrob Agents Chemother* 49:3575–3577.

3. eMarketer, Inc. (2014) 2013: The Year of the Smartphone in Latin America. *eMarketercom*. Available at: http://www.emarketer.com/Article/2013-Year-of-Smartphone-Latin-America/1010545 [Accessed March 9, 2014].

4. eMarketer, Inc. (2013) Major Bump in Mobile Web Use in Urban Russia. *eMarketercom*. Available at: http://www.emarketer.com/Article/Major-Bump-Mobile-Web-Use-Urban-Russia/1010076 [Accessed March 9, 2014].

5. eMarketer, Inc. (2013) Russia's Digital Ecosystem Shaped by Market Nuances. *eMarketercom*. Available at: http://www.emarketer.com/Article/Russias-Digital-Ecosystem-Shaped-by-Market-Nuances/1009653 [Accessed March 9, 2014].

6. eMarketer, Inc. (2014) Forecast: mobile phone users in Russia 2011-2017. Available at: http://www.statista.com/statistics/274770/forecast-of-mobile-phone-users-in-russia/ [Accessed March 9, 2014].

7. eMarketer, Inc. (2012) Smartphones Speed the Digital Revolution in India. *eMarketercom*. Available at: http://www.emarketer.com/Article/Smartphones-Speed-Digital-Revolution-India/1009551 [Accessed March 9, 2014].

8. eMarketer, Inc. (2014) Forecast: Mobile phone users in India 2011-2017. Available at: http://www.statista.com/statistics/274658/forecast-of-mobile-phone-users-in-india/ [Accessed March 9, 2014].

9. eMarketer, Inc. (2014) Forecast: Smartphone user penetration in India 2010-2016. Available at: http://www.statista.com/statistics/257048/smartphone-user-penetration-in-india/ [Accessed March 9, 2014].

10. eMarketer, Inc. (2013) The Mobile Ad Boom Reaches China. *eMarketercom*. Available at: http://www.emarketer.com/Article/Mobile-Ad-Boom-Reaches-China/1010293 [Accessed March 9, 2014].

11. Rao M (2012) Mobile Southeast Asia Report 2012: Crossroads of Innovation. *Mobile Monday*. Available at: http://www.mobilemonday.net/reports/SEA_Report_2012.pdf. [Accessed March 9, 2014].

12. Nie ZZ et al. (2010) Electrochemical sensing in paper-based microfluidic devices. *Lab Chip* 10:477–483.